REPORT NO.
UCB/EERC-88/02
JANUARY 1988

EARTHQUAKE ENGINEERING RESEARCH CENTER

EXPERIMENTAL EVALUATION OF SEISMIC ISOLATION OF MEDIUM-RISE STRUCTURES SUBJECT TO UPLIFT

by

M.C. GRIFFITH
J.M. KELLY
V.A. COVENEY
C.G. KOH

Report to the National Science Foundation

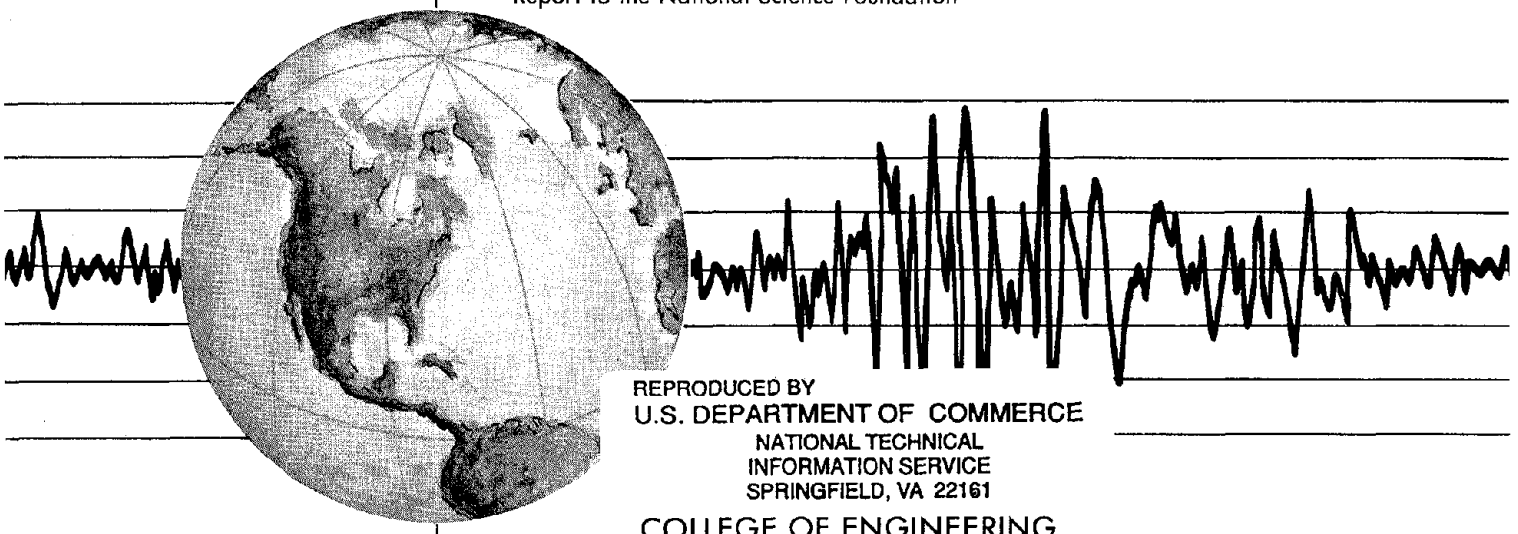

COLLEGE OF ENGINEERING

UNIVERSITY OF CALIFORNIA AT BERKELEY

DISCLAIMER

Any opinions, findings, and conclusions or recommendations expressed in this publication are those of the authors and do not necessarily reflect the views of the National Science Foundation or the Earthquake Engineering Research Center, University of California at Berkeley.

REPORT DOCUMENTATION PAGE	1. REPORT NO. NSF/ENG-88041	2.	3. PB91-217950

4. Title and Subtitle
Experimental Evaluation of Seismic Isolation of Medium-Rise Structures Subject to Uplift

5. Report Date
January 1988

6.

7. Author(s)
M.C. Griffith, J.M. Kelly, V.A. Coveney, C.G. Koh

8. Performing Organization Rept. No.
UCB/ENG-88/02

9. Performing Organization Name and Address
Earthquake Engineering Research Center
University of California, Berkeley
1301 S 46th St.
Richmond, CA 94804

10. Project/Task/Work Unit No.

11. Contract(C) or Grant(G) No.
(C)
(G) ECE-8414036

12. Sponsoring Organization Name and Address
National Science Foundation
1800 G. St. NW
Washington, DC 20550

13. Type of Report & Period Covered

14.

15. Supplementary Notes

16. Abstract (Limit: 200 words)

Earthquake simulator tests were performed on a base-isolated 1/5-scale 7-story reinforced concrete structure with a height-to-width ratio of 1.23. The scale model had been previously tested to failure as a fixed base structure, so it had to be modified to accept the base isolation devices as would be required in a rehabilitation project. Lightweight, low-cost bearings were tested to determine whether such bearings would be suitable for base isolation of smaller structures and houses in less well developed countries where earthquakes pose a major hazard. The test results were compared with values given by the tentative base isolation design provisions proposed by the seismology committee of SEAONC.

The study found that base isolation of medium-rise structures provides significant reductions in story and base shears and story accelerations, but the shear connection between the bearing and the column must be maintained during column uplift. In addition, the favorable test results indicated that the rehabilitation of the damaged structure was successful. The performance of the lightweight bearings was nearly identical to that of the more conventional sets used, except that they appeared to be slightly more flexible in shear. The use of lightweight bearings is particularly promising for base isolation of low-cost housing.

17. Document Analysis a. Descriptors
earthquake simulator tests
base isolation
rehabilitation
bearings
lightweight, low-cost
medium-rise structures

b. Identifiers/Open-Ended Terms

c. COSATI Field/Group

18. Availability Statement:
Release Unlimited

19. Security Class (This Report)
unclassified

20. Security Class (This Page)
unclassified

21. No. of Pages
181

22. Price

EXPERIMENTAL EVALUATION OF SEISMIC ISOLATION OF MEDIUM-RISE STRUCTURES SUBJECT TO UPLIFT

by

M. C. Griffith

J. M. Kelly

V. A. Coveney

C. G. Koh

Report No. UCB/EERC-88/02

Earthquake Engineering Research Center

College of Engineering

University of California, Berkeley

January 1988

ACKNOWLEDGMENTS

The research reported herein was supported by the National Science Foundation under Grant No. ECE-8414036 and was conducted at the Earthquake Simulator Laboratory of the University of California at Berkeley. The views and conclusions expressed in this report are those of the authors and not necessarily those of the National Science Foundation. Professor James Kelly was the principal investigator for this project.

The authors would also like to thank the Malaysian Rubber Producers Research Association in Hertford, England, for providing the base isolation bearings and Messrs C. J. Derham and A. G. Thomas for their advice. In addition, the authors wish to thank Mr. I. Aiken for his invaluable assistance with the experimental portion of the research program and his invaluable advice and assistance with the preparation of this report.

The staff of the Earthquake Engineering Research Center, especially Messrs. D. Clyde, I. Van Asten and Drs. J. Dimsdale, C.M. Uang, and B. Bolt provided invaluable assistance and advice over the course of the experimental program.

ABSTRACT

Earthquake simulator tests were performed on a 1/5-scale 7-story reinforced concrete structure with a height to width ratio of 1.23. The three main objectives of this study were:

(1) to evaluate the feasibility of base isolation for medium-rise structures subject to column uplift during severe seismic loads;

(2) to evaluate the effectiveness of base isolation for rehabilitation of damaged structures. The scale model in this study had been previously tested to failure as a fixed base structure, so it had to be modified to accept the base isolation devices as would be required in a rehabilitation project.

(3) Lightweight, low-cost bearings were tested to determine whether such bearings would be suitable for base isolation of smaller structures and houses in less well developed countries where earthquakes pose a major hazard.

The test results were compared with values given by the tentative base isolation design provisions proposed by the seismology committee of The Structural Engineers Association of Northern California (SEAONC).

The study found that base isolation of medium-rise structures provides significant reductions in story and base shears and story accelerations, but the shear connection between the bearing and the column must be maintained during column uplift. In addition, the favorable test results indicated that the rehabilitation of the damaged structure was successful. The performance of the lightweight bearings was nearly identical to that of the more conventional sets used, the only difference being that they appeared to be slightly more flexible in shear. The use of lightweight bearings is particularly promising for base isolation of low-cost housing.

Table of Contents

List of Tables

Table **Page**

List of Figures

Figure **Page**

1. INTRODUCTION

Base isolation is a strategy for reducing the effects of earthquake ground motions on a building by uncoupling the building from the horizontal components of the earthquake motion while simultaneously supporting the vertical weight of the structure. It is becoming widely accepted that this technique provides additional structural safety against earthquake ground motions for buildings up to about 5 stories in height [1], and the question "What is the height above which base isolation is no longer effective?" has been frequently asked. Of course the answer depends on several factors — building period, slenderness of structure and, as was so dramatically illustrated by the 1985 Mexico City earthquake, soil conditions.

It has generally been accepted that the longest feasible period for a base isolated structure is about 2 to 3 seconds. In general, the taller the structure the less practical it is to use base isolation. Building slenderness has some relation to period but, more important, it plays a large part in determining whether a building will uplift off parts of its base during extreme lateral loadings, and this is not something that is accommodated by usual base isolation devices. Finally, soil conditions play an important part in whether base isolation is feasible for a particular structure and site. For instance, there is little point in uncoupling a structure from ground motions already filtered by the soil. Each of these factors must be considered when trying to answer the question of whether to isolate a taller building.

The main purpose of the research described here was to study the behavior of elastomeric bearing pads used to isolate a medium-rise structure with a tendency to uplift. An additional aspect of the study was an investigation of the effectiveness of base isolation as a scheme for rehabilitation of damaged structures. The performance of low-cost lightweight bearings was also investigated. There is a potential use for inexpensive bearings which are also lightweight. In particular, these could be manufactured in developing countries not having available the current technology to make the more conventional

style of bearing.

Shaking table tests were performed on a 1/5-scale model of a 7-story reinforced concrete shear wall structure which had been severely damaged when used in prior earthquake shaking table tests as a fixed-base structure. The fixed-base structure was first modified to incorporate the base isolation scheme, then the main structural joints and the first story shear wall were repaired.

The base isolated model was found to uplift slightly off the outer bearings under extreme earthquake loadings, but the isolation scheme significantly reduced the peak values of base shear from those seen in the fixed-base tests. Since base isolation reduces the strength demands on a structure it is a promising method for rehabilitation of damaged or understrength structures. The model, when base isolated, responded almost as a rigid unit on the horizontally flexible system of bearings, thereby providing a fairly simple problem to model analytically.

Finally, the low-cost bearings were tested and their behavior was similar to bearings of a more expensive, conventional design. Thus, the thickness of the steel reinforcing shims used in bearings may be greatly reduced without jeopardizing bearing strength significantly.

2. EXPERIMENTAL MODEL

The experimental tests were performed on a 1/5-scale reinforced concrete shear wall structure. The model had been tested previously [2] as a fixed-base structure. A brief description of the model characteristics and previous test results follow.

2.1 Model Details

The structure was fabricated by a private contractor using, as nearly as possible, geometrically-scaled materials (reinforcing bar and concrete aggregate) as well as specially treated steel to approximate the stress-strain properties of the full-scale structure [3]. The stress-strain details for the steel reinforcing bars used in the construction of the model and other material properties of the concrete can be found in reference 3. One of the distinguishing characteristics of the model was the inclusion of internal force transducers (IFTs) in the ten exterior columns. The IFTs were designed to have axial, shear, and bending stiffnesses similar to those of the length of concrete column that they replaced. Details of these devices are presented in a report by Sause and Bertero [4]. The same IFTs were used in this study to provide accurate records of the forces experienced by the base isolation system during the various loadings to which the base-isolated structure was subjected. The scale factors necessary for converting scale model response quantities into values for the prototype structure are given in Table 2.1.

2.2 Previous Test Results

The concrete structure had been badly damaged by the sequence of tests performed previously [2]. A diagram of the cracks in the shear wall and some of the beams is shown in Figure 2.1. The structure had experienced a peak base shear of 50.8% of its weight (V_b = 53.8 kips, 243 kN) when subjected to the time-scaled Taft ground motion which had a peak table acceleration of 0.403g. Table 2.2 lists the peak base shear at different magnitudes of peak table acceleration for the Taft and Miyagi-Ken-Oki earthquake ground motions.

2.3 Repair of Model and Modification for Isolation Tests

In view of the severity of the damage incurred during the previous fixed-base test program it was decided to separate the model from its base at the midcolumn height of the first story just below the internal force transducers (Figure 2.2).

The major part of the repair work involved replacement of the first story shear wall and its adjacent columns which had been completely destroyed during the previous tests. All large cracks, wider than 0.008 inch (0.2mm), in the vicinity of all beam-column joints were pressure grouted. The first story shear wall and its two adjacent columns were rebuilt down to a level of 7.58 inches (193mm) below the bottom of the first floor slab. The isolators were placed at this level. Since the shear force carried by the shear wall had to be transferred to the columns at the base, a pair of 5 x 3.5 x 0.5 inch (130 x 89 x 13mm) steel angles was bolted to each row of columns in the direction of shaking (Figure 2.3) to transfer the column shear directly from the first floor slab to the bearings. The axial stiffness of the angles ensured that the lateral displacements of each isolator were the same. The isolators were designed to have the same horizontal stiffness so the shear force in each bearing was nearly identical.

The stiffened structure was placed on the set of IFTs with the IFTs placed between the top of each bearing and the bottom of each column stub (Figure 2.3). The force transducers recorded accurate time histories of the forces acting on the bearings. Figure 2.4 shows the base-isolated model ready for testing.

3. BASE ISOLATION BEARINGS

3.1 Bearing Design and Rubber Formulations

Three sets of bearings were constructed for these experiments. The designs are shown in Figure 3.1. The plan dimensions of each bearing were 6 inches (153mm) square.

The first set of bearings was made using a natural rubber formulation similar to one used commercially in seismic isolation bearings and which conforms to the British Standard for bridge bearings (BS 5400). The ingredients and cure of the elastomer were chosen to accentuate the high stiffness at low strains and the high damping needed for isolation bearings. Each of the first set of bearings was designed to have a horizontal stiffness of approximately 1 kip/inch (180 kN/m) at a shear strain of about 50%. Assuming rigid body behavior, the first mode frequency of the bearing-plus-model structure would be approximately 1.1 Hz under a design load of 10 kips (45 kN); then for a model scaling of 5 the natural frequency of the full-size structure would be 0.5 Hz.

In contrast, each of the second and third sets of bearings was designed to have a horizontal stiffness of approximately 0.53 kip/inch (95 kN/m) giving a first mode frequency of approximately 0.72 Hz for the model structure. The purpose of choosing a lower natural frequency was threefold; first, to assess the effectiveness of a softer base isolation system for the seismic protection of a damaged building, and secondly to assess the feasibility of using base isolation for protection against low-frequency strong ground motion. For tests with the first and second sets of bearings the scale of the model was assumed to be 1/5. Thirdly, a tentative assessment of the feasibility of base isolation for protection of a small building (mass 50 to 200 tons) against a range of earthquakes was to be made. In this set of tests the model would be tested as if it were both a full-scale and a 1/2-scale structure.

For base isolation of a light building, low weight is a desirable attribute for the bearings themselves, since heavy bearings require equipment for lifting and moving into

place. Lightweight bearings can be moved and installed at the construction site by hand. Hence, the third set of bearings was of an experimental design incorporating 0.012 inch (0.3mm) thick steel (inter-rubber) shims.

In contrast to the rubber formulation used in the first set of bearings, that used in the second and third sets was an experimental natural rubber compound subject to continuing development.

3.2 Physical Testing of the Rubber Formulations

Shear test specimens (Figure 3.2) of the two types of rubber were subjected to sinusoidal strain histories. Typical results of the tests are presented in Tables 3.1 and 3.2. The shear moduli (G) in terms of ksi and MN/m^2 are given as functions of shear strain amplitude. Values of the phase angle (δ) between shear force and displacement are also shown.

Force versus displacement hysteresis loops for the two compounds are shown in Figures 3.3 and 3.4. The equivalent loss angle can be calculated from the ratio of the area of one cycle (A_c) to that of the circumscribing rectangle (A_r) by

$$\delta = \arcsin\frac{4A_c}{\pi A_r} .$$

The modulus of the complex stiffness (k^*) can be calculated from the ratio of height to width of the circumscribing rectangle. In spite of the nonlinearity of the hysteresis loops it was found that the values for δ obtained using a Solatron/Schlumberger signal analyzer were in close agreement with the values obtained directly from the hysteresis loops (see Figure 3.5). There was negligible difference between the values of stiffness obtained from the analyzer and those obtained directly from the hysteresis loops.

For the rubber formulations used the frequency dependence of the shear modulus is low (approximately 10% increase or less from 0.5 Hz to 10 Hz for strain amplitudes greater than 10%) and the frequency dependence of the loss angle is comparably low.

3.3 Design of Bearings

The plan dimensions of all three sets of bearings were 6 inches (153mm) square. All were made with very thin cover layers ($\approx$ 0.06 inch, 1.5mm) to facilitate the study of bearing performance in spite of the fact that thin cover layers tend to increase stress concentrations at plate edges.

3.3.1 1st Set of Bearings

The design elastomer large shear-strain modulus (G) for this set of bearings was 102 psi (0.7MN/m^2). Since the intended load per bearing was small the tilting compliance was ignored and the simple shear formula was used to calculate the horizontal stiffness (k_h) from the shear modulus, the cross sectional area (A) and the height of rubber in the bearing (h_r)

$$k_h = \frac{G\,A}{h_r}\,. \tag{3.1}$$

A height of rubber of 3.41 inches (86.6mm) was chosen to give a first order design horizontal stiffness of 1.0 kip/inch (180 kN/m).

The simple single degree-of-freedom natural frequency (f_o) is given by:

$$f_o = \frac{1}{2\pi}\sqrt{\frac{k}{m}} \tag{3.2}$$

where m is the total mass of the model structure and k is the total horizontal stiffness of the bearings. For a load of 10 kips (4545 kg) per bearing and k = 12 kips/inch, f_o = 1.0 Hz.

The model as used in the shaking table tests was slightly lighter than originally envisaged so the average load per bearing was 8.7 kips (39 kN). This decrease in mass increased the horizontal natural frequency to 1.1 Hz.

For experimental reasons related to the study of building uplift the vertical stiffness of these bearings had to be high and a bearing with 16 layers of rubber, each 0.213 inch

(5.41mm) thick, was selected. The rubber layers were separated by 0.0625 inch (1.6mm) thick mild steel shims.

The shape factor (S) of a bearing is defined as the ratio of the area of one loaded face to the area of the unloaded faces for a single layer of rubber. The shape factor for bearings of the first set was 6.9. The equation for the compression modulus of a bonded rubber layer reduces to $E_c = 6GS^2$ for $S^2 >> 1$ and ignoring rubber compressibility.

The shear modulus, G, for this equation will not be less than the high strain value of 102 psi (0.7MN/m^2). Therefore, $E_c \geq 29$ ksi (0.2 MN/m^2) and the compressive stiffness $K_c \geq 287$ kips/inch (51 MN/m). Calculations based on the material data in Table 3.1(b) and the above equations indicate that for a compressive load of 8.2 kips (37 kN) the equivalent shear strain in the rubber is about 10%, and that for a compressive load of 14 kips (63 kN) it is about 20%; the corresponding calculated compressive (chord) stiffnesses are 400 kips/inch (71 MN/m) and 320 kips/inch (58 MN/m).

The dynamic stiffness of a bearing depends on the magnitude of the dynamic load and in general will be higher than the chord stiffness. Thus the ratio of vertical to horizontal (large strain) stiffness will be greater than 58000/180 = 322 and the corresponding ratio of the vertical and horizontal frequencies will be greater than 18.

The buckling load (F_b) for a rectangular cross-section bearing can be calculated from the following equation [5]:

$$F_b = \frac{GAh_t(\sqrt{1+\pi^2 a^2 f/l^2}-1)}{2h} \quad , \tag{3.3}$$

where

$$f = \frac{6a^2 q}{\pi^4 h^2} + 1$$

and

$$q = \sum_{n=1}^{n=\infty} \left(\frac{1}{n^4} - \frac{a}{n^5 \pi b} \tanh\,(n\pi b/a) \right)$$

where:

G = shear modulus of rubber;

A = cross–sectional area of bearing;

h = thickness of one rubber layer;

h_t = h plus the thickness of one steel shim;

a = length of shorter side;

b = length of longer side;

n = number of layers;

$l = n \times h_t$

By using the large strain shear modulus (102 psi or 0.7MN/m^2) in the equations above, a conservative estimate of 56 kips (250 kN) was obtained for the buckling load.

3.3.2 2nd Set of Bearings

The design shear modulus for the rubber for this set of bearings was 55 ksi (0.38MN/m^2). A total height of rubber of 3.56 inches (90.5mm) was chosen to give a design horizontal stiffness of 0.53 kips/inch (95 kN/m); see Equation 3.1. For a load of 10 kips (45 kN) per bearing the first-order design horizontal natural frequency was 0.72 Hz ($0.32\sqrt{5}$ Hz or $0.51\sqrt{2}$ Hz). For a load of 8.7 kips (39 kN) per bearing the first-order design horizontal natural frequency was 0.77 Hz ($0.34\sqrt{5}$ Hz or $0.54\sqrt{2}$ Hz).

There were two major purposes in deciding on these design parameters for the second set of bearings. The first purpose was to investigate the feasibility of using base isolation in situations of low frequency strong ground motion. The second purpose was to investigate the feasibility of using earthquake base isolation for small buildings ($\approx$ 50 to 200 tons).

The vertical stiffness of these bearings had to be sufficient to ensure little coupling between fundamental horizontal and vertical modes. The design arrived at had 18 layers of rubber, each 0.198 inch (5.03 mm) thick, separated by 0.037 inch (0.93 mm) mild steel shims. The shape factor was therefore 7.4 for this set of bearings. Hence a conservative estimate for compressive stiffness, obtained using G = 58 psi ($0.38 MN/m^2$) and $E_c = 6GS^2$, is 170 kips/inch (30 MN/m). Taking account of material nonlinearity and assuming a compressive load of 10 kips (45 kN), however, gives a design compressive stiffness of 245 kips/inch (43 MN/m).

Thus the ratio of compressive stiffness (for 10 kips or 45 kN normal load) to the large strain horizontal stiffness is approximately 43000/95 = 453, so the corresponding ratio of design frequencies was greater than 21.

A conservative estimate of 26 kips (117 kN) was obtained for the buckling load for this design by using the large strain shear modulus: 58 psi ($0.4 MN/m^2$).

3.3.3 3rd Set of Bearings

The third set of bearings extended the investigation of the possible use of isolation bearings for small buildings. These bearings were designed to be identical to the second set in all but one respect: very thin 0.012 inch (0.3 mm) thick mild steel shims were used between the rubber layers so as to reduce the overall weight of the bearings.

4. CYCLIC LOADING TESTS ON INDIVIDUAL BEARINGS

4.1 Test Rig

A test rig was designed to subject the three sets of bearings to combined static vertical and cyclic lateral loads. The rig is a modification of a fixture previously used for testing masonry piers [6]; it consists of two heavily-braced reaction frames supporting a horizontal hydraulic actuator and two vertical actuators (Figure 4.1). The horizontal actuator moves according to the command signal from a controller (model 443 manufactured by MTS of Minnesota). The vertical actuators apply through a beam a compressive force on the bearing to simulate the gravity load effect. An electronic IC circuit controls the vertical actuators such that the total compression load is maintained at a specified constant load while the differential displacement between the actuators is always zero (within experimental error). This is done to reproduce the correct boundary condition in an actual base-isolated building.

A force transducer is located under the bearing specimen to measure the shear force and bending moment. A bottom reaction block composed of a concrete base and a wide flange steel beam provides anchorage to the test floor. A rigid spacer is placed between the transducer and the bottom beam to maximize the length of the vertical actuators so that the change of vertical load component in the actuators due to lateral displacements becomes insignificant. The setup was designed for testing bearings of 8 inches (20.3cm) in height. Shorter bearings can be tested by inserting spacer plates above or below the transducer. Two struts connected perpendicular to the top beam enhance the transverse stability of the setup.

The maximum dynamic load which may be developed by the horizontal actuator is 75 kips (334 kN), using a hydraulic pressure of 3000 psi (20.7MPa). The maximum stroke is $\pm$ 6 inches (15.2 cm), the maximum piston velocity is 26 in./s (66 cm/s) and the flow capacity of the servovalve is 200 gpm (12.6 l/s). Either displacement or load can be controlled with these actuators. A vertical load up to 300 kips (1335 kN) can be applied

through each of the vertical actuators and the servovalve capacity is 25 gpm (1.6 l/s).

4.1.1 Instrumentation

The loads applied by the actuators are measured by pre-calibrated load cells. The compression load on the bearing is calculated from the measured forces in the vertical actuators. The shear force and bending moment are measured by the force transducer mentioned earlier. An LVDT (linear variable differential transformer) in the horizontal actuator measures the lateral displacement of the bearing. Two linear potentiometers are attached to the left and right vertical actuators as feedbacks for the electronic control. Four DCDTs (direct current differential transformers) measure the vertical displacement of the top beam near the four corners of the top bearing plate. To account for any shortening of spacer plates and other components below the specimen, two more DCDTs are connected between the bottom beam and the bottom plate of the bearing.

4.1.2 Data Acquisition and Data Processing

The data acquisition was performed by an LSI 11/23 microcomputer manufactured by Digital Equipment Corporation. The analog signals were multiplexed through a 12 bit analog to digital converter at a burst rate of 250k samples per second. For the cyclic loading tests, the channel list was scanned typically at a rate of 100 times per second. The digitized data was then stored permanently on a magnetic tape and transferred to a VAX 11/750 computer for data processing.

4.1.3 Natural Rubber Bearings

Three sets of natural rubber bearings were used in the experiment and they were specially made by MRPRA for the shaking table tests of the 1/5-scale model of a 7-story reinforced concrete building. They are all 6 inch x 6 inch (15cm x 15cm) in plan but differ in height or formulation of rubber. The first set of bearings was made using a rubber formulation which conforms to the demanding British standard for bridge bearings. The second and third sets were made of softer rubber using an experimental formulation. Bearings of the second set have approximately the same dimensions as

bearings of the first set, whereas bearings of the third set are shorter because they have thinner steel plates. Bearings of the first set have 16 layers of rubber and 15 steel reinforcing plates. Bearings of the second set have 18 rubber layers and 17 steel reinforcing plates. The thickness of a rubber layer is 0.213 inch (5.41mm) for bearings of the first set, and 0.198 inch (5.03mm) for bearings of the second and third sets. The thickness of a steel reinforcing plate is 0.063 inch (1.6mm), 0.037 inch (0.93mm) and 0.012 inch (0.3mm) for the first, second and third sets of bearings, respectively. All were made with very thin cover layers to facilitate the study of bearing performance. At each end of the bearing, there is a 0.625 inch (16mm) steel plate with holes for dowels which key the bearings to the force transducer below and the loading beam above.

4.2 Test Results

In each test, the bearing specimen was subjected to a sinusoidal horizontal displacement under a constant compression load (P). A number of such tests was carried out with varying compression loads so as to study the effect of the compression load on the behavior of the bearing. To eliminate any frequency dependence of the material properties, all tests were conducted at about 0.5 Hz (which is typically the design horizontal natural frequency of a base isolation system). In each of the tests, a hysteresis loop of horizontal force versus horizontal displacement was obtained. The experimental hysteresis loop was used to calculate:

$$\text{dynamic shear stiffness} \equiv K_d = \frac{f_o}{d_o} \tag{4.1}$$

$$\text{damping factor} \equiv \sin\phi = \frac{A_{loop}}{\pi f_o d_o} \tag{4.2}$$

where f_o and d_o are the amplitudes of the horizontal force and displacement, respectively, and A_{loop} is the area of the hysteresis loop per cycle. For plotting convenience, $\sin\phi$ is used instead of $\tan\phi$ since the value of $\sin\phi$ is between 0 and 1. The hysteresis loop was also used to obtain:

$$\Delta h_{max} = \text{maximum } \Delta h(t) - \text{minimum } \Delta h(t) \, . \tag{4.3}$$

In this calculation, correction was made to the DCDT measurements to account for horizontal displacement (the "arc" effect) and also the change in bearing height due to slight variation in the actual compression load.

A sequence of tests was also carried out with varying displacements to study the effect of shear strain on the bearing shear stiffness. The test programs and the test results for the three sets of bearings are summarized in Tables 4.1 to 4.6.

4.3 Application of Analytical Models

The parameters that determine the dynamic shear stiffness (K_d) and the loss angle (ϕ) of the elastomeric bearing can be grouped into the following terms:

(i) l, the combined height of the elastomeric layers and steel plates (not including the top and bottom end plates);

(ii) δ, the loss angle of elastomer;

(iii) $(GA_s)_{eff}$, the effective GA_s of the elastomer-steel (composite) bearing. If l_r is the total thickness of elastomeric layers, G the shear modulus of elastomer and $A = 4b^2$ the cross-sectional area,

$$(GA_s)_{eff} = GA\, l/l_r \, . \tag{4.4}$$

(iv) $(EI)_{eff}$, the effective EI of the elastomer-steel bearing. For square bearings,

$$(EI)_{eff} = EI\, g(S^2,\nu)\, l/l_r \tag{4.5}$$

where E is the Young's modulus of elastomer, $I = 4b^4/3$ is the area moment of inertia and $g(S^2,\nu)$ is a dimensionless function defined by

$$g(S^2,\nu) = \frac{144S^2}{1+\nu} \sum_{n=1}^{\infty} \frac{1}{\bar{\alpha}_n^2 \bar{\beta}_n^2} \left[1 - \frac{\tanh(\bar{\beta}_n)}{\bar{\beta}_n}\right]$$

in which

$$\bar{\alpha}_n = n\pi$$

$$\bar{\beta}_n = [\bar{\alpha}_n^2 + 72\frac{1-2\nu}{1+\nu}S^2]^{\frac{1}{2}} .$$

Note that $(EI)_{eff}$ in Equation (4.5) takes into account the presence of steel plates which are assumed to be rigid in comparison with the elastomer.

4.3.1 Parameter Identification

For thin bonded elastomeric layers $(EI)_{eff}$ can be many times greater than EI, especially for nearly incompressible material. Using Equations (4.4) and (4.5), we can relate $(EI)_{eff}$ to $(GA_s)_{eff}$:

$$(EI)_{eff}/l^2 = \eta\,(GA_s)_{eff} \tag{4.6}$$

where

$$\eta = \frac{E}{G}\frac{b^2}{3l^2}g(S^2,\nu) . \tag{4.7}$$

Nevertheless, the exact value of ν for elastomer (and thus η) is rarely known. Therefore $(EI)_{eff}$ is treated here as an independent parameter to be identified.

Although data sheets for elastomers are available in some cases, the elastomer used in the bearing may have somewhat different properties from the elastomer used in the tests pertaining to the data sheets. It has been observed in past experiments that a bearing usually has a higher damping factor than the small elastomer specimen used in tests for obtaining the data sheets; but the reason is not fully understood. The curing time for the actual bearings was longer than that for the small elastomer sample, leading to some significant increase in the stiffness. For these practical reasons, the values of G and δ were determined from the tests of actual specimens of elastomeric bearings rather than taken from the data sheets for the elastomer. To reduce the computational effort in the parameter identification, it was assumed that ν is independent of the shear deformation. A computer program was written to estimate the dynamic shear stiffness (K_d) by least

squares, assuming different $(GA_s)_{eff}$ values but the same η value for different displacement amplitude tests. Both the first-mode consistent model and the 2-spring physical model were used [7]. The damping factor ($\sin\delta$) of the rubber was estimated from the initial flat portion of the $\sin\phi$ versus P curve since $\sin\phi \approx \sin\delta$ at and near $P = 0$. Slight adjustment in the value of $\sin\delta$ was sometimes necessary to achieve a better correlation, because of inevitable experimental errors in obtaining data for the initial flat portion of the curve.

4.3.2 1st Set of Bearings

The parameters for the analytical models were identified by the previously described routine and are shown in Table 4.7. Figures 4.2 to 4.4 compare the experimental data of K_d, $\sin\phi$ and Δh_{max} (for 3.5 inch tests only) with the analytical results. Once again it is seen that the analytical models can reproduce the variations of K_d and $\sin\phi$ due to the influence of axial load. The prediction of Δh_{max} by the analytical models is, however, not satisfactory. As pointed out before, the discrepancy can likely be attributed to the asymmetry of the setup, measurement accuracy problems and other inevitable experimental errors. In addition, the assumption that ν was independent of the shear strain is not strictly correct, and this assumption contributes partly to the discrepancy in this case. We can reduce the discrepancy by relaxing this assumption and assuming only that η was independent for each set of tests. Considering only the 3.5 inch tests, the model parameters are identified independently of the 1 inch and 3 inch tests (Table 4.8). With these parameters, the predicted height reductions agree fairly well with the experimental data (Figure 4.4(b)).

In order to study the effect of shear strain on bearing shear stiffness one specimen from the first set of bearings was cycled over a range of displacements. The bearing was loaded with 10 kips axial compression load and tested at a frequency of 0.5 Hz with the shear strain ranging between 2% and 125%. The test results are shown in Figure 4.5.

4.3.3. 2nd Set of Bearings

Twelve specimens from the second set of bearings were used, each of which went through a standard cyclic test ($d_o = 1$ inch, $P = 5$ kips) to see if there were any significant differences among them since they had previously been used in shaking table tests. It was found that only one specimen (Specimen V24) showed abnormally high horizontal stiffness. Excluding this specimen, the rest of the bearings had a dynamic shear stiffness of 1.092 ± 0.075 kip/inch in the standard tests. The model parameters that best fit K_d were found and are presented in Table 4.9. The plots for K_d, $\sin\phi$ and Δh_{max} are shown in Figures 4.6 to 4.8. Agreement between the experimental results (including Δh_{max}) and the analytical curves is generally good despite the fact that the eleven specimens were not identical.

In order to study the effect of shear strain on shear stiffness for the rubber used in the second set of bearings one specimen from the second set of bearings was tested over a range of shear strain. The results of this test are shown in Figure 4.9. The experimental rubber mix had lower stiffness than the rubber used for the first set of bearings.

4.3.4. 3rd Set of Bearings

Ten specimens from the third set of bearings were used. Again, each specimen went through a standard test (1 inch displacement and 5 kips compression). The specimens were found to have a K_d of 1.019 ± 0.062 kips/inch. Since none of the specimens showed large deviation from the others, all specimens were used for the data analysis. The only difference between the second and third sets of bearings is that the bearings of the third set have thinner steel plates (by about 3 times). The assumption of *rigid* steel plates is questionable in this case. Without resorting to a more complicated model to include the flexibility of steel plates, the experimental K_d values were fitted to the same analytical models. The model parameters are shown in Table 4.10 and the plots for K_d, $\sin\phi$ and Δh_{max} in Figures 4.10 to 4.12. It can be seen that the agreement for K_d and $\sin\phi$ is still good, but the predictions for Δh_{max} are not. The discrepancies in Δh_{max} could very

likely be due to the significant flexibility of the steel plates as well as to the other sources of experimental error discussed previously..

A specimen from the third set of bearings was also tested over a range of shear strain. This bearing had essentially the same shear stiffness as the specimen from the second set of bearings, within experimental error. The test results are shown in Figure 4.13.

5. TEST PROGRAM FOR BASE ISOLATED MODEL

5.1 Model Instrumentation

The test structure was instrumented with a combination of accelerometers, linear potentiometers (LPs), direct current linear voltage differential transformers (DCDTs), and internal force transducers (IFTs) to record the response of the structure to all input loads. The IFTs were used to record the forces of axial, shear and moment in the column stubs immediately above the rubber bearings. The support reactions (and thus the forces on the bearings) were measured by the IFTs.

A total of 81 channels of data was recorded for each test; 14 channels recorded shaking table responses and 67 channels recorded model responses. Figure 5.1 shows the instrumentation and Table 5.1 lists the instruments and the corresponding model or table response.

Two accelerometers were placed on each floor to measure the horizontal acceleration of that floor. Another two accelerometers were placed on top of the end columns of Frame B to measure vertical acceleration and two accelerometers were placed on the face at the top of the end columns of Frame A to measure horizontal accelerations of the floor perpendicular to the direction of shaking. In addition, an accelerometer was placed on each corner of the model above the steel stiffeners to measure the vertical acceleration of the model above the bearings. These accelerometers helped determine when uplift of the model from its bearing supports took place. Two DCDTs were placed on each end of Frame B, one between the shaking table and the top of the model, the other between the steel stiffeners and the model. These also helped detect column uplift.

Seven LPs were used to measure displacement of the model. Two LPs were used to record the relative displacement of the rubber bearings under columns 1-A and 1-C. Two LPs each on the fourth floor and the 7th floor recorded the total horizontal displacement at those levels and one LP was used to record the relative displacement of the model in the direction perpendicular to the direction of input motion of the shaking

table.

5.2 Dynamic Test Program

The test program for the structure on each set of natural rubber bearings consisted cf free vibration tests, harmonic base input tests, white noise input tests, and earthquake input tests. The first three types of test were performed to determine the dynamic characteristics of the model and to evaluate the effectiveness of existing analytical methods for predicting these quantities.

The free vibration test was performed to determine the fundamental frequency, the torsional frequency, and the approximate equivalent viscous damping ratio of the model. This test was performed by enforcing an initial lateral displacement in the bearings and releasing the structure from this position. A shear force of approximately 5 kips was applied to the model by pulling the structure just above the top of the bearings. This load was applied by a cable and a turnbuckle connected by shackles to the cable. In line with the cable was a short length of 0.625 inch (15.9mm) diameter threaded rod which, after the lateral load was applied, was cut using bolt cutters. This instantly released the structure from its displaced position. Story accelerations and displacements, bearing displacements and column axial and shear forces and moment were monitored as the structure underwent transient response ending in static equilibrium.

The equivalent viscous damping ratio was estimated from the column shear force measurements taken just above the rubber bearings. The natural frequency of the model was estimated by taking the Fast Fourier transform (FFT) of the shear force time history and noting the frequencies associated with the peaks in the Fourier spectra. The natural frequency was also estimated directly from the shear force time history by counting the number of zero crossings.

In order to determine the fundamental torsional frequency of the model, the model was pulled just above the top of the rubber bearing located at the corner of the structure (column 4-C) and released. The fundamental torsional frequency was estimated from the

column shear force time history in a manner similar to that described above.

The harmonic vibration test was conducted to determine the fundamental frequency, the torsional frequency, and the approximate viscous damping ratio of the structure. The model was loaded dynamically with sinusoidal base input of fixed frequency. The model was subjected to this input and once the model reached a steady-state harmonic motion, data from the table and the model were monitored for three seconds. This test procedure was repeated for a range of frequencies around the expected natural frequency of the structure. The peak story acceleration normalized to peak table acceleration was plotted against frequency, and from these plots the fundamental and torsional frequencies were estimated. These quantities were also estimated by taking FFTs of the story acceleration and bearing displacement time histories.

The modal frequencies of the structure were determined from a white noise vibration test. The test consisted of subjecting the isolated model to white noise table displacement in the frequency range 0-20 Hz. This motion was applied for 30 seconds during which the response quantities of floor accelerations and displacements, relative bearing displacements and column forces of axial, shear, and moment were monitored.

The FFT of ideal white noise input over a frequency 0-20 Hz should have a constant Fourier amplitude for that range of frequency. Note than in Figure 5.2, which shows the actual table displacement time history and the FFT of the table displacement time series, that the frequency content is really only reasonably constant for the frequency range of 0-10 Hz. While the input base displacement was not purely white noise, for the purposes of these tests it was sufficient to allow the estimation of the modal frequencies below 10 Hz by taking FFTs of the roof acceleration and relative bearing displacement time histories.

The test program for each set of bearings concluded with extensive testing of the model subjected to eight different earthquake base motion inputs described in the following section. This was done in order to evaluate the ability of the different rubber bearing

pads to isolate the structure from earthquake ground accelerations. The tests were designed to show the effectiveness of base isolation for different earthquake ground motions. The earthquake inputs were varied in amplitude (with respect to peak horizontal base acceleration) to study the effect of the bearing displacement magnitude and column uplift on the effectiveness of the base isolation system.

The test programs for each set of bearings are given in Tables 5.2 to 5.7. The table span refers to the setting of the amplitude of shaking table displacement. A span setting of 1000 corresponds to ± 5 inches of table displacement (the maximum possible). Fractions of span 1000 setting vary approximately linearly so that a span setting of 500 would correspond to a peak input table displacement of approximately 2.5 inches.

5.3 Earthquakes Used in Dynamic Test Program

The isolated models were tested for their response to eight different earthquake input motions. The earthquakes used varied from those with predominantly low frequency content, such as the 1985 Mexico City Earthquake, to earthquakes with predominantly high frequency content, for example the 1957 San Francisco Earthquake. The following earthquake ground motions were used for input [8,9,10,11]:

(1) Imperial Valley Earthquake (El Centro) of May 18, 1940 - S00E component;

(2) Kern County Earthquake (Taft Lincoln School Tunnel) of July 21, 1952 - S69E component;

(3) San Francisco Earthquake (Golden Gate Park) of March 22, 1957 - S80E component;

(4) Parkfield Earthquake (Cholame, Shandon, Calif. Array No.2) of June 27, 1966 - N65E component;

(5) San Fernando Earthquake (Pacoima Dam) of February 9, 1971 - S14W component;

(6) Bucharest Earthquake (Building Research Institute) of March 7, 1977 - EW component;

(7) Miyagi-Ken-Oki Earthquake (Tohoku University) of June 12, 1978 - S00E component;

(8) Mexico City Earthquake (Mexico City Station SCT) of September 19, 1985 - S60E component.

The records were time scaled by a factor of $\sqrt{5}$ to satisfy similitude requirements for the 1/5-scale model. A list of the earthquakes used in the test program and the symbols subsequently used to refer to each earthquake are given in Table 5.8.

Plots of the real-time earthquake ground motions normalized to 1g peak acceleration and their FFTs are given in Figure 5.3. As can be seen in the FFT plots for each earthquake, there is a wide range of earthquake characteristics represented by this group. The real-time Mexico City signal has a frequency content concentrated almost entirely in the region of 0.5 Hz. The real-time Bucharest signal has a significant amount of low frequency content which gradually decreases to nearly zero at a frequency of about 5 Hz. The real-time El Centro record has most of its frequency content between 1 Hz and 3 Hz and the Miyagi-Ken-Oki record has most of its frequency content around 1 Hz. Parkfield has a frequency range of 0.5 Hz to 3 Hz while the frequency content of the Pacoima Dam signal ranges between 1 Hz and 4 Hz. The frequency of the San Francisco record has two peaks, one near 4 Hz and another at about 7 Hz. The Taft earthquake record has a broad range of frequency content (0.5 Hz to 5 Hz).

6. TEST RESULTS FOR MODEL ON 1ST SET OF BEARINGS

6.1 Free Vibration Test Results

The initial displacement of 0.10 inch (2.5mm) resulted from a force of 5.45 kips (24.6 kN) applied to the stiffeners just above bearing 4-B. Because of the strong nonlinearity of the bearing stiffness, it is important to note the shear strain in the bearings when comparing frequency evaluated from this test with model frequencies evaluated from the other tests. In fact, the 2.45 Hz natural frequency indicated by this test corresponded to an initial strain level of 3.5%. The approximate equivalent viscous damping obtained from the log decrement curve (Figure 6.1) was 5% of critical, the fundamental torsional frequency was found to be 3.1 Hz, and the second lateral mode frequency was 7.6 Hz (Figure 6.2).

6.2 Harmonic Vibration Test Results

The model was next subjected to harmonic base motion at a variety of frequencies ranging from 0.5 Hz to 6.0 Hz (Table 5.2 lists the input frequencies). The peak lateral floor acceleration normalized to peak lateral table acceleration at each frequency of input is plotted against frequency in Figure 6.3. From these plots the fundamental lateral and torsional frequencies were estimated. These frequencies were then confirmed by taking FFTs of the story acceleration and bearing displacement time histories. From this test, the fundamental lateral frequency was estimated to be 1.15 Hz and the fundamental torsional frequency to be 2.3 Hz. Since the range of frequencies tested included that of the second lateral mode, the second lateral mode frequency was estimated to be 4.9 Hz. In view of the nonlinearity of the bearings, it was noted that these frequencies were obtained at shear strains of about 32%.

The loss angle, δ, of the rubber bearing was determined from the hysteresis loops, at resonance, for bearing shear force versus relative bearing displacement shown in Figure 6.4:

$$\delta = \arcsin \frac{4A_c}{\pi A_r} \ ;$$

and then the approximate equivalent viscous damping ratio

$$\xi = 0.5 \tan\delta$$

was calculated and found to be 11.5% of critical.

6.3 White Noise Vibration Test Results

The isolated structure was then subjected to the white noise base input motion described earlier (Section 5.2). By taking FFTs of the roof acceleration and the bearing displacement time histories (Figures 6.5 and 6.6), the modal frequencies were estimated. The peak magnitude of bearing displacement during this test was such that the peak shear strain in the rubber was 6.5%. From this test, the fundamental lateral frequency was estimated to be 1.3 Hz, the fundamental torsional frequency was 2.2 Hz, and the second mode frequency was 5.0 Hz.

6.4 Discussion of Preliminary Tests

The decrease in stiffness that the rubber underwent with increasing strain amplitude made direct comparisons between the free vibration, harmonic vibration and white noise vibration tests difficult. However, as a first step, the following proportionality was assumed

$$f_{res} = C_p \sqrt{G\, \epsilon_{max}} \tag{6.1}$$

between the resonant frequency (f_{res}) and the shear modulus of the rubber (G), where C_p is a constant of proportionality. The shear modulus was taken as that given by Table 3.1 at the maximum shear strain (ϵ_{max}) during the test.

Following this simple approach, the free vibration test which gave a fundamental frequency of 2.45 Hz at 3% shear strain implied a frequency of 1.43 Hz at 100% shear strain. In contrast, the harmonic tests gave a fundamental frequency of 1.15 Hz for a 32% shear strain implying a frequency of 0.94 Hz at 100% shear strain.

The white noise test result for fundamental frequency of 1.3 Hz at 6.5% shear strain implied a frequency of 0.85 Hz at 100% shear strain. The harmonic and white noise results were therefore reasonably consistent with each other and, unlike the free vibration result, they were in fairly good agreement with the design frequency of 1 Hz at large strain. Furthermore, the value of 11.5% of critical damping calculated from the harmonic tests (at 32% shear strain) was in good agreement with the damping of the rubber at similar strain levels (11.3% of critical). The results are shown in Table 6.1.

The fact that the damping indicated by the free vibration test (5.2% of critical at 3% strain) was about one third of that obtained for the rubber at comparable strains emphasizes the fact that other factors need to be taken into account in the case of low-strain free vibration. It seems likely that, because of the relatively high stiffness of the bearings at low strain, the assumption that the damaged structure was acting approximately as a rigid body on flexible supports was a poor one.

The natural frequency of the model on the first set of bearings was calculated to be 0.96 Hz using the single degree-of-freedom Equation 3.2, where k = 9.8 kips/inch (1.75MN/m) and m = 104 kips (470kN). The results are presented in Table 6.2.

The natural frequencies of the isolated structure determined by the harmonic test were about 2% lower than those given by simple rigid body theory and the white noise test results were about 12% lower than the rigid body results. This suggests that model flexibility was playing a part in determining the overall performance. The stiffness of bearing V1 under 10 kips (45 kN) axial load tested singly was 1.46 kips/inch (263 kN/m) at 30% shear strain; the value for k_h at 33% strain implied in Figure 4.5 was

$$4\pi^2 \left(\frac{104}{12\ (386.4)} \right) 1.33 = 1.17 \text{ kips/inch} \qquad (207 \text{ kN/m}).$$

The design stiffness of the bearing at 30% shear strain was about 1.25 kips/inch (225 kN/m).

6.5 Earthquake Motion Test Results

The model supported on the first set of bearings was designed primarily to be a 1/5-scale model of a building isolated against strong ground motions in firm soil conditions — the conventional approach. The natural frequency of the isolated model was approximately 1 Hz for large bearing displacements — corresponding to approximately 0.5 Hz for the full-size building represented. It was clear, however, that the natural frequency was somewhat lower than the intended 1.1 Hz because of building flexibility. It was apparent that the building had been considerably damaged in the previous fixed-base tests and that repairs had been effective only to a limited extent.

The isolated model was subjected to the time-scaled earthquakes listed in Table 5.3. Each earthquake was input at three levels of peak table acceleration (typically 0.2g, 0.5g, and 0.8g). Thus, the effect of increasing shear strain in the rubber and the consequent change in structural response of the system was studied. The effectiveness of isolation was studied as a function of earthquake magnitude. Also, the shape of the story acceleration profiles and their relationship to uplift were studied.

By studying the acceleration profiles (Figure 6.7) for a given earthquake at different values of peak acceleration it becomes clear that as the peak acceleration was increased the isolation effect (peak table acceleration divided by peak structure acceleration) increased. The peak story acceleration values used for these plots did not necessarily all occur at the same time. The values used were the maximum accelerations for each floor over the duration of the earthquake motion. Thus, the profiles are really envelopes defining the maximum value of the acceleration at each story for the earthquake signal. It was also apparent that the effectiveness of the isolation system depended greatly on the earthquake frequency content. That is, for an earthquake rich in frequencies near the resonant frequency of the isolated structure, the isolation system's effectiveness was limited and, in fact, if sufficient damping had not been provided in the isolation system then a significant increase in structure acceleration divided by ground acceleration would have

resulted. It was also clear for earthquakes with the dominant portion of their frequency content well away from the isolated frequency that the isolation system provided significant reductions in structural accelerations divided by ground accelerations, on the order of 1/4 in some cases (San Francisco, for example).

It was noted that during shaking table tests where uplift occurred a pulse of vertical acceleration occurred at both ends of the model as it came back into contact with the foundation. This would have to be a design consideration if uplift were allowed. Another consideration for base isolation of buildings with uplift would have to be the design of connections between the bearings and the structure. If uplift were to occur, the usual shear key connections may disconnect. This phenomenon was witnessed during tests of the structure using the El Centro ground motion. The basic mechanism by which the bearings disengaged themselves from the shear key involved uplift of the base of the structure at the time of peak lateral bearing displacement. When base uplift exceeded the height of the shear key the bearing disconnected at its top and straightened instantly before the structure came back down on the bearing in this position. The structure then rode out the remainder of the ground motion in this position. The shear key could not be increased in height in the limited time available since it was nearly as high as the top and bottom plate thicknesses of the bearings already. It was noted that uplift of the structure when subjected to the El Centro ground motion occurred at a displacement of about 2 inches (50mm) which was much less than the 3.6-inch (92mm) displacement predicted for bearing roll-out to occur [12]. Thus, it is unlikely that the disconnection of the bearings was due to bearing roll-out.

In order to ascertain whether the horizontal responses of the model structure were affected by vertical ground motions, the El Centro ground motion was used twice in succession to excite the model. For both runs the horizontal table control setting was set at a span of 200. In the first case (860124.02) only horizontal motion was supplied to the shaking table. The peak horizontal acceleration for the table was 0.449g and the peak

horizontal acceleration in the model was 0.398g.

In the second case (860124.03) both horizontal and vertical motions were input to the table. The peak horizontal accelerations in the table and model were 0.452g and 0.378g, respectively. It appeared, then, that the addition of vertical motion had very little influence on the horizontal responses of the model.

6.6 Interpretation of Earthquake Test Results

Peak model acceleration against peak table acceleration was plotted in Figure 6.8 for a variety of earthquakes. The results show that peak model acceleration increases monotonically with peak table acceleration. It certainly appears that the ratio of peak model acceleration to peak table acceleration decreased for larger accelerations for the El Centro, Miyagi-Ken-Oki, and Bucharest input. There is some confusion about the points associated with uplift as higher lateral accelerations may have been induced by uplift or the consequences of uplift.

It is interesting to note that for the lower frequency earthquakes (Miyagi-Ken-Oki, and Bucharest) peak model acceleration versus peak table acceleration followed trends similar to the trends for the higher frequency earthquakes. If the model had not been in such a damaged and fragile condition it would have been feasible to increase the shaking table accelerations to a level where the nonlinear isolation system became more effective, for Miyagi-Ken-Oki and Bucharest as well as for El Centro. In spite of this the earthquakes can be ranked for effectiveness of the isolation system as follows: El Centro (most effective), Miyagi-Ken-Oki, Bucharest (least effective).

Figure 6.9 shows the acceleration time histories of all seven stories superimposed for each earthquake signal used in this set of tests. For all but the San Francisco signal it indicates that, generally, all the stories were moving in phase. This is important to note since the use of simple design formulae based on site design response spectra for analysis of base isolated structures implies an assumption of single degree-of-freedom behavior, which floor accelerations being in phase would help justify.

Another point of interest is the comparison between the peak base shear obtained in these tests and in the fixed-base tests performed by Bertero et al. [2]. It should be noted that the fixed-base results were obtained at levels of structural deformation well into the nonlinear range. Consequently, the fixed-base structure experienced a decrease in natural frequency with each subsequent test performed on it. Also, the fixed-base model was a 7-story model while the base isolated model was essentially a 6-story model. Thus, the two sets of test results cannot be compared directly. However, it made sense to compare base shears from the two tests in terms of peak base shear ratio — peak base shear as a percentage of the total weight of the structure, W. Comparison of the results in Table 6.3 with those in Table 2.2 shows that the base isolated model experienced a base shear ratio of 30.4% whereas this ratio was 41.7% for the fixed-base model for the Miyagi-Ken-Oki ground motion, at peak table accelerations of 0.304g and 0.247g, respectively. For the Taft ground motion, the base shear ratio for the base isolated model was 19.2% compared with 50.8% for the fixed-base model for peak table accelerations of 0.539g and 0.403g, respectively. These results indicate the reductions in base shear achievable with base isolation.

Figure 6.10 shows a plot of base shear ratio versus bearing shear strain for the El Centro ground motion. This plot is typical for all the earthquake ground motions tested. Only the magnitude of the base shear ratio varied somewhat (see Table 6.3). The shape of the curve in Figure 6.10 is due to the nonlinearity of the rubber, not due to yielding of the structure.

7. TEST RESULTS FOR MODEL ON 2ND SET OF BEARINGS

After the first set of tests was completed on the model it was isolated with a second set of natural rubber bearings. These bearings were made of a different rubber compound but had the same dimensions as the bearings of the first set. The structure on the second set of bearings was also subjected to a set of preliminary dynamic tests before being tested with earthquake ground motions. The results of these tests are presented in the following sections.

7.1 Free Vibration Test Results

The free-vibration tests conducted on the model supported by the second set of bearings indicated that the fundamental frequency of the isolated model was 1.72 Hz (Figure 7.1). The initial displacement of 0.138 inch (3.5mm), the result of 5 kips (22.6 kN) of force applied to the stiffener above bearing 4B, corresponded to an initial shear strain of 3.8% in the rubber of the bearings. The second lateral mode frequency was 5.9 Hz (Figure 7.2) and the fundamental torsional frequency was 2.6 Hz. The approximate equivalent viscous damping ratio found from the log decrement curve was 7% of critical.

7.2 Harmonic Vibration Test Results

The model supported on the second set of bearings was subjected to harmonic base motion at a variety of frequencies ranging from 0.7 Hz to 3.0 Hz (see Table 5.4 for the list of input frequencies). The model responses of peak lateral floor accelerations normalized to peak table acceleration at each input frequency were plotted against frequency (Figure 7.3). The fundamental frequencies were determined from these plots and by taking FFTs of lateral story acceleration time histories and relative bearing displacement time histories.

The fundamental lateral frequency indicated by this test was 0.95 Hz at a peak shear strain of about 35% in the rubber. The fundamental torsional frequency was 2.1 Hz and the second lateral mode frequency was 4.8 Hz. The loss angle of the rubber was determined from the hysteresis loops for bearing shear force versus relative bearing

displacement (Figure 7.4) and the damping ratio was calculated to be 9.5% of critical.

7.3 White Noise Vibration Test Results

The model supported by the second set of bearings was then subjected to white noise base motion. By taking FFTs of the lateral roof acceleration time histories and the relative bearing displacement time histories and noting the frequencies associated with the peaks in the Fourier spectra the modal frequencies were estimated (Figures 7.5 and 7.6). The level of peak shear strain in the rubber for this test was 7%. The first lateral mode frequency was 1.2 Hz, the second lateral mode frequency was 4.5 Hz, and the fundamental torsional frequency was 2.1 Hz.

7.4 Discussion of Preliminary Tests

The nonlinear relationship between bearing shear stiffness and shear strain made direct comparisons of preliminary test results difficult, so the test results were adjusted as discussed in Section 6.4. The free vibration test result of a fundamental frequency of 1.72 Hz at 3.8% shear strain corresponds to a frequency of 1.16 Hz at 100% shear strain. The harmonic test result of 0.95 Hz for a fundamental frequency at 35% shear strain corresponds to a frequency of 0.81 Hz at 100% shear strain. Finally, the result of the white noise test — 1.2 Hz at 7% shear strain — corresponds to a fundamental frequency of 0.81 Hz at 100% shear strain. These results are presented in Tables 7.1 and 7.2.

Again, the free vibration test indicated a higher value for fundamental lateral frequency of the isolated model than the other two tests. To some extent this was expected since the bearings were so stiff at small shear strains that the assumption of rigid body behavior at these strains was a poor one. The harmonic vibration and white noise test results were identical at 100% shear strain.

The value for k_h, based on Equation 3.1, was calculated using the linearly interpolated values for the shear modulus at 100% shear strains from Table 3.2. This was found to be $k_h = 0.592$ kips/inch (106.6 kN/m). An estimate of the fundamental lateral frequency of the model based on the rigid body formula (Equation 3.2) was found to be

0.82 Hz. The comparison of this value with the adjusted experimental values for the different preliminary tests is given in Table 7.2. As can be seen, the harmonic and white noise test results compare very closely with the rigid body estimate. Only the free vibration result was significantly different. On the basis of these results and those for the first set of bearings it seemed reasonable to discontinue using the free vibration test to estimate the fundamental frequency if the bearings could not be deformed significantly. These results seem to confirm the results of the first set of tests that the harmonic and white noise base vibration tests were the most successful for determining frequencies of the model structure.

7.5 Earthquake Motion Test Results

The 1/5-scale model isolated on the second set of bearings had a natural frequency of about 0.8 Hz, which would correspond to a prototype fundamental frequency of 0.36 Hz (2.76 second natural period). This isolation system was therefore significantly softer than the first system tested and was deemed to be more suitable for base isolation of a reinforced concrete structure on a soft soil site (i.e. Mexico City). Therefore, the Mexico City signal was included in the group of earthquake signals used to test the isolation system. The list of earthquake tests performed on this system is given in Table 5.5.

Each earthquake was input at a level of peak table acceleration which caused a peak relative bearing displacement of about 2 inches (50mm) which corresponded to about 60% shear strain in the rubber. This was done in order to compare the responses of the structure to a large group of earthquakes at similar bearing shear strain levels. Because of the high frequency content of the San Francisco signal, a maximum bearing displacement of only about 1 inch (25mm) was possible.

As was done previously, the acceleration profile of the structure was plotted for each of these earthquakes (Figure 7.7). From these profiles it was seen again that the effectiveness of the isolation system depended greatly on the earthquake characteristics. For example, the Mexico City signal caused peak structural accelerations about twice

that of the shaking table, the Bucharest signal caused model accelerations about equal to the table, and the model accelerations were smaller than the table accelerations for the remainder of the signals. By observing the FFT plots (Figure 5.3) for each earthquake and noting that the 1/5-scale model frequency of 0.8 Hz corresponds to a full-scale frequency of 0.36 Hz it can be seen why the Mexico City earthquake was most severe in terms of lack of isolation, Bucharest next, and the other signals less severe. It was also noted that the shape of the acceleration profiles implied nearly rigid body behavior in the isolated structure, more so than the results for the tests on the first set of bearings. To confirm that the model was responding predominantly in the first mode, story acceleration time history plots were superimposed for the different earthquakes. From these plots (Figure 7.8) it can be seen that the story acceleration responses were generally in phase for most of the large amplitude oscillations in the time histories, except for the San Francisco signal.

The structure on the second set of bearings was also tested with a sequence of large amplitude El Centro ground motions. These tests caused bearing displacements of nearly 4 inches (100mm) — over 100% rubber shear strain. At this level of input the story accelerations and story shear force distribution were sufficient to cause the columns to uplift off the bearings and become disconnected. The manner in which the devices became unattached indicated that the result was not a simple case of column uplift. Unlike the manner in which the model columns lifted off the first set of bearings, the model supported on the second set of bearings did not appear to uplift sufficiently for the shear key to become disconnected from the top of the bearing. This was confirmed by the DCDT measuring devices used to measure column uplift. It appeared that a combination of column uplift and bearing roll-out had occurred. The predicted roll-out displacement for the second and third sets of bearings, based on the 100% shear strain stiffness from Figure 4.9, is 4.2 inches (107mm) [12]. This could have happened if the top plates had rotated sufficiently to allow the shear key to slide out of the hole at a

reduced amount of column uplift. Alternatively, it could have happened if the column faces had rotated sufficiently to lift the shear key out of the hole.

The peak base shear ratio (peak base shear as a percentage of the total weight of the structure) was plotted against bearing shear strain (Figure 7.9) for the El Centro ground motion; the shape of the curve again illustrates the softening of the isolation system with increasing displacements. The values of peak base shear ratio in Table 7.3 were compared with the fixed-base results in Table 2.2 and the first isolation system results in Table 6.3. The second set of isolators seemed to be more effective isolators in terms of reducing the story accelerations and the degree to which the structure acted in the first mode for the earthquakes tested. However, there did not appear to be any appreciable difference in the magnitude of peak base shear ratios for the model on either of the first two sets of bearings used to isolate the structure.

7.6 Fixed-Base Tests

At this stage, it was decided to test the model as a fixed-base structure with a white noise base input and an El Centro earthquake signal. For these tests the structure was restrained against displacement at the level just above the base isolators and the input signal magnitudes were very low so the structure would not suffer any more damage. These tests provided some information about the condition of the model and what sort of response the structure would exhibit when subjected to an earthquake as a fixed-base structure.

Based on the results of the white noise test, the 1/5-scale fixed-base structure had a fundamental frequency of about 7.5 Hz (Figure 7.10). Thus, the shift in natural frequency from 7.5 Hz for the fixed-base model to the isolated frequency of about 1 Hz was substantial. The peak base shear of the model for the El Centro test was 12.92 kips (58.36 kN) (Table 7.7). This value, if it were to be scaled elastically by the ratio of the other El Centro earthquake table accelerations to the fixed-base table acceleration, would be significantly larger than the base isolated base shears. The roof acceleration time

history for the base isolated case for the El Centro motion at 0.783g peak table acceleration and the roof acceleration time history for the fixed base test multiplied by a factor of 0.783/0.146 are plotted together in Figure 7.11 to illustrate the differences in response. In particular, the roof acceleration response of the isolated structure has visibly lower frequency content. Also of interest is the shape of the story acceleration profile in Figure 7.12 for the fixed-base structure. Keeping in mind that the plotted values are maximum values over time the profile reflects the first mode shape for a fixed-base structure. This is also evident in the superimposed plots of the story acceleration time histories in Figure 7.13.

8. TEST RESULTS FOR MODEL ON 3RD SET OF BEARINGS

The free vibration test was not conducted on the reinforced concrete model on the third set of bearings since it was felt that the test did not give an accurate estimate of the natural frequency, certainly not as accurate as either the harmonic or white noise vibration tests. The reasons for this have been discussed in Sections 6.4 and 7.4.

8.1 Harmonic Vibration Test Results

The model was subjected to harmonic base excitation at constant frequency over the range of frequencies from 0.7 Hz to 2.0 Hz (Table 5.6) The model frequencies were determined using the same combination of techniques used in the previous harmonic vibration tests (Figure 8.1). The fundamental lateral frequency determined from this test at a peak shear strain of about 37% was 1.0 Hz, the second lateral mode frequency was 4.8 Hz, and the fundamental torsional frequency was 2.1 Hz. The approximate equivalent viscous damping ratio obtained from the hysteresis loops (Figure 8.2) for bearing shear force versus relative displacement was 10.5% of critical.

8.2 White Noise Vibration Test Results

The model supported on the third set of bearings was then subjected to the same white noise input as described in Section 5.2. From the FFTs of the lateral floor acceleration time histories and bearing relative displacement time histories (Figures 8.3 and 8.4) the model frequencies were determined to be 1.1 Hz for the first lateral mode, 4.3 Hz for the second lateral mode, and 2.1 Hz for the first torsional mode. These frequencies corresponded to peak shear strains of about 7% in the rubber.

8.3 Discussion of Preliminary Test Results

Again, the nonlinear stiffness properties of the rubber had to be accounted for before comparing results of the two preliminary tests with each other or with the rigid body theory. The third set of bearings was manufactured from the same type of rubber as that used to make the second set of bearings. The only significant difference between the

second and third sets of bearings was the thickness of the steel reinforcing shims. The third set used much thinner shims — 0.012 inch (0.3mm) instead of 0.037 inch (0.93mm). Thus the results were adjusted using the relationship of Equation 6.1 and the MRPRA shear modulus values at peak shear strains in Table 3.2.

Using this procedure, the harmonic vibration test result corresponds to a fundamental frequency of 0.77 Hz at 100% shear strain and the white noise test result corresponds to a 0.74 Hz fundamental frequency at 100% shear strain. The results for these tests are presented in Table 8.1. If it were assumed that the steel shims did not affect the horizontal stiffness significantly, then the bearing stiffness, k_h, for the third set of bearings should have been the same as for the second set. Using the same equations and stiffness, the rigid body theory predicted the same fundamental frequency as for the second system — 0.82 Hz. These results are given in Table 8.2.

It seems logical that thinner steel shims would result in a "softer" bearing, thereby resulting in a lower natural frequency. Both tests seem to confirm this. The harmonic test result at 100% shear strain was about 5% lower than the rigid body theory and the white noise test result at 100% shear strain was about 10% lower than the rigid body theory.

The damping values indicated by the harmonic vibration test (10.5%) were consistent with the MRPRA results at similar shear strain levels and also close to the results for the harmonic vibration test on the second set of bearings.

8.4 Earthquake Test Results

On the basis of the preliminary tests, the 1/5-scale model isolated on the third set of bearings had a fundamental frequency of about 0.75 Hz which corresponded to a full-scale natural frequency of 0.335 Hz (2.98 seconds natural period). The Mexico City signal was included in the earthquake test series on this set of bearings since the isolation was felt to be "soft" enough to provide some isolation from the low frequency earthquake motion. The earthquake test series is listed in Table 5.7, and a summaries and

discussions of the results for some of the earthquake tests follow.

As was done for the tests on the second set of bearings each earthquake signal was input at a magnitude sufficient to cause a peak bearing displacement of about 2 inches (50mm). In addition, the El Centro and Mexico City earthquake signals were input at several different levels to study the effect of increasing bearing displacement on the response of the structure. The behavior of the model at the point of bearing uplift or roll-out was of particular interest because of the very thin steel shims used.

By studying the acceleration profiles of the structure for the group of earthquakes used (Figure 8.5) it is seen that the structure on the third isolation system responded mostly in a rigid body manner. Only for the Mexico City signal is there any appreciable increase in the story accelerations at higher levels in the model. The degree of isolation is almost identical to that for the second set of isolators except for the Mexico City earthquake. Peak base shear ratios similar to those recorded for tests on the second set of bearings were also experienced (Table 8.3). This indicates that in terms of structure accelerations the third system was just as effective. In fact, the relative bearing displacements were also very similar for the second and third sets of bearings for all the earthquake signals except Mexico City. Curiously, the third set of bearings provided much better isolation for the Mexico City signal than either of the first two sets of bearings. This indicates that the third set of bearings was softer; a fact confirmed by the individual bearing tests (Figures 4.9 and 4.13) and the preliminary dynamic tests on the base isolated structure (Tables 7.2 and 8.2).

Two sequences of earthquake tests were also performed on the third isolation system to study the effect of increasing bearing displacement on the isolation effectiveness. The sequence of El Centro earthquakes demonstrated improved isolation with increase in peak table acceleration. That is, the slope of the plot of the peak base shear ratio versus bearing shear strain decreased as the peak table acceleration increased (Figure 8.6). This was also observed for the series of Mexico City earthquake signals, although there was

one data point which seemed to be inconsistent with the other points (Figure 8.7).

The most dramatic result of this set of tests was the improvement of the isolation over that of the second set of bearings for the Mexico City earthquake signal. It was expected that the behavior of the structue would be similar for both of these sets since the bearing properties were so similar but there was a significant improvement in isolation with the third set of bearings for the Mexico City signal. The ratio of peak model to peak table acceleration was about 2.5 for the model on the second set of bearings (860130.13-Table 5.5). This ratio dropped to approximately 1.0 for the model on the third set of bearings for the same Mexico City signal at a slightly higher peak table acceleration (860227.07-Table 5.7). This result was due to the fact that the slight increase in the period of the structure was sufficient to move the period away from the predominant frequency content of the earthquake signal. This also explains why the bearing displacements were smaller for the Mexico City tests on the third set of bearings than for similar tests on the second set. This is illustrated by considering the response spectrum (Figure 8.8) of the $\sqrt{5}$ time-scaled shaking table acceleration record for the Mexico City test signal. For a change in structural period from 1.23 seconds to 1.33 seconds, the spectral displacements and accelerations both decrease.

To get an idea of how well the isolated structure behaved as a rigid body on a system of isolators the story acceleration time history plots were superimposed for each earthquake (Figure 8.9). As for the other isolation systems, the story accelerations were in phase for most of the large amplitude swings in the response time histories. The isolated structure responded most like a rigid body when subjected to the low frequency signals (Bucharest and Mexico City).

Another point that should be mentioned was the behavior of the structure at uplift. The structure on the third set of bearings exhibited a tendency to uplift similar to that of the structure on the second isolation system. Displacement magnitudes for the bearings were similar for the El Centro signal and are shown in Tables 5.5 and 5.7. As was

the case for the second isolation system, the observed "uplift" seemed to be a combination of bearing roll-out and column uplift. The bearing displacements were greater than 3.5 inches (89mm) when uplift occurred for the El Centro ground motion. This corresponded to about 100% shear strain in the rubber. The roll-out displacement for the third set of bearings was predicted to be 4.2 inches (107mm) [12]. The model also exhibited a slight amount of uplift for the largest Mexico City input signal. In contrast to the El Centro motion this motion resulted in a peak bearing displacement of only about 2.8 inches (71mm) and a peak model acceleration of about 0.327g. These values were much less than what was felt necessary to cause column uplift. A uniform story acceleration of about 0.4g was estimated to be required to cause uplift.

A final point of consideration was the degree to which the thin steel shims might encourage interaction between the vertical and horizontal responses of the structure. To study this, the San Francisco and El Centro earthquake signals were input at the same table input settings for horizontal motion and run twice — once with horizontal motions only and once with horizontal and vertical motion input. On the basis of those tests, there appeared to have been a slight increase (about 5% for El Centro, 11% for San Francisco) in the peak model acceleration when the vertical motion was included. The resulting bearing displacements decreased about 5% for the El Centro and increased about 1% for San Francisco with the vertical motion included. These differences in the test results were not felt to be significant enough to warrant testing of the base isolated structure with vertical motion for each earthquake signal.

9. SEAONC BASE ISOLATION DESIGN FORMULA

The Structural Engineers Association of California (SEAOC) has recognized the "need to supplement existing codes with design requirements developed specifically for seismically isolated buildings. This need is shared by the public which requires assurance that seismically isolated buildings are *safe* and by the engineering profession which requires a minimum standard upon which design and construction can be based." Out of this need the "Tentative Seismic Isolation Design Requirements, September, 1986" were developed by the Base Isolation Subcommittee of the Seismology Committee of the Structural Engineers Association of Northern California (SEAONC) [13]. These requirements were intended to supplement the SEAOC "Tentative Lateral Force Requirements, October, 1985" document [14]. These seismic isolation design requirements are tentative and at the time of writing had not been adopted by the SEAOC Seismology Committee. The basic design philosophy and design formulae recommended by this document are discussed here and experimental results from the tests discussed in Chapters 6-8 are compared with values given by the proposed design formulae.

9.1 Summary of SEAONC Design Procedure

The general design philosophy requires that: (1) the base isolated structure should remain stable for required design displacements; (2) the isolation system should provide resistance which increases with increases in displacement; (3) the system should be capable of repeated cyclic loads without any significant degradation; (4) the isolation system should have quantifiable engineering parameters.

Either of two design procedures are permitted under the proposed design guidelines. The first uses a set of simple equations to prescribe design values of displacement and base shear. These formulae are similar to the seismic lateral force formulae now in use for conventional building design. The second procedure requires a dynamic analysis to determine the peak responses of the base-isolated structure pertinent to design. This procedure would be required of any structure with geometric irregularities or of any

especially flexible structure.

The tentative design provisions are based on a level of earthquake ground motion which corresponds to a 500 year earthquake as described by the ATC 3-06 recommended ground motion spectra [15]. The provisions require the base isolation system and all structural components at or below this level to withstand the full force and effects of this ground motion without damage. Structural elements above the isolation level are not, however, required to be designed for the full force of this motion. A small amount of inelastic damage is allowed above the isolation level if sufficient ductility is provided. The overall philosophy is that base isolated structures should be at least as safe as conventional buildings during extreme earthquake loadings. The inelastic factor of 2.76 for the 500 year earthquake is meant to ensure elastic response of the structure for ground motions less severe than the 50 to 100 year earthquake.

The purpose of the following comparisons between shaking table test results and values for bearing displacement and base shear given by the simple design equations is to evaluate the reliability of the design formulas for this particular structural system. Further work is being conducted in this area for a wide range of isolation systems.

9.2 Comparison of Experimental and Design Displacements

The shaking table test displacements for the 1/5-scale test structure were to be compared with the displacements predicted by the SEAONC Tentative Seismic Isolation Design Requirements [13]. The SEAONC base isolation code formula for displacement is given by Equation (1) from Section B.2; it applies, however, to prototype displacements D_{prot}.

$$D_{prot} = \frac{10\ Z\ N\ S\ T}{B} \tag{9.1}$$

where the terms are defined as follows:

D_{prot} = minimum displacement for which the isolation system must be designed;

Z = earthquake zone factor (0.3 or 0.4 for California);

N = coefficient depending on distance from fault;

S = soil factor ranging between 1.0 and 2.7;

T = period of the isolated structure;

W = weight of isolated structure above and including the isolation surface;

g = acceleration due gravity;

k_{min} = minimum effective stiffness of the isolation system;

B = damping coefficient ranging between 0.8 and 2.0 .

The period for the prototype isolated structure should be calculated from the equation

$$T = 2\,\pi \sqrt{\frac{W}{k_{min}\, g}} \tag{9.2}$$

where the prototype values are defined as above, and g = acceleration due to gravity.

In order to make comparisons between the experimental displacements and values given by the proposed code Equation 9.2, the code equation had to be modified to account for the scale factor of the experimental model. The SEAONC code for base isolation is derived from the ATC 3-06 formula $S_A = A_a\,(T_o/T)\,g$, where A_a is the acceleration factor, for example 0.4, and T is the fundamental period in seconds. S_A is the design acceleration in g's and the equation is set up so that $S_A = A_a\,g$ when $T = 1$ second. Thus, $T_o = 1$ second and does not explicitly appear in the formula. This formula was scaled for experimental purposes and the following relationships were used, where F is used to denote the model scale factor:

$$\text{length}_{model} = \frac{1}{F}\,\text{length}_{prot}\ ;$$

$$\text{time}_{model} = \frac{1}{\sqrt{F}}\,\text{time}_{prot}\ ;$$

$$\text{accel}_{\text{model}} = \text{accel}_{\text{prot}} \ .$$

Therefore, when applying the formula to the scale model the following values must be used:

$$S_{A_{\text{model}}} = S_{A_{\text{prot}}} \ , \quad A_{a_{\text{model}}} = A_{a_{\text{prot}}} \ , \quad T_{o_{\text{model}}} = \frac{1}{\sqrt{F}} T_{o_{\text{prot}}} \ .$$

The formula was extended to base isolation applications as

$$D_{\text{prot}} = 10 \, A_{a_{\text{prot}}} \, T_{\text{prot}} \ .$$

This was derived from the following equations:

$$S_D = \frac{S_A}{\omega^2} \quad \text{where} \quad \omega = \frac{2\pi}{T}$$

and

$$S_D = A_a \frac{T_o}{T} \, g \, \frac{T^2}{(2\pi)^2} = \frac{g}{(2\pi)^2} A_a \, T_o \, T \ .$$

Using the scaled quantities

$$D_{\text{model}} = \frac{1}{F} D_{\text{prot}} \ , \quad T_{\text{model}} = \frac{1}{\sqrt{F}} T_{\text{prot}} \ , \quad T_{o_{\text{model}}} = \frac{1}{\sqrt{F}} T_{o_{\text{prot}}}$$

and substituting into the equation for D gives the expression

$$F \, D_{\text{model}} = \frac{g}{(2\pi)^2} A_a \sqrt{F} \, T_{o_{\text{model}}} \sqrt{F} \, T_{\text{model}} \ ;$$

$$D_{\text{model}} = \frac{g}{(2\pi)^2} T_{o_{\text{model}}} \, T_{\text{model}} \, A_a \ .$$

For the prototype $\frac{g}{(2\pi)^2} \approx 10$ and $T_o = 1$ second, therefore $D = 10 \, A_a \, T$ for the prototype. For the model, $T_{o_{\text{model}}} = \frac{1}{\sqrt{F}}$ so that $D_{\text{model}} = \frac{10}{\sqrt{F}} A_a \, T_{\text{model}}$. For this study $F = 5$, so that the coefficient for the scaled formula is 4.47. Thus, the code based displacements for the 1/5-scale model were calculated using the formula

$$D_{model} = 4.47 \frac{Z\,N\,S\,T_{model}}{B} \quad . \tag{9.3}$$

The values for S and B used in the calculations are explained below. A value for S of 2.7 was used for the Mexico City earthquake since the soil condition at the data collection site for that signal falls into the S_4 category. A value of 2.0 was used for S for the Bucharest earthquake signal since that signal corresponds to a soft soil site, although not as soft as for the Mexico City signal. A value of 1.0 was used for the San Francisco signal and a value of 1.5 was used for all the other earthquake signals. The isolated period was calculated from Equation 9.2 using the value of k_{min} from Figures 4.5, 4.9 and 4.13 based on the shear strain corresponding to the experimental displacement, D_{exp}, for the particular shaking table test. Finally, since the three sets of bearings each had damping ratios of about 10%, a value of 1.2 was used for B. Three different types of values were used for ZN in Equation 9.3. They were:

- the peak table acceleration, PGA;
- the coefficient A_a based on the effective peak acceleration (as defined by ATC 3-06) for each of the time-scaled table signals;
- the coefficient A_v based on the effective peak velocity (as defined by ATC 3-06) for each of the time-scaled table signals.

Using these parameters in Equations 9.2 and 9.3, displacement values for the different shaking table tests were calculated and the ratio D_{model}/D_{exp} was computed for the series of tests and tabulated in Table 9.1.

The use of the design formula with ZN = PGA gave conservative results for all the earthquake test signals except Bucharest and Mexico City. These two signals are both low frequency motions and as such the model responses are more velocity dependent than acceleration dependent. The design procedure is not applicable for low frequency motions and this is illustrated here. The use of the effective peak acceleration coefficient A_a was less conservative than the use of the PGA coefficient, and while the effective peak

velocity coefficient A_v sometimes gave more conservative results than the A_a coefficient it was still generally less conservative than the PGA coefficient results.

9.3 Comparison of Experimental and Design Base Shear

Base isolation decreases the magnitude of peak base shear from levels for fixed base structures by decreasing the magnitude of accelerations experienced by the structure. The peak base shear, V_{exp}, for the three sets of tests is tabulated in Table 9.2. The design values of peak base shear are given by the SEAONC Equation 3 (from Section B.3.1)

$$V_b = \frac{k_{max}\, D}{1.5} \tag{9.4}$$

where k_{max} is the maximum effective bearing stiffness.

The values for k_{max} were obtained from Figures 4.5, 4.9 and 4.13 for the appropriate set of bearings and shear strain corresponding to the experimental displacement D_{exp} listed in Table 9.1. Because of the consistency of the shear hysteresis loops for the rubber base isolation bearings, k_{min} is effectively equal to k_{max}. This is illustrated by the hysteresis loops in Figures 6.4, 7.4, and 8.2. The calculated values, V_{PGA}, for peak base shear based on the displacements, D_{PGA}, are listed in Table 9.2 along with the experimental values of peak base shear, V_{exp} and the ratio of the calculated peak base shear over the experimental peak base shear, V_{PGA}/V_{exp}. The ratio was less than one for tests of the structure on each set of bearings when subjected to the Mexico City and Bucharest earthquake signals. The ratios for the tests with the El Centro and Parkfield signals were near or less than one. In general, the ratio was less for peak base shear than for peak bearing displacement for each test.

The structural elements above the isolation level must be designed to resist a minimum shear force V_s given by the SEAONC Equation 4 (from section B.3.2) where

$$V_s = \frac{2\, k_{max}\, D}{R_w} \tag{9.5}$$

and R_w is a numerical coefficient related to the type of structural system and its ductility capabilities. If Equations 9.4 and 9.5 are compared, it can be seen that a factor of 3 for R_w would cause $V_s \equiv V_b$.

Calculated values of V_s were not compared with shears experienced in the structure since the measured peak base shear was the same just above the isolators as it was just below. However, it should be noted that for elastic behavior of the structure above the isolators, the elastic design value for shear, V_s, should be at least as great as V_b. Then the structural elements would remain elastic for any shear $V \leq V_b$.

9.4 Additional SEAONC Design Considerations

It was of interest to note that the ratios of the fixed-base period to the isolated period for the three sets of bearings tested were 0.13, 0.10, and 0.10, respectively. Section B.4 in the tentative SEAONC provisions for design of base isolated buildings requires that a dynamic analysis be performed for isolated structures where the ratio of the fixed base period to the isolated period exceeds 0.20. This is to account for interaction between the structure and the isolation system which would show up as modal responses for modes greater than one. In these tests this requirement was well satisfied.

Implicit in the tentative design provisions is the assumption of uniform lateral acceleration distributed over the height of the structure. The story shear forces are calculated on the basis of this assumption by the equation

$$F_j = \frac{V_s \, w_j}{\sum_{i=1}^{n} w_i}$$

where F_j is the story shear at level j, V_s is the total base shear, and w_j is the weight (or mass) at level j.

The degree to which the structure behaved as a rigid body and therefore had a uniform story acceleration distribution is discussed in Chapters 6 to 9. The peak acceleration profile distributions are given in Figures 6.7, 7.5, and 8.5. They illustrate the degree

to which the structure responded as a single degree-of-freedom system and on the basis of these results it is felt that the assumption above is reasonable.

For this particular structure the possibility of uplift existed. The tentative code provisions address this problem in Section E.1.6. The provisions allow local uplift, which did occur during large magnitude El Centro earthquake tests on the three sets of bearings. The factor of safety against global overturning must be greater than or equal to 1.0. This must be considered for all gravity and seismic load combinations required by the 1985 SEAOC code. The seismic forces for overturning calculations should be based on the maximum base shear force given by $k_{max}D$, with the story shear forces distributed as before and a restoring force due to the weight of the structure W. The structure on the first set of bearings experienced uplift sufficient to cause the base isolators to become disconnected at one end of the structure. This would have to be taken into consideration in the design process.

10. IMPLICATIONS OF THE TEST RESULTS

10.1 Rehabilitation of Damaged Structures

The 1/5-scale model structure tested in this study had been tested previously to failure. It was originally designed as a fixed-base 7-story reinforced concrete shear wall structure. Because major repairs were necessary before the model could be tested, this study was considered an ideal opportunity to illustrate the use of base isolation to repair a damaged structure.

The major task encountered in this project was incorporation of the base isolation system into the already existing foundation system of the structure. Some modifications to the structure had to be made in order to do this and the majority of the repair cost was related to this modification. In order to base isolate the structure, the structure had to be stiffened — or "tied together" — just above the isolators. This ensured that the bearings worked in parallel and provided some redundancy in the isolation system. Other work, such as repair of the first story shear wall down to the level of the isolators and beam-column joint repairs, was also carried out but this would most likely have had to be done for any rehabilitation scheme.

On the basis of the shaking table tests it is felt that the damaged structure was successfully rehabilitated by the base isolation scheme. The benefits of the base isolation system include reduced base shear and story shear magnitudes in comparison with those experienced in the fixed-base tests. The base isolators, the modifications to the structure to accommodate the isolators, and the replacement or repair of any nonstructural elements which cross the isolation gap are all costs associated with the base isolation of damaged structures.

10.2 Base Isolation of Medium-Rise Structures

Until now base isolation has been used only on relatively low-rise structures. One of the objectives of this study was to investigate the effect base isolation would have on structures taller than those base isolated to date. The structure that was tested in this

study had an aspect ratio (height to width) of about 1.23 in the direction of shaking. It was felt that a uniform horizontal story acceleration of about 0.4g would cause the columns to begin to uplift off the bearings. This level of story acceleration was easily achieved in the fixed-base model. It was not certain, however, whether story accelerations of this magnitude would result in the base isolated model.

Tests of the structure on the three sets of bearings showed that uplift would occur. For the structure on the first set of bearings column uplift was measured to be about 0.5 inch (13mm) during the El Centro earthquake test which had a peak table acceleration of about 0.7g. The peak structural acceleration (roof) for this test was about 0.5g although the average story acceleration was closer to 0.4g. The magnitude of this test signal, in terms of effective peak acceleration (EPA) as defined in the ATC 1985 design code, was about 0.7g.

As mentioned in Chapters 7 and 8, uplift was generated in the structure on the second and third sets of bearings as well. The amount of uplift measured was less than the 13 mm recorded during the tests of the structure on the first set of bearings. Results of these tests showed that the peak structural acceleration experienced by the model on the second set of bearings was only 0.411g for the 0.685g El Centro signal (860204.05 in Table 5.5) and 0.491g for the 0.786g El Centro signal (860304.07 in Table 5.7) on the third set of bearings. Both of these tests exhibited large bearing displacements, 3.526 inches (90mm) and 3.494 inches (89mm), respectively. While these displacements were less than the predicted roll-out displacement of 4.2 inches (107mm), bearing roll-out was thought to play a part in the way the bearings became disconnected from the structure at acceleration levels and displacements below those thought necessary for column uplift to occur.

Column uplift was a major factor considered in the design of the structure-to-bearing connections. For this study, each set of bearings was designed to allow 0.5 inch (13mm) of uplift before the bearings would disengage themselves from the base of the

column. The uplift occurred at times of peak lateral bearing displacement so that when uplift exceeded the height of the shear key the bearings disengaged themselves and snapped back into an upright position before the column came back to rest on the bearing where it rode out the rest of the earthquake signal. This behavior is clearly undesirable since the reduction in peak base shear due to uplift was not especially significant (Figures 6.10, 7.9, 8.6, and 8.7) and the event tended to damage the shear key connections.

Several schemes for preventing this phenomenon were proposed but none were implemented during this study. The first proposal required the bearings to be bolted to the column base plates and the foundation. This solution would have been fairly simple to implement but required the bearings to carry tensile forces during uplift. Not enough was known about the tensile strength of the bearings at that time to do this confidently. Another proposal was to increase the shear key height. This required that the holes into which the shear keys were inserted be deepened but the holes were already at their limit. Finally, a set of bearings acting in shear in the vertical direction was proposed but this system was too complicated to implement easily. Thus the tests were carried out without any uplift prevention devices in place. Nevertheless, these tests show that structural and base shear forces are reduced in a medium-rise base isolated structure even with the occurrence of column uplift.

10.3 Small Buildings and Low-Cost Housing

Another objective of this study was to determine if inexpensive lightweight bearings could be made which would perform well and have satisfactory engineering properties. This type of bearing could be used for base isolation of smaller structures and low-cost structures. With the decreased cost per bearing and less rigorous manufacturing techniques required the principle of base isolation could be more easily introduced into third world countries where inexpensive construction procedures and materials are usual.

The third set of bearings tested was such a design. These bearings were manufactured of the same rubber used in the second set, however the steel shim thickness was reduced by a factor of about three. The steel shims were only 0.012 inch (0.3mm) thick, compared with the 0.037 inch (0.93mm) thickness in the second set. Besides the savings in steel costs and manufacturing costs the bearings also weighed less than the conventional bearings and could thus be placed at a construction site without expensive equipment.

The third set of bearings performed in a manner almost identical to the performance of the second set. As mentioned in detail in Chapter 8, the only significantly different result was for the Mexico City earthquake for which the bearing displacements were smaller and the isolation was improved. All the other test results were similar for both sets of bearings. The third set was only slightly softer in shear than the second set and this resulted in a slightly longer period. They were slightly less stiff vertically as well, and at very large shear strains ($>100\%$) the top plate of the bearing exhibited some rotation. In general, the third set of bearings performed extremely well and test results indicate that further experimental and analytical investigation is warranted.

REFERENCES

[1] J. M. Kelly, "Aseismic Base Isolation: Review and Bibliography," *Soil Dynamics and Earthquake Engineering*, Vol. 5, No. 3, (1986).

[2] V. V. Bertero, A. E. Aktan, F. A. Charney and R. Sause, "Earthquake Simulation Tests and Associated Studies of a 1/5th-Scale Model of a 7-Story R/C Frame-Wall Test Structure," Report No. UCB/EERC-84/05, Earthquake Engineering Research Center, University of California, Berkeley, (1984).

[3] V. V. Bertero, A. E. Aktan, H. G. Harris and A. A. Chowdhury, "Mechanical Characteristics of Materials Used in a 1/5 Scale Model of a 7-Story Reinforced Concrete Test Structure," Report No. UCB/EERC-83/21, Earthquake Engineering Research Center, University of California, Berkeley, (1983).

[4] R. Sause and V. V. Bertero, "A Transducer for Measuring the Internal Forces in the Columns of a Frame-Wall Reinforced Concrete Structure," Report No. UCB/EERC-83/05, Earthquake Engineering Research Center, University of California, Berkeley, (1983).

[5] C. J. Derham and H. G. Thomas, "The Stability of Rubber/Steel Laminated Building Bearings," *Natural Rubber Technology*, Vol. 14, No. 3, (1983).

[6] P. A. Hidalgo, R. L. Mayes, H. D. McNiven, and R. W. Clough, "Cyclic Loading Tests of Masonry Single Pier: Volume 1 -- Height to Width Ratio of 2," Report No. UCB/EERC-78/27, Earthquake Engineering Research Center, University of California, Berkeley, (1978).

[7] C. G. Koh and J. M. Kelly, "Modelling of Dynamic Response of Elastomeric Isolation Bearings," Report No. UCB/EERC-86/12, Earthquake Engineering Research Center, University of California, Berkeley, (1986).

[8] Earthquake Catalog of California, January 1, 1900 to December 31, 1974, Charles R. Read et. al., California Division of Mines and Geology, Special Publication No. 52, 1st Edition and Cal. Tech. Report No., EERL 80-01, D.M. Lee, P.C. Jennings, G.W. Housner, (1980).

[9] N. Ambraseys, "The Romanian Earthquake of March 4, 1977," Preliminary Report of UNESCO Earthquake Reconnaissance Mission, (1977).

[10] Bruce Ellingwood (Ed.), "An Investigation of the Miyagi-Ken-Oki, Japan, Earthquake of June 12, 1978," National Bureau of Standard Center for Building Technology, Washington, D. C., (1980).

[11] S. Suzuki and A. S. Kiremidjian, "The Mexico Earthquake of September 19, 1985, A Preliminary Report," The John A. Blume Earthquake Engineering Center, Dept. of Civil Engineering, Stanford University, Report No. 77, (1986).

[12] J. M Kelly, I. G. Buckle and H. C. Tsai, "Earthquake Simulator Testing of a Base-Isolated Bridge Deck," Report No. UCB/EERC-85/09, Earthquake Engineering

Research Center, University of California, Berkeley, (1985).

[13] "Tentative Seismic Isolation Design Requirements," Report prepared by the Base Isolation Subcommittee of the Seismology Committee of the Structural Engineers Association of Northern California, (1986).

[14] "Tentative Lateral Force Requirements: October 1985," Report prepared by the Seismology Committee of the Structural Engineers Association of California, (1985).

[15] "Tentative Provisions for the Development of Seismic Regulations for Buildings," ATC Publication No. ATC 3-06, prepared by the Applied Technology Council, (1978).

TABLES

PARAMETER	1/5-SCALE MODEL/PROTOTYPE	
Length	L	1/5
Time	$\sqrt{L}$	1/2.24
Mass	L^2	1/25
Displacement	L	1/5
Acceleration	1	1/1
Stress	1	1/1
Strain	1	1/1
Force	L^2	1/25
Area	L^2	1/25

Table 2.1 Similitude Scale Factors for Full-Scale Responses

Test Signal Acceleration (%g)	Effective Frequency	Maximum Base Shear (%W)	Maximum Overturning Moment (%WH)	Maximum Top Acceleration (%g)
MO 5.0	4.2 Hz	9.9% W (3.83 sec)	6.72% WH (3.83 sec)	15.1 (3.84 sec)
MO 9.7	3.9 Hz	17.5% W (3.86 sec)	11.5% WH (3.86 sec)	27.4 (3.84 sec)
MO 14.7	2.9 Hz	27.3% W (3.11 sec)	18.2% WH (4.67 sec)	44.5 (4.65 sec)
MO 24.7	2.7 Hz	41.7% W (7.27 sec)	27.1% WH (7.26 sec)	65.2 (7.23 sec)
MO 28.3	2.1 Hz	46.8% W (5.50 sec)	30.9% WH (5.26 sec)	81.3 (5.45 sec)
T 40.3	1.8 Hz	50.8% W (3.14 sec)	33.7% WH (3.14 sec)	88.8 (3.18 sec)
T 46.3	1.5 Hz	47.8% W (3.26 sec)	30.5% WH (3.58 sec)	78.4 (1.95 sec)

Table 2.2 - Maximum Response of Fixed-Base Model

Displ. amplitude (mm)	Shear Strain	1st up Sweep k x 10^{-5} (N/m)	G (MN/m^2)	G (ksi)	δ (degrees)	% Critical Damping
0.12	0.020	5.3	3.14	0.456	16.0	0.143
0.3	0.051	3.4	2.01	0.292	17.8	0.160
0.6	0.101	2.45	1.45	0.211	16.5	0.148
1.2	0.202	1.8	1.07	0.155	14.3	0.127
3.0	0.505	1.25	0.74	0.107	12.1	0.107
6.0	1.010	1.0	0.59	0.086	10.9	0.096

Displ. amplitude (mm)	Shear Strain	1st down Sweep k x 10^{-5} (N/m)	G (MN/m^2)	G (ksi)	δ (degrees)	% Critical Damping
0.12	0.020	3.3	1.95	0.283	17.0	0.153
0.3	0.051	2.35	1.39	0.202	17.0	0.153
0.6	0.101	1.85	1.10	0.160	15.5	0.139
1.2	0.202	1.5	0.89	0.129	14.0	0.125
3.0	0.505	1.1	0.65	0.094	11.5	0.102
6.0	1.010	0.9	0.53	0.077	10.7	0.094

Displ. amplitude (mm)	Shear Strain	2nd up Sweep k x 10^{-5} (N/m)	G (MN/m^2)	G (ksi)	δ (degrees)	% Critical Damping
0.12	0.02	3.02	1.79	0.260	17.0	0.153
0.3	0.051	2.2	1.30	0.189	17.1	0.154
0.6	0.101	1.8	1.07	0.155	15.5	0.139
1.2	0.202	1.5	0.89	0.129	13.7	0.122
3.0	0.505	1.1	0.65	0.094	11.4	0.101
6.0	1.010	0.9	0.53	0.077	10.3	0.091

Specimen identification: V6-3-7,22-67-101-01,15+5 min. @ 150°C
Test dates: 31 July, 1985 & 5 Aug., 1985.
Values taken from graph.
G = shear modulus and δ = loss angle.

Table 3.1 - Preliminary Tests of Elastomer, 1st Set of Bearings

Shear Strain 1st Cycle	G (MN/m^2)	G (ksi)	δ (degrees)	% Critical Damping
0.023	1.22	0.177	14.3	0.127
0.054	0.96	0.139	15.0	0.134
0.106	0.77	0.112	13.7	0.122
0.209	0.63	0.091	11.7	0.104
0.517	0.48	0.070	8.6	0.076
1.040	0.40	0.058	8.1	0.071

Shear Strain 2nd Cycle	G (MN/m^2)	G (ksi)	δ (degrees)	% Critical Damping
0.023	1.16	0.168	14.8	0.132
0.054	0.92	0.136	14.3	0.127
0.106	0.74	0.107	13.2	0.117
0.209	0.62	0.090	11.1	0.098
0.517	0.48	0.070	8.6	0.076
1.040	0.39	0.057	7.6	0.067

Table 3.2 - Preliminary Tests of Elastomer, 2nd and 3rd Sets of Bearings

d_0	P (kips)	K_d (kips/in.)	$\sin\phi$ (%)	Δh_{max} (in.)
1	4.8	1.486	24.50	*
	20.3	1.308	28.53	*
	29.6	1.168	34.05	*
	40.3	1.042	41.18	*
	45.1	0.986	43.94	*
	50.1	0.975	45.84	*
	55.8	0.894	52.45	*
	60.3	0.840	55.93	*
2	4.9	1.137	20.94	*
	10.0	1.126	20.66	*
	20.1	0.993	26.09	*
	29.8	0.880	33.08	*
	40.2	0.768	42.80	*
	45.2	0.700	48.29	*
	50.0	0.594	60.05	*
3.5	10.1	0.981	19.48	0.093
	20.2	0.828	25.61	0.123
	29.6	0.663	36.36	0.135
	40	0.465	59.54	0.148

Note: * Measurement of height reduction too small to be accurate.

Table 4.1 - Cyclic Loading Test Results for 1st Set of Bearings -

P (kips)	d_0 (in.)	Strain(%)	K_d (kips/in.)
10	0.068	2	4.27
	0.170	5	3.34
	0.341	10	2.63
	0.852	25	1.80
	1.705	50	1.37
	2.558	75	1.19
	3.41	100	1.10
	4.262	125	1.00

Table 4.2 - Cyclic Loading Test Results for 1st Set of Bearings

d_0	P (kips)	K_d (kips/in.)	$\sin\phi$ (%)	Δh_{max} (in.)	Specimen
1	5.2	1.056	19.38	*	V14
	5.2	1.079	18.36	*	V15
	4.9	1.081	18.44	*	V16
	5.1	1.164	17.11	*	V17
	5.2	1.101	18.70	*	V18
	5.1	1.096	17.93	*	V19
	5.3	1.137	17.19	*	V20
	5.1	1.035	19.62	*	V21
	5.3	1.110	19.75	*	V22
	5.4	1.017	18.96	*	V23
	4.9	1.257	17.89	*	V24**
	5.2	1.140	18.07	*	V25
	10.0	0.998	19.29	*	V15
	20.2	0.828	25.61	*	V16
	30.1	0.752	33.66	*	V17
	34.8	0.621	43.34	*	V18
	40.4	0.553	53.45	*	V19
2	5.2	0.821	18.79	*	V14
	9.9	0.802	18.06	*	V15
	20.0	0.678	24.80	*	V16
	30.1	0.608	34.45	*	V17
	34.7	0.384	60.06	*	V14
	35.1	0.431	53.15		V18
	40.4	0.423	59.65	*	V19
3.5	5.2	0.698	16.61	0.060	V20
	5.1	0.686	16.83	0.058	V20
	9.8	0.658	18.70	0.097	V21
	20.0	0.566	29.41	0.141	V22
	24.8	0.542	34.11	0.125	V25
	29.9	0.332	60.01	0.149	V15
	30.0	0.323	64.86	0.165	V23

Notes: * Measurement of height reduction too small to be accurate

** Specimen V24 shows abnormally high stiffness; data disregarded

Table 4.3 - Cyclic Loading Test Results for 2nd Set of Bearings

P (kips)	d_0 (in.)	Strain (%)	K_d (kips/in.)
10	0.068	2	2.26
	0.170	5	1.85
	0.341	10	1.44
	0.852	25	1.12
	1.705	50	0.87
	2.558	75	0.78
	3.41	100	0.71
	4.262	125	0.67

Table 4.4 - Cyclic Loading Test Results for 2nd Set of Bearings

d_0	P (kips)	K_d (kips/in.)	$\sin\phi$ (%)	Δh_{max} (in.)	Specimen
1	4.9	1.034	19.35	*	V27
	4.9	0.957	19.64	*	V28
	5.1	1.017	18.89	*	V29
	5.2	1.081	17.91	*	V30
	5.4	1.053	18.15	*	V33
	5.1	1.017	18.23	*	V34
	5.1	1.040	17.65	*	V36
	5.2	1.002	18.01	*	V37
	4.9	1.054	17.65	*	V40
	5.3	1.071	18.02	*	V41
	9.7	0.880	20.83	*	V28
	10.4	0.946	20.73	*	V27
	10.2	0.851	22.89	*	V28
	15.2	0.871	23.54	*	V27
	20.1	0.689	30.52	*	V28
	25.1	0.659	34.61	*	V29
	30.5	0.706	36.07	*	V30
	30.2	0.584	42.63	*	V27
	35.3	0.592	47.83	*	V33
3.5	5.1	0.671	16.69	0.088	V41
	10.2	0.647	18.23	0.095	V34
	15.1	0.564	23.54	0.101	V41
	20.1	0.542	28.14	0.106	V36
	24.9	0.458	38.52	0.116	V37
	29.8	0.339	57.82	0.129	V40

Note: * Measurement of height reduction too small to be accurate.

Table 4.5 - Cyclic Loading Test Results for 3rd Set of Bearings

P (kips)	d_0 (in.)	Strain (%)	K_d (kips/in.)
10	0.068	2	4.27
	0.170	5	3.34
	0.341	10	2.63
	0.852	25	1.80
	1.705	50	1.37
	2.558	75	1.19
	3.41	100	1.10
	4.262	125	1.00

Table 4.6 - Cyclic Loading Test Results for 3rd Set of Bearings

		Consistent Model		Physical Model	
d_0 (in)	tanδ	$(GA_s)_{eff}$ (kip)	$(EI)_{eff}$ (kip-in^2)	$(GA_s)_{eff}$ (kip)	$(EI)_{eff}$ (kip-in^2)
1	0.24	6.157	1897	6.178	2222
2	0.21	4.983	1535	4.988	1794
3.5	0.20	4.155	1280	4.158	1496

Table 4.7 - Parameters Identified for the 1st Set of Bearings

		Consistent Model		Physical Model	
d_0 (in)	tanδ	$(GA_s)_{eff}$ (kip)	$(EI)_{eff}$ (kip-in^2)	$(GA_s)_{eff}$ (kip)	$(EI)_{eff}$ (kip-in^2)
3.5	0.20	4.452	988	4.466	1150

Table 4.8 - Parameters Identified for the 1st Set of Bearings

		Consistent Model		Physical Model	
d_0 (in)	tanδ	$(GA_s)_{eff}$ (kip)	$(EI)_{eff}$ (kip-in^2)	$(GA_s)_{eff}$ (kip)	$(EI)_{eff}$ (kip-in^2)
1	0.19	4.422	1142	4.429	1324
2	0.17	3.668	947	3.677	1099
3.5	0.165	3.083	796	3.076	919

Table 4.9 - Parameters Identified for the 2nd Set of Bearings

		Consistent Model		Physical Model	
d_0 (in)	tanδ	$(GA_s)_{eff}$ (kip)	$(EI)_{eff}$ (kip-in^2)	$(GA_s)_{eff}$ (kip)	$(EI)_{eff}$ (kip-in^2)
1	0.185	3.744	868	3.760	988
3.5	0.15	2.799	648	2.807	737

Table 4.10 - Parameters Identified for the 3rd Set of Bearings

Channel	Instr.	Variable	Channel	Instr.	Variable
1	DCDT	hor. table dis.	43	IFT	column 4c axial
2	DCDT	ver. table dis.	44	IFT	column 4c shear
3	ACCL	hor. table acc.	45	IFT	column 4c mom.
4	ACCL	ver. table acc.	46	DCDT	column 1b tvdisp
5	ACCL	pit. table acc.	47	DCDT	column 1b rvdisp
6	ACCL	roll table acc.	48	DCDT	column 4b tvdisp
7	ACCL	twi. table acc.	49	DCDT	column 4b rvdisp
8	DCDT	v1 table dis.	50	LP	7th floor hdisp.-1a
9	DCDT	v2 table dis.	51	LP	7th floor hdisp.-1b
10	DCDT	v3 table dis.	52	LP	4th floor hdisp.-1a
11	DCDT	v1 table span.	53	LP	4th floor hdisp.-1b
12	DCVT	hor. table vel.	54	LP	bearing hdisp. -1a
13	IFT	column 1a axial	55	LP	bearing hdisp. -1c
14	IFT	column 1a shear	56	LP	perp. bearing disp.
15	IFT	column 1a mom.	57	LP	not activated
16	IFT	column 2a axial	58	LP	not activated
17	IFT	column 2a shear	59	ACCL	1st hacc., frame b
18	IFT	column 2a mom.	60	ACCL	2nd hacc., frame b
19	IFT	column 4a axial	61	ACCL	3rd hacc., frame b
20	IFT	column 4a shear	62	ACCL	4th hacc., frame b
21	IFT	column 4a mom.	63	ACCL	5th hacc., frame b
22	IFT	column 1b axial	64	ACCL	6th hacc., frame b
23	IFT	column 1b shear	65	ACCL	7th hacc., frame b
24	IFT	column 1b mom.	66	ACCL	1st hacc., frame a
25	IFT	column 2b axial	67	ACCL	2nd hacc., frame a
26	IFT	column 2b shear	68	ACCL	3rd hacc., frame a
27	IFT	column 2b mom.	69	ACCL	4th hacc., frame a
28	IFT	column 3b axial	70	ACCL	5th hacc., frame a
29	IFT	column 3b shear	71	ACCL	6th hacc., frame a
30	IFT	column 3b mom.	72	ACCL	7th hacc., frame a
31	IFT	column 4b axial	73	ACCL	7th vacc., column b
32	IFT	column 4b shear	74	ACCL	7th vacc., column b
33	IFT	column 4b mom.	75	ACCL	7th pacc., column
34	IFT	column 1c axial	76	ACCL	7th pacc., column
35	IFT	column 1c shear	77	ACCL	1st vacc., column 1a
36	IFT	column 1c mom.	78	ACCL	1st vacc., column 4a
37	IFT	column 2c axial	79	ACCL	1st vacc., column 1c
38	IFT	column 2c shear	80	ACCL	1st vacc., column 4c
39	IFT	column 2c mom.	81	ACCL	not activated
40	IFT	column 3c axial	82	DCDT	horiz. table displ.
41	IFT	column 3c shear	83	DCDT	horiz. table displ.
42	IFT	column 3c mom.			

DCDT - Direct Current Displacement Transducer

DCVT - Direct Current Velocity Transducer

ACCL - Accelerometer

IFT - Internal Force Transducer

LP - Linear Voltage Displacement Transducer

Table 5.1 - Model Instrumentation List

FILE NO.	RUN	SPAN	PK. TABLE ACCEL.(g's)	PK. MODEL ACCEL.(g's)	REL. BEARING DISPL.(in.)	UPLIFT (Y/N)
860116.02	.5hz Sine	20	.026	.024	.018	N
860116.03	.7hz Sine	20	.050	.035	.036	N
860116.04	.9hz Sine	20	.060	.064	.123	N
860116.05	1.0hz Sine	20	.065	.080	.240	N
860116.06	1.1hz Sine	20	.084	.220	1.136	N
860116.07	1.15hz Sine	20	.081	.212	1.082	N
860116.08	1.2hz Sine	20	.078	.198	.966	N
860116.09	1.3hz Sine	20	.090	.172	.788	N
860116.10	1.4hz Sine	20	.105	.162	.655	N
860116.11	1.6hz Sine	20	.126	.168	.496	N
860116.12	1.8hz Sine	20	.150	.159	.392	N
860123.03	2.0hz Sine	20	.030	.068	.066	N
860123.04	3.0hz Sine	20	.081	.086	.038	N
860123.05	4.0hz Sine	20	.152	.147	.012	N
860123.06	4.5hz Sine	20	.184	.210	.019	N
860123.07	4.7hz Sine	20	.209	.278	.056	N
860123.08	4.8hz Sine	20	.146	.197	.036	N
860123.09	4.9hz Sine	20	.205	.385	.123	N
860123.10	5.0hz Sine	20	.207	.369	.140	N
860123.11	5.1hz Sine	20	.190	.322	.126	N
860123.12	5.2hz Sine	20	.214	.298	.128	N
860123.13	5.3hz Sine	20	.244	.292	.134	N
860123.14	5.4hz Sine	20	.256	.274	.131	N
860123.15	6.0hz Sine	20	.307	.195	.108	N

Table 5.2 - Preliminary Tests of R.C. Model on 1st Set of Bearings

FILE NO.	RUN	SPAN	PK. TABLE ACCEL.(g's)	PK. MODEL ACCEL.(g's)	REL. BEARING DISPL.(in.)	UPLIFT (Y/N)
860116.13	√5 ec1	20	.218	.075	.048	N
860116.14	√5 taft1	50	.300	.100	.127	N
860116.15	√5 ec1	100	.164	.173	.278	N
860116.16	√5 ec1	100	.163	.178	.272	N
860116.17	√5 ec1	100	.005	.007	.004	N
860117.01	√5 ec1	300	.465	.386	1.304	N
860117.02	√5 ec1	450	.699	.454	2.298	Y
860117.03	√5 ec1	450	.728	.485	2.467	Y
860121.01	√5 ec1	450	.705	.510	2.226	Y
860122.01	√5 ec2	100	.233	.267	.424	N
860122.02	√5 taft2	100	.225	.242	.445	N
860122.03	√5 park2	100	.130	.191	.266	N
860122.04	√5 pac2	100	.183	.168	.490	N
860122.05	√5 miyagi	100	.147	.164	.370	N
860122.06	√5 sf2	100	.284	.183	.183	N
860123.16	√5 sf2	100	.802	.371	.480	N
860123.17	√5 sf2	200	1.338	.516	.984	N
860123.18	√5 sf2	230	1.418	.554	1.135	N
860123.19	√5 ec2	230	.532	.411	1.506	N
860123.20	√5 taft2	220	.539	.368	1.020	N
860123.21	√5 park2	220	.324	.316	1.005	N
860123.22	√5 pac2	220	.412	.267	1.222	N
860123.23	√5 miyagi	220	.304	.313	1.202	N
860123.24	√5 miyagi	330	.443	.401	1.717	N
860123.25	√5 miyagi	350	.492	.415	1.815	N
860123.26	√5 taft2	350	.919	.447	1.612	N
860123.27	√5 park2	350	.538	.465	1.708	N
860123.28	√5 pac2	350	.646	.361	1.932	N
860123.29	√5 ec2	350	.792	.549	2.921	Y
860124.01	√5 ec2	200	.006	.020	.005	N
860124.02	√5 ec2	200	.449	.398	1.184	N
860124.03	√5 ec2	200	.452	.378	1.181	N
860124.04	√5 sf2	300	1.588	.648	1.436	N
860124.05	√5 ec1	100	.166	.179	.266	N
860124.06	√5 buc1	100	.126	.168	.417	N
860124.07	√5 buc1	200	.212	.257	1.289	N
860124.08	√2 ec2	200	.251	.252	.887	N
860124.09	√2 ec2	300	.340	.285	1.336	N

Table 5.3 - Earthquake Tests of R.C. Model on 1st Set of Bearings

FILE NO.	RUN	SPAN	PK. TABLE ACCEL.(g's)	PK. MODEL ACCEL.(g's)	REL. BEARING DISPL.(in.)	UPLIFT (Y/N)
860129.03	.7hz Sine	20	.058	.040	.173	N
860129.04	.8hz Sine	20	.066	.068	.392	N
860129.05	.9hz Sine	20	.063	.213	1.853	N
860129.06	.95hz Sine	20	.069	.176	1.529	N
860129.07	1.0hz Sine	20	.076	.156	1.309	N
860129.08	1.02hz Sine	20	.080	.149	1.234	N
860129.09	1.2hz Sine	20	.091	.111	.825	N
860129.10	1.1hz Sine	20	.083	.132	1.012	N
860129.11	1.5hz Sine	20	.146	.122	.548	N
860129.12	2.0hz Sine	20	.207	.115	.390	N
860129.13	2.5hz Sine	20	.288	.133	.326	N
860129.14	3.0hz Sine	20	.402	.194	.269	N
860130.14	Random Noise	40	.902	.128	.133	N

Table 5.4 - Preliminary Tests of R.C. Model on 2nd Set of Bearings

FILE NO.	RUN	SPAN	PK. TABLE ACCEL.(g's)	PK. MODEL ACCEL.(g's)	REL. BEARING DISPL.(in.)	UPLIFT (Y/N)
860129.19	ec2	100	.091	.103	.411	N
860129.20	ec2	200	.156	.166	1.066	N
860129.21	√2 ec2	100	.139	.097	.496	N
860129.22	√2 ec2	200	.259	.154	.922	N
860129.23	√5 ec2	200	.508	.315	2.192	N
860129.24	√2 ec2	350	.370	.241	1.761	N
860129.25	ec2	400	.267	.278	2.122	N
860130.01	√5 taft2	300	.771	.302	2.009	N
860130.02	√2 taft2	375	.370	.283	2.107	N
860130.03	taft2	500	.243	.238	1.540	N
860130.04	√5 miyagi	450	.579	.309	1.702	N
860130.05	√2 miyagi	450	.279	.317	2.350	N
860130.06	miyagi	450	.138	.238	1.992	N
860130.07	√5 buc1	200	.230	.250	2.080	N
860130.08	√2 buc1	400	.221	.255	2.271	N
860130.09	buc1	500	.144	.190	1.595	N
860130.10	√5 park2	325	.489	.366	1.991	N
860130.11	√5 pac2	325	.636	.272	1.852	N
860130.12	√5 sf2	250	1.478	.355	1.151	N
860130.13	√5 mex2	150	.105	.252	2.181	N
860131.03	√5 ec2	350	.803	.364	3.880	Y
860131.04	√5 ec2	350	.774	.353	3.889	Y
860131.05	√5 ec2	350	.783	.369	3.952	Y
860204.04	√5 ec2	300	.678	.384	3.501	Y
860204.05	√5 ec2	300	.685	.411	3.526	Y
860204.06	√2 taft2	200	.189	.160	.800	N
860204.07	√2 ec2	450	.465	.304	2.568	N

Table 5.5 - Earthquake Tests of R.C. Model on 2nd Set of Bearings

FILE NO.	RUN	SPAN	PK. TABLE ACCEL.(g's)	PK. MODEL ACCEL.(g's)	REL. BEARING DISPL.(in.)	UPLIFT (Y/N)
860211.01	.7hz Sine	50	.086	.086	.512	N
860211.02	.8hz Sine	35	.078	.112	.820	N
860211.03	.9hz Sine	20	.053	.130	.982	N
860211.04	.95hz Sine	15	.0554	.116	.840	N
860211.05	1.0hz Sine	15	.048	.132	.910	N
860211.06	1.05hz Sine	15	.050	.122	.794	N
860211.07	1.1hz Sine	20	.069	.132	.857	N
860211.08	1.2hz Sine	25	.110	.113	.698	N
860211.09	1.5hz Sine	26	.164	.126	.588	N
860211.10	2.0hz Sine	20	.166	.099	.316	N
860211.11	Random Noise	40	1.370	.252	.250	N

Table 5.6 - Preliminary Tests of R.C. Model on 3rd Set of Bearings

FILE NO.	RUN	SPAN	PK. TABLE ACCEL.(g's)	PK. MODEL ACCEL.(g's)	REL. BEARING DISPL.(in.)	UPLIFT (Y/N)
860211.12	√2 ec2	350	.382	.259	1.707	N
860211.13	√5 ec2	200	.471	.341	2.158	N
860211.14	√5 ec2	300	.624	.429	3.196	Y
860211.15	√5 ec2	300	.674	.435	3.415	Y
860211.16	√2 ec2	450	.466	.298	2.512	N
860211.17	√2 ec2	450	.460	.299	2.532	N
860227.01	√5 taft2	300	.783	.299	2.105	N
860227.02	√5 miyagi	450	.568	.289	1.703	N
860227.03	√5 buc1	200	.220	.248	2.174	N
860227.04	√5 park2	325	.483	.379	1.996	N
860227.05	√5 pac2	325	.646	.286	1.864	N
860227.06	√5 sf2	250	1.457	.343	1.119	N
860227.07	√5 mex2	150	.161	.181	1.292	N
860227.08	√5 ec2	350	.839	.467	3.782	Y
860228.01	√5 taft2	250	.233	.218	1.159	N
860304.01	√5 miyagi	450	.565	.293	1.728	N
860304.02	√5 miyagi	450	.558	.290	1.658	N
860304.03	√5 miyagi	450	.579	.292	1.658	N
860304.04	√5 sf2	250 h&v	1.454	.382	1.127	N
860304.05	√5 mex2	200	.204	.240	1.653	N
860304.06	√5 mex2	250	.241	.272	2.070	N
860304.07	√5 ec2	350 h&v	.786	.491	3.494	Y
860304.08	√5 mex2	300	.270	.317	2.564	N
860304.09	√5 mex2	350	.361	.327	2.775	Y
860304.10	√5 ec2	350 h&v	.780	.475	3.660	Y

Table 5.7 - Earthquake Tests of R.C. Model on 3rd Set of Bearings

SYMBOL	EARTHQUAKE	DATE	PGA (g)
ec1,ec2	Imperial Valley El Centro Site	May 18,1940 S00E	0.35
taft1,taft2	Kern County, Calf. Taft Lincoln School Tunnel	July 21,1952 S69E	0.18
sf1,sf2	San Francisco Golden Gate Park	March 22,1957 S80E	0.10
park1,park2	Parkfield, Calf. Cholame,Shandon,CA array #2	June 27,1966 N65E	0.49
pac1,pac2	San Fernando Pacoima Dam, Calif.	Feb. 9,1971 S14W	1.08
miyagi	Miyagi-Ken-Oki Tohoku University	June 12th 1978 S00E	0.24
buc1	Bucharest Building Research Inst.	March 7th, 1977 EW	0.21
mex1,mex2	Mexico City SCT Site	September 19, 1985 S60E	0.20

Note: In this report, if the symbol for the earthquake has a suffix of "1", then no additional filtering was applied to the signal. A suffix of "2" means that the un-time-scaled signal was high pass filtered at 0.1 Hz. For example, "ec1" is unfiltered, "ec2" was high pass filtered.

All are digitized records at EERC Richmond, California.

Table 5.8 - Earthquake Signals Used In Tests

Test	Rubber Shear Strain (%)	Damping Ratio (%)	Fund. Horiz. Freq. (Hz.)	Fund. Tors. Freq. (Hz.)	2nd Horiz. Freq. (Hz.)
Free Vibration	3.5	5	2.45	3.1	7.6
Harmonic Vibration	32	11.5	1.15	2.3	4.9
White Noise	6.5	n.a.	1.3	2.2	5.0

Table 6.1 - Preliminary Shaking Tests, 1st Set of Bearings.

Test	Fund. Horiz. Frequency (Hz.)	Rigid Body Theory (Hz.)
Free Vibration	1.43	0.96
Harmonic Vibration	0.94	0.96
White Noise	0.85	0.96

Table 6.2 - Comparison of Results at 100% Shear Strain

EARTHQUAKE	PK. TABLE ACCEL.(g's)	BASE SHEAR (kips)	BASE SHEAR RATIO (% W)
Bucharest	.126g	10.41	10.2
Bucharest	.212g	21.41	24.0
El Centro	.233g	10.95	10.8
El Centro	.532g	23.35	22.9
El Centro	.792g	31.11	30.5
Miyagi	.147g	10.64	10.4
Miyagi	.304g	20.83	20.4
Pacoima Dam	.183g	12.21	12.0
Pacoima Dam	.412g	20.66	20.3
Pacoima Dam	.646g	28.59	28.1
Parkfield	.130g	8.29	8.1
Parkfield	.324g	19.31	19.0
Parkfield	.538g	26.15	25.7
San Francisco	.802g	13.17	12.9
San Francisco	1.338g	19.00	18.7
San Francisco	1.418g	20.16	19.8
Taft	.225g	12.36	12.1
Taft	.539g	18.25	17.9
Taft	.919g	24.97	24.5

Table 6.3 - Peak Base Shear, 1st Set of Bearings

Test	Rubber Shear Strain (%)	Damping Ratio (%)	Fund. Horiz. Freq. (Hz.)	Fund. Tors. Freq. (Hz.)	2nd Horiz. Freq. (Hz.)
Free Vibration	7.0	7	1.72	2.6	5.9
Harmonic Vibration	35	9.5	0.95	2.1	4.8
White Noise	7.0	n.a.	1.2	2.1	4.5

Table 7.1 - Preliminary Shaking Tests, 2nd Set of Bearings.

Test	Fund. Horiz. Frequency (Hz.)	Rigid Body Theory (Hz.)
Free Vibration	1.16	0.82
Harmonic Vibration	0.81	0.82
White Noise	0.81	0.82

Table 7.2 - Comparison of Results at 100% Shear Strain

EARTHQUAKE	PK. TABLE ACCEL.(g's)	BASE SHEAR (kips)	BASE SHEAR RATIO (%W)
Bucharest	.230g	20.51 kips	20.0%
El Centro*	.146g	12.92 kips	12.6%
El Centro	.508g	22.54 kips	22.0%
El Centro	.678g	28.28 kips	27.6%
El Centro	.783g	26.19 kips	25.6%
Mexico	.105g	21.51 kips	21.0%
Miyagi	.579g	18.86 kips	18.4%
Parkfield	.489g	21.40 kips	20.9%
Pacoima Dam	.636g	19.78 kips	19.3%
San Francisco	1.478g	14.69 kips	14.3%
Taft	.771g	21.61 kips	21.1%

Table 7.3 - Peak Base Shear, 2nd Set of Bearings

Test	Rubber Shear Strain (%)	Damping Ratio (%)	Fund. Horiz. Freq. (Hz.)	Fund. Tors. Freq. (Hz.)	2nd Horiz. Freq. (Hz.)
Harmonic Vibration	37	10.5	0.90	2.1	4.8
White Noise	7.0	n.a.	1.1	2.1	4.3

Table 8.1 - Preliminary Shaking Tests, 3rd Set of Bearings.

Test	Fund. Horiz. Frequency (Hz.)	Rigid Body Theory (Hz.)
Harmonic Vibration	0.77	0.82
White Noise	0.74	0.82

Table 8.2 - Comparison of Results at 100% Shear Strain

EARTHQUAKE	PK. TABLE ACCEL.(g's)	BASE SHEAR (kips)	BASE SHEAR RATIO (%W)
Bucharest	.220g	20.50 kips	20.1%
El Centro	.471g	23.02 kips	22.6%
El Centro	.674g	30.88 kips	30.3%
El Centro	.839g	29.76 kips	29.2%
Mexico	.161g	14.04 kips	13.8%
Mexico	.204g	17.12 kips	16.8%
Mexico	.241g	19.96 kips	19.6%
Mexico	.270g	21.41 kips	21.0%
Mexico	.361g	23.25 kips	22.8%
Miyagi	.568g	17.68 kips	17.4%
Parkfield	.483g	20.94 kips	20.6%
Pacoima Dam	.646g	19.34 kips	19.0%
San Francisco	1.457g	14.37 kips	14.0%
Taft	.233g	13.14 kips	12.8%
Taft	.783g	21.23 kips	20.7%

Table 8.3 - Peak Base Shear, 3rd Set of Bearings

1st Set of Bearings

EQ Signal	PGA	A_a	A_v	D_{exp} (in.)	$\frac{D_{PGA}}{D_{exp}}$	$\frac{D_a}{D_{exp}}$	$\frac{D_v}{D_{exp}}$
Bucharest	.212g	.143	.387	1.29	0.98	0.67	1.79
El Centro	.792g	.572	.859	2.92	1.21	0.88	1.33
Miyagi	.304g	.216	.425	1.20	1.13	0.81	1.58
Pacoima Dam	.646g	.520	.492	1.93	1.50	1.20	1.13
Parkfield	.538g	.340	.315	1.71	1.41	0.89	0.83
San Francisco	1.418g	1.460	.628	1.14	3.71	3.82	1.65
Taft	.919g	.647	.623	1.61	2.55	1.80	1.72

2nd Set of Bearings

EQ Signal	PGA	A_a	A_v	D_{exp} (in.)	$\frac{D_{PGA}}{D_{exp}}$	$\frac{D_a}{D_{exp}}$	$\frac{D_v}{D_{exp}}$
Bucharest	.230g	.150	.389	2.08	0.83	0.54	1.40
El Centro	.783g	.584	.861	3.95	1.11	0.83	1.22
Mexico	.105g	.081	.248	2.18	0.49	0.37	1.18
Miyagi	.579g	.372	.863	1.70	1.91	1.22	2.84
Pacoima Dam	.636g	.520	.492	1.85	1.92	1.57	1.49
Parkfield	.489g	.311	.434	1.99	1.38	0.87	1.21
San Francisco	1.478g	1.545	.693	1.15	4.79	5.00	2.24
Taft	.771g	.562	.532	2.01	2.14	1.56	1.48

3rd Set of Bearings

EQ Signal	PGA	A_a	A_v	D_{exp} (in.)	$\frac{D_{PGA}}{D_{exp}}$	$\frac{D_a}{D_{exp}}$	$\frac{D_v}{D_{exp}}$
Bucharest	.220g	.149	.387	2.17	0.76	0.51	1.34
El Centro	.839g	.591	.863	3.78	1.24	0.87	1.28
Mexico	.361g	.191	.848	2.78	1.31	0.69	3.05
Miyagi	.568g	.379	.874	1.70	1.87	1.25	2.87
Pacoima Dam	.646g	.520	.492	1.86	1.94	1.56	1.47
Parkfield	.483g	.306	.434	2.00	1.35	0.86	1.22
San Francisco	1.457g	1.536	.702	1.12	4.85	5.11	2.33
Taft	.783g	.560	.541	2.10	2.08	1.49	1.43

Table 9.1 - Design and Experimental Bearing Displacements

1st Set of Bearings

EQ Signal	PK. TABLE ACCEL.(g's)	D_{meas} (in.)	k_{max} (kips/in.)	D_{calc} (in.)	V_{meas} (kips)	V_{calc} (kips)	$\frac{V_{calc}}{V_{meas}}$
Bucharest	.212	1.289	1.58	3.56	21.41	45.0	2.10
El Centro	.792	2.921	1.15	5.81	31.11	53.5	1.72
Miyagi	.304	1.202	1.62	1.87	20.83	54.5	2.62
Pacoima Dam	.646	1.932	1.32	4.41	28.59	46.6	1.63
Parkfield	.538	1.708	1.37	3.59	26.15	39.3	1.50
San Francisco	1.418	1.135	1.66	8.63	20.16	114.6	5.68
Taft	.919	1.612	1.42	6.05	24.97	68.7	2.75

2nd Set of Bearings

EQ Signal	PK. TABLE ACCEL.(g's)	D_{meas} (in.)	k_{max} (kips/in.)	D_{calc} (in.)	V_{meas} (kips)	V_{calc} (kips)	$\frac{V_{calc}}{V_{meas}}$
Bucharest	.230	2.080	.84	5.32	20.51	35.8	1.74
El Centro	.783	3.952	.69	7.37	26.19	40.7	1.55
Mexico	.105	2.181	.83	2.43	21.51	16.1	0.75
Miyagi	.579	1.702	.89	4.82	18.86	34.3	1.82
Pacoima Dam	.636	1.852	.86	5.35	19.78	36.8	1.86
Parkfield	.489	1.991	.85	4.16	21.40	28.3	1.32
San Francisco	1.478	1.151	1.05	11.33	14.69	95.2	6.48
Taft	.771	2.009	.85	6.55	21.61	44.5	2.06

3rd Set of Bearings

EQ Signal	PK. TABLE ACCEL.(g's)	D_{meas} (in.)	k_{max} (kips/in.)	D_{calc} (in.)	V_{meas} (kips)	V_{calc} (kips)	$\frac{V_{calc}}{V_{meas}}$
Bucharest	.220	2.174	.85	5.05	20.50	34.3	1.68
El Centro	.839	3.782	.72	7.76	29.76	44.7	1.50
Mexico	.361	2.775	.80	8.53	23.25	54.6	2.35
Miyagi	.568	1.703	.90	4.69	17.68	33.8	1.91
Pacoima Dam	.646	1.864	.88	5.38	19.34	37.9	1.96
Parkfield	.483	1.996	.87	4.07	20.94	28.3	1.35
San Francisco	1.457	1.119	.99	11.53	14.37	91.3	6.35
Taft	.783	2.105	.86	6.59	21.23	45.3	2.14

Table 9.2 - Design and Experimental Base Shear

FIGURES

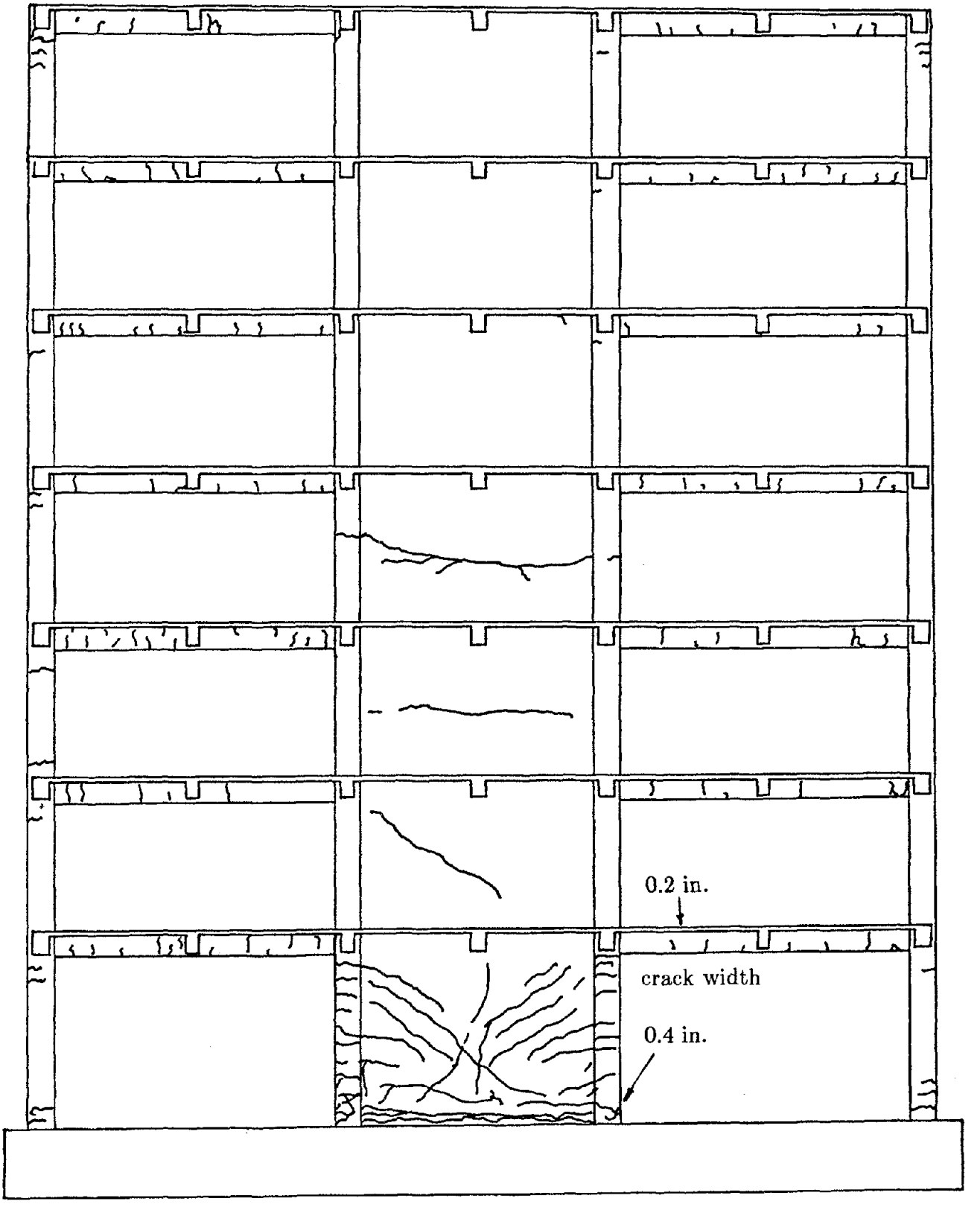

Figure 2.1 - Diagram of Cracks in Fixed-Base R.C. Shear Wall Model

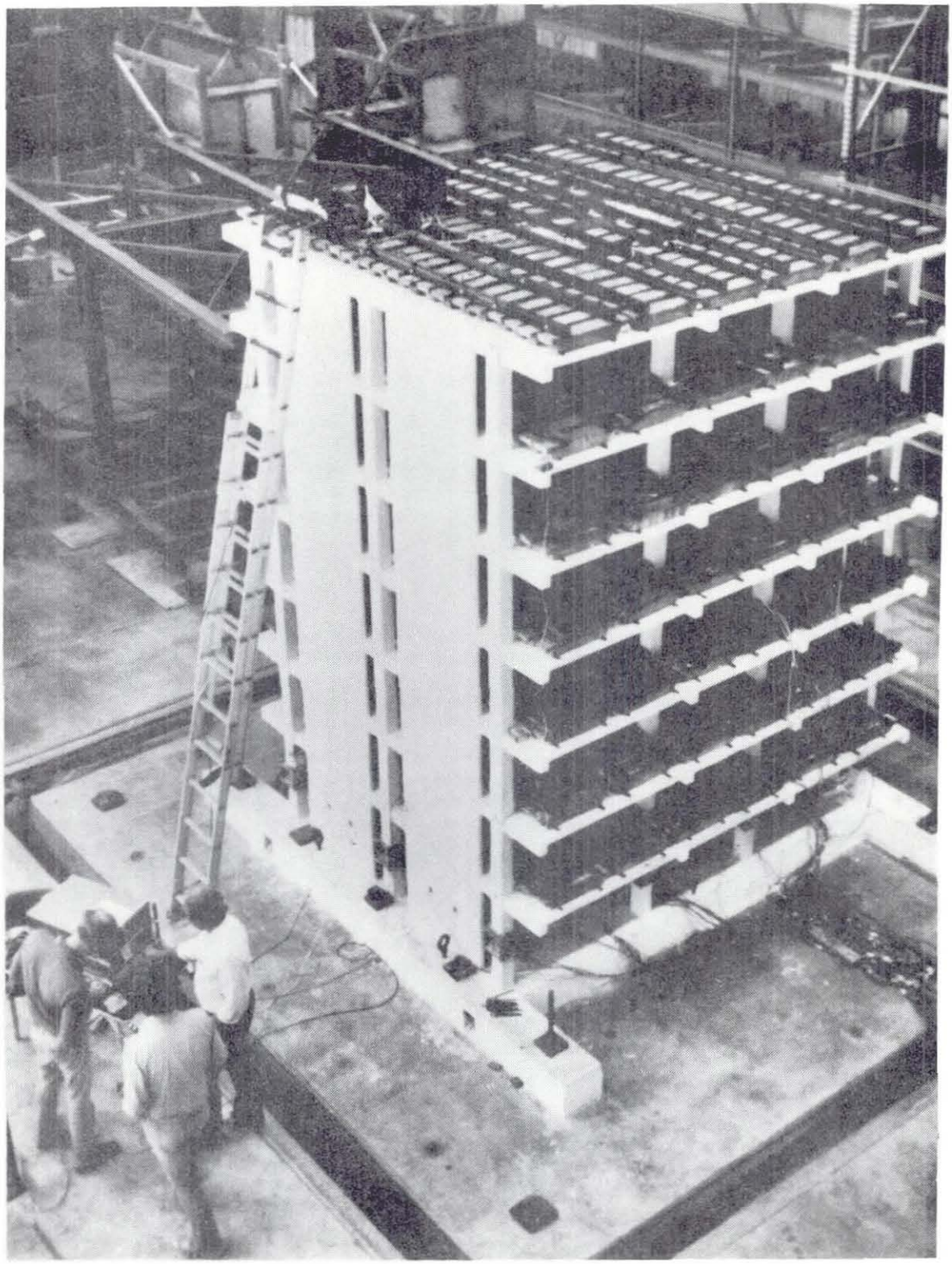

Figure 2.2 - Overview of Fixed-Base R.C. Model

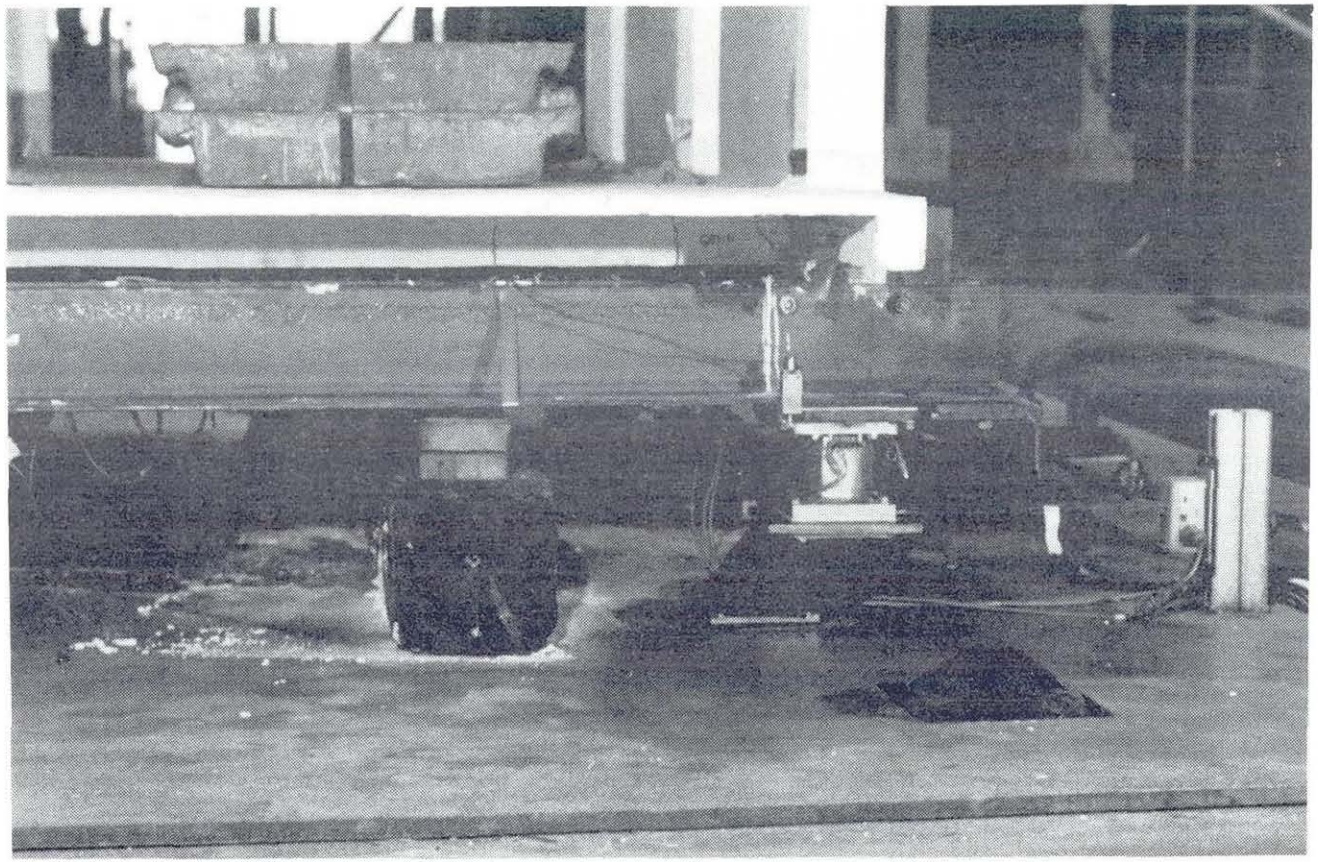

Figure 2.3 - Close-up of Base-Isolated R.C. Model

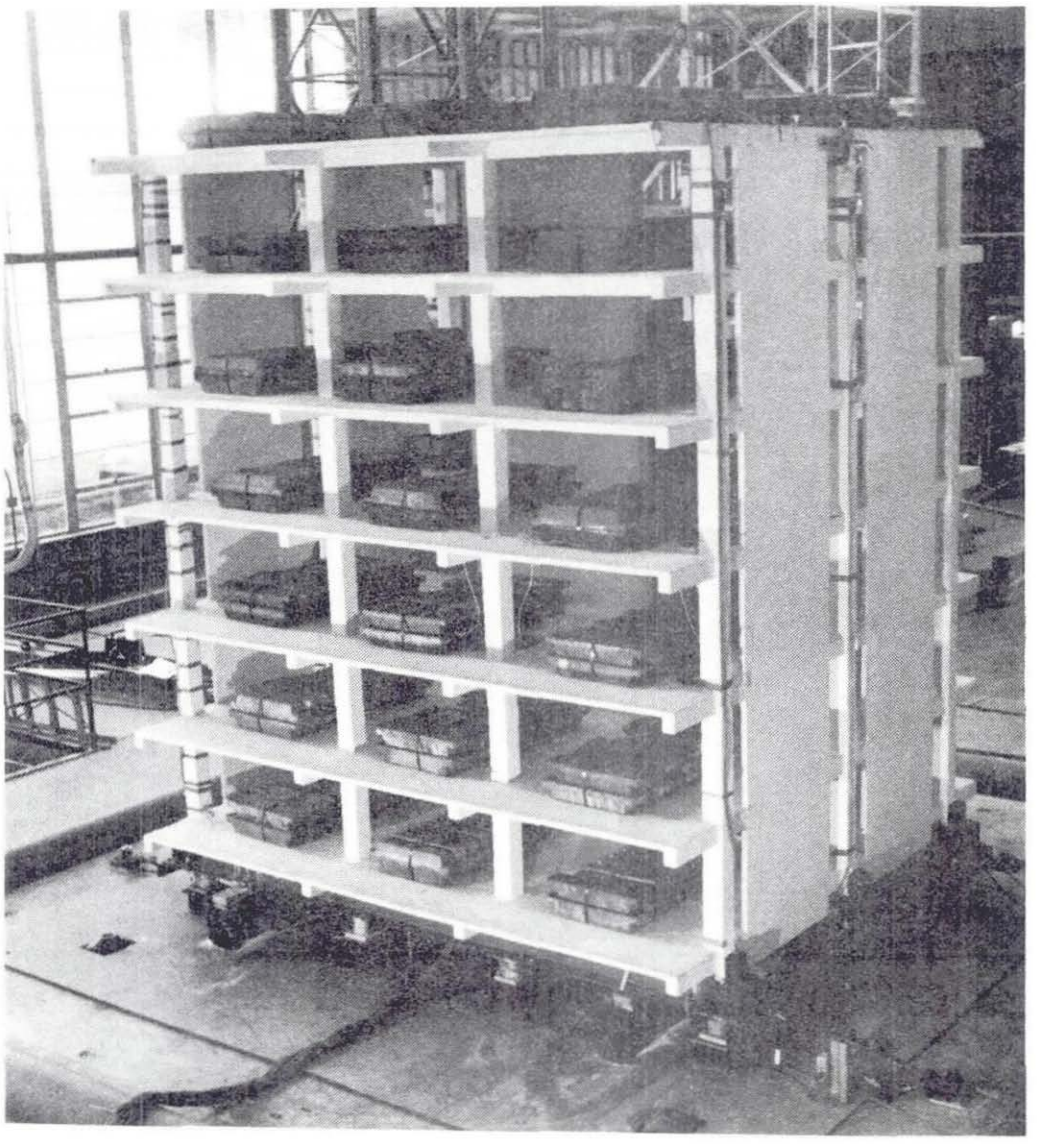

Figure 2.4 - Overview of Base-Isolated R.C. Model

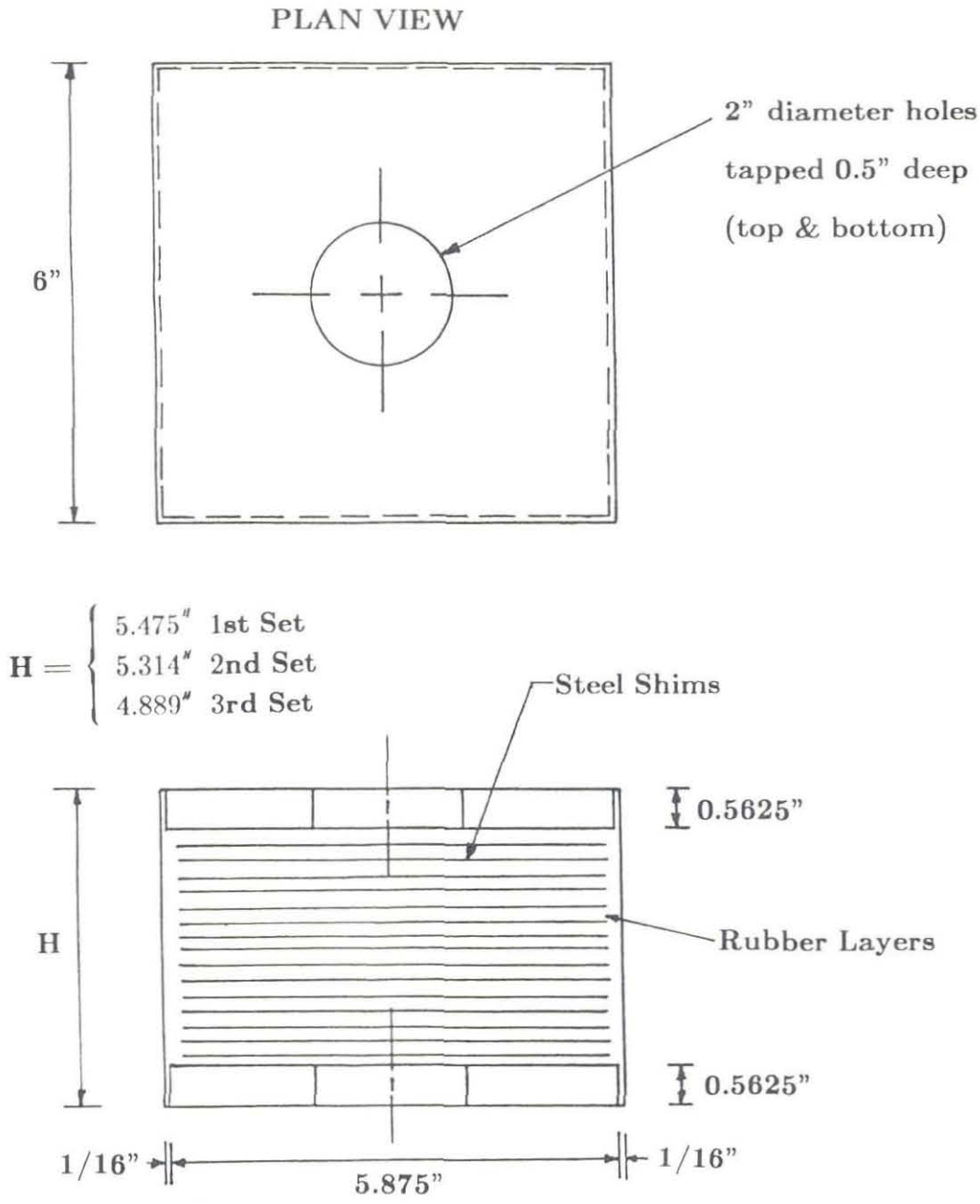

15 - 0.06" Steel Shims (1st Set) 16 - 0.213" Rubber Layers (1st Set)

17 - 0.037" Steel Shims (2nd Set) 18 - 0.198" Rubber Layers (2nd & 3rd Sets)

17 - 0.012" Steel Shims (3rd Set)

Figure 3.1 - Base Isolation Bearing Designs

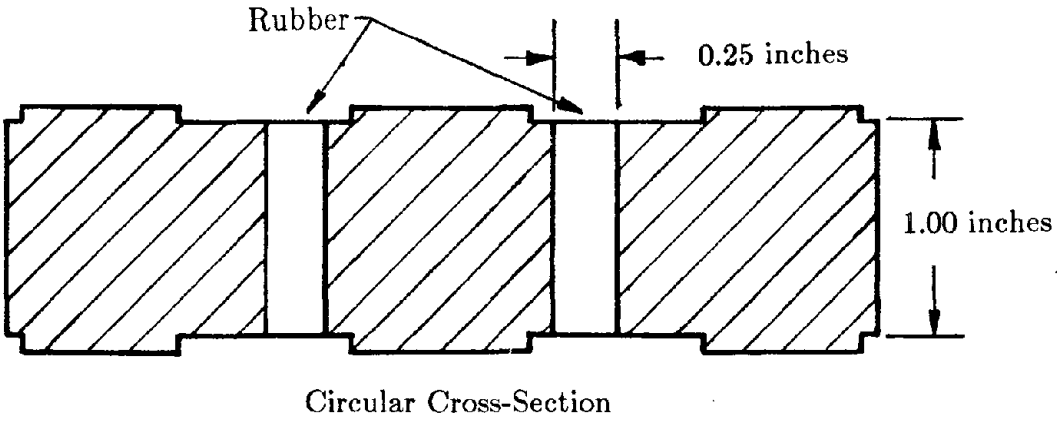

Figure 3.2 - Natural Rubber Shear Test Specimens

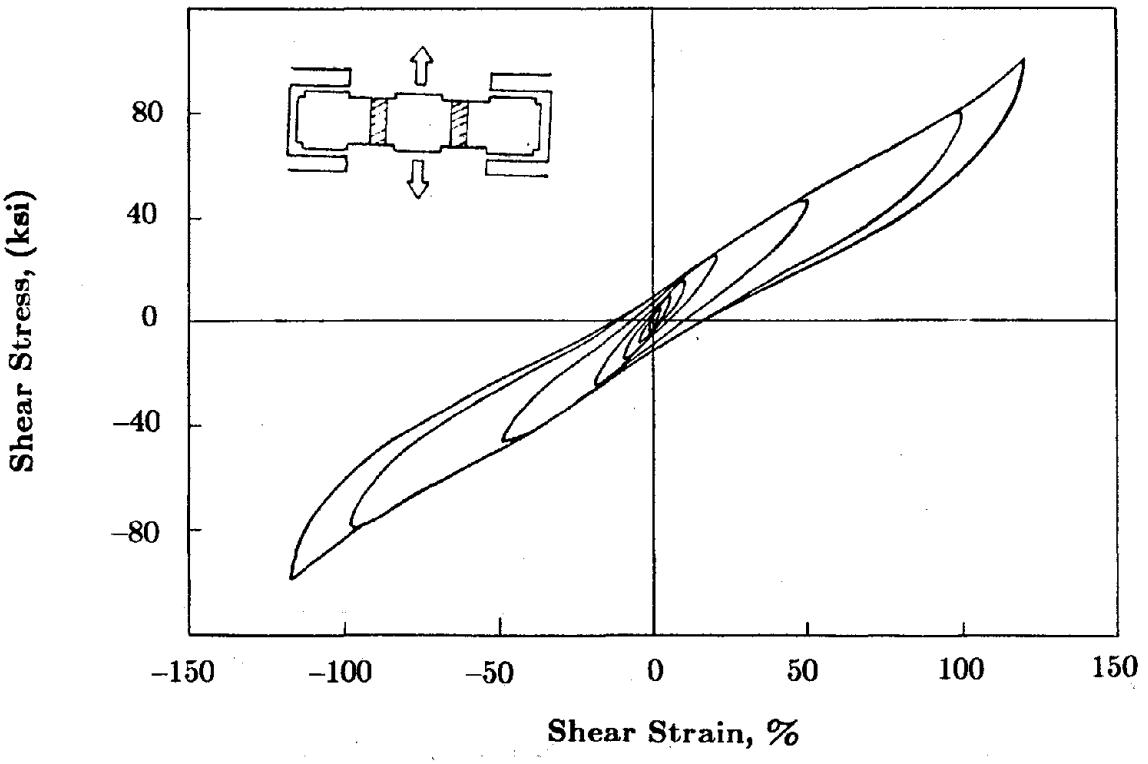

Figure 3.3 - Hysteresis Loops for Shear Tests at MRPRA

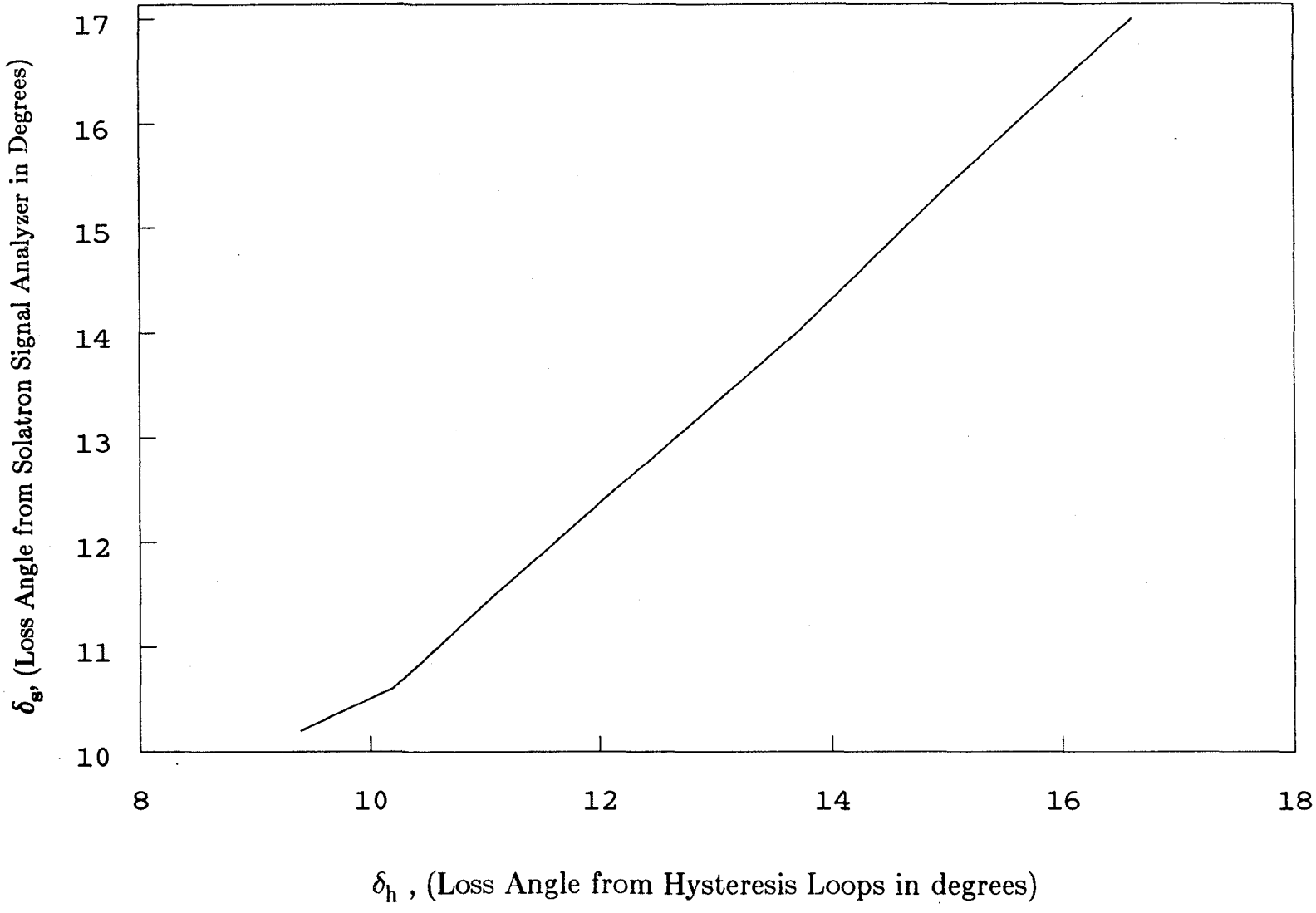

Figure 3.4 - Signal Analyzer Results from Tests at MRPRA

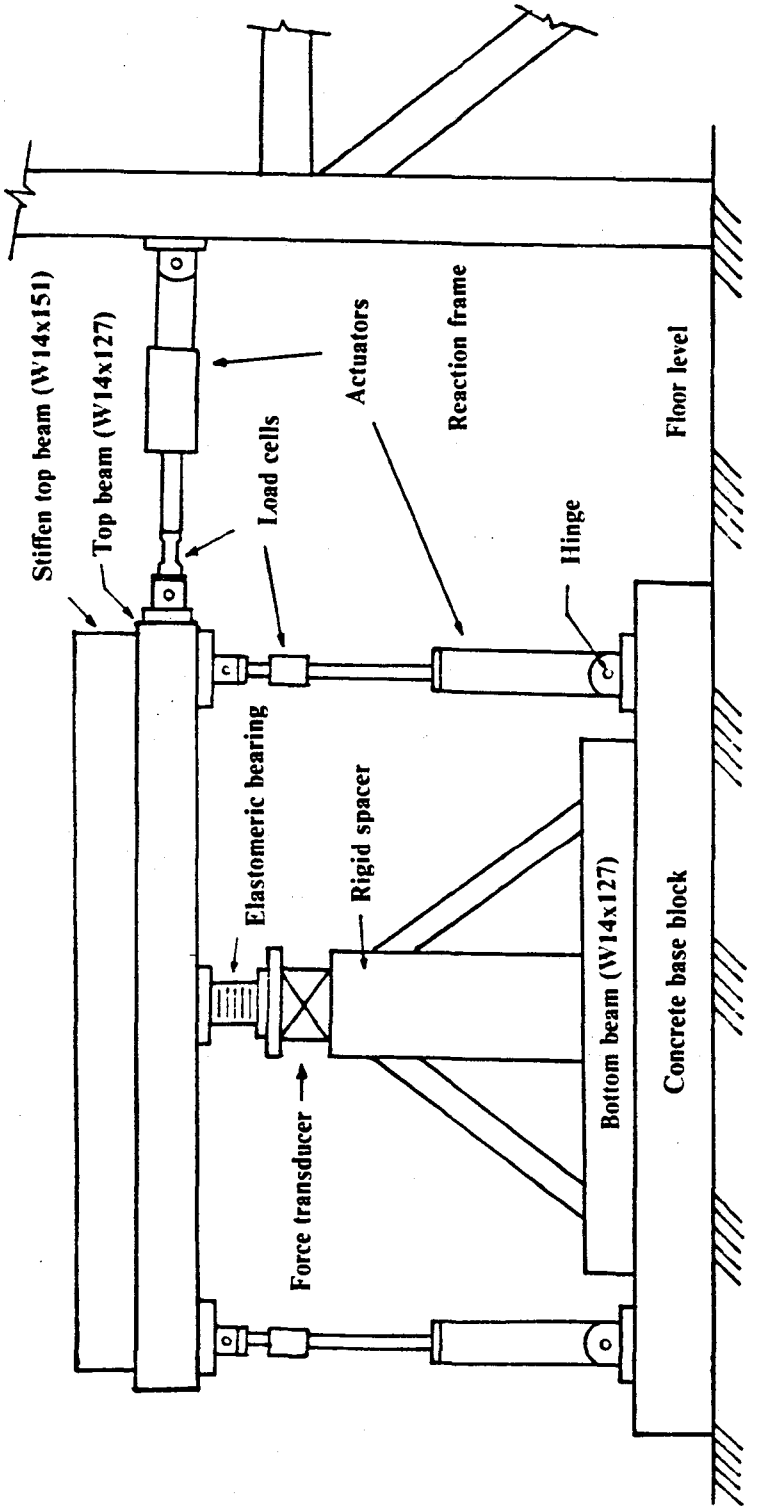

Figure 4.1 - Diagram of EERC Shear Test Apparatus

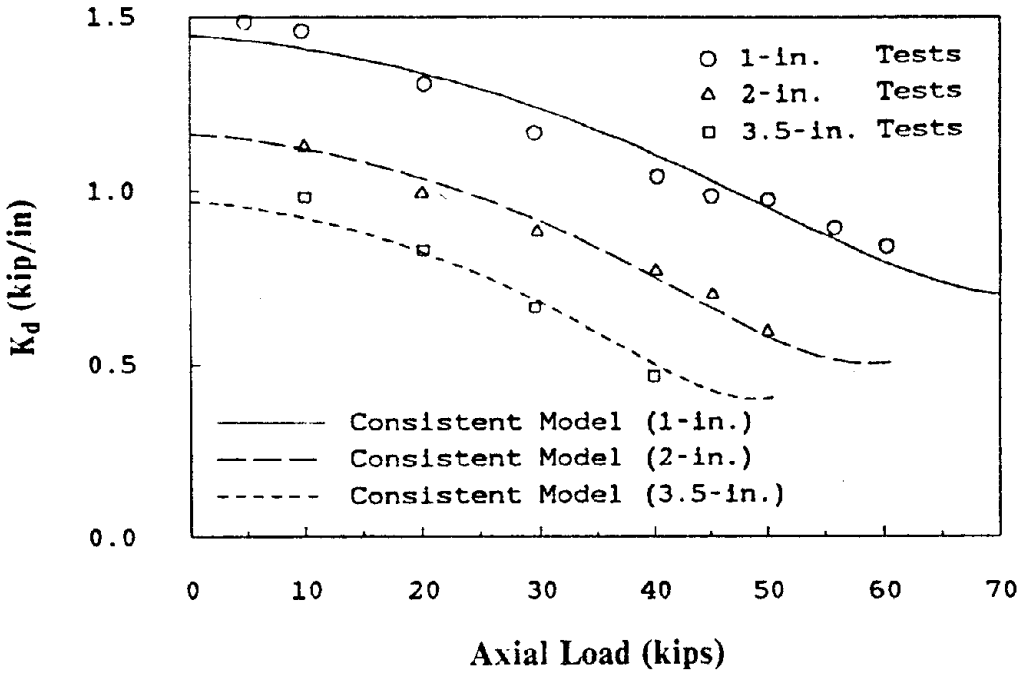

(a) Consistent Model

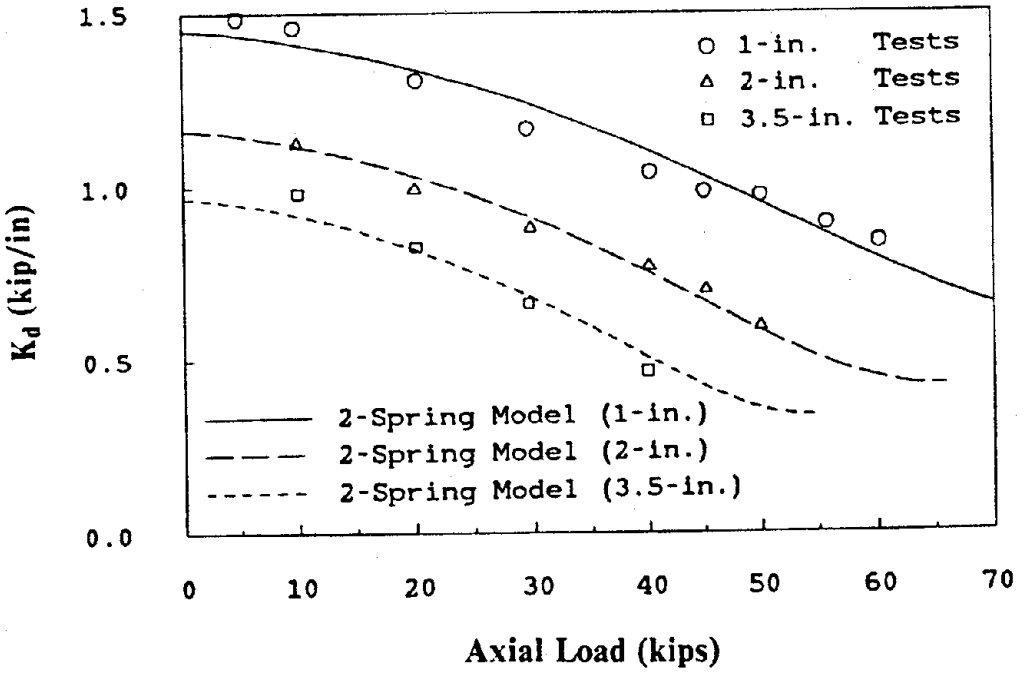

(b) 2-Spring Model

Figure 4.2 - Dynamic Shear Stiffness of 1st Set of Bearings

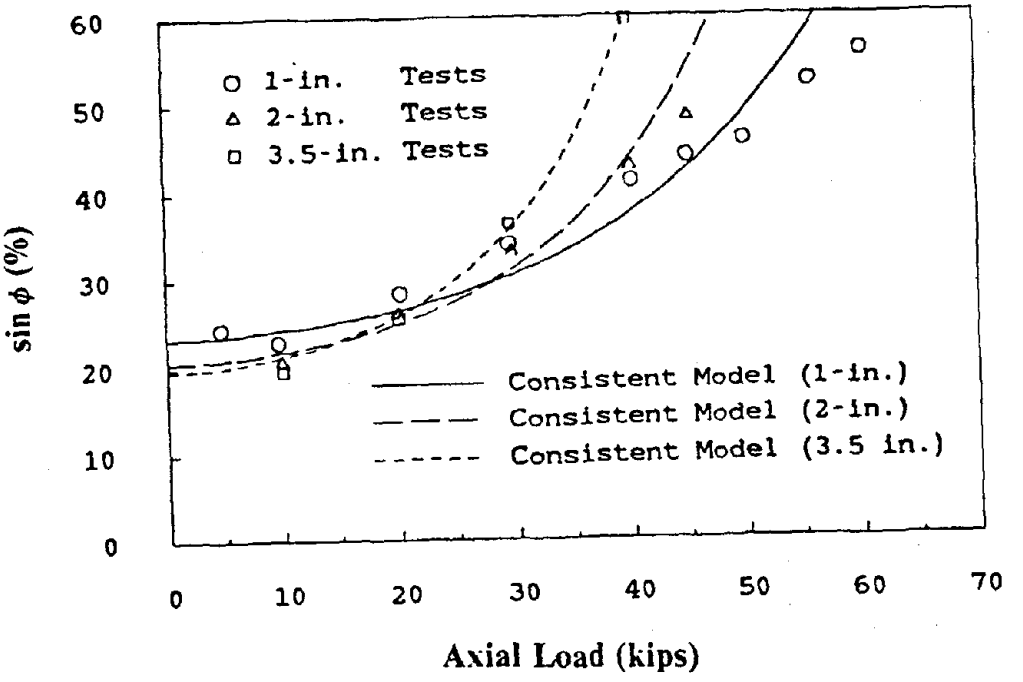

(a) Consistent Model

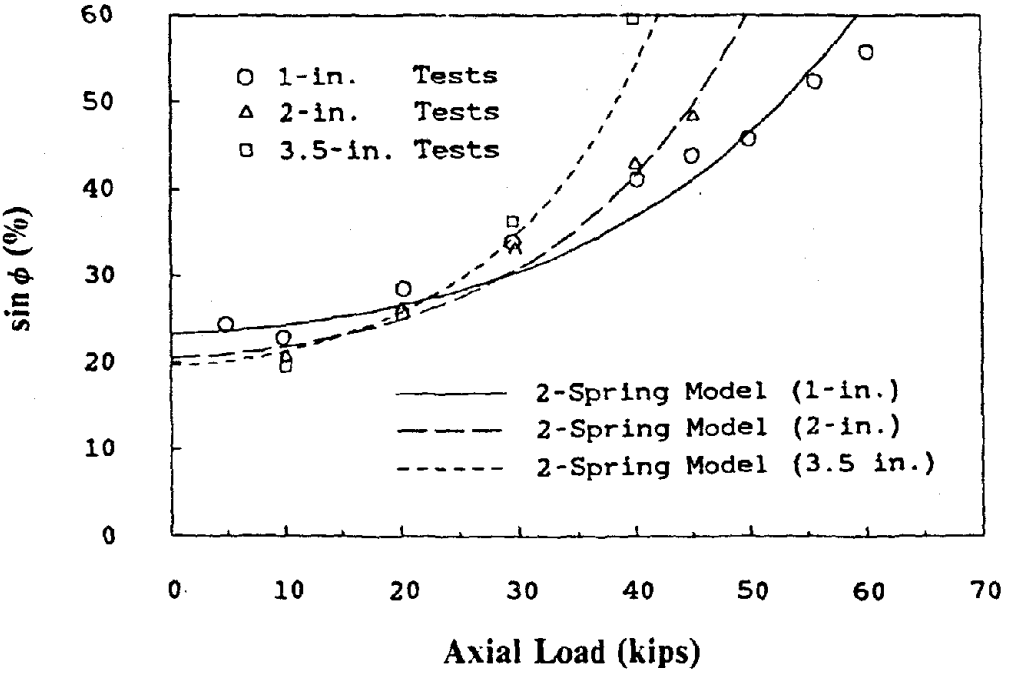

(b) 2-Spring Model

Figure 4.3 - Damping Factor of 1st Set of Bearings

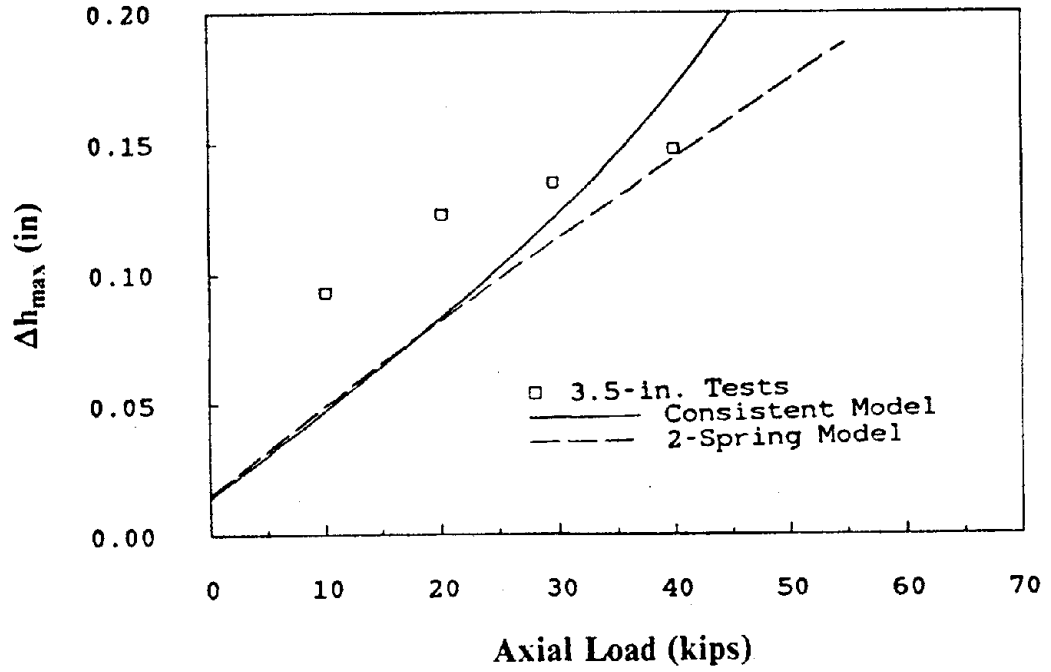

(a) assuming μ the same for all tests

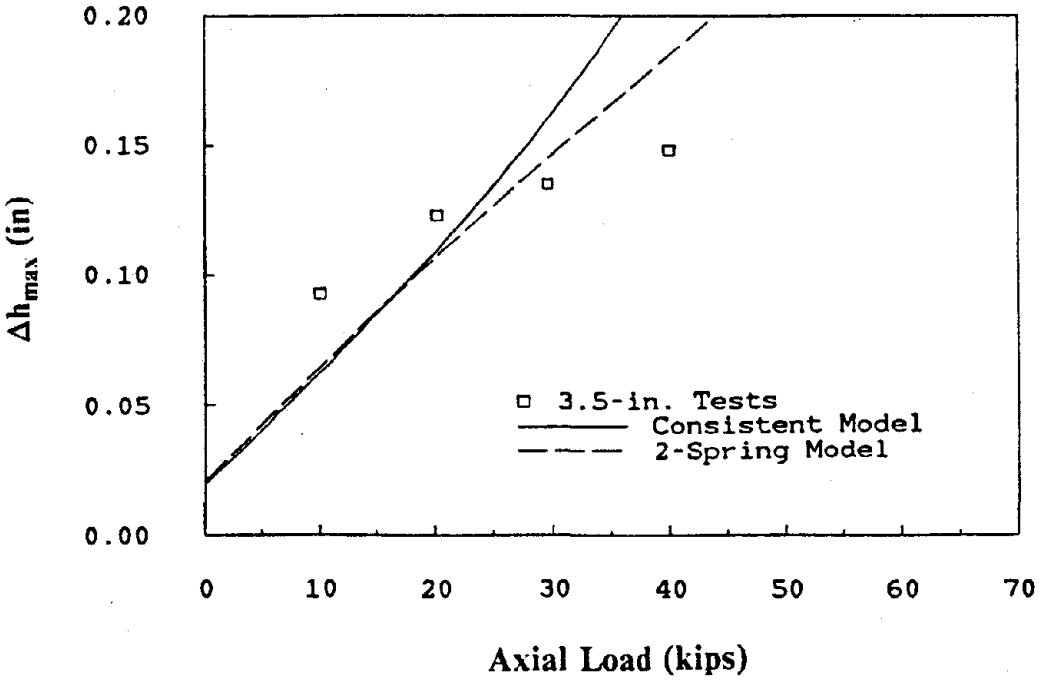

(b) assuming μ constant for only 3.5" tests

Figure 4.4 - Height Reduction of 1st Set of Bearings

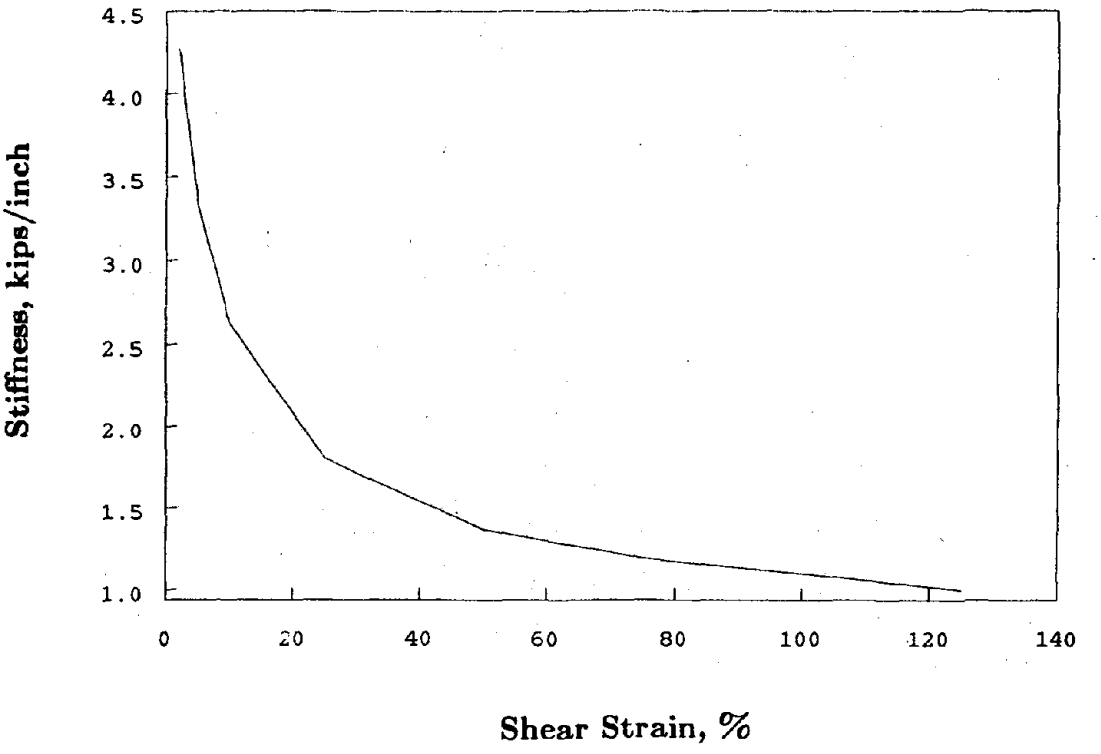

Figure 4.5 - Dynamic Shear Stiffness vs. Shear Strain for 1st Set of Bearings

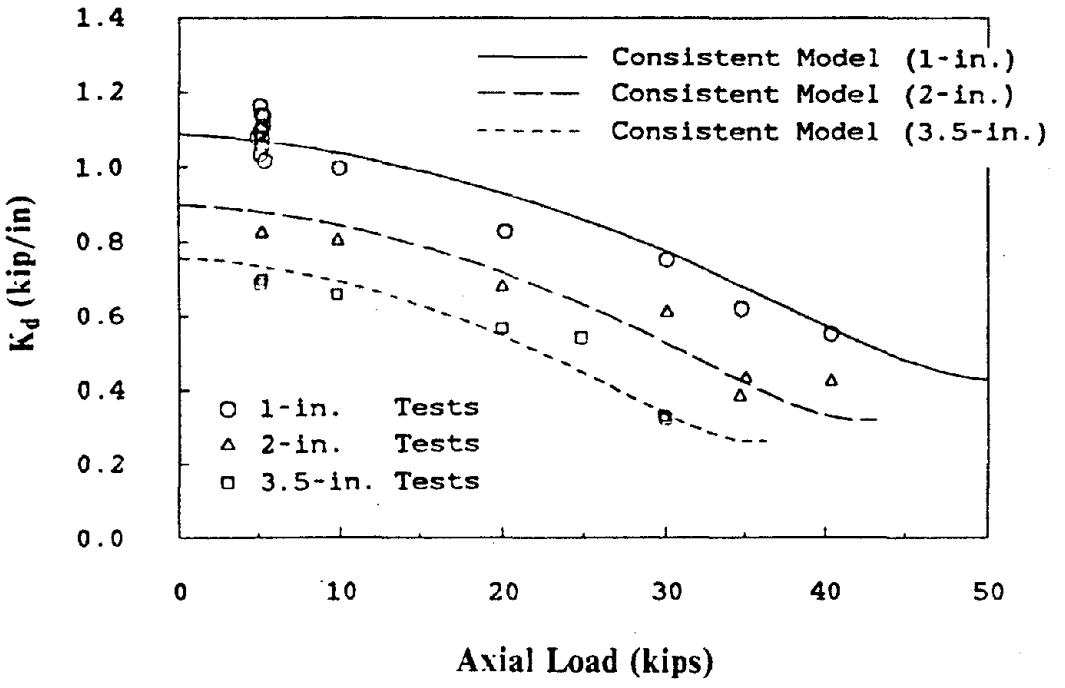

(a) Consistent Model

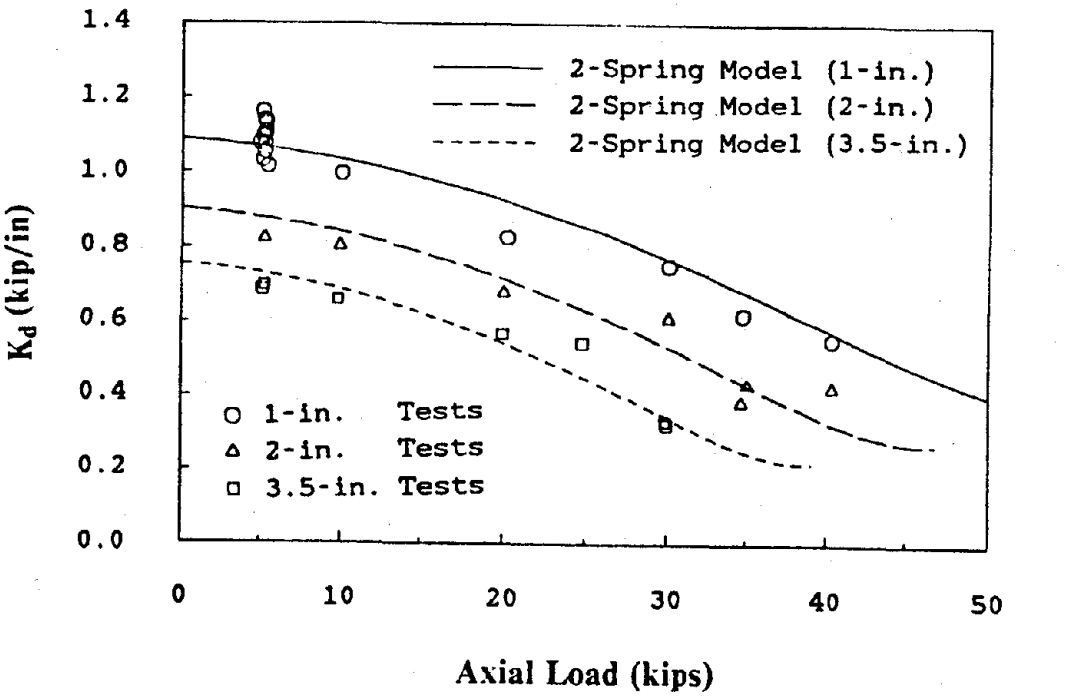

(b) 2-Spring Model

Figure 4.6 - Dynamic Shear Stiffness of 2nd Set of Bearings

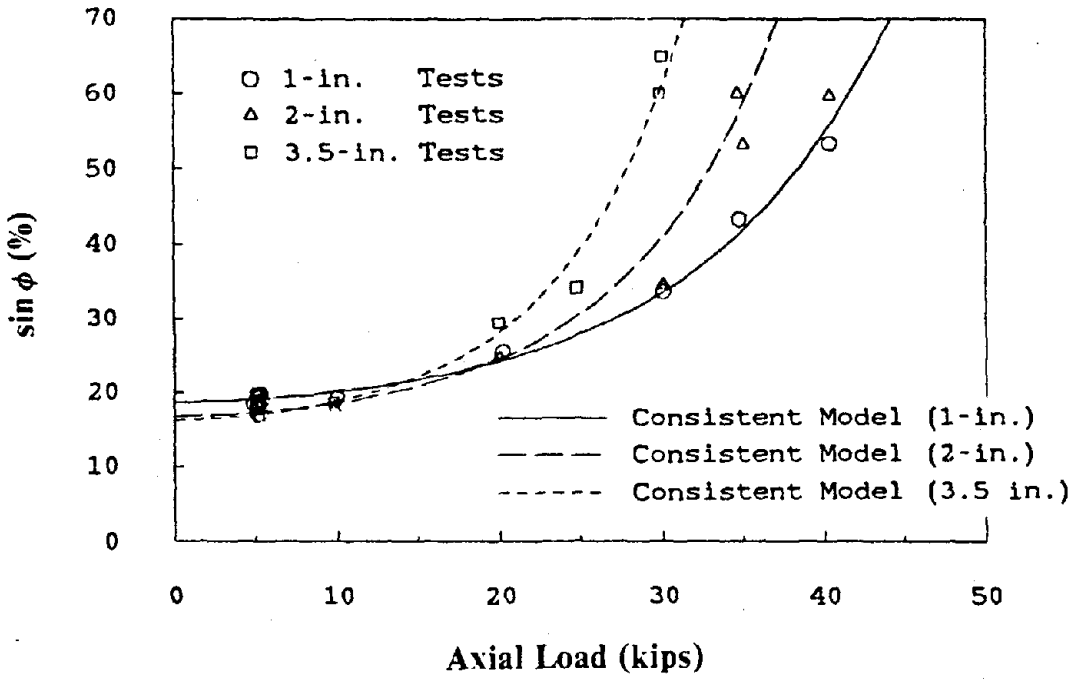

(a) Consistent Model

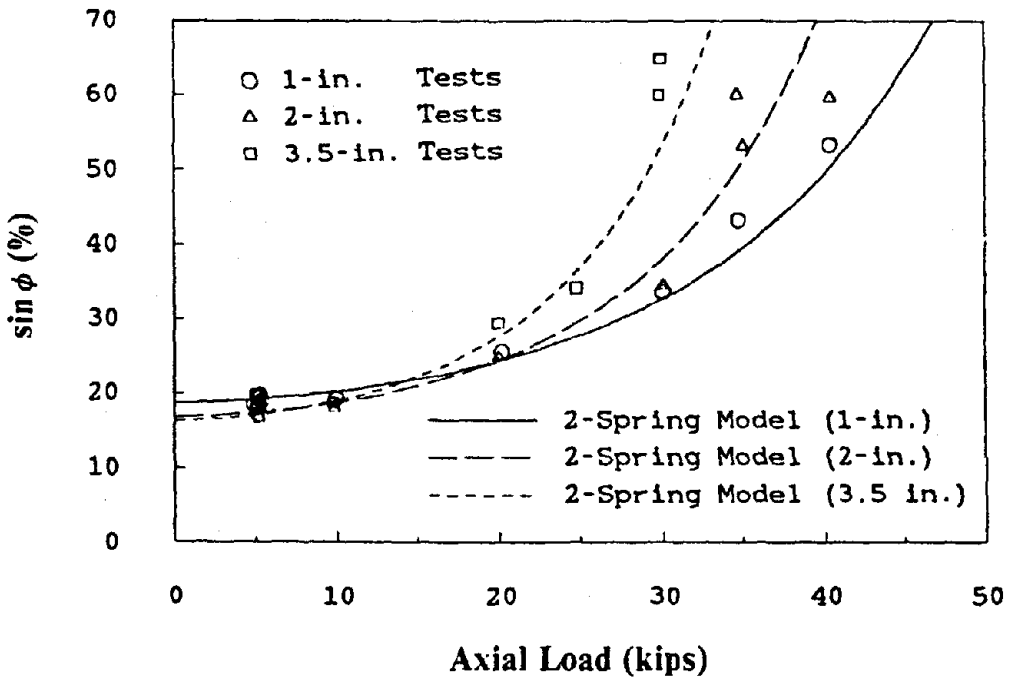

(b) 2-Spring Model

Figure 4.7 - Damping Factor of 2nd Set of Bearings

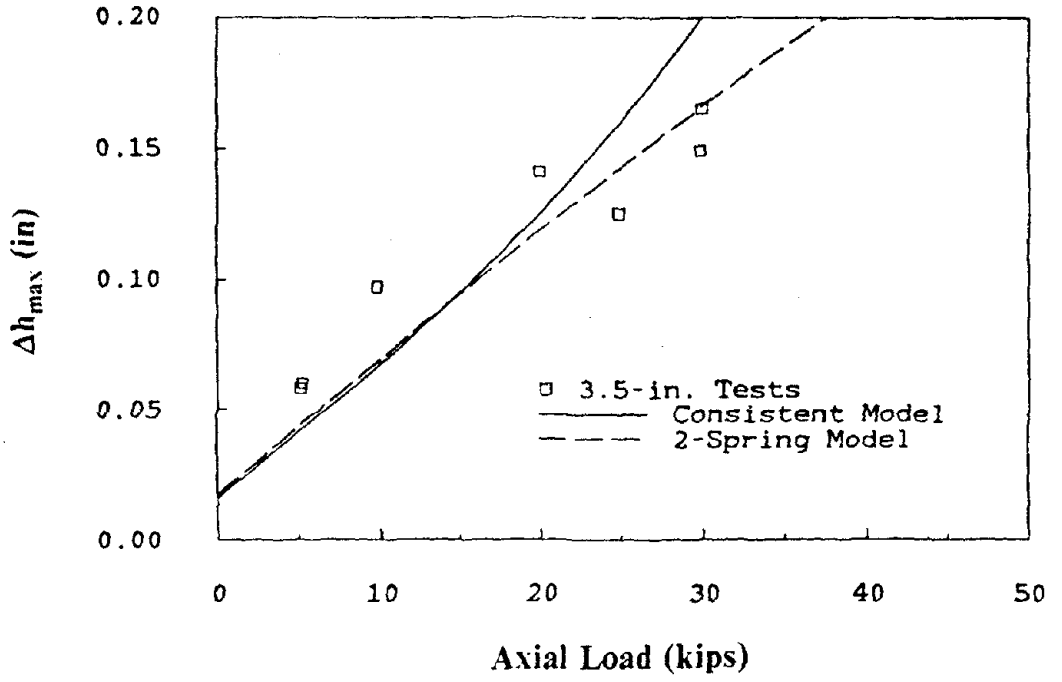

Figure 4.8 - Height Reduction of 2nd Set of Bearings

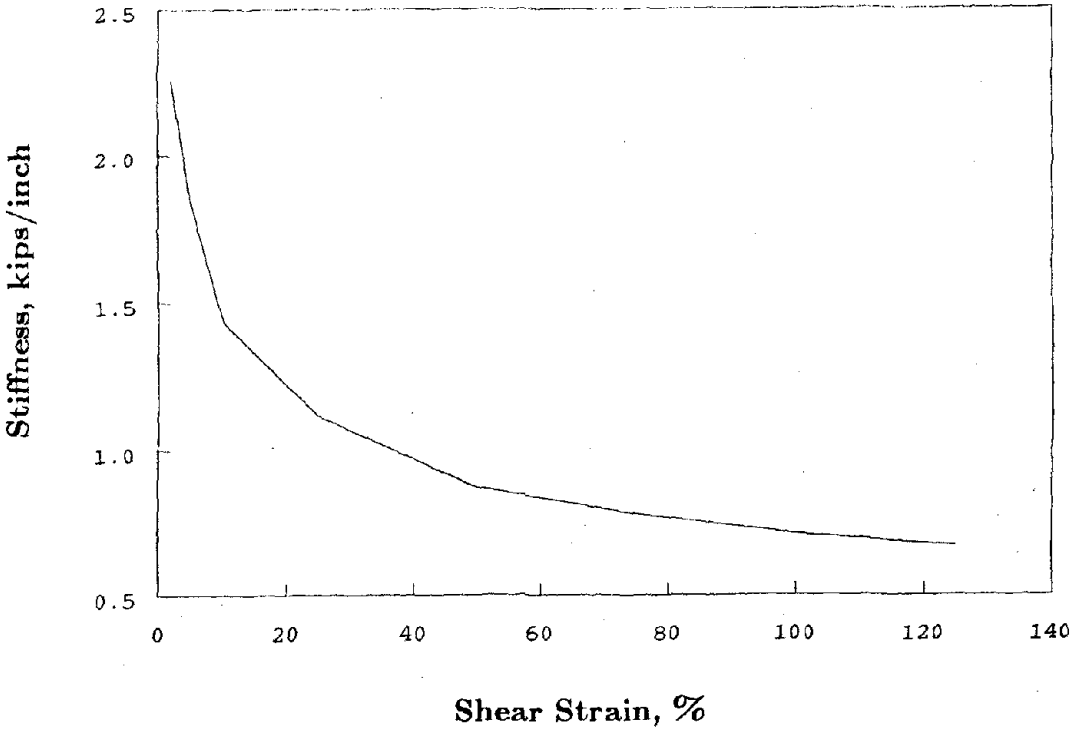

Figure 4.9 - Dynamic Shear Stiffness vs. Shear Strain for 2nd Set of Bearings

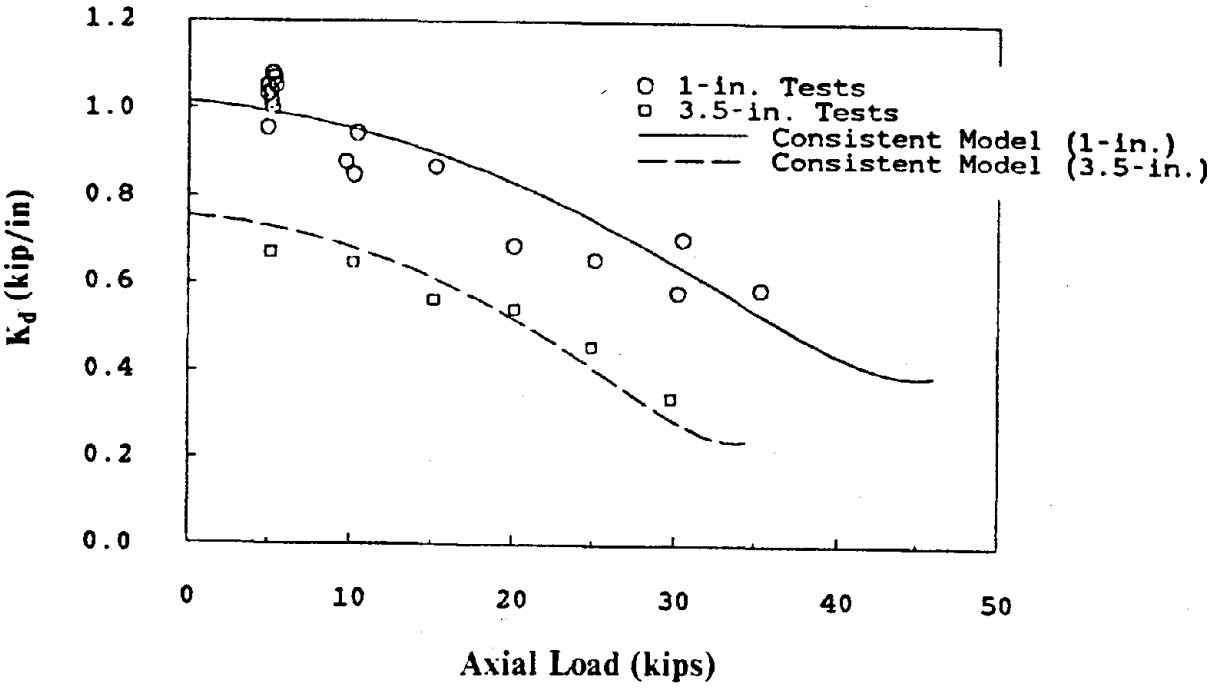

(a) Consistent Model

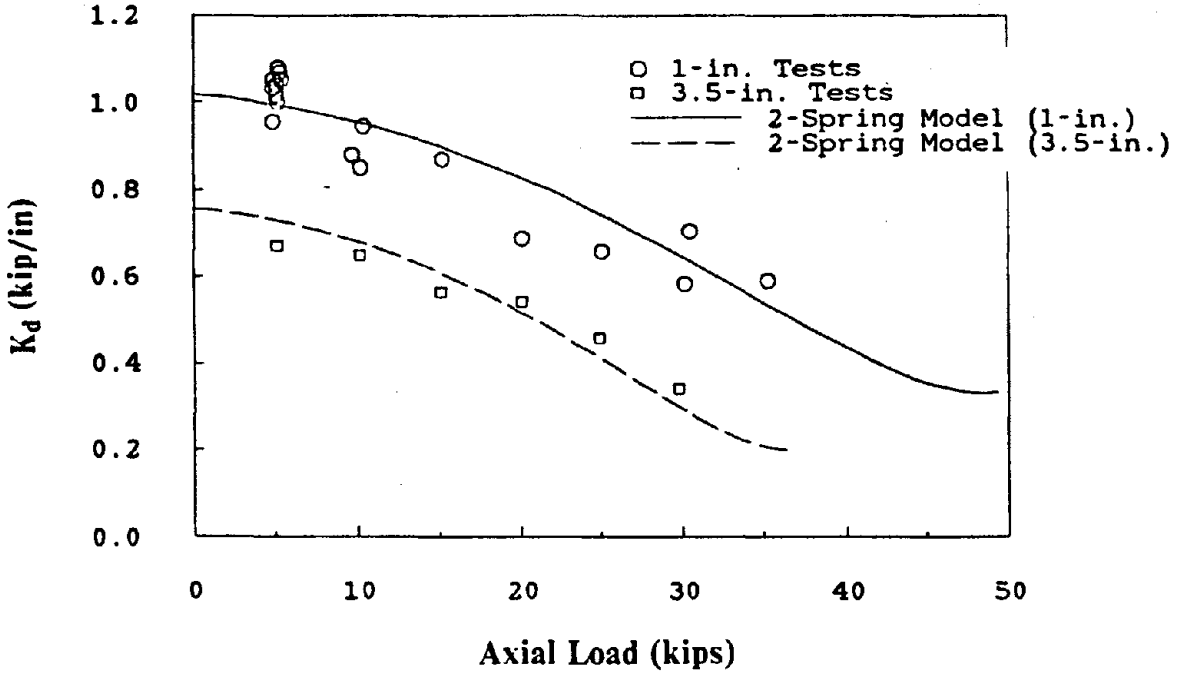

(b) 2-Spring Model

Figure 4.10 - Dynamic Shear Stiffness of 3rd Set of Bearings

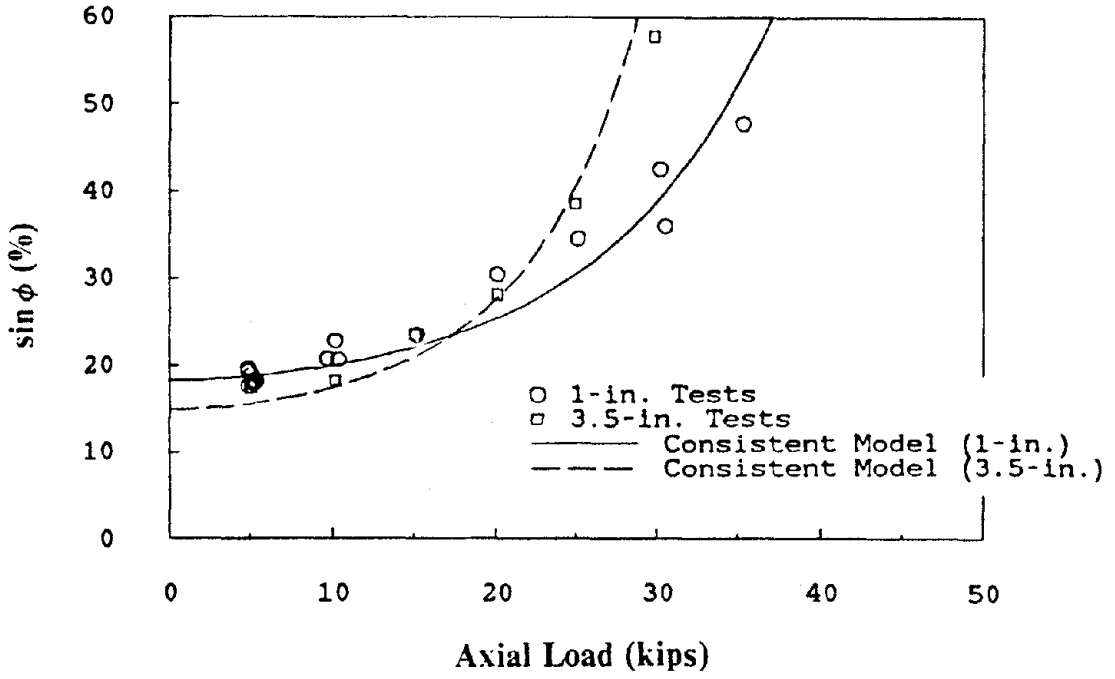

(a) Consistent Model

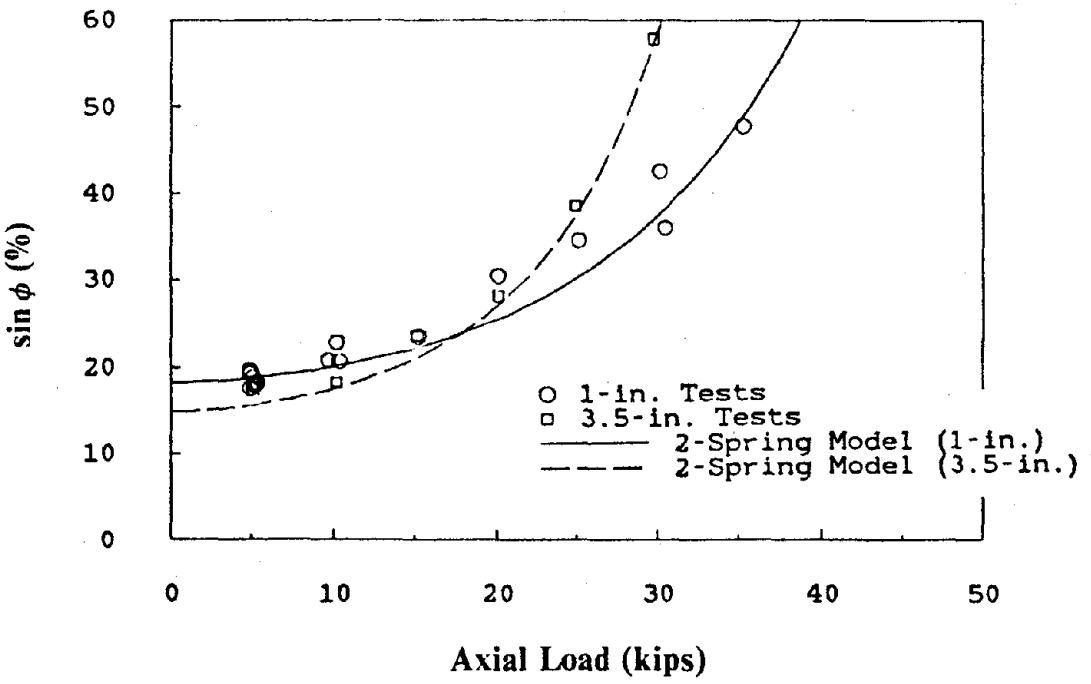

(b) 2-Spring Model

Figure 4.11 - Damping Factor of 3rd Set of Bearings

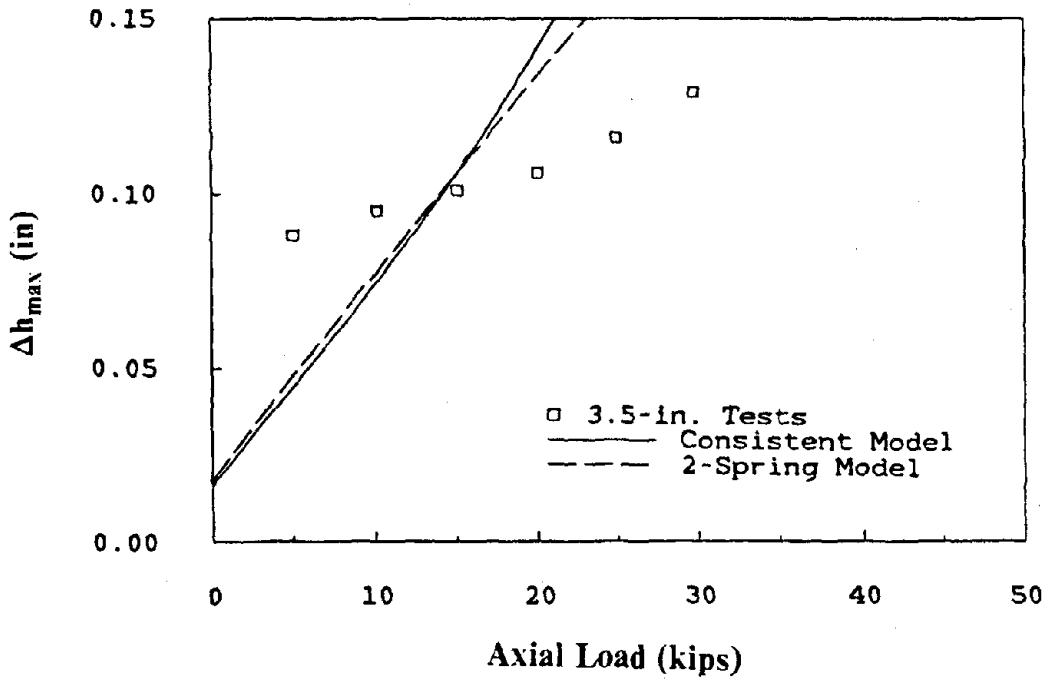

Figure 4.12 - Height Reduction of 3rd Set of Bearings

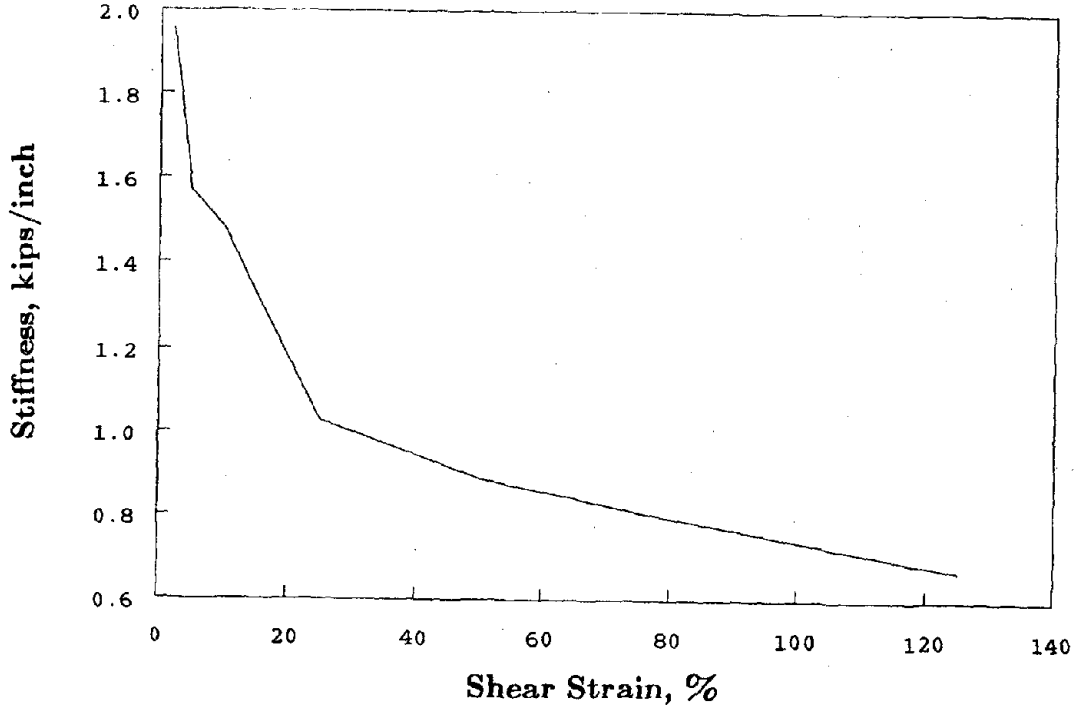

Figure 4.13 - Dynamic Shear Stiffness vs. Shear Strain for 3rd Set of Bearings

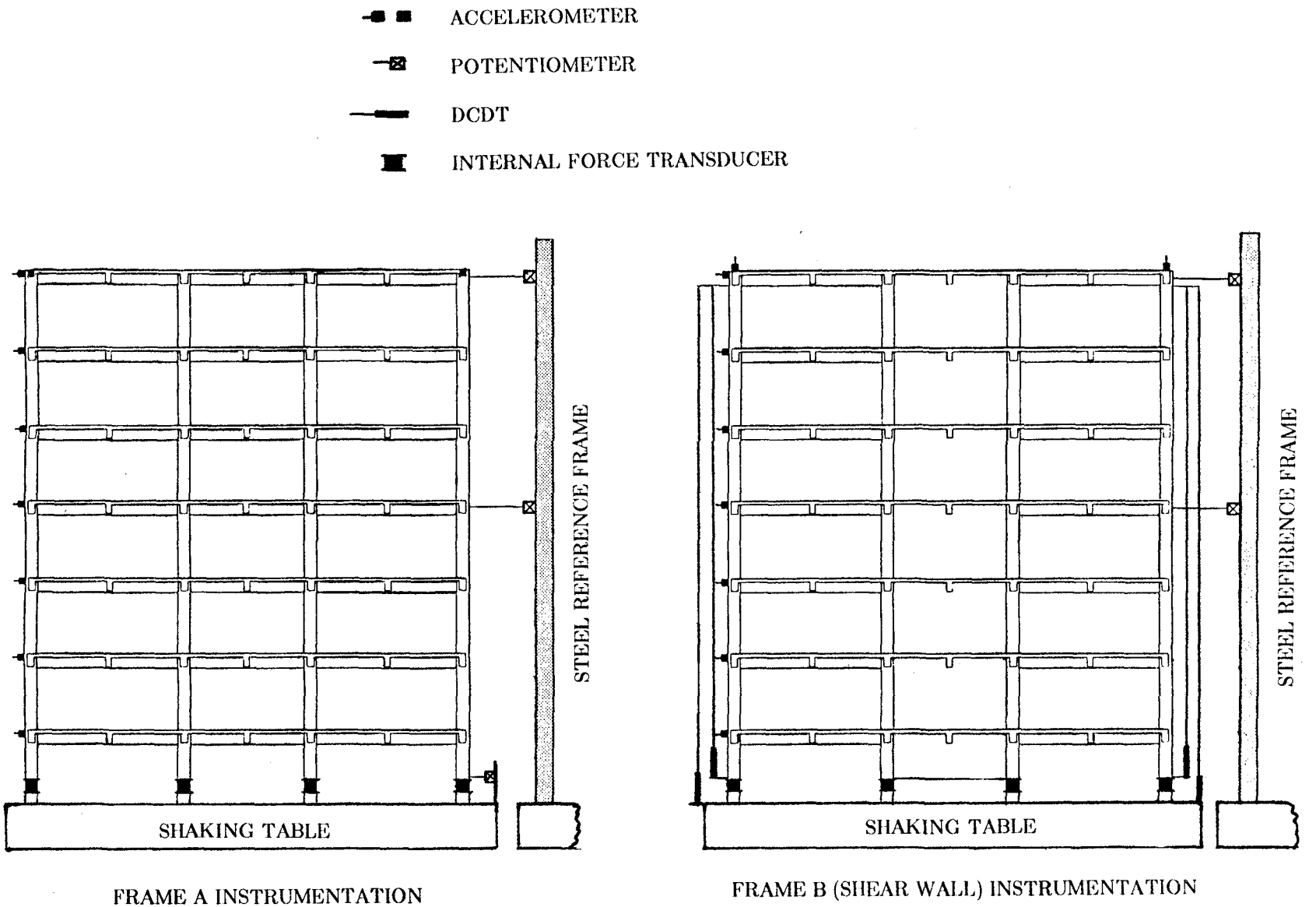

Figure 5.1 - Model Instrumentation Diagram

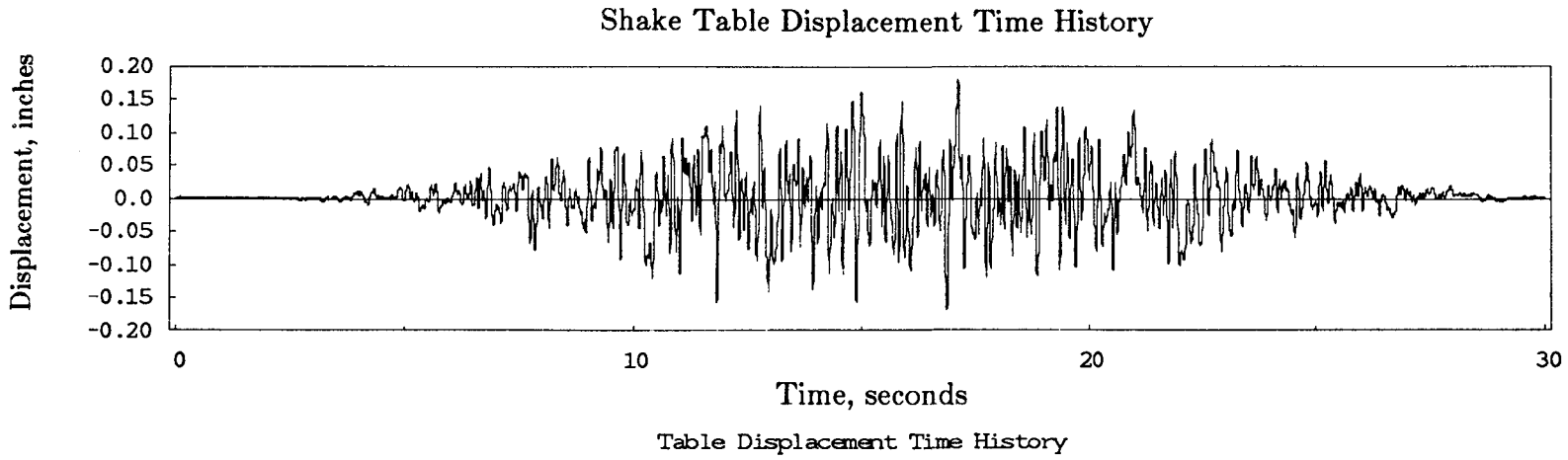

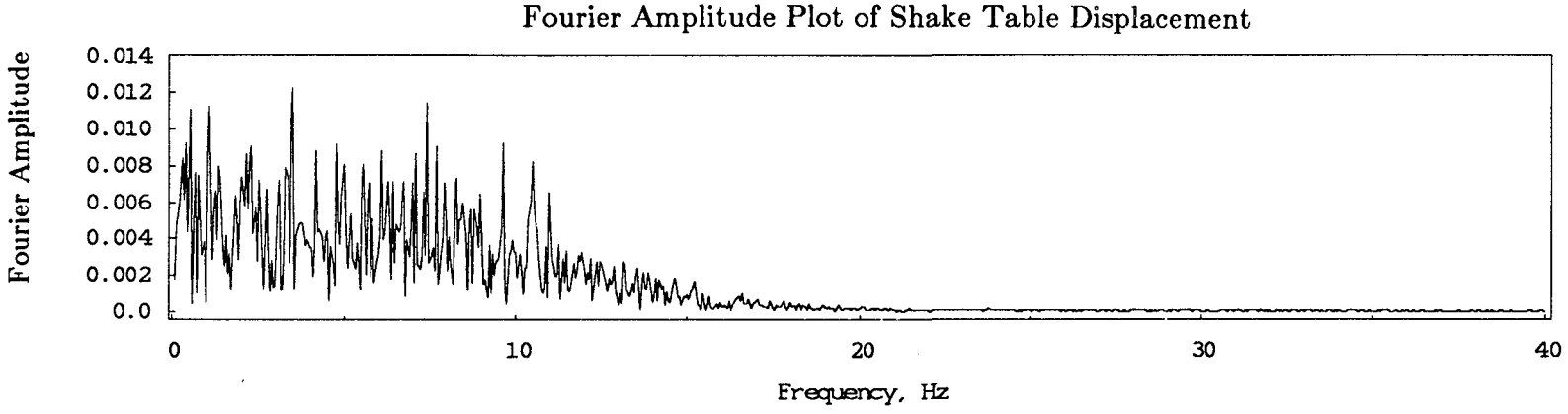

Figure 5.2 - Plot of White Noise Table Displacement Motion and its Fourier Amplitude

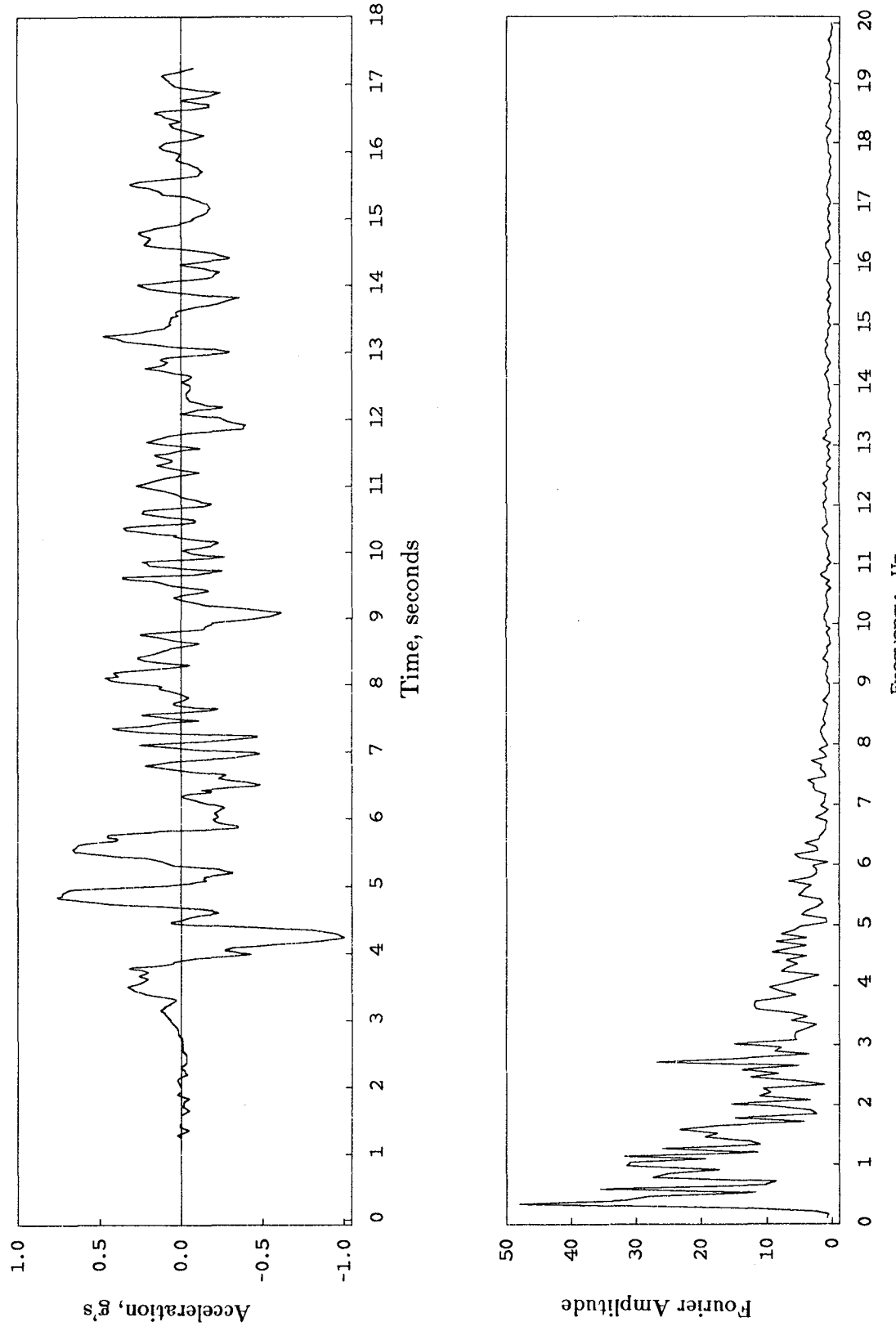

(a) Bucharest

Figure 5.3 - Normalized Real-Time Earthquake Record and its Fourier Amplitude

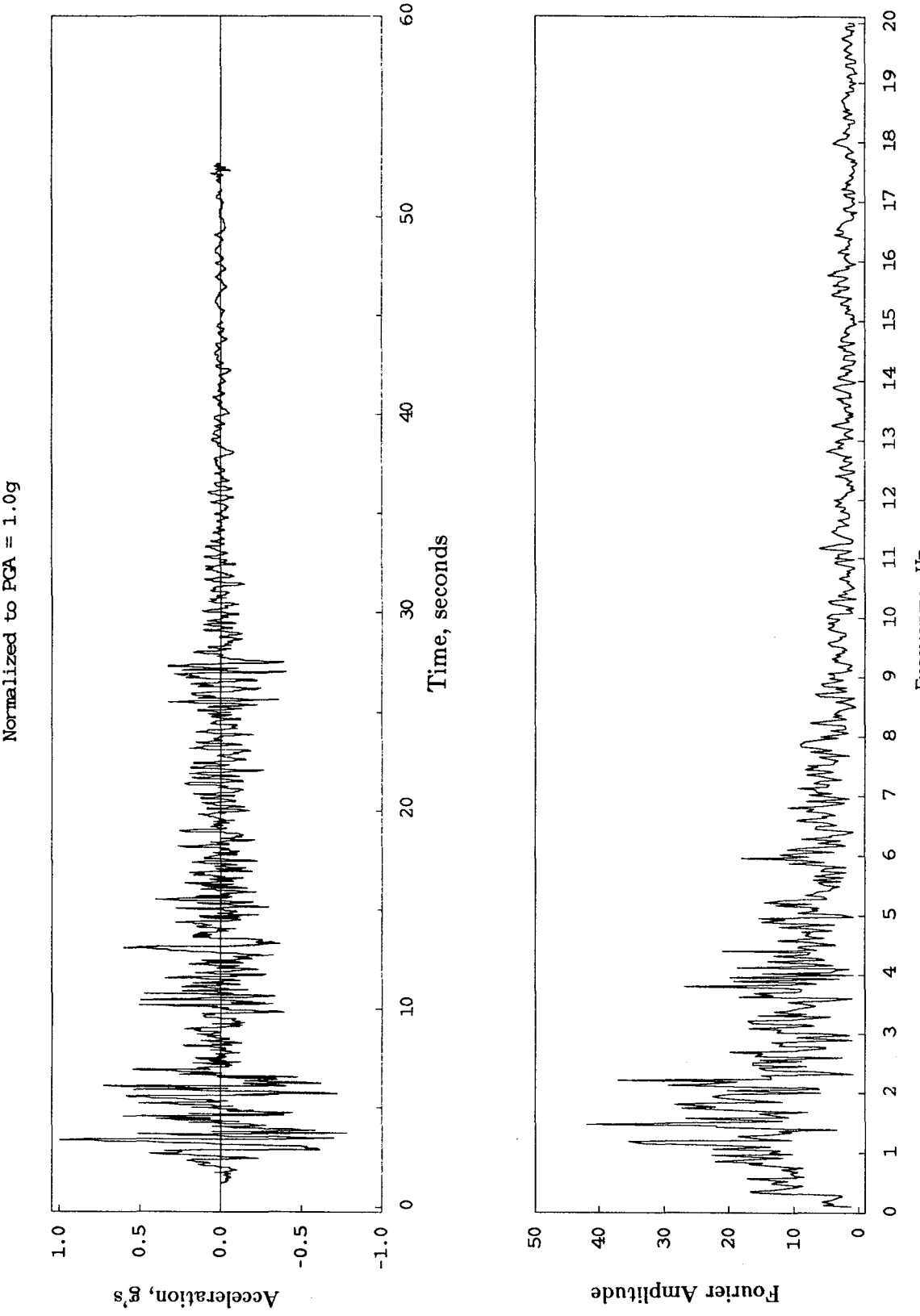

(b) El Centro

Figure 5.3 - Continued

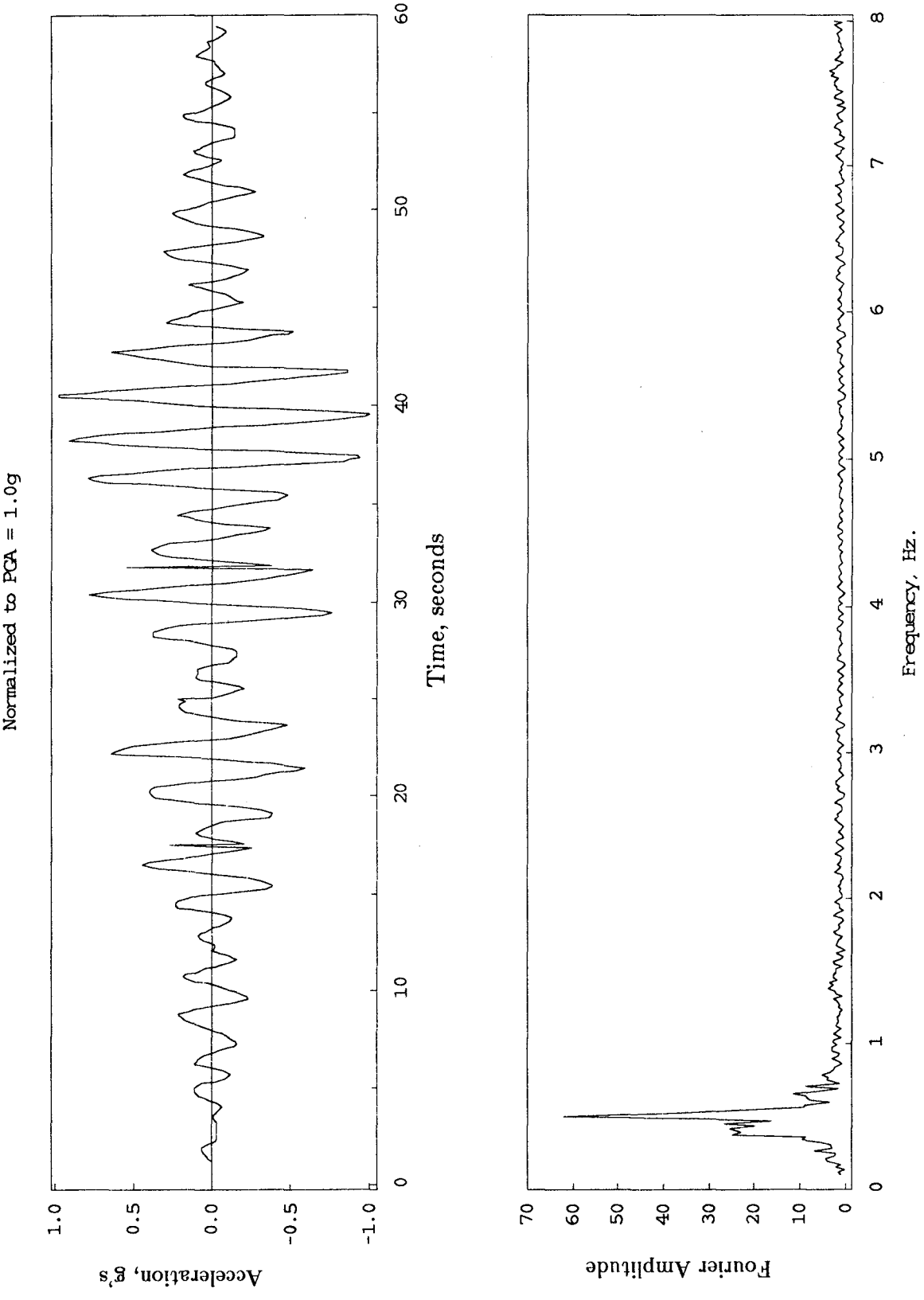

(c) Mexico City

Figure 5.3 - Continued

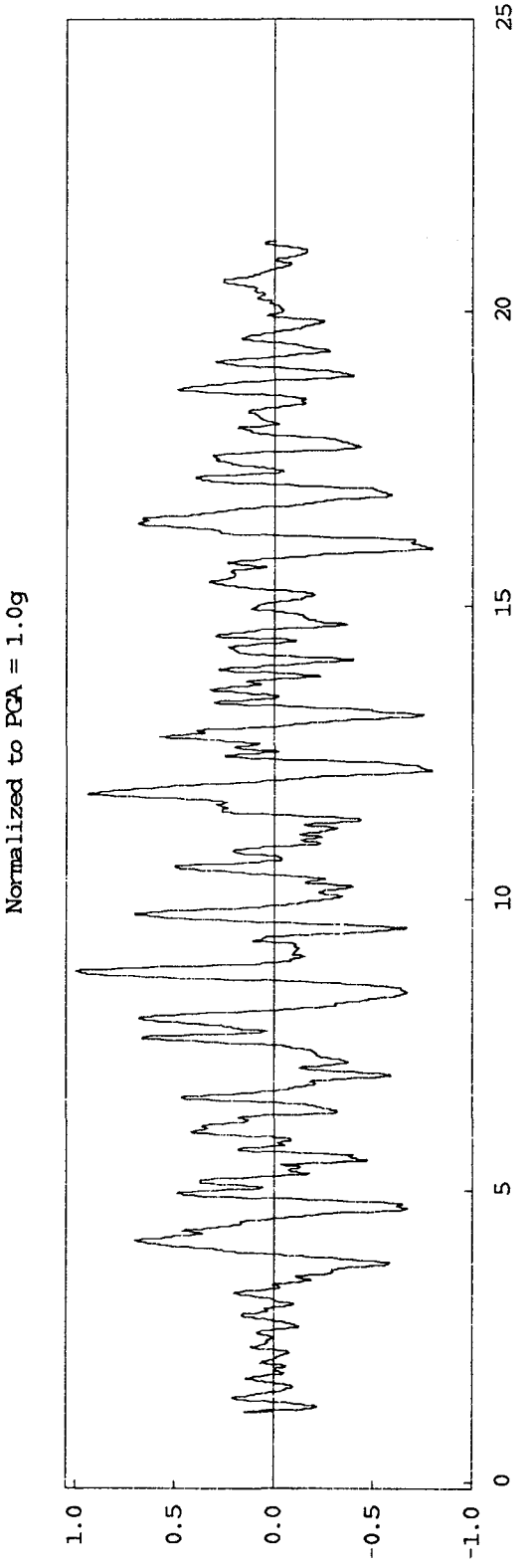

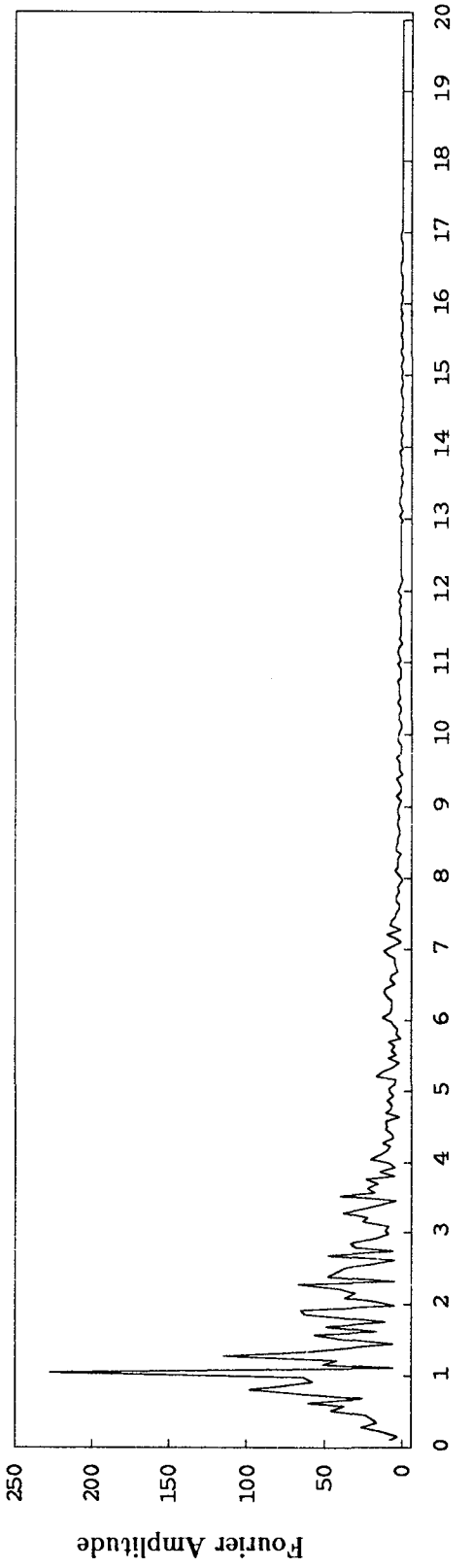

(d) Miyagi-Ken-Oki

Figure 5.3 - Continued

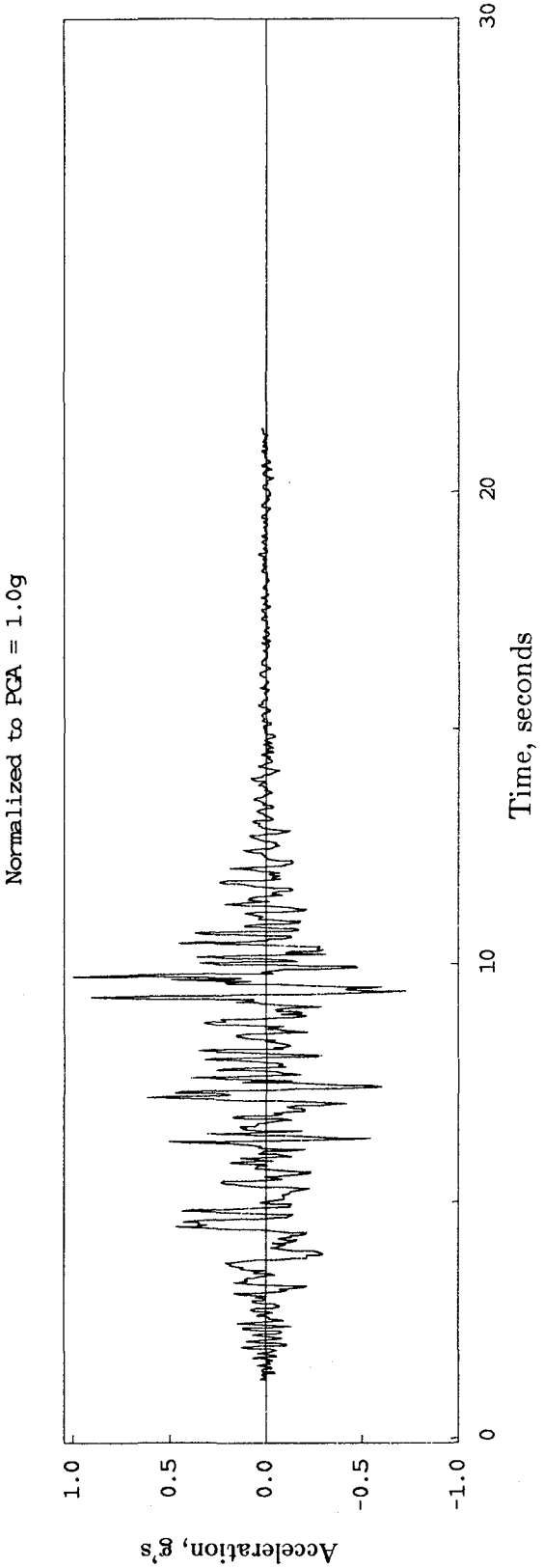

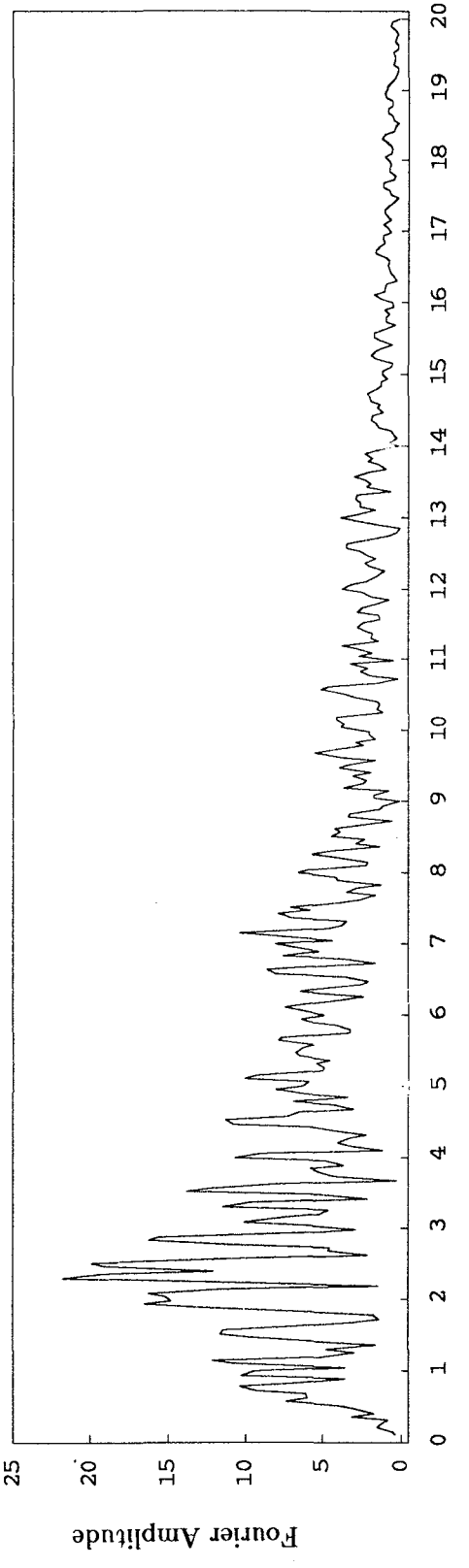

(e) Pacoima Dam

Figure 5.3 - Continued

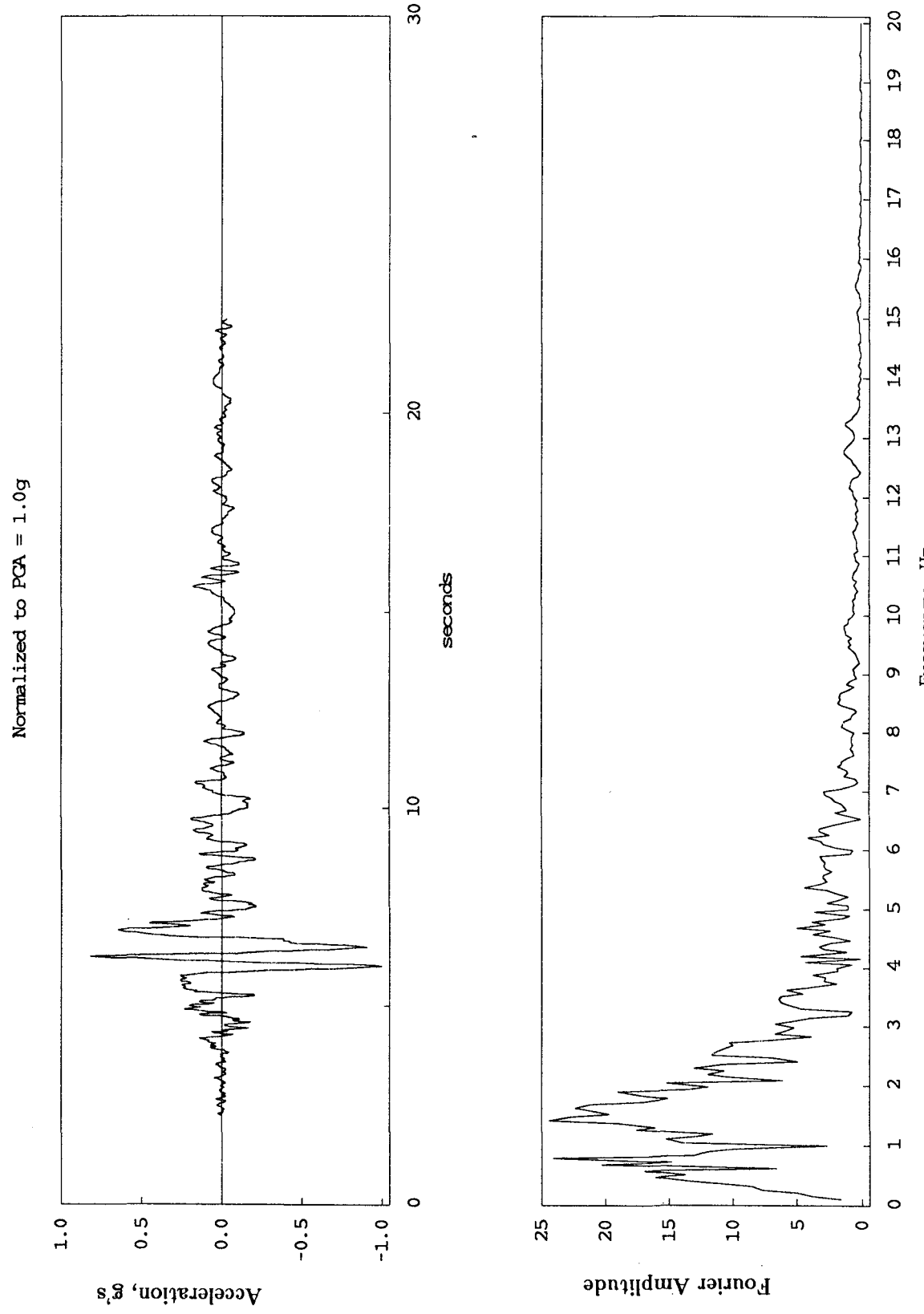

(f) Parkfield

Figure 5.3 - Continued

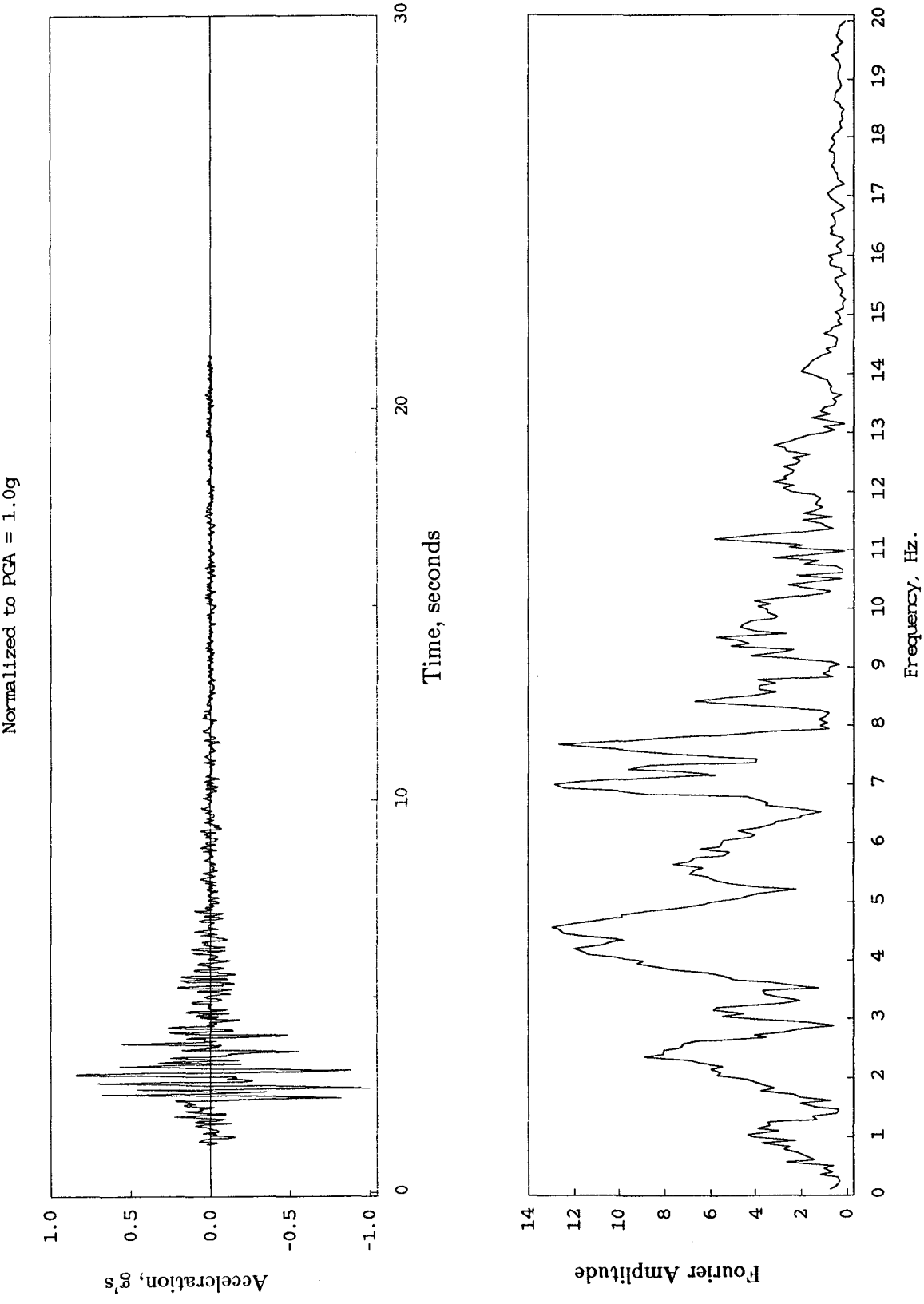

(g) San Francisco

Figure 5.3 - Continued

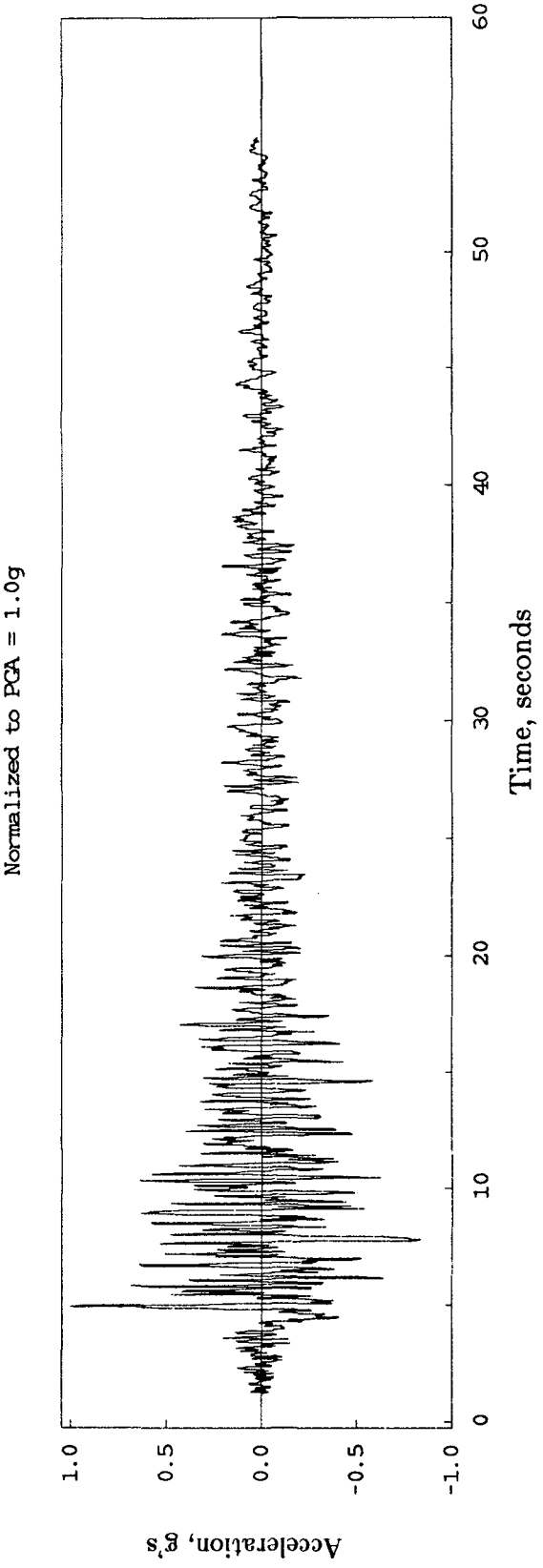

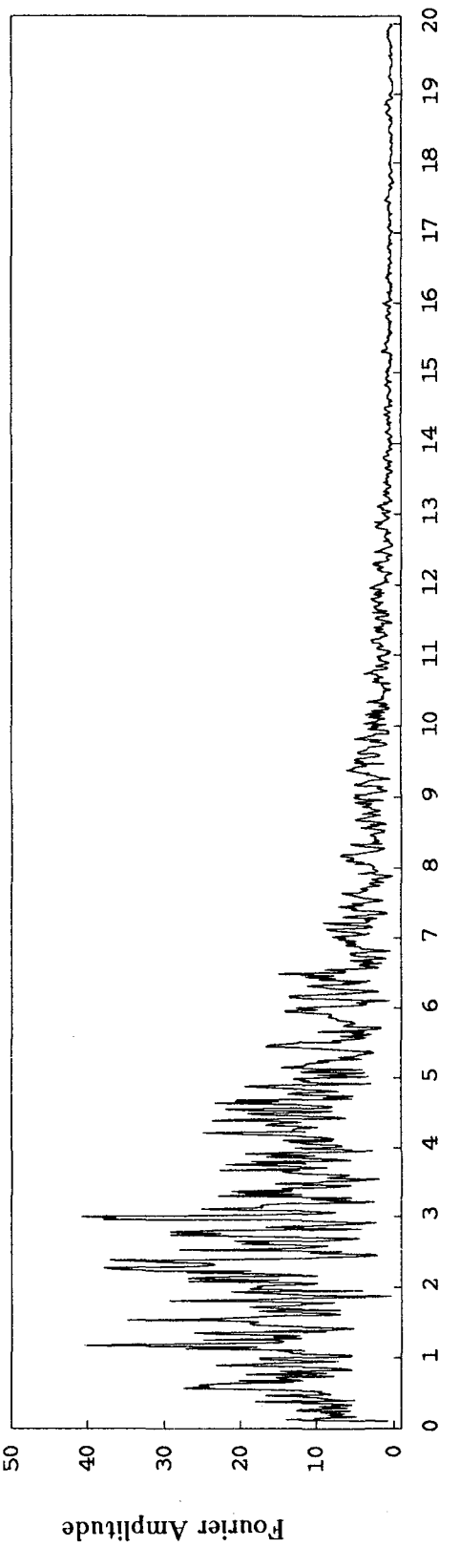

(h) Taft

Figure 5.3 - Continued

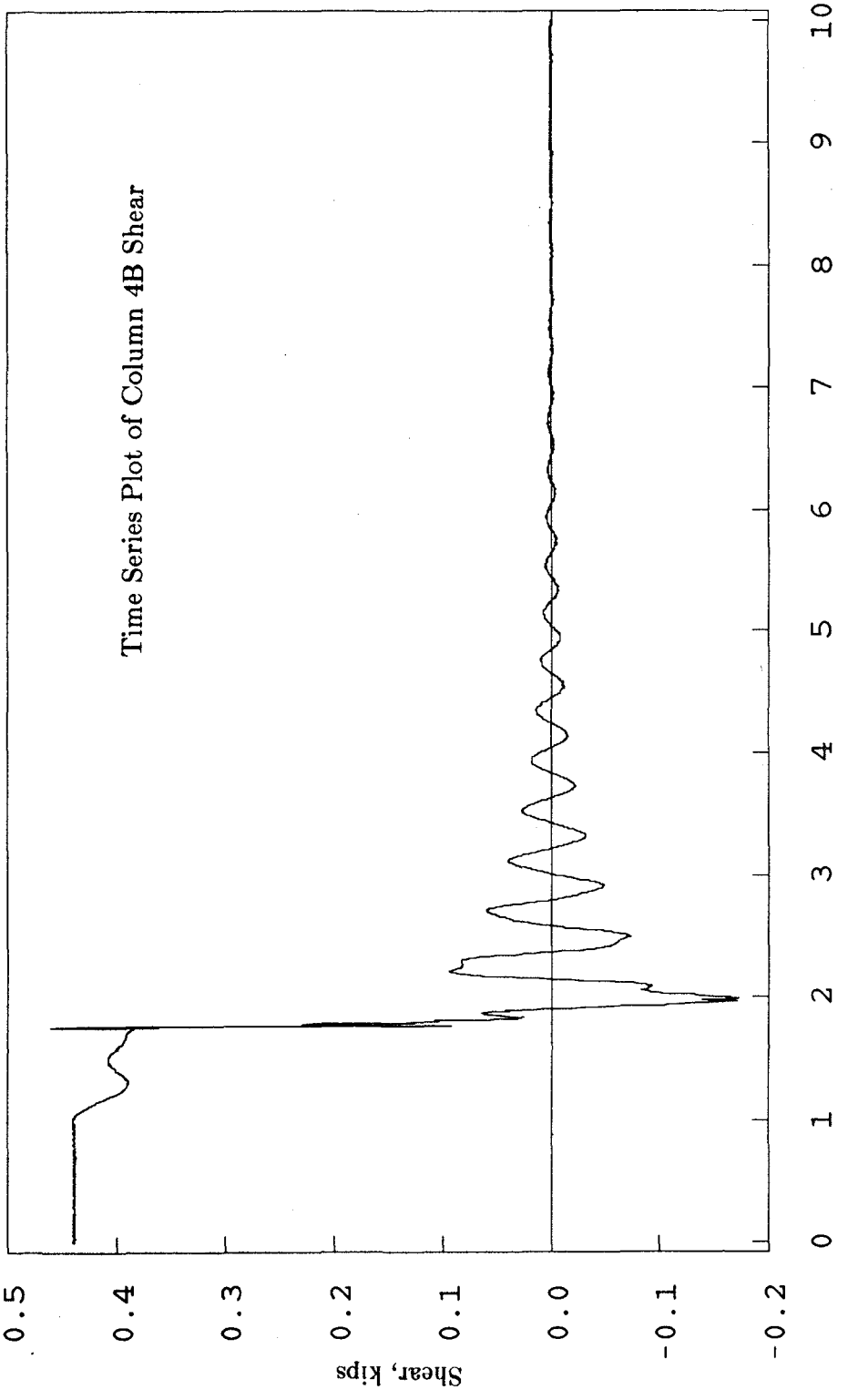

Figure 6.1 - Free-Vibration Test Log-Dec. Curve, 1st Set of Bearings

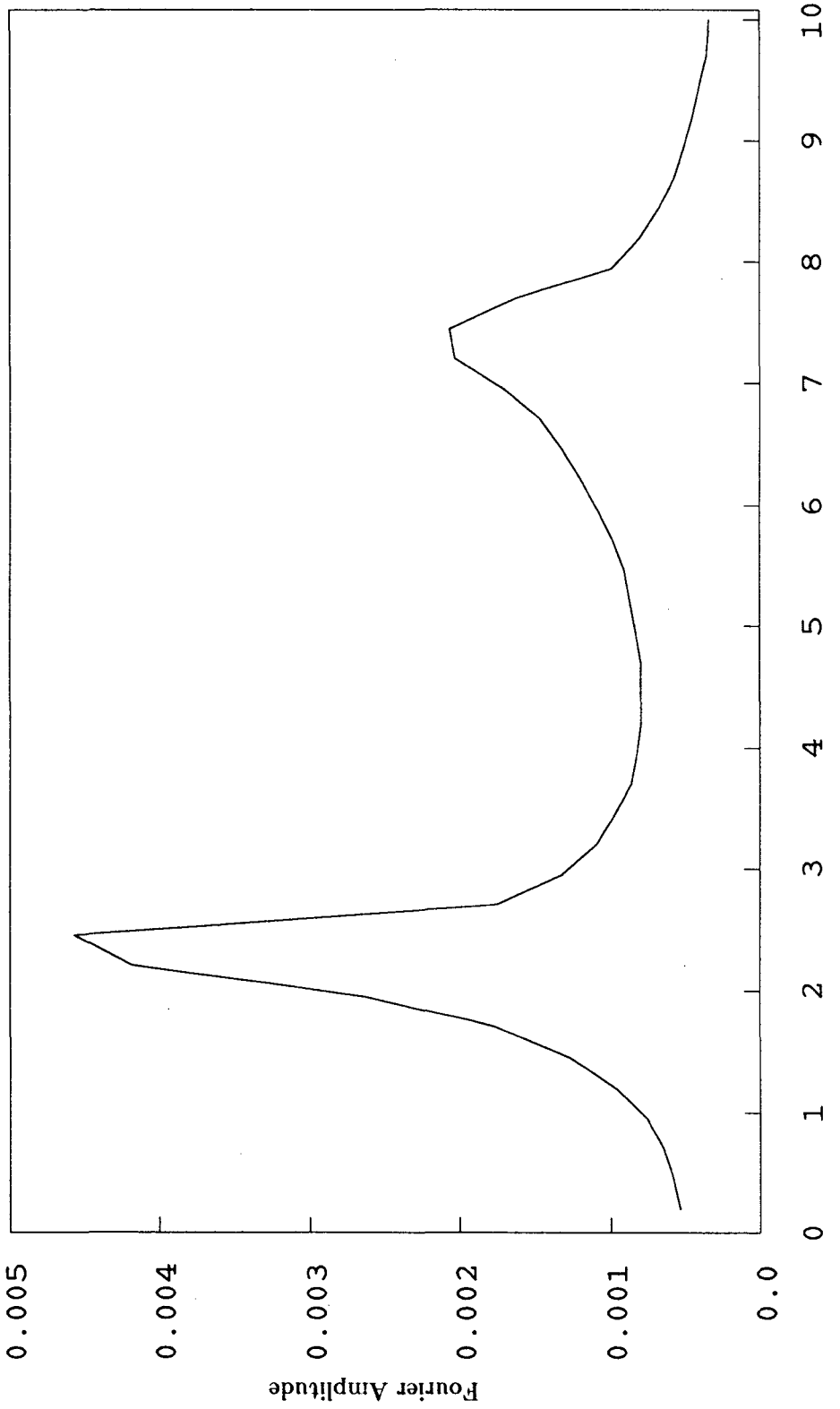

Figure 6.2 - Free-Vibration Test, 1st Set of Bearings

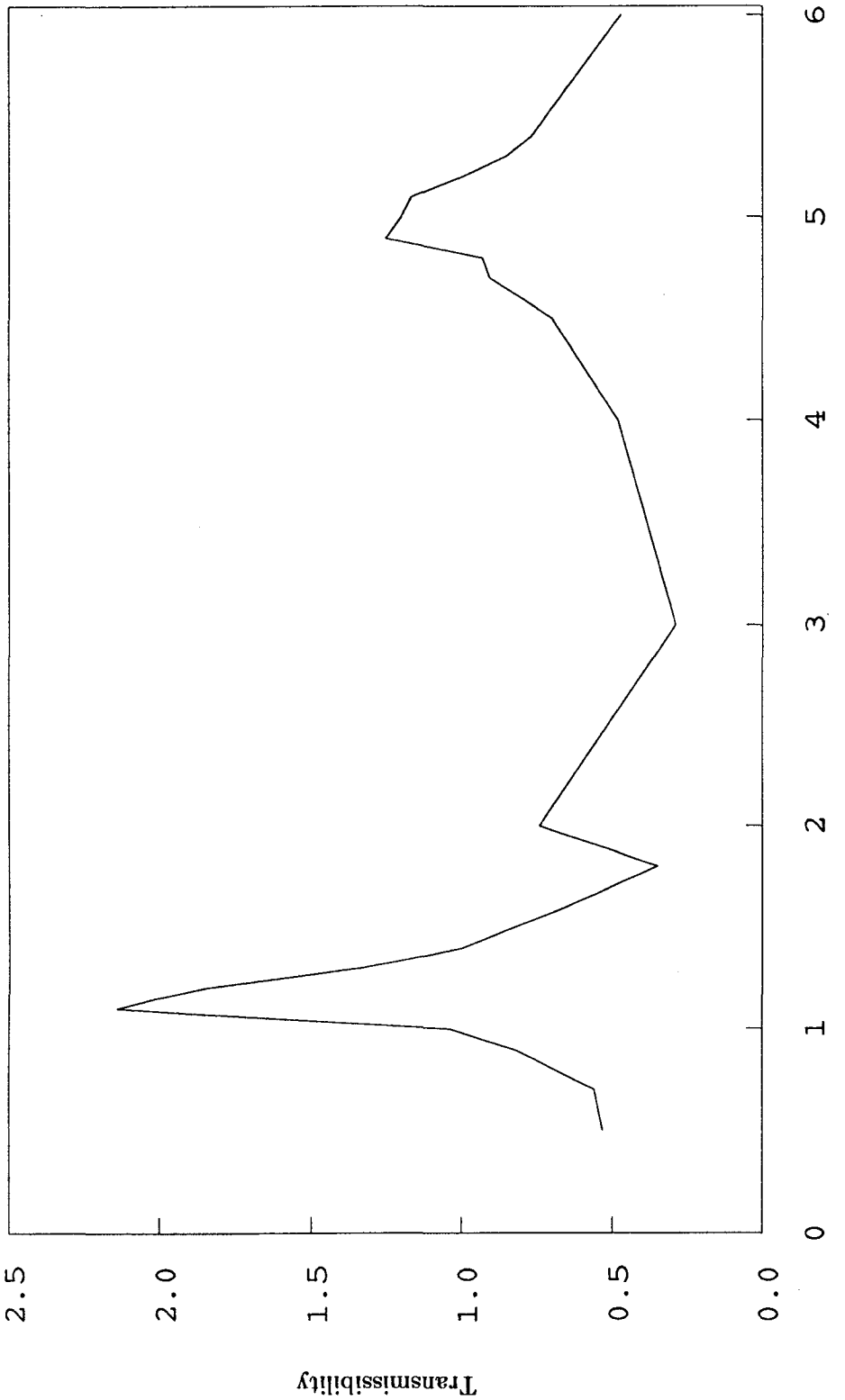

Figure 6.3 - Sine Test Transmissibility Plot, 1st Set of Bearings

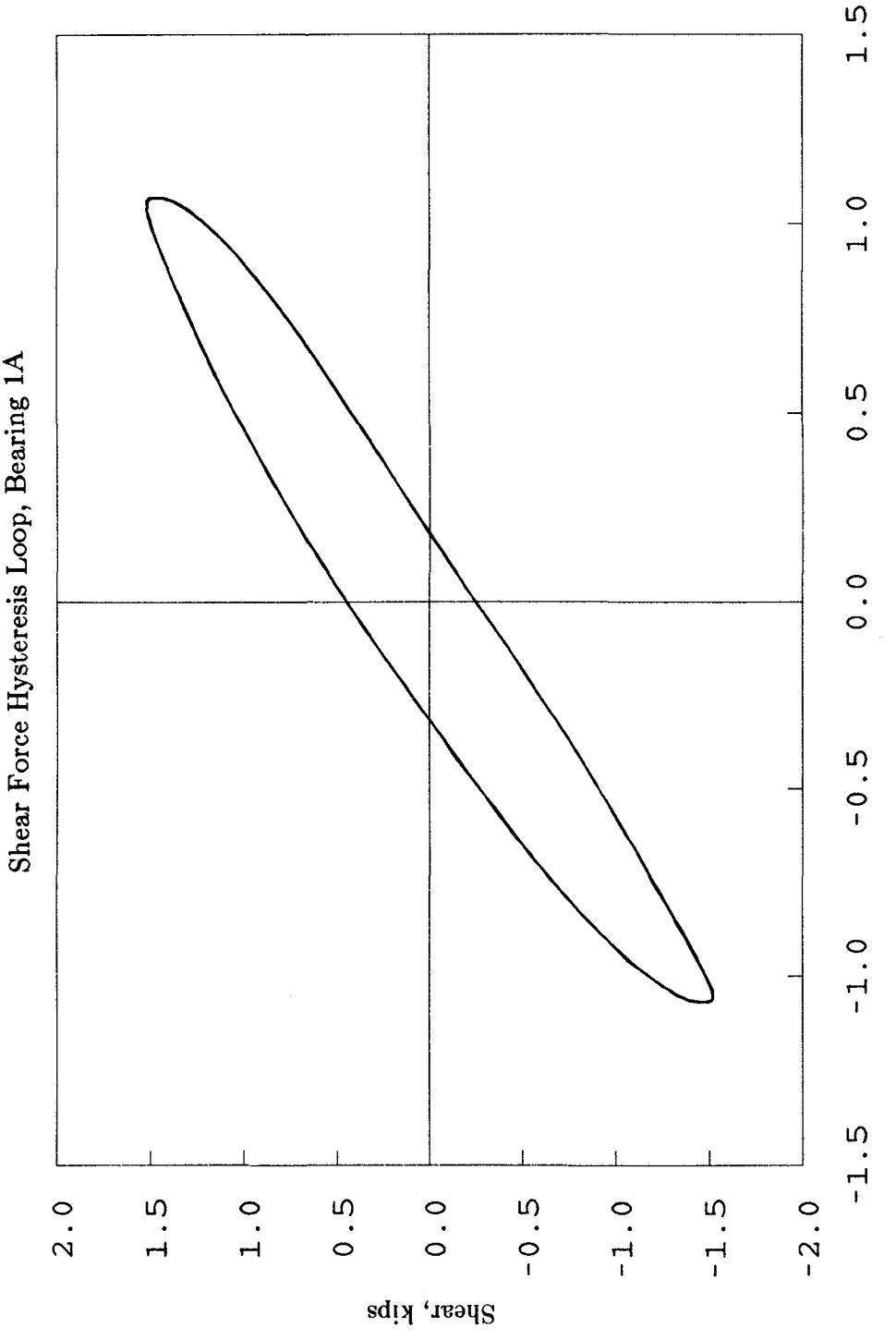

Figure 6.4 - Sine Test Hysteresis Loops, 1st Set of Bearings

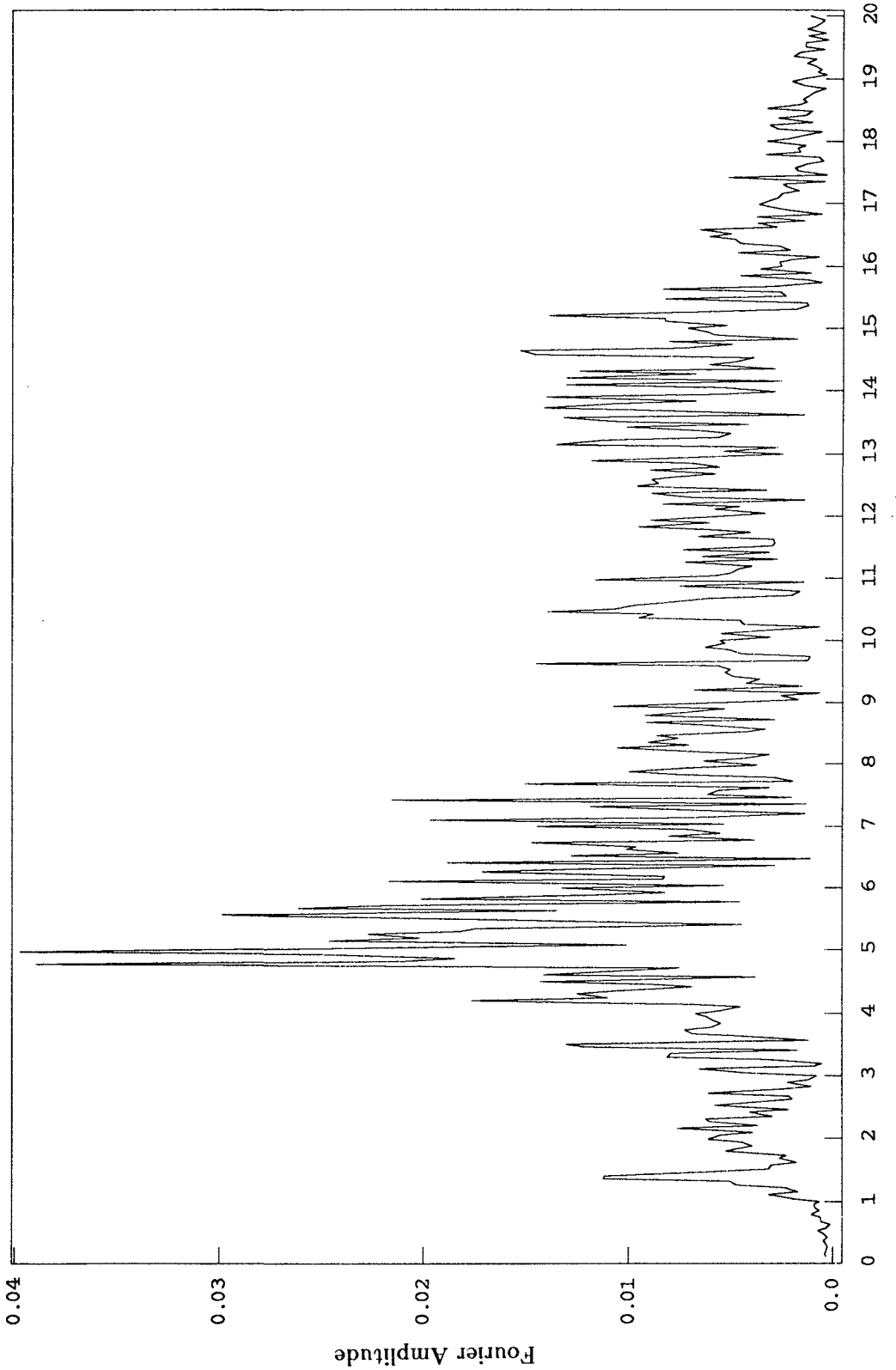

Figure 6.5 - White Noise Test, Roof Acceleration

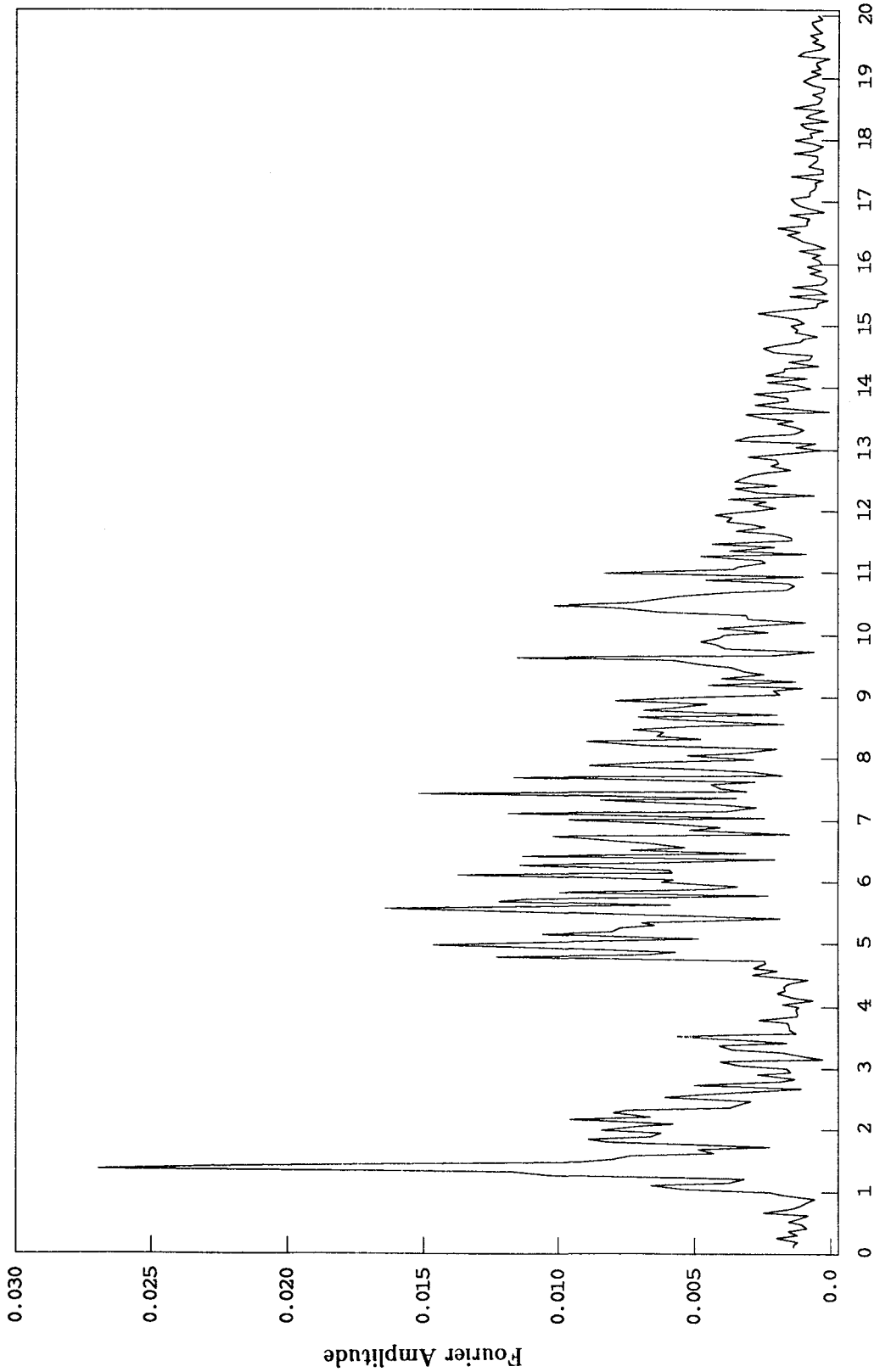

Figure 6.6 - White Noise Test, Bearing Displacement

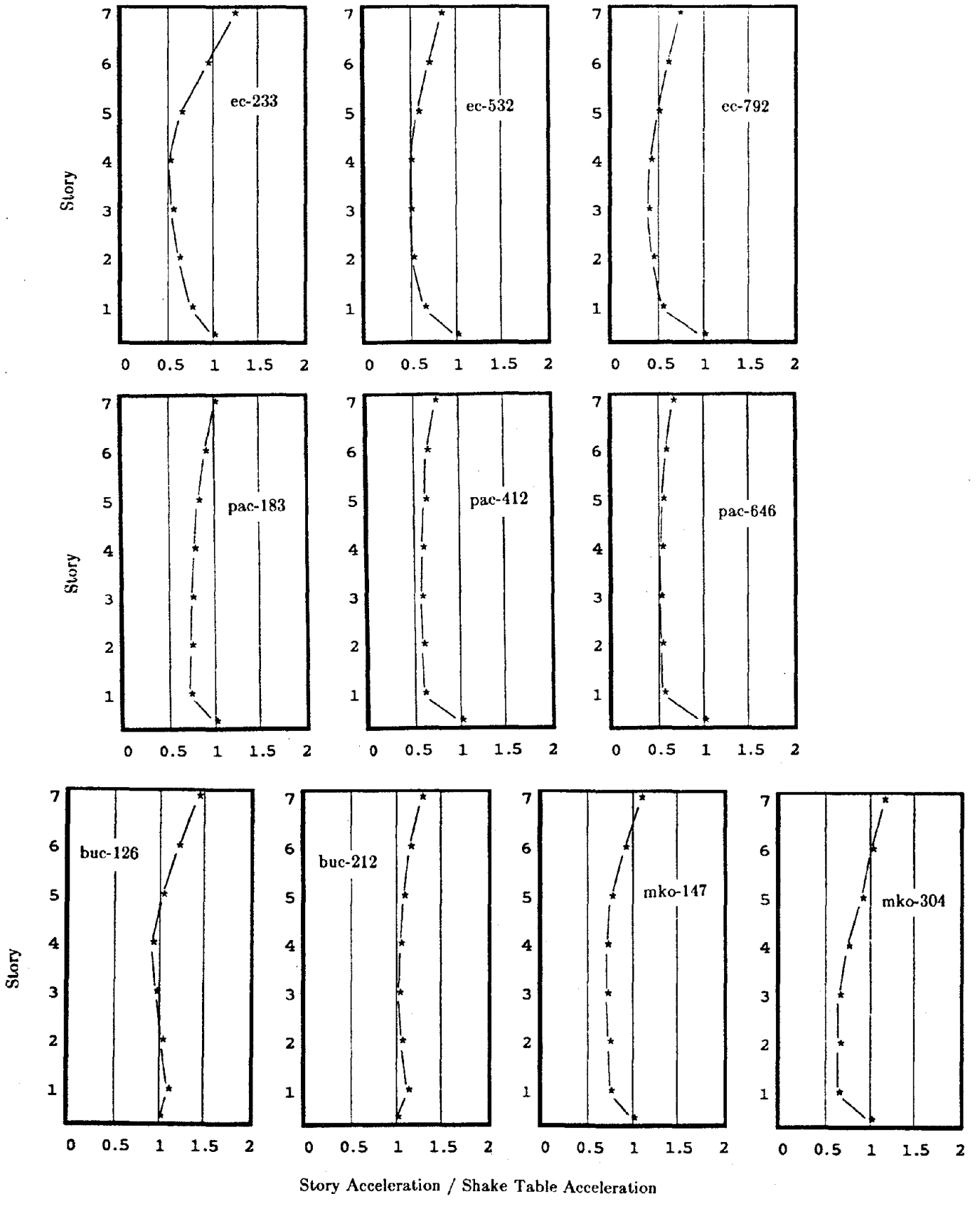

Figure 6.7 - Peak Acceleration Profiles, 1st Set of Bearings

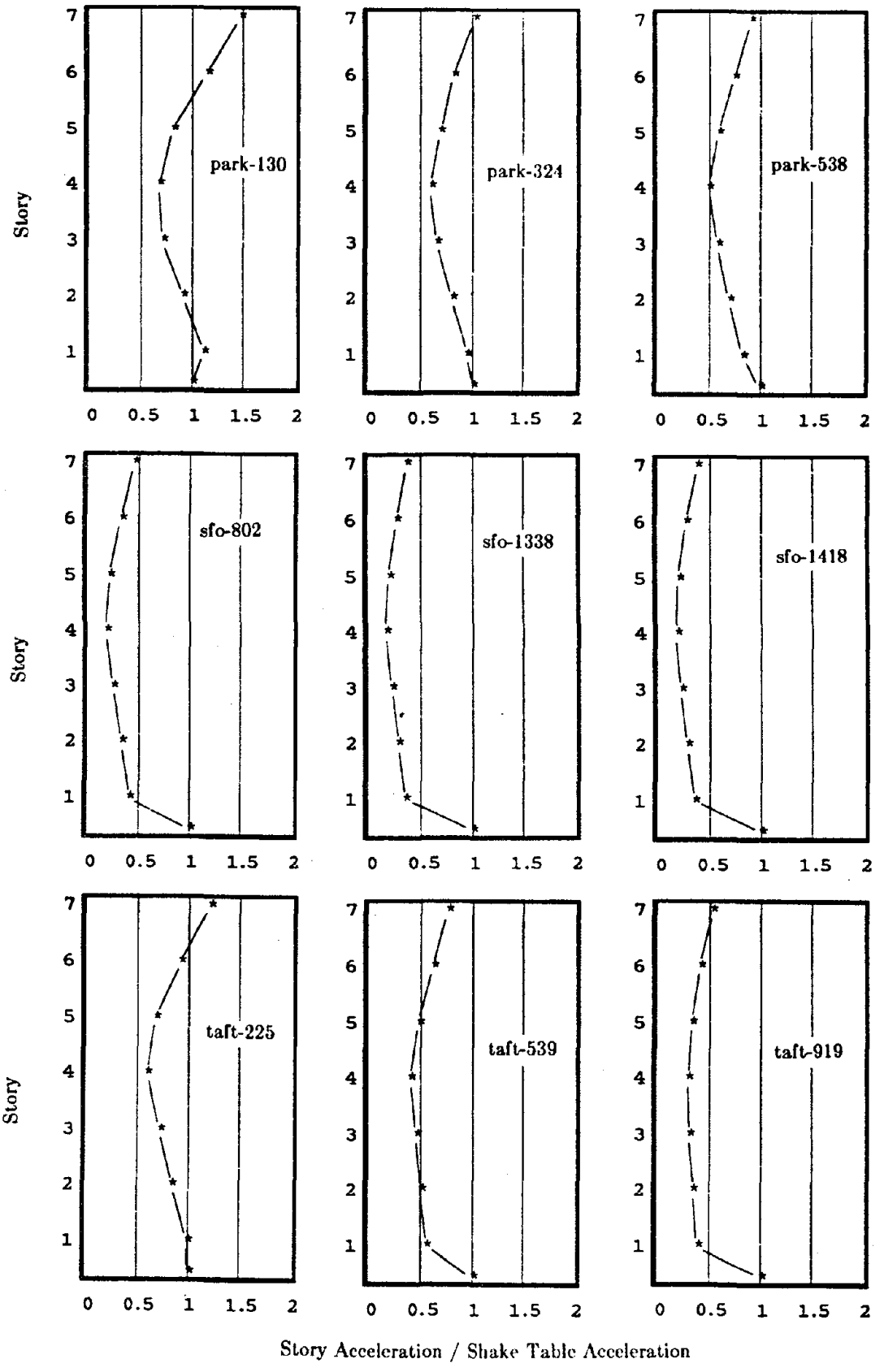

Figure 6.7 - Continued

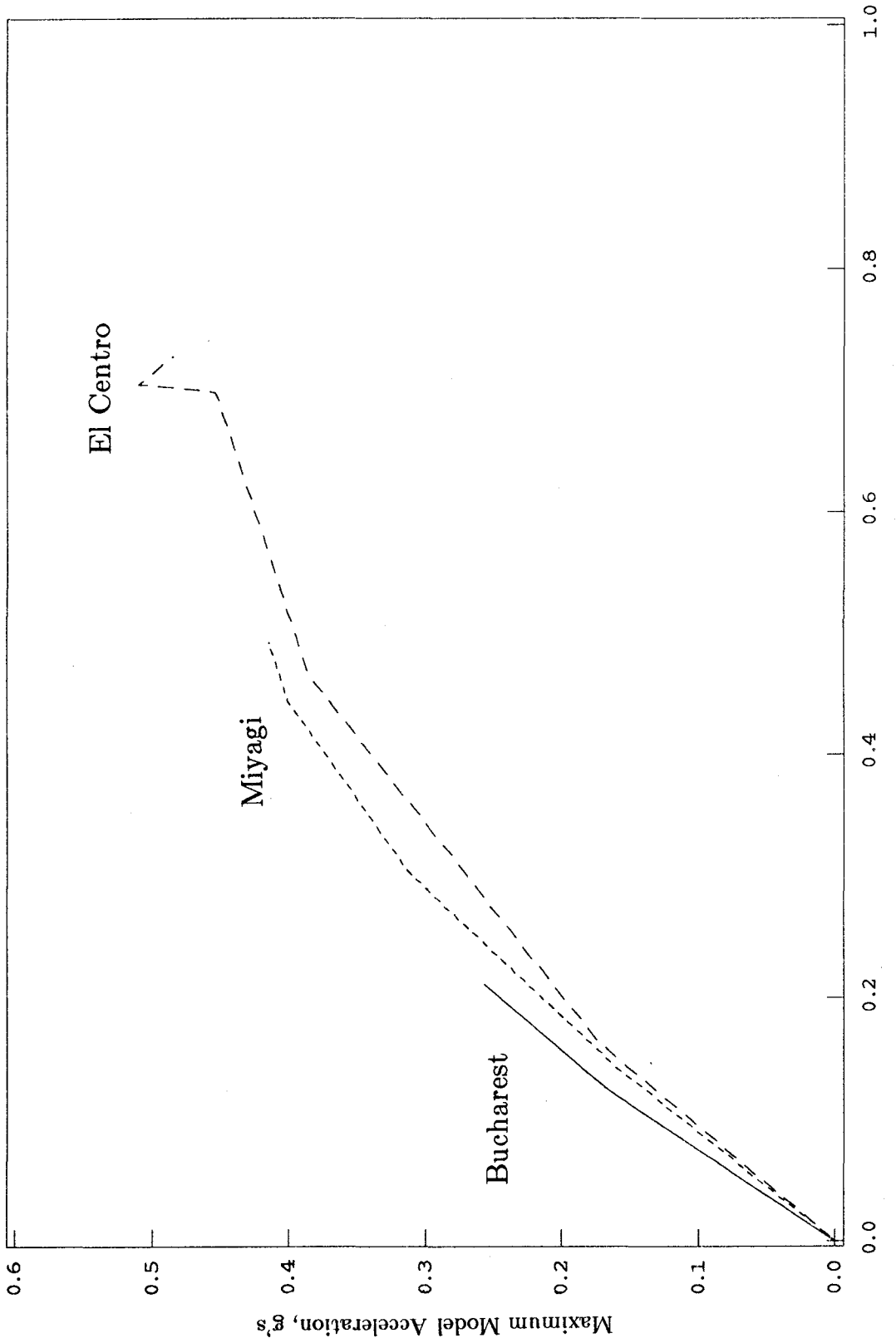

Figure 6.8 - Peak Model vs. Peak Shaking Table Acceleration

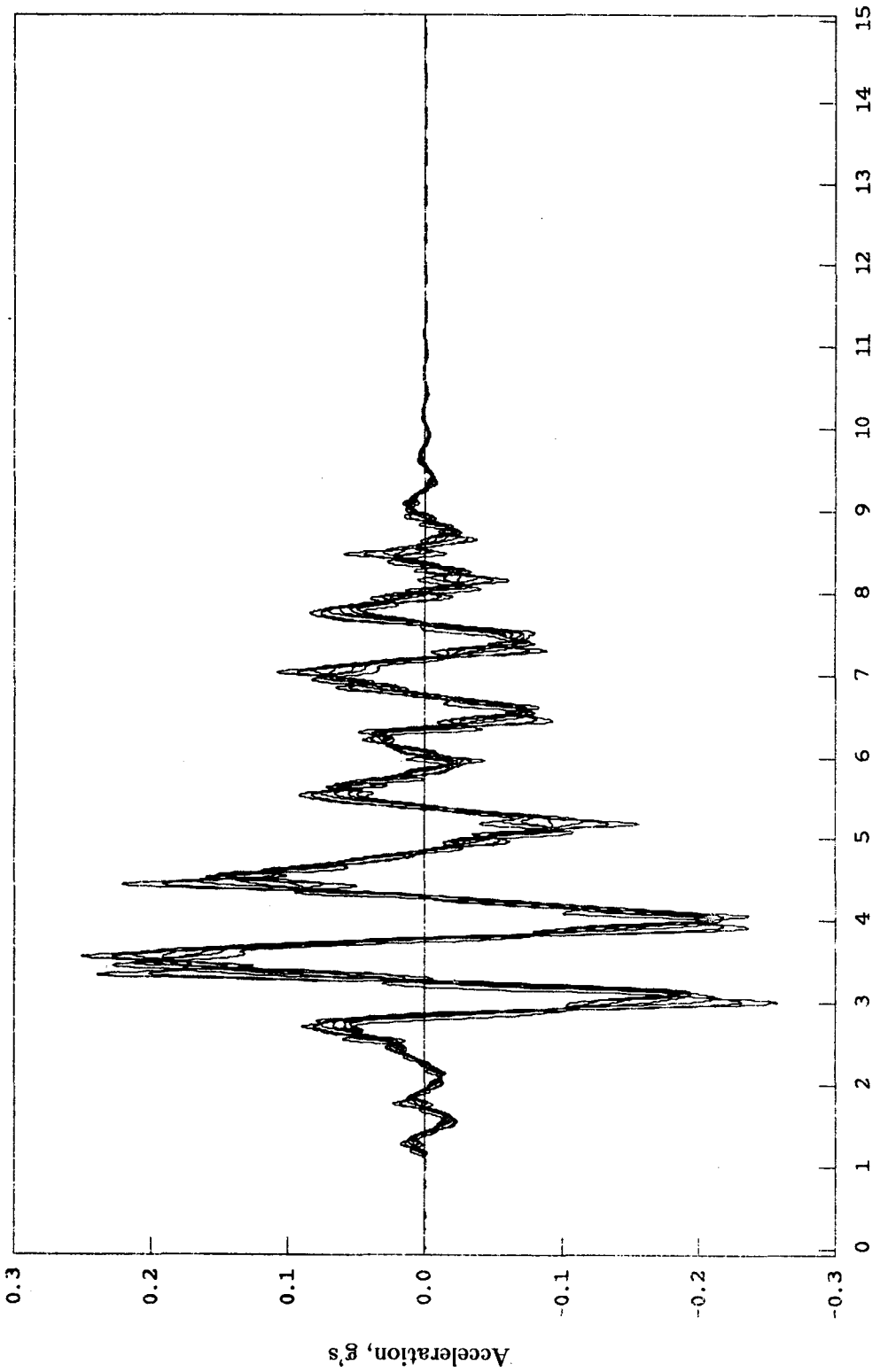

(a) Bucharest

Figure 6.9 - Story Accelerations, 1st Set of Bearings

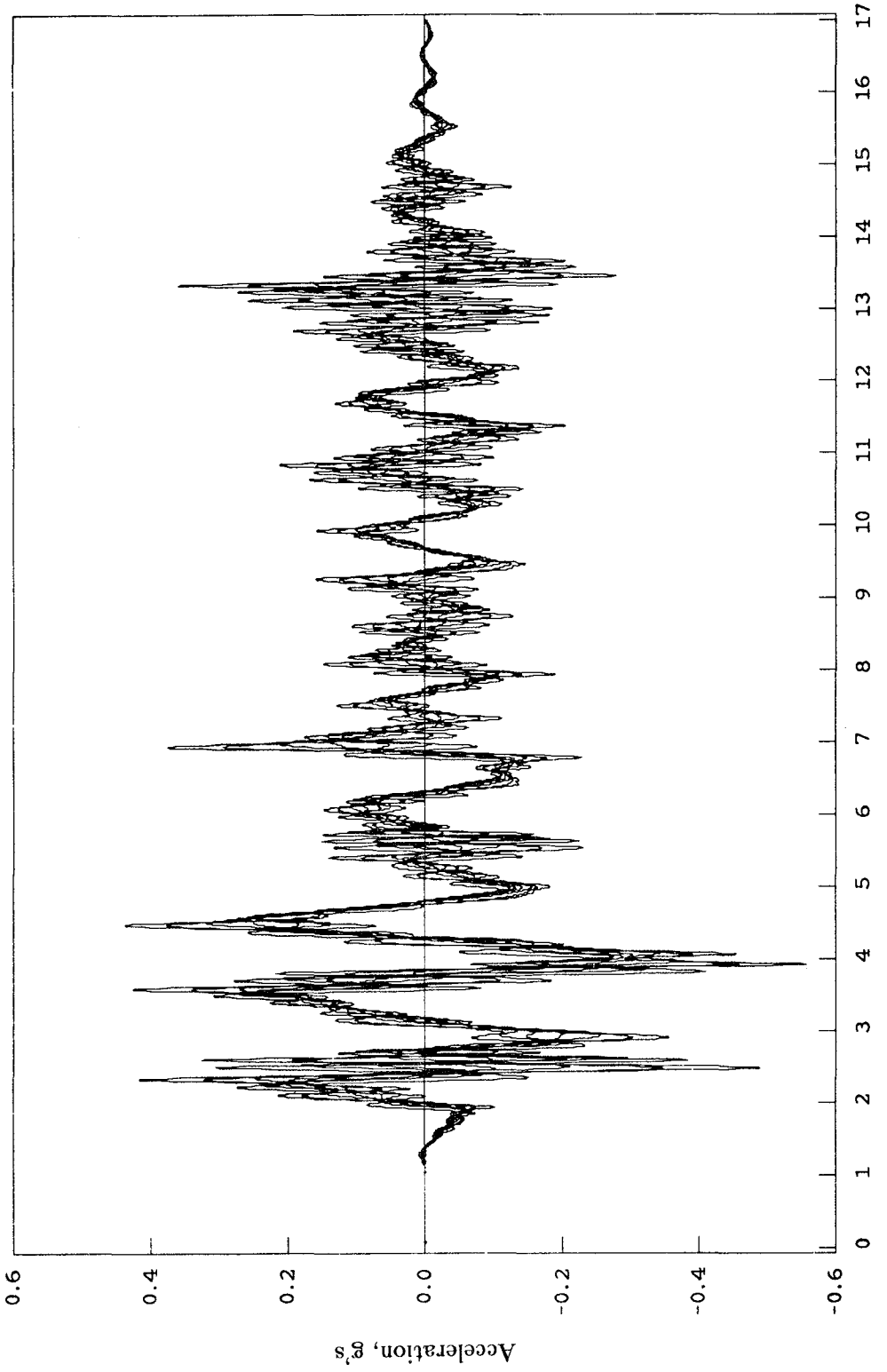

(b) El Centro

Figure 6.9 - Continued

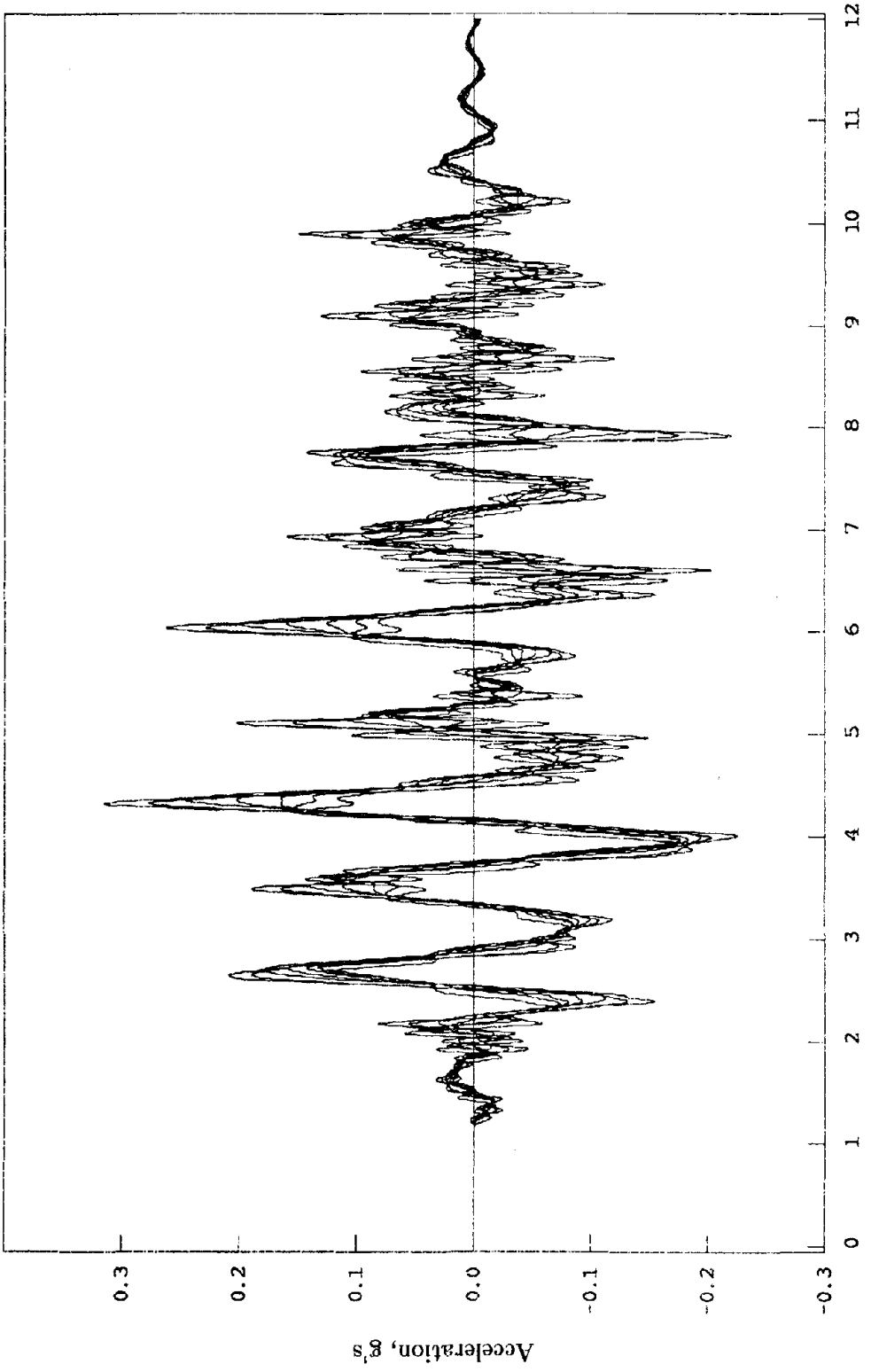

(c) Miyagi-Ken-Oki

Figure 6.9 - Continued

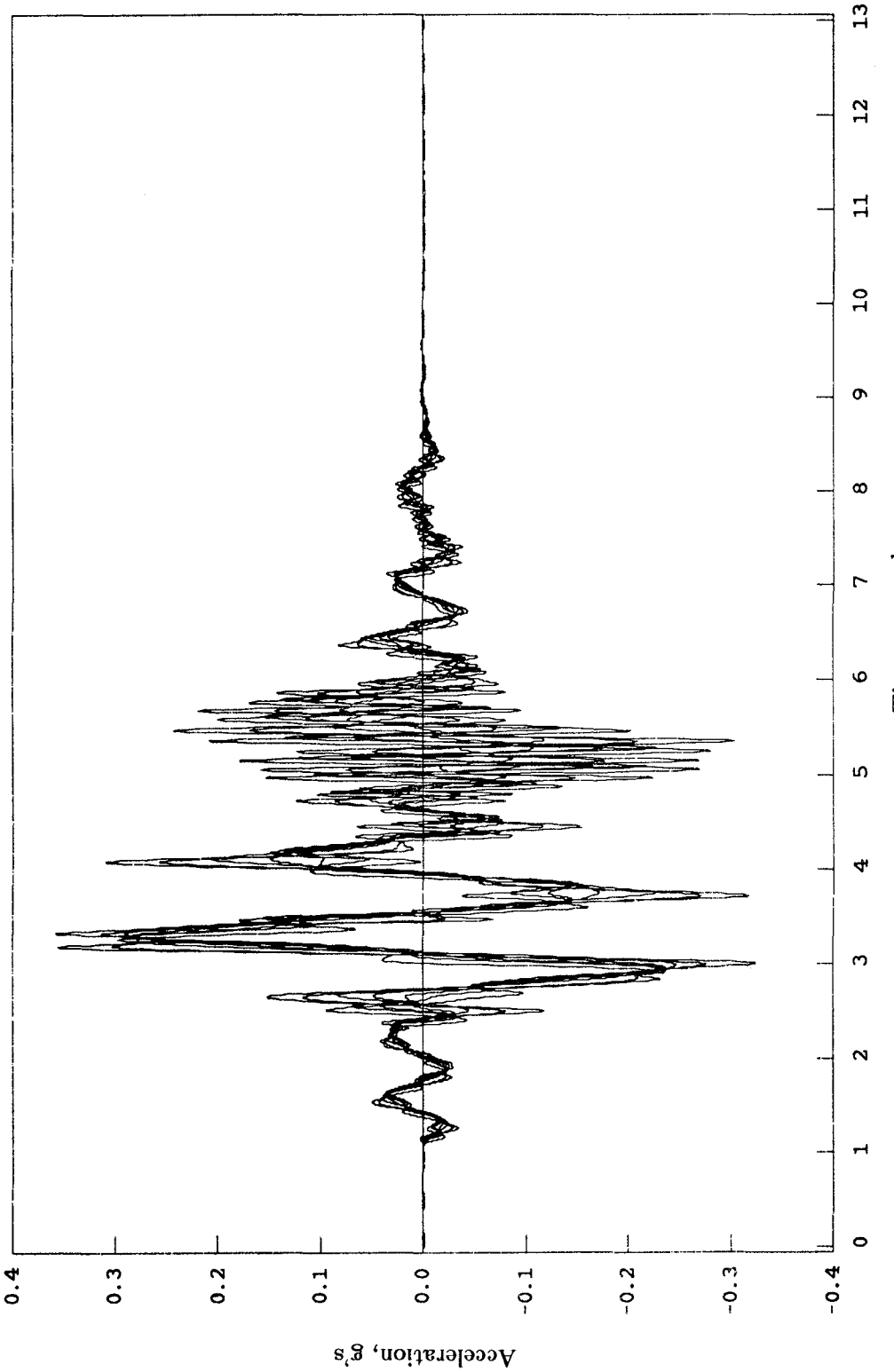

(d) Pacoima Dam

Figure 6.9 - Continued

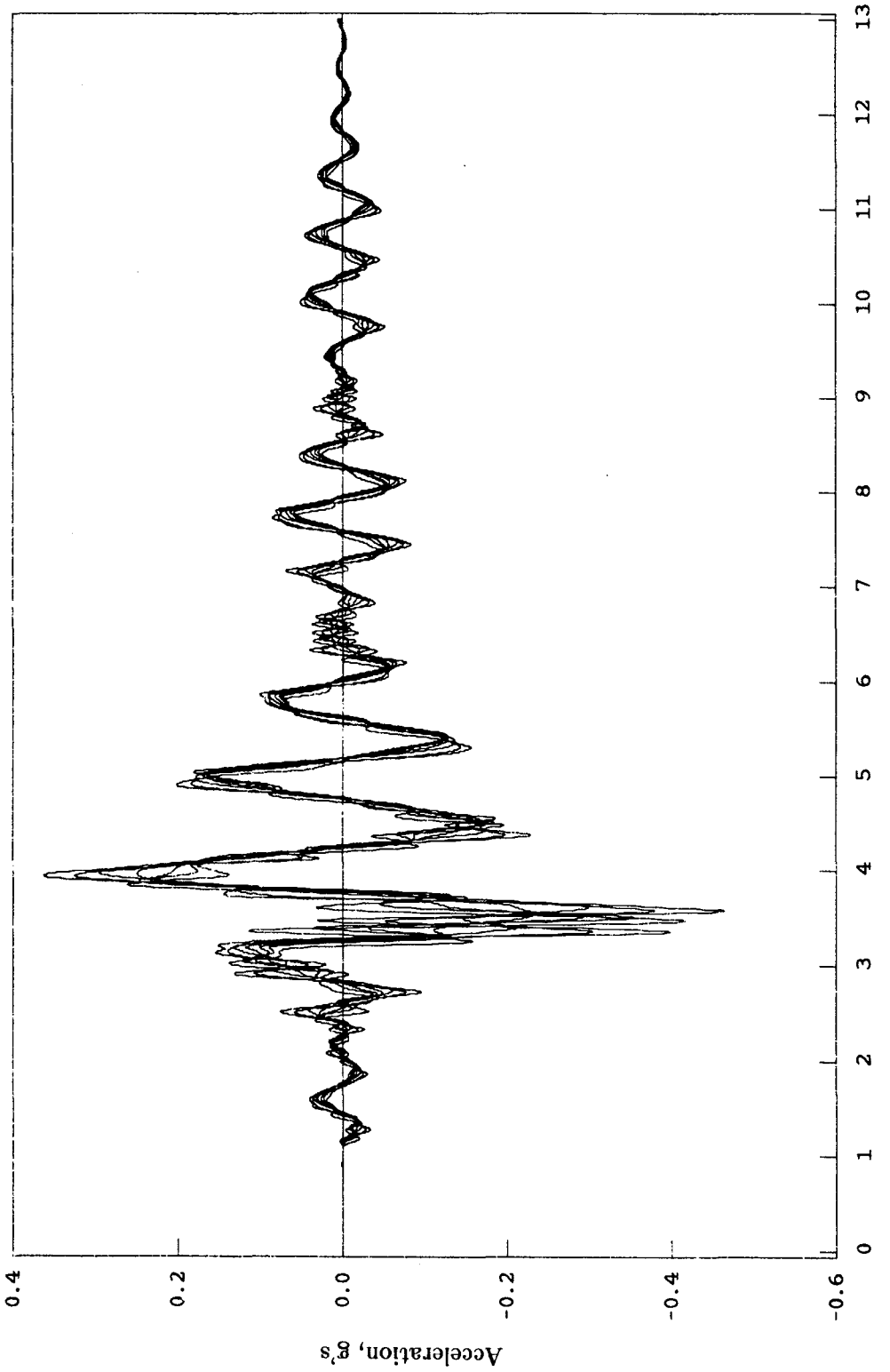

(e) Parkfield

Figure 6.9 - Continued

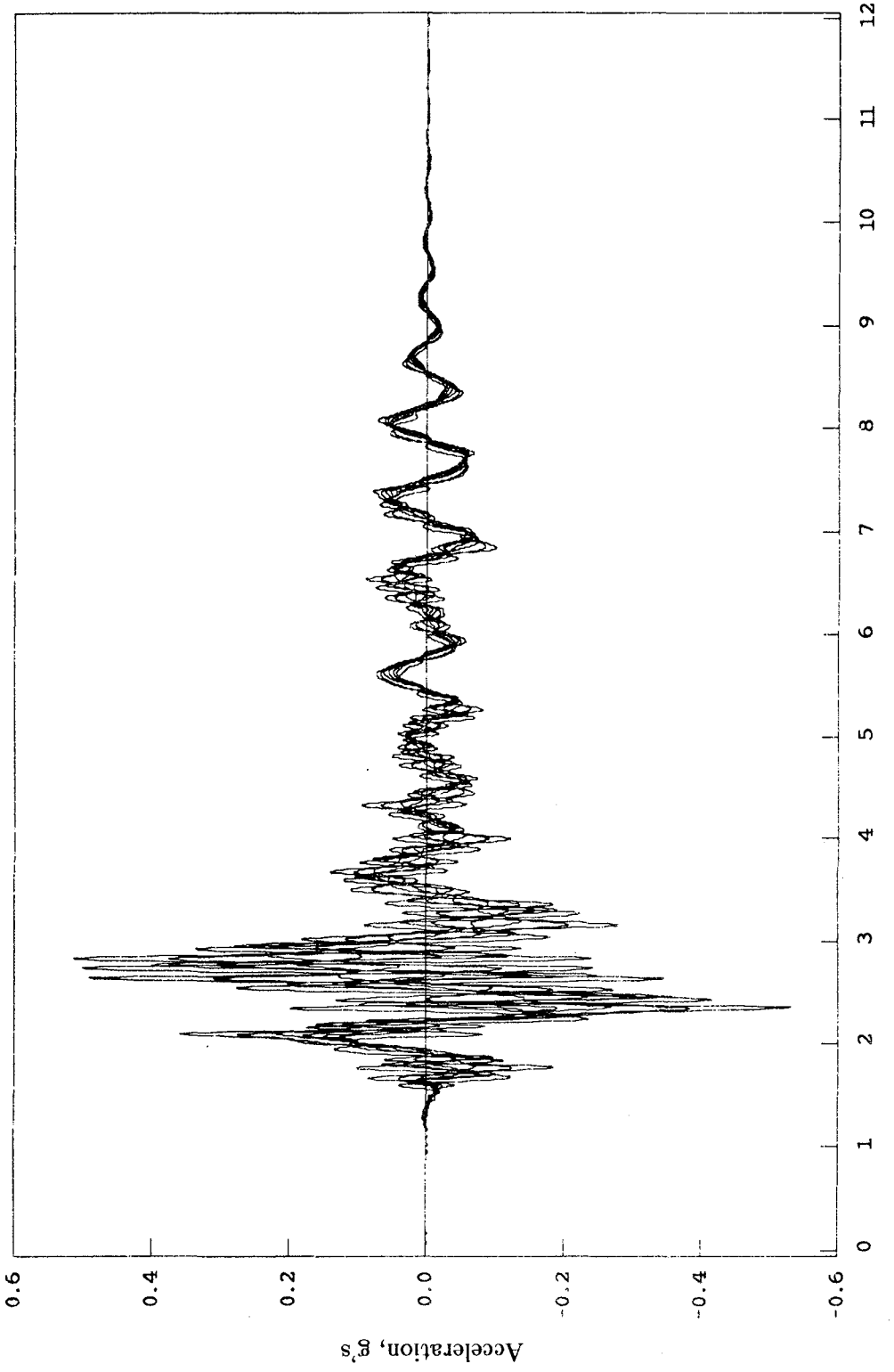

(f) San Francisco

Figure 6.9 - Continued

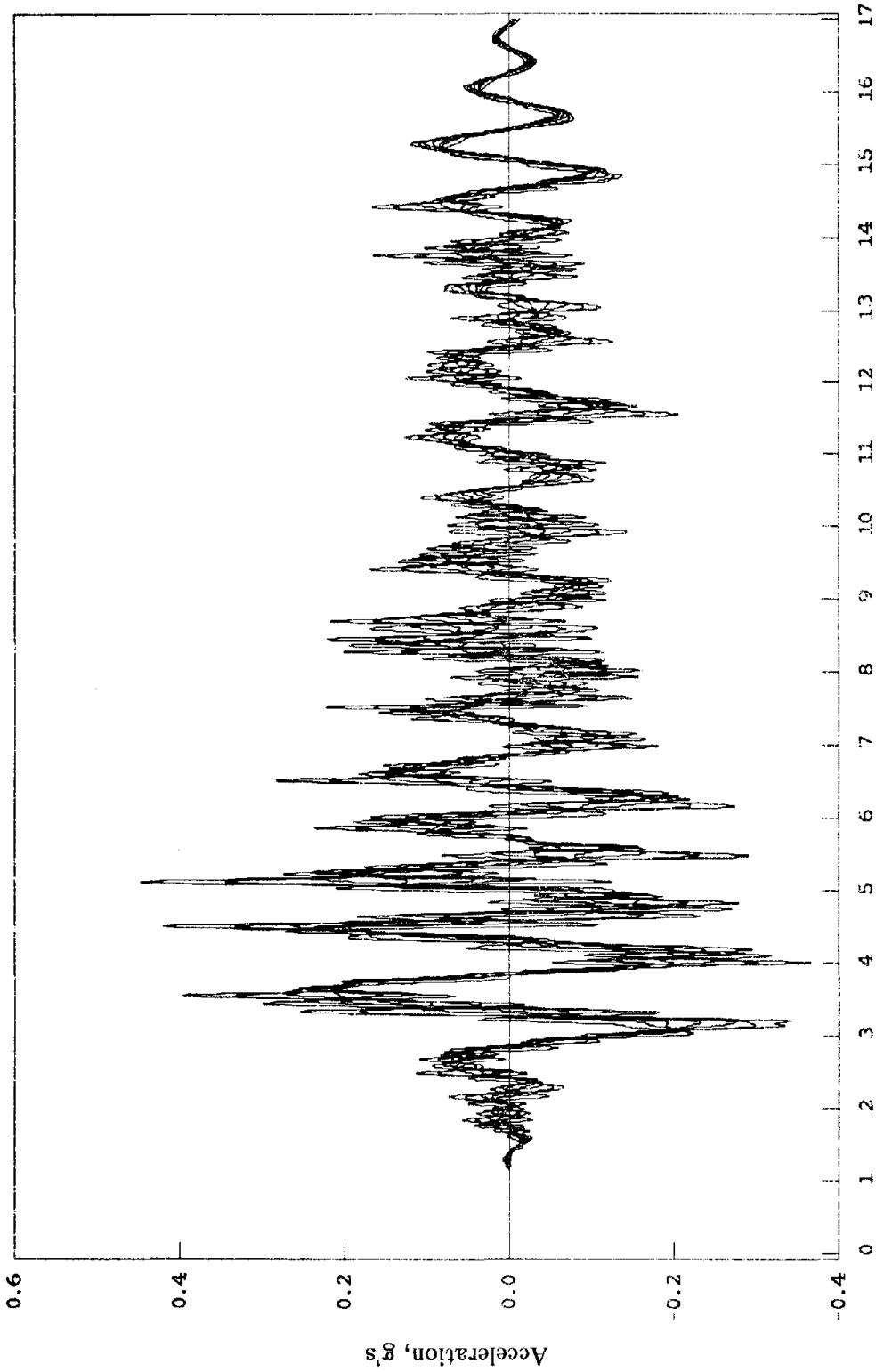

(g) Taft

Figure 6.9 - Continued

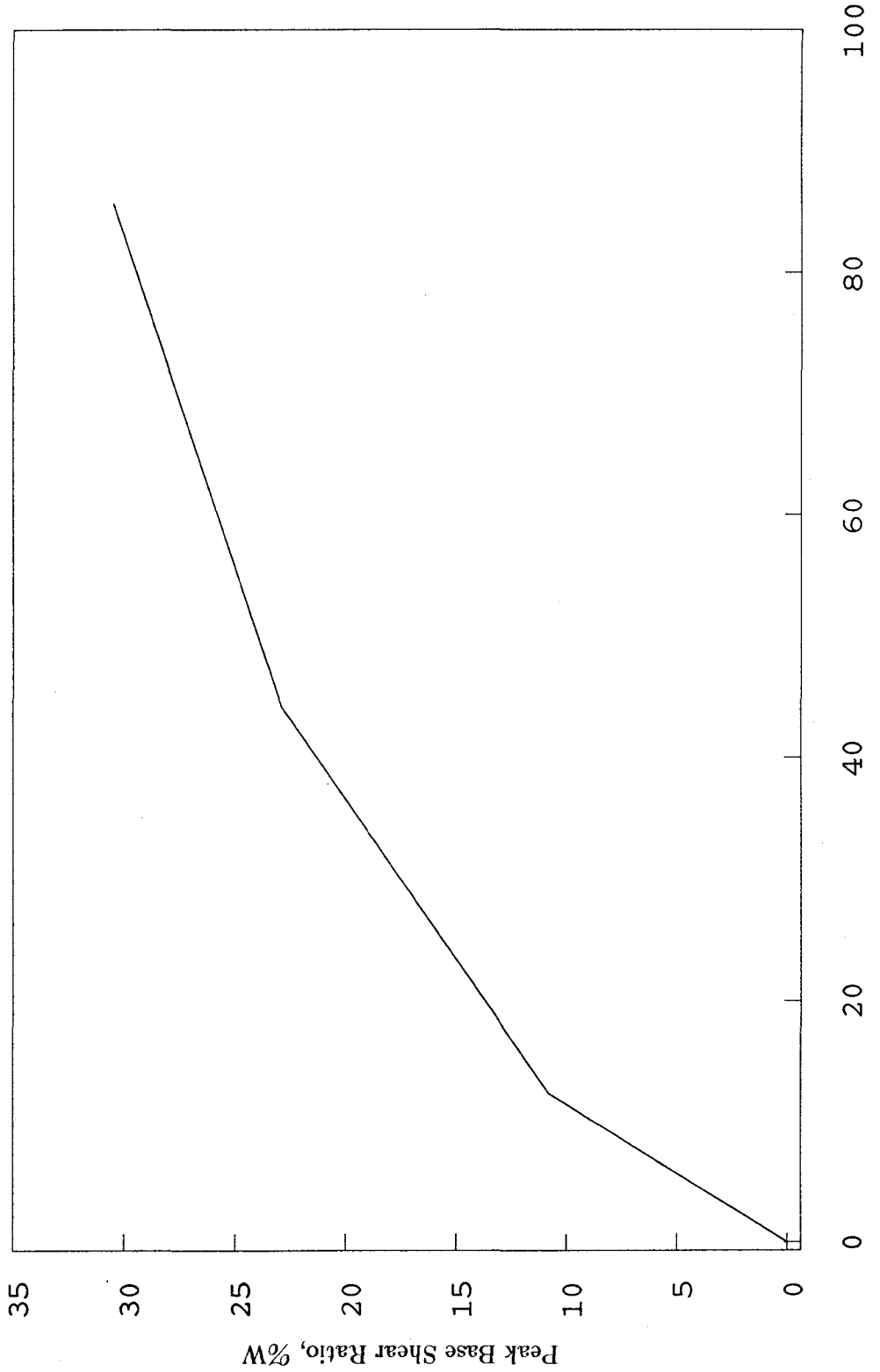

Figure 6.10 - Peak Base Shear Ratio for El Centro Earthquake - 1st Set of Bearings

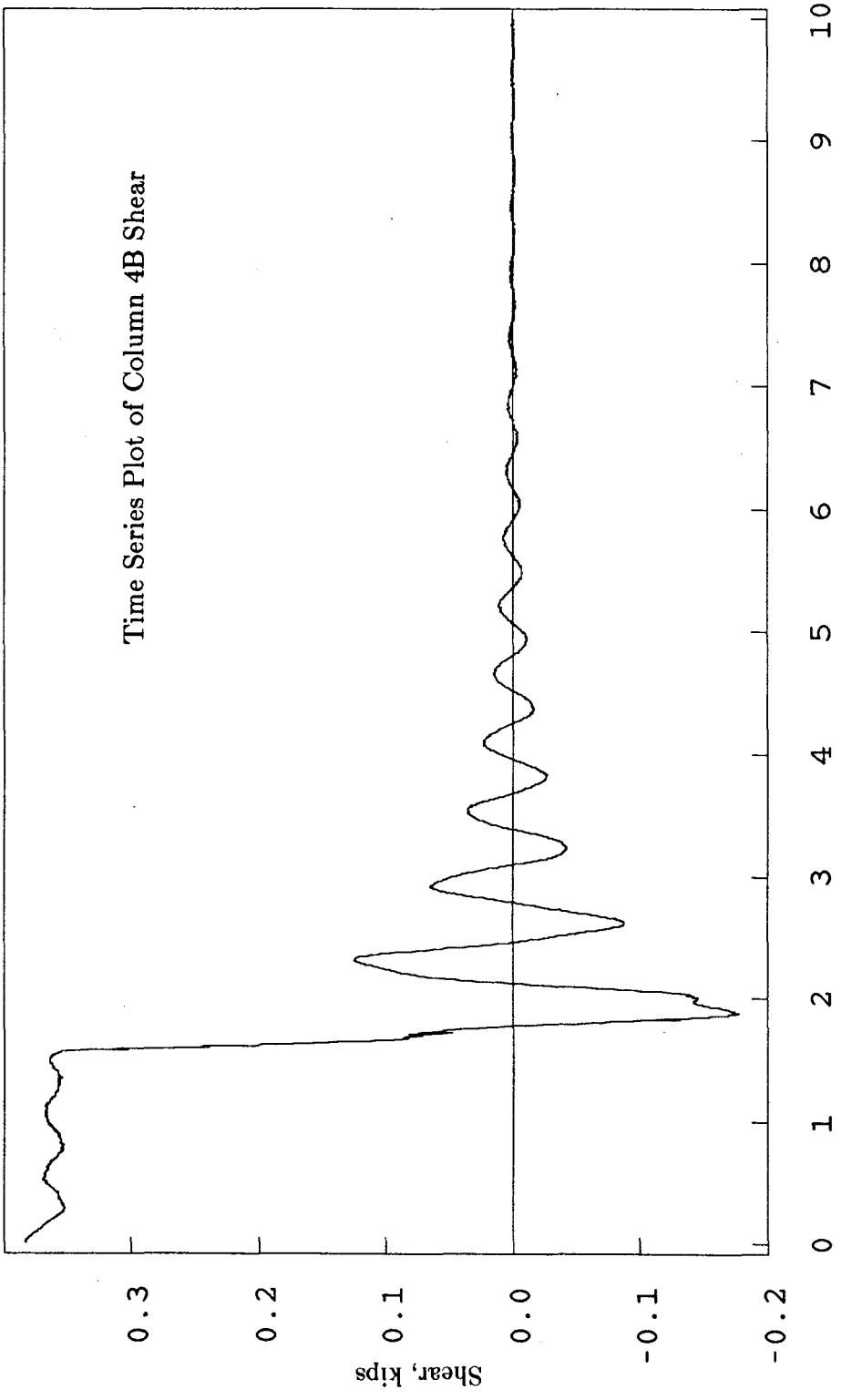

Figure 7.1 - Free-Vibration Test Log-Dec. Curve, 2nd Set of Bearings

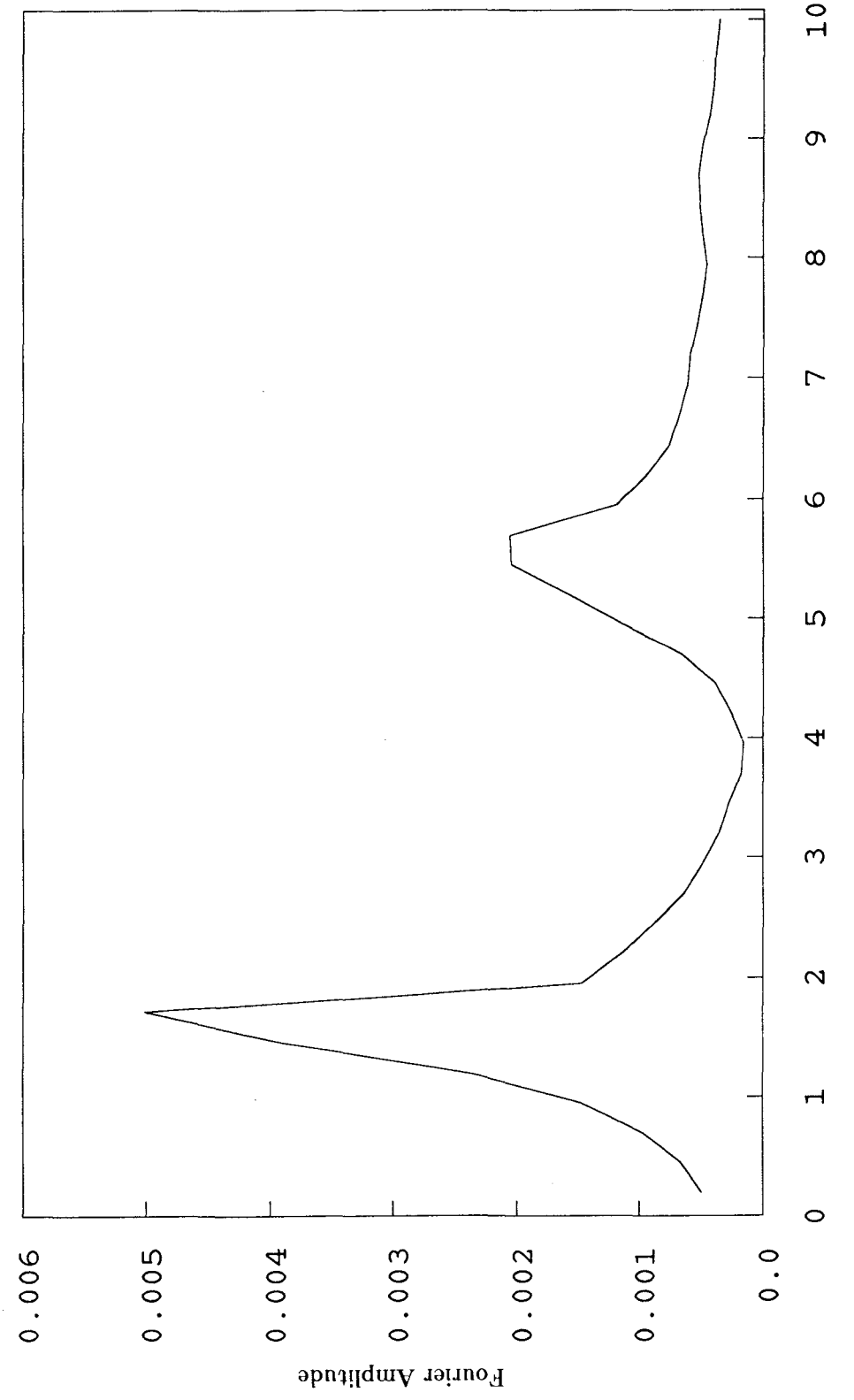

Figure 7.2 - Free-Vibration Test, 2nd Set of Bearings

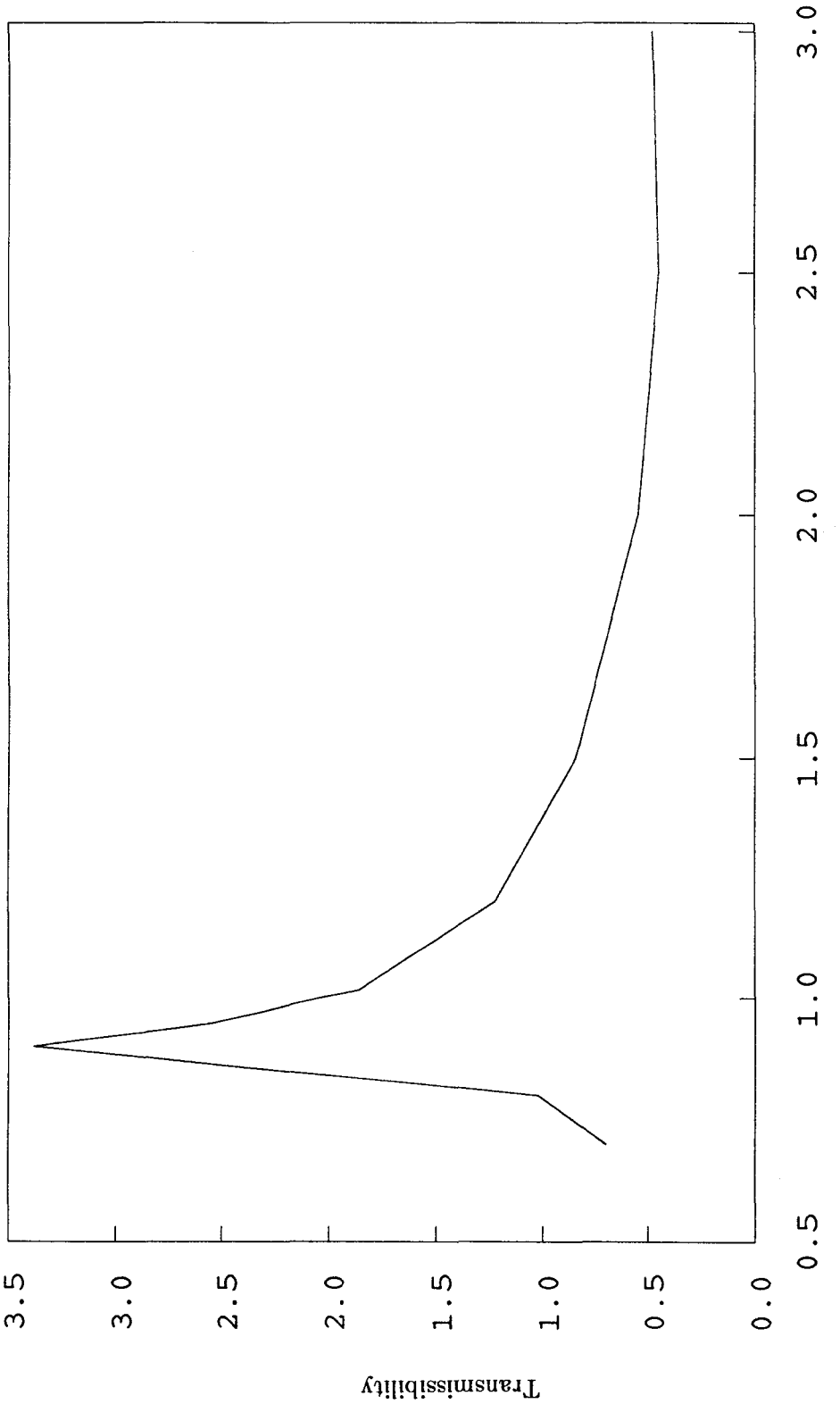

Figure 7.3 - Sine Test Transmissibility Plot, 2nd Set of Bearings

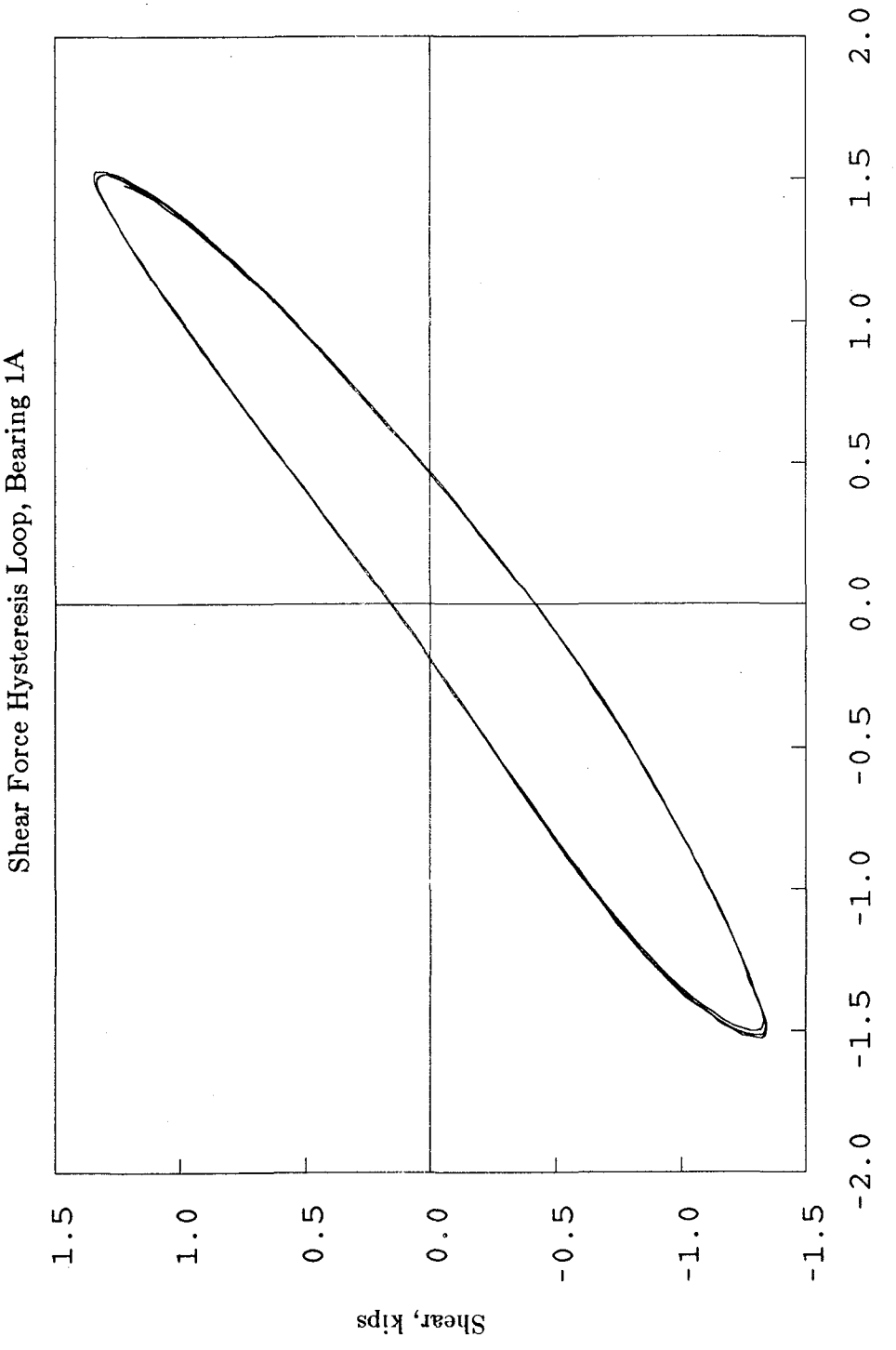

Figure 7.4 - Sine Test Hysteresis Loops, 2nd Set of Bearings

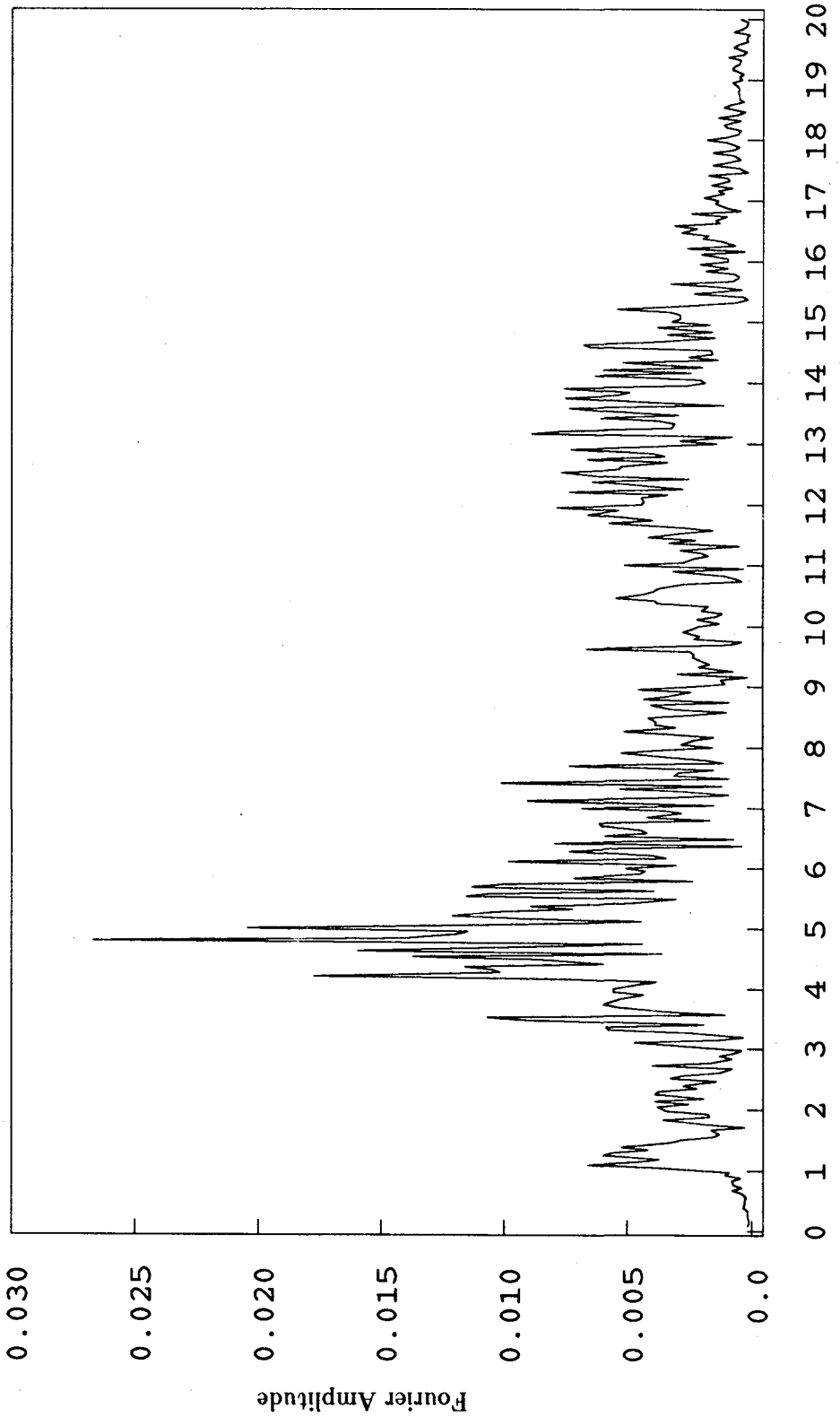

Figure 7.5 - White Noise Test, Roof Acceleration

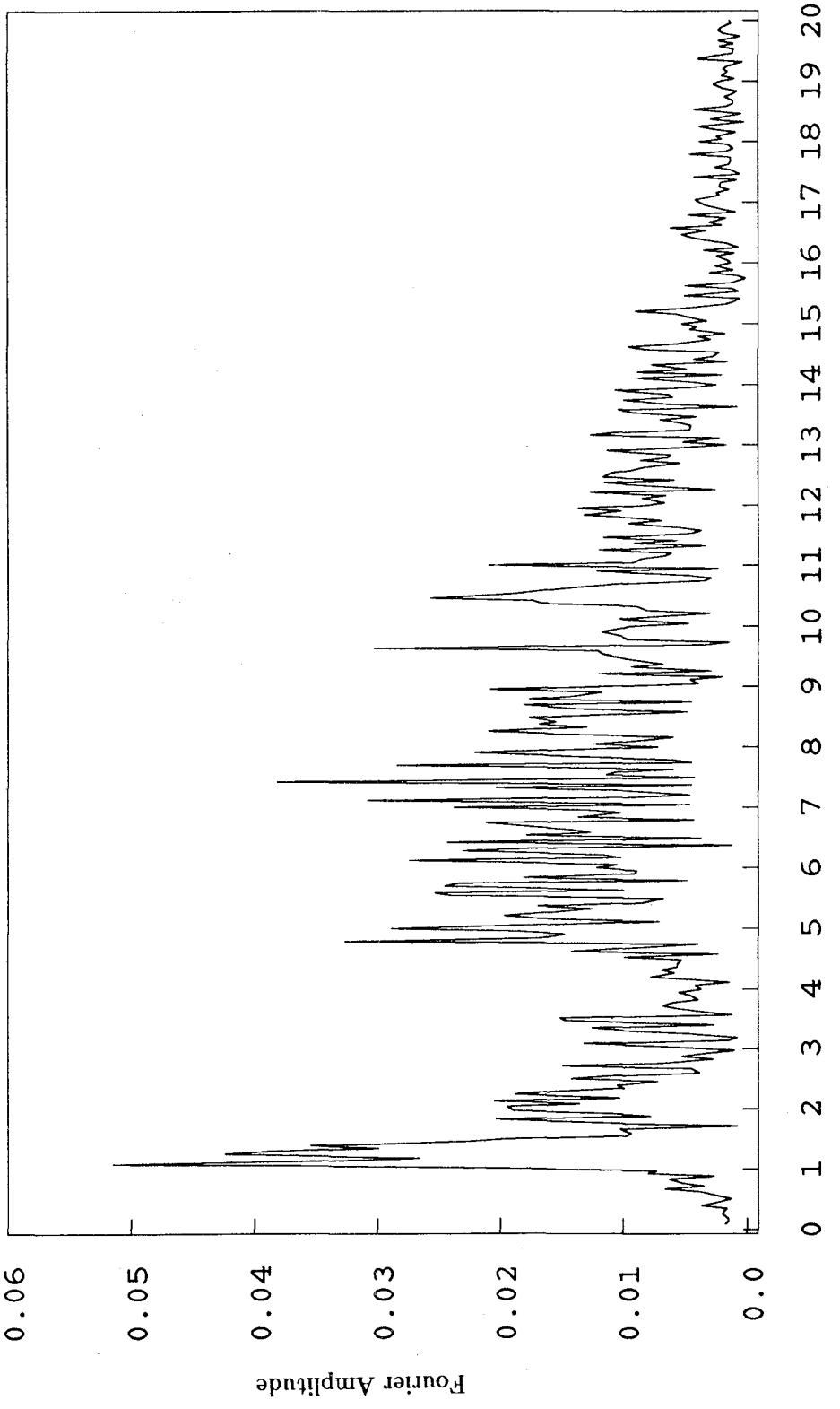

Figure 7.6 - White Noise Test, Bearing Displacement

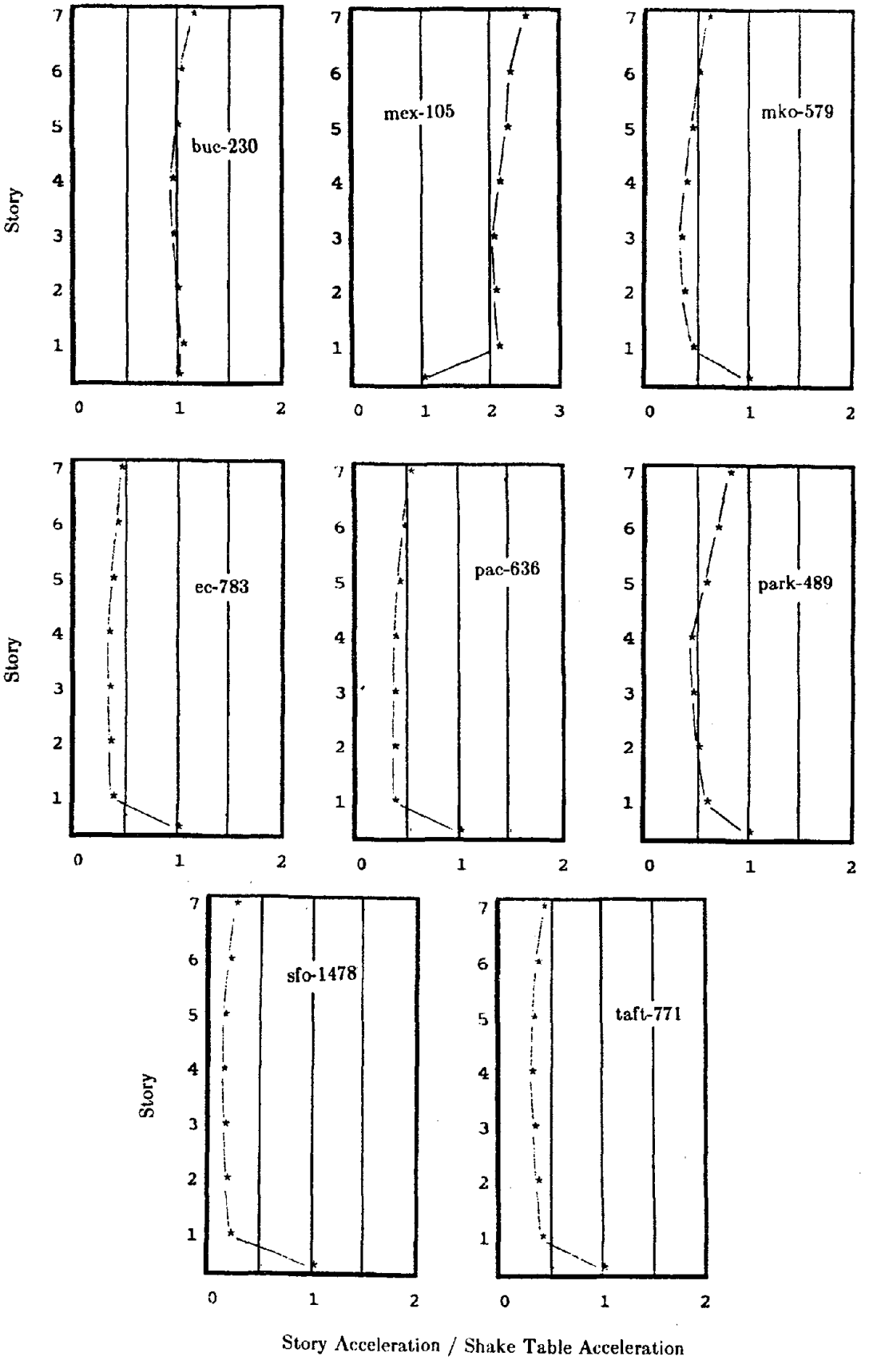

Figure 7.7 - Peak Acceleration Profiles, 2nd Set of Bearings

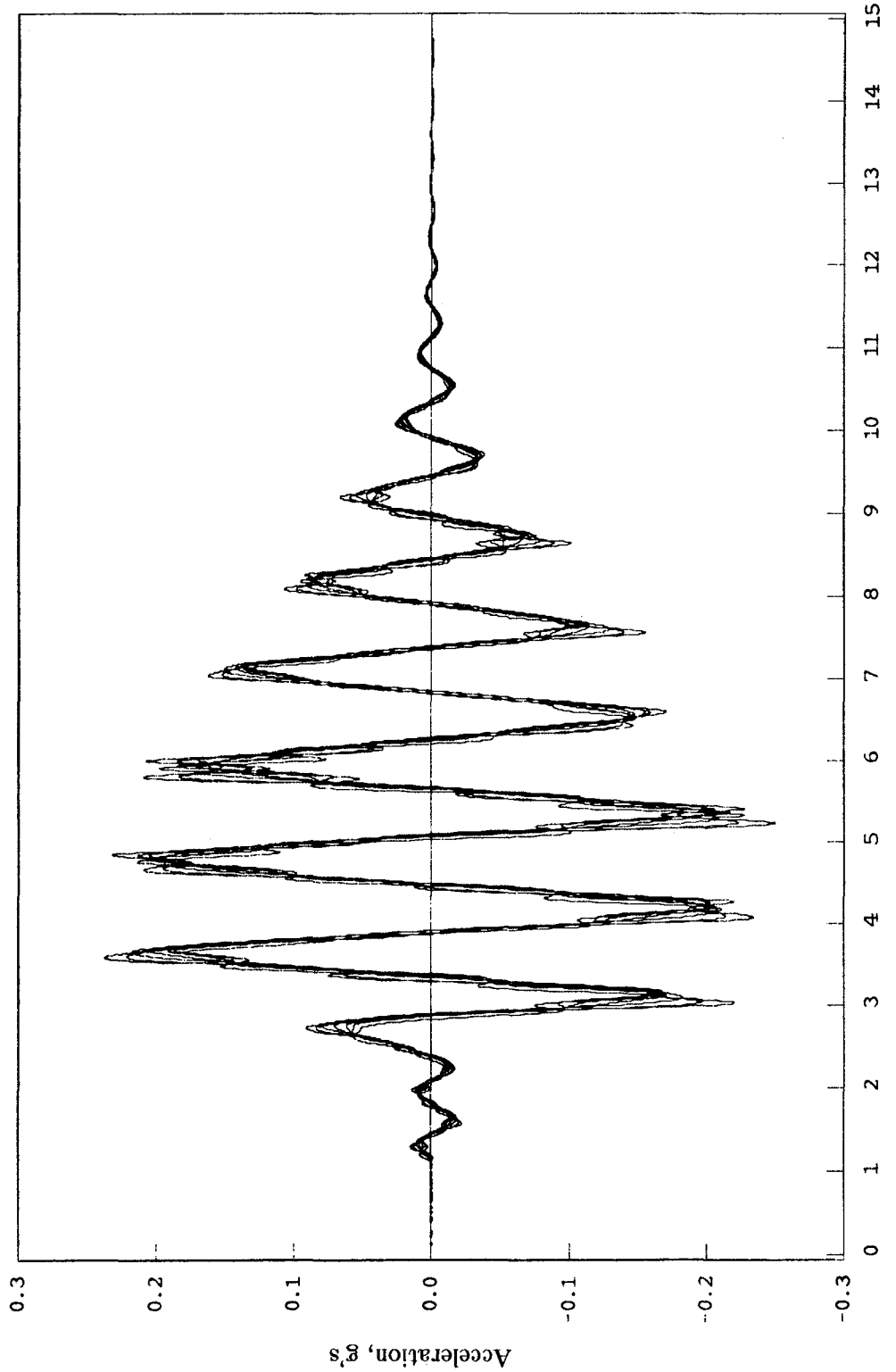

(a) Bucharest

Figure 7.8 - Story Accelerations, 2nd Set of Bearings

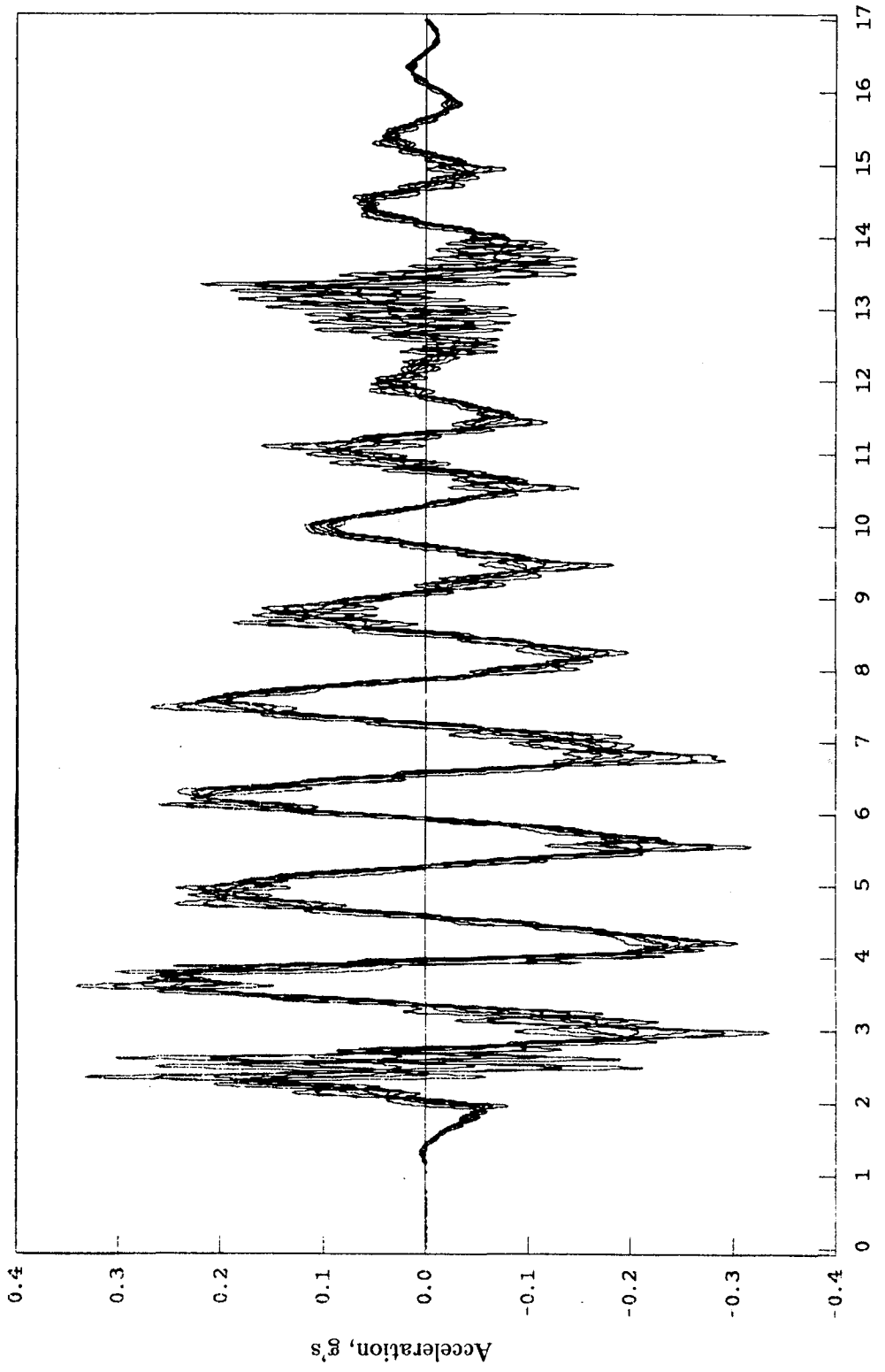

(b) El Centro

Figure 7.8 - Continued

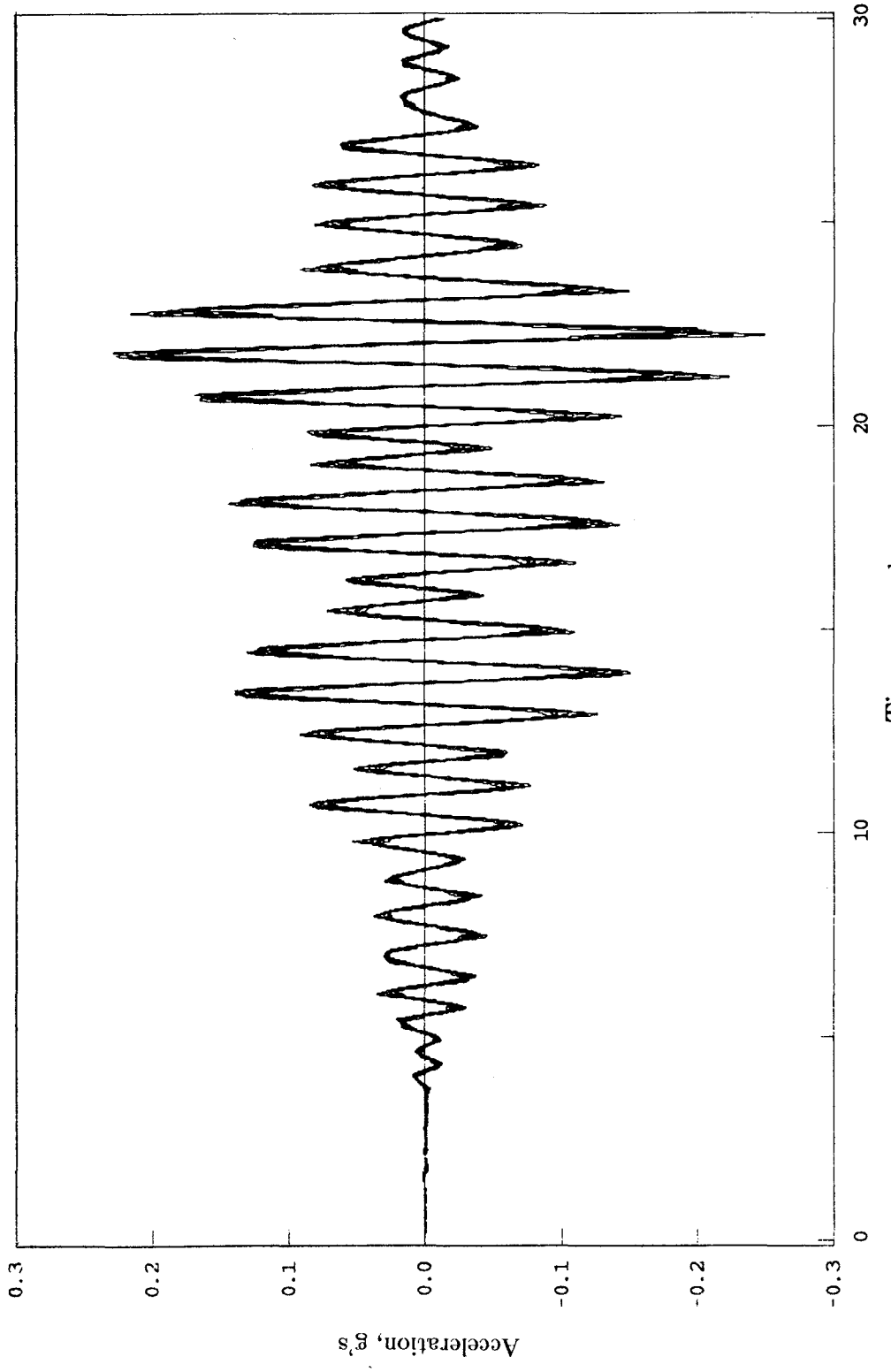

(c) Mexico City

Figure 7.8 - Continued

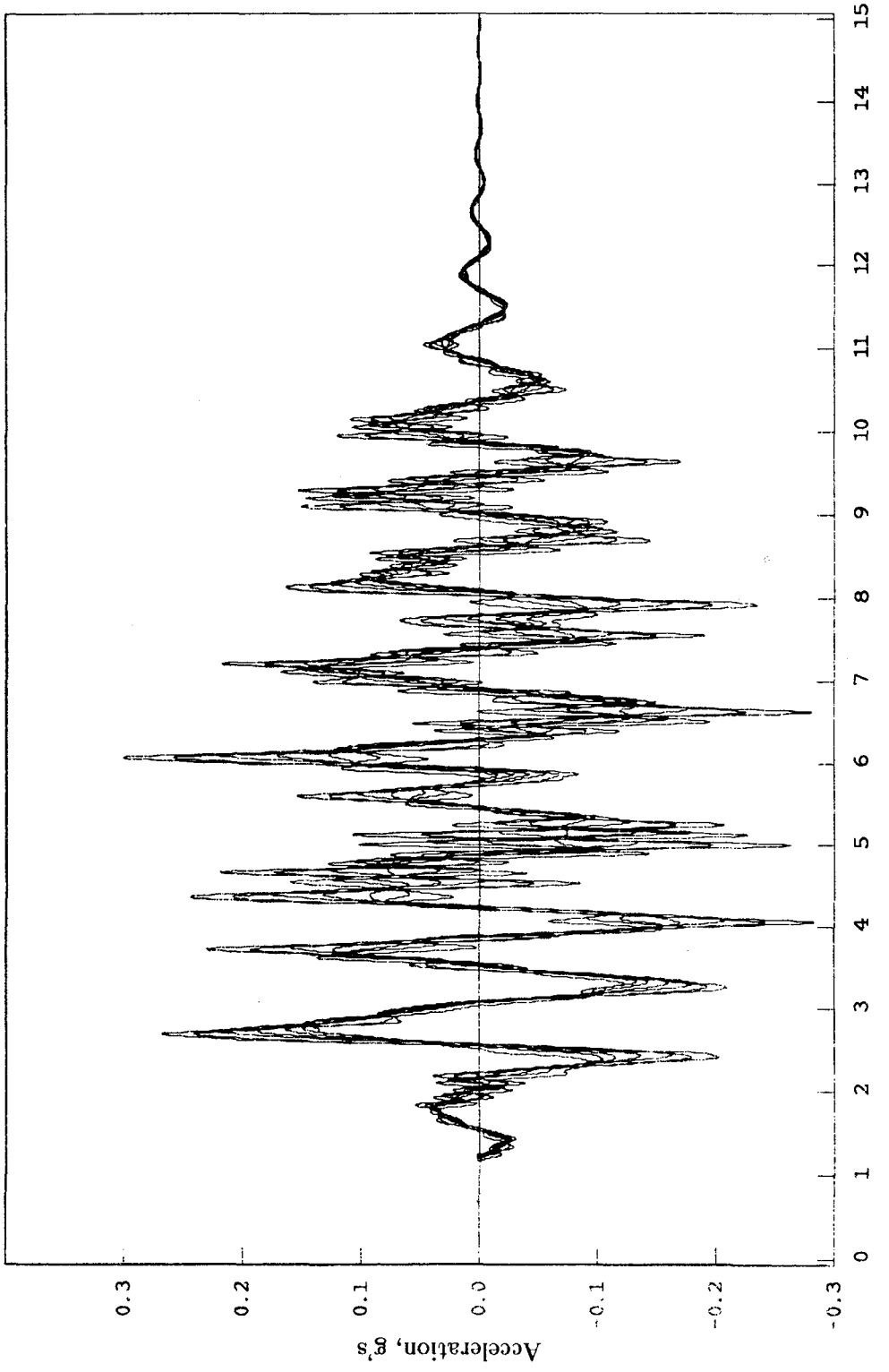

(d) Miyagi-Ken-Oki

Figure 7.8 - Continued

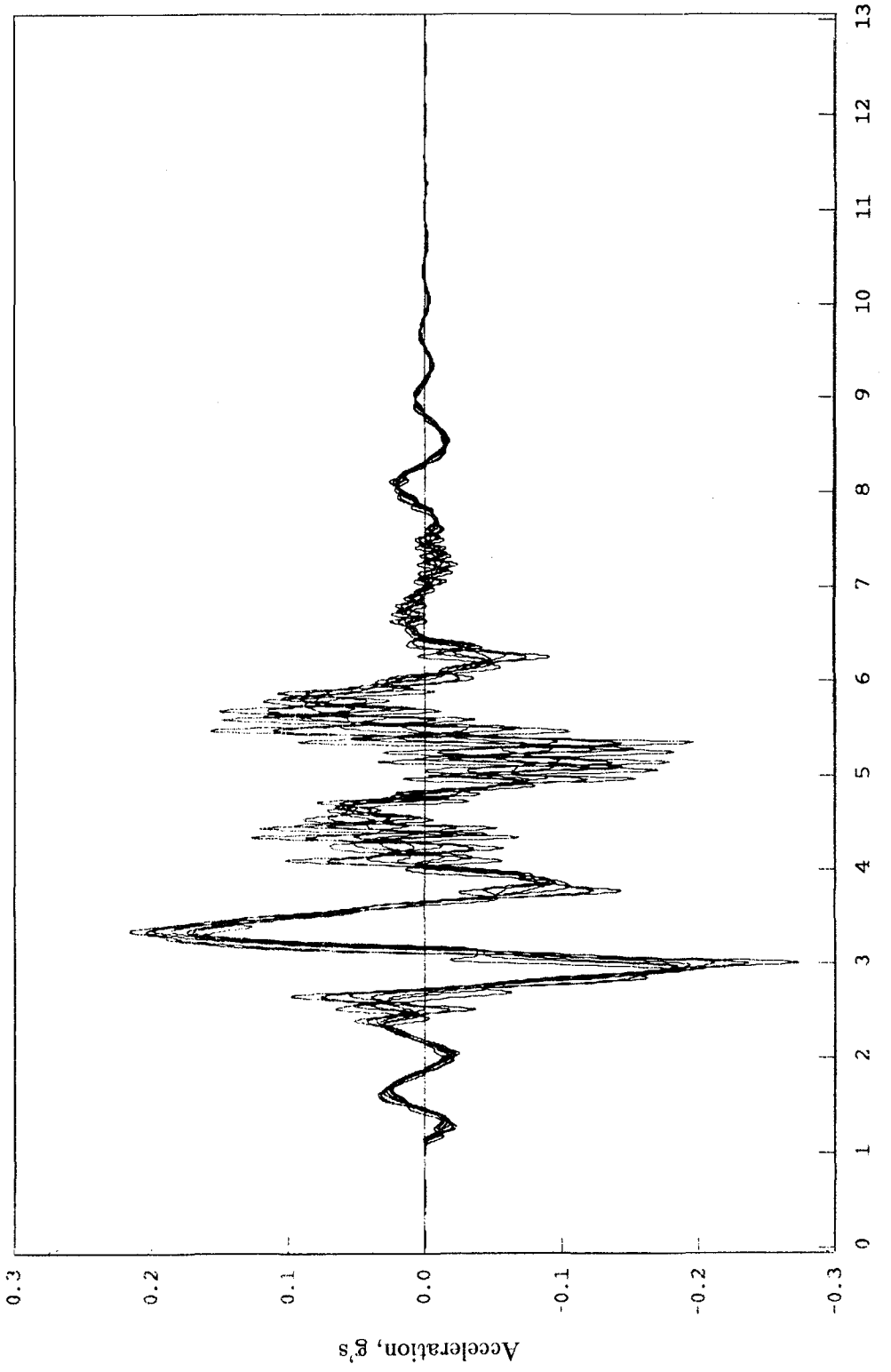

(e) Pacoima Dam

Figure 7.8 - Continued

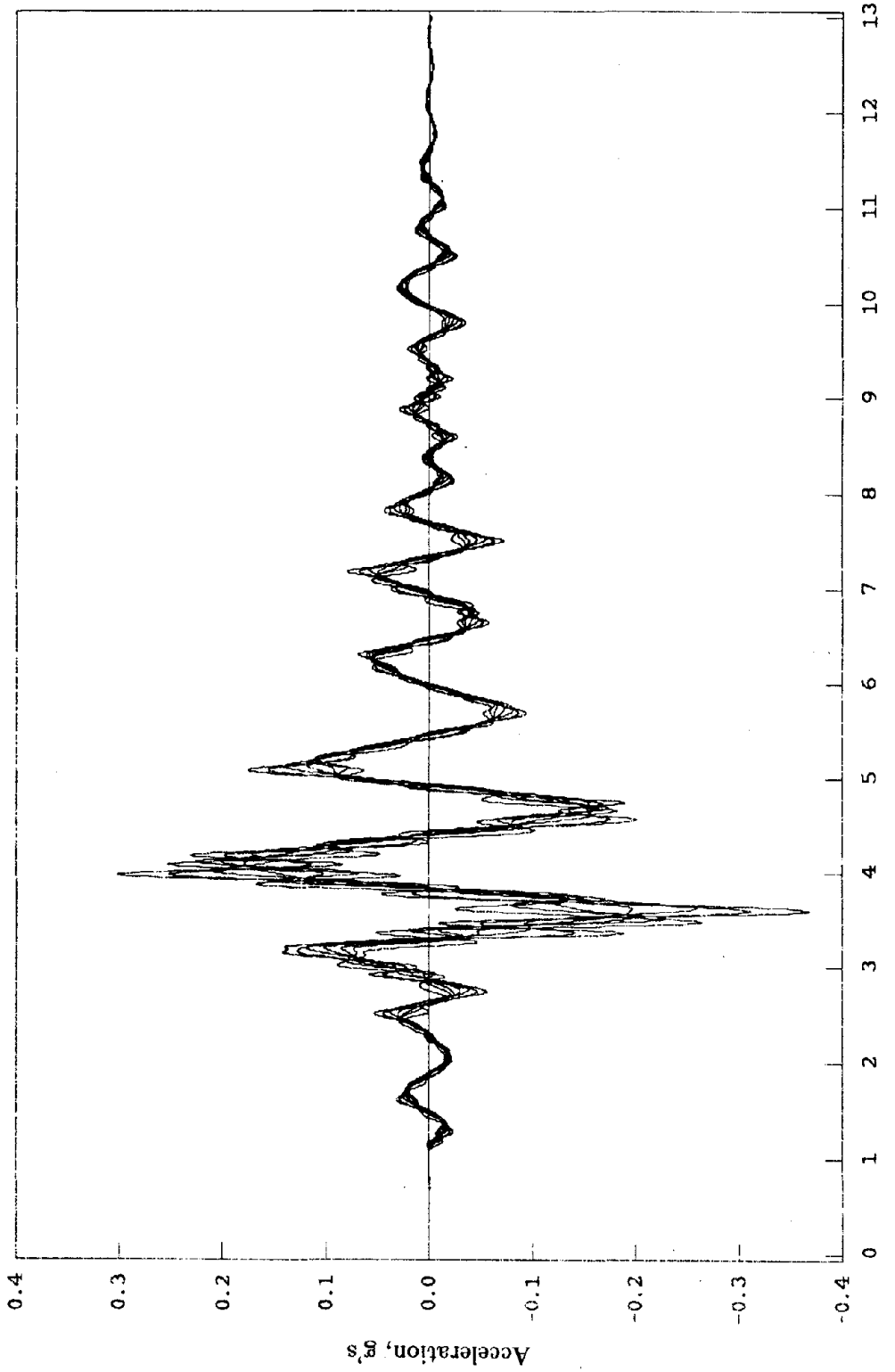

(f) Parkfield

Figure 7.8 - Continued

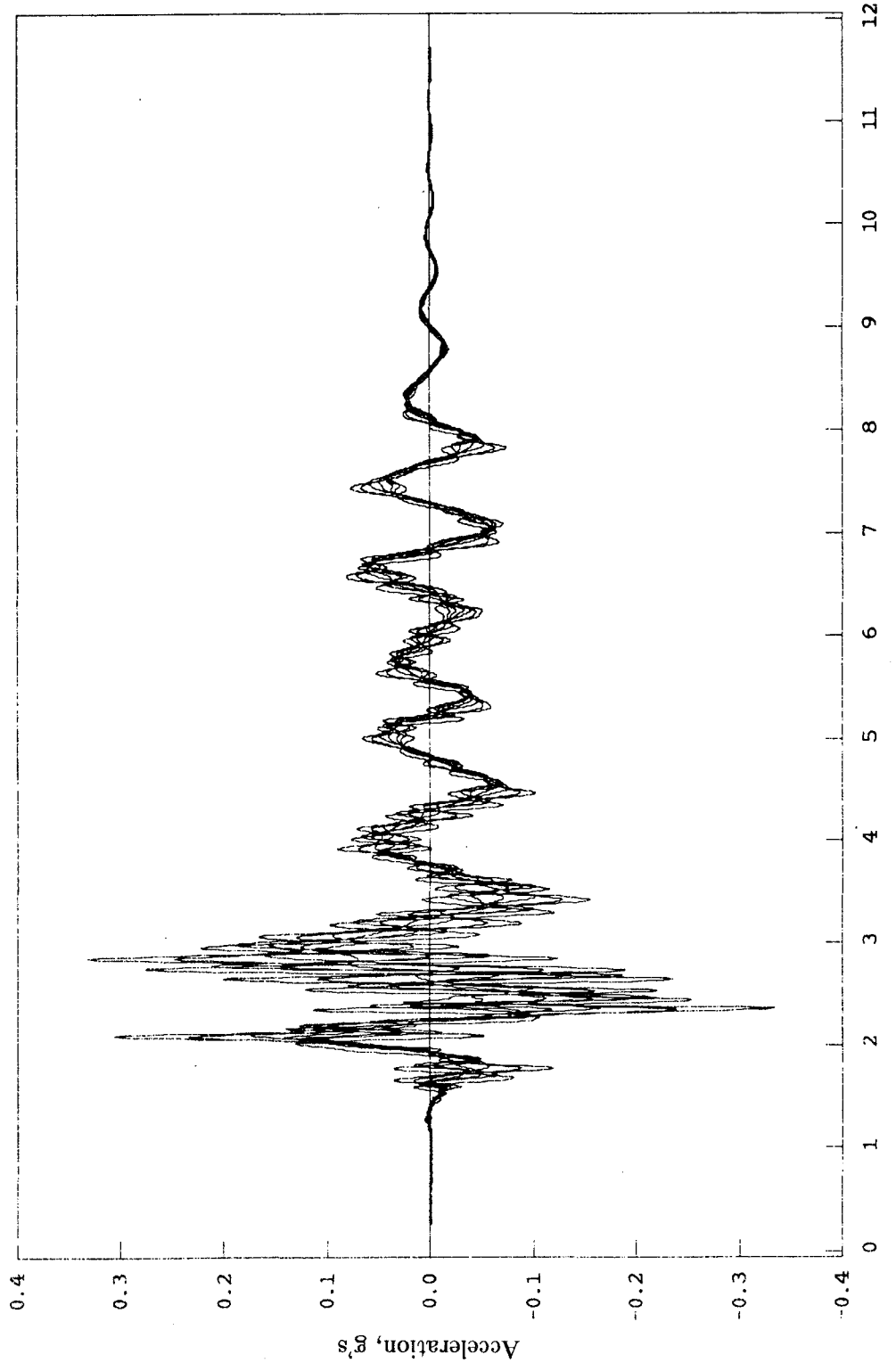

(g) San Francisco

Figure 7.8 - Continued

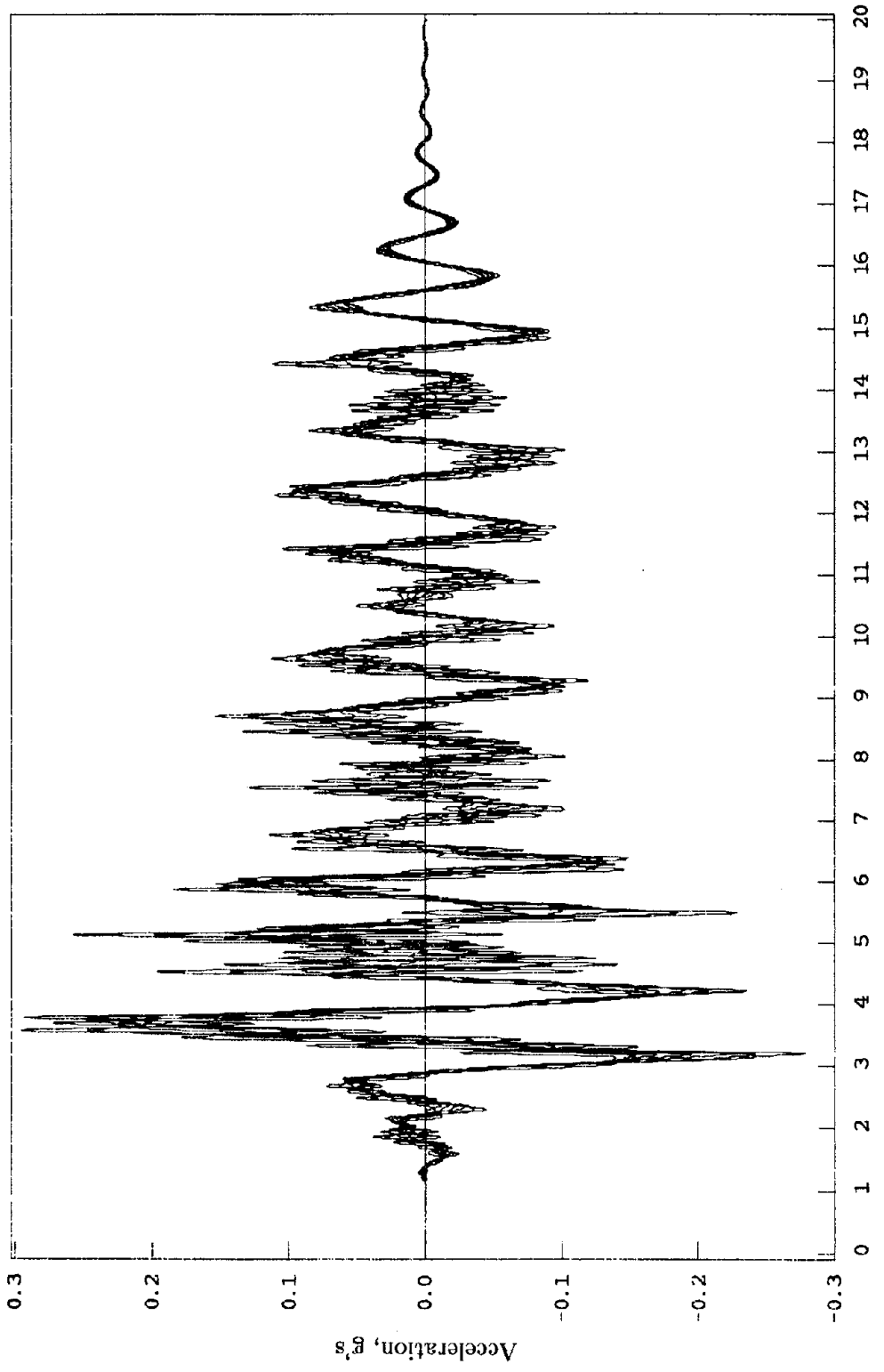

(h) Taft

Figure 7.8 - Continued

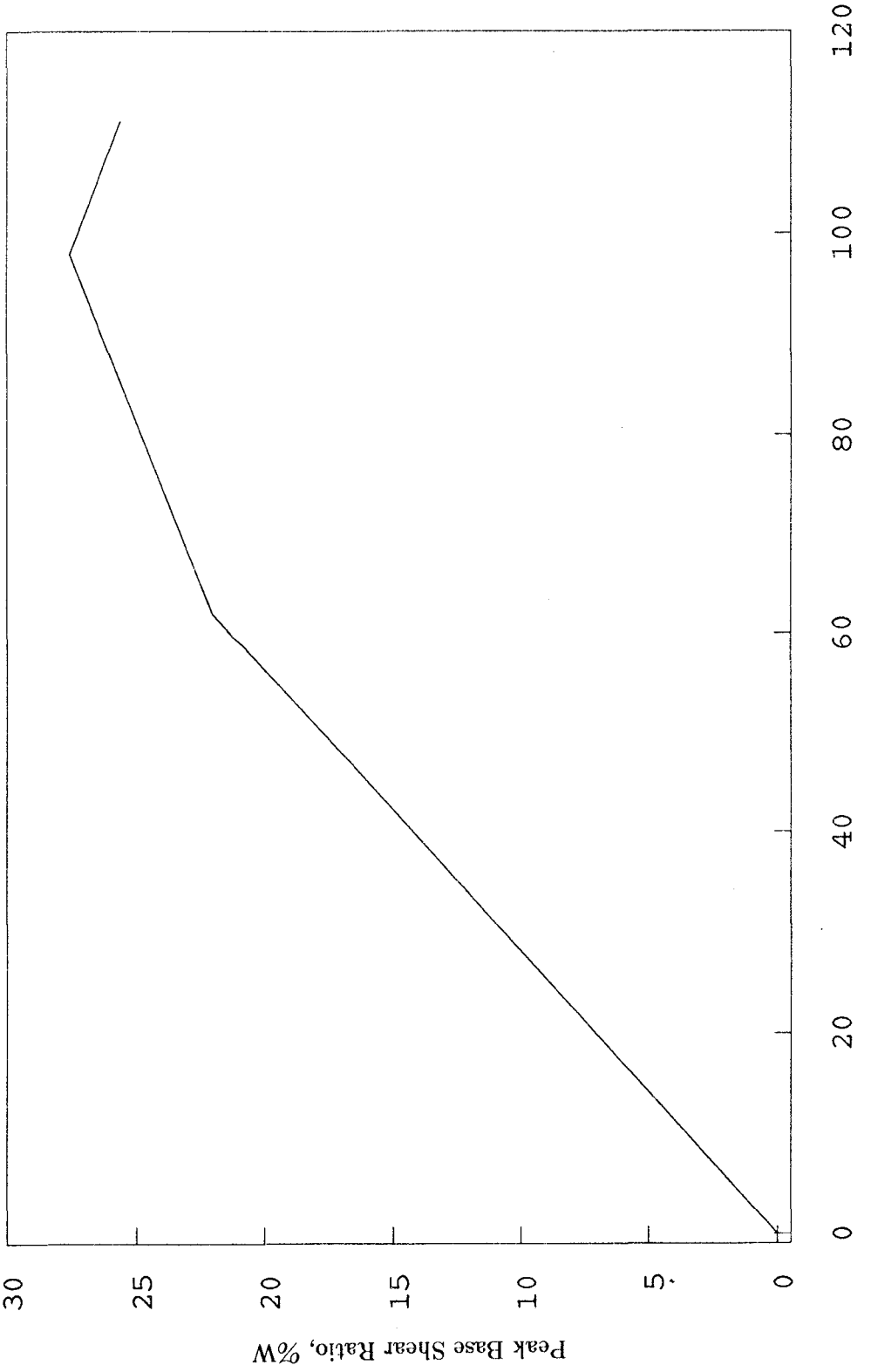

Figure 7.9 - Peak Base Shear Ratio for El Centro Earthquake 2nd Set of Bearings

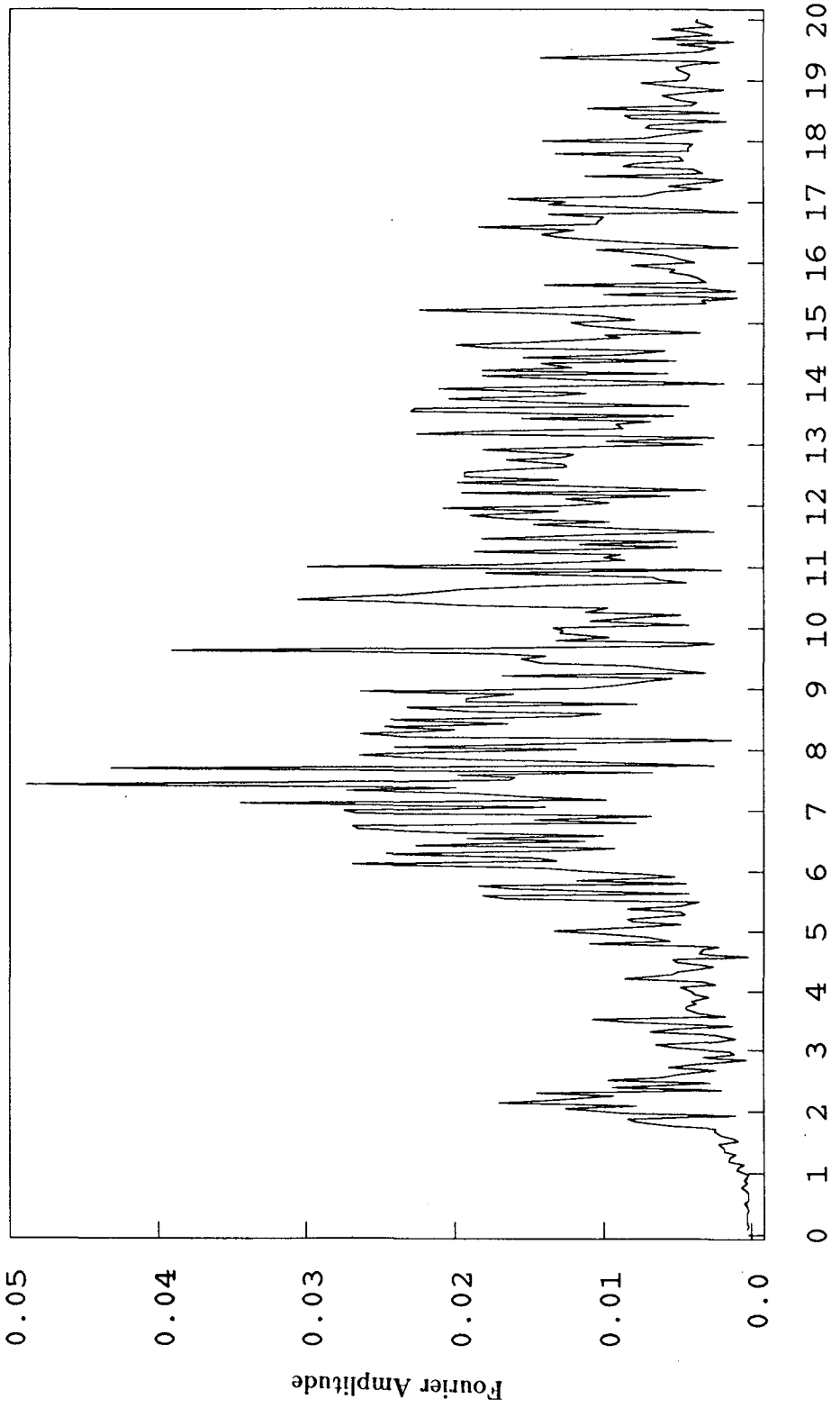

Figure 7.10 - White Noise Test, Roof Acceleration, Fixed-Base R.C. Model

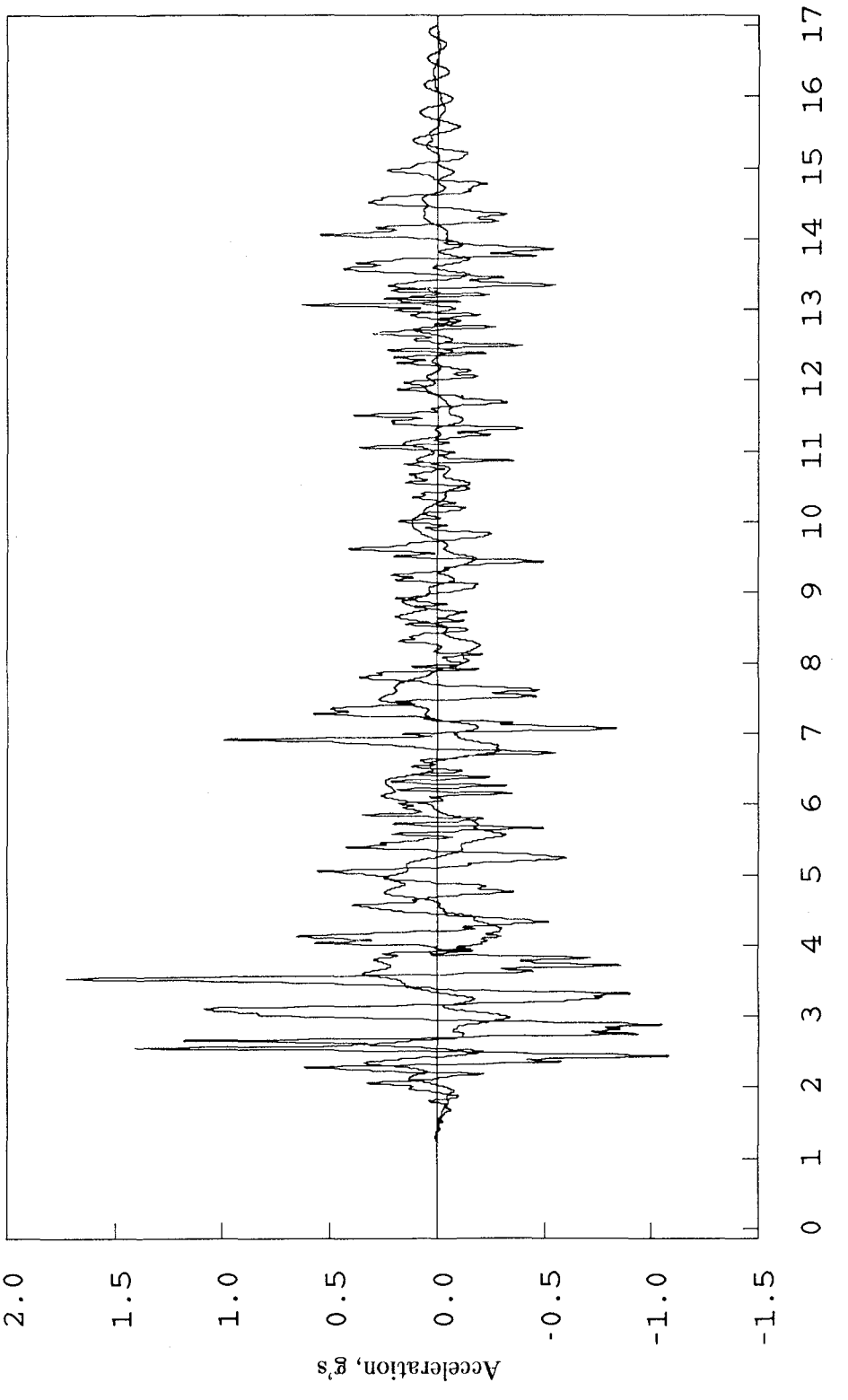

Figure 7.11 - Fixed-Base and Base-Isolated Roof Accelerations, El Centro Earthquake

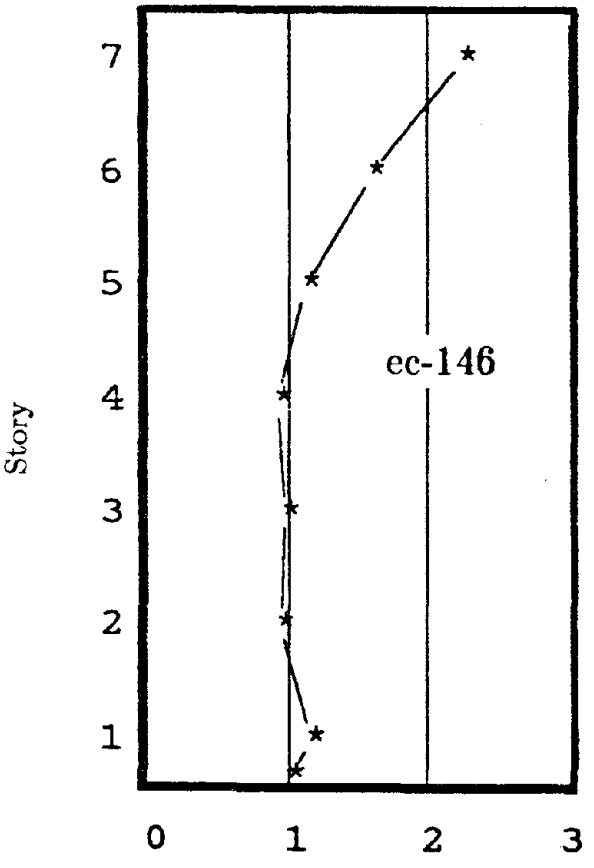

Figure 7.12 - Peak Acceleration Profile, Fixed-Base R.C. Model

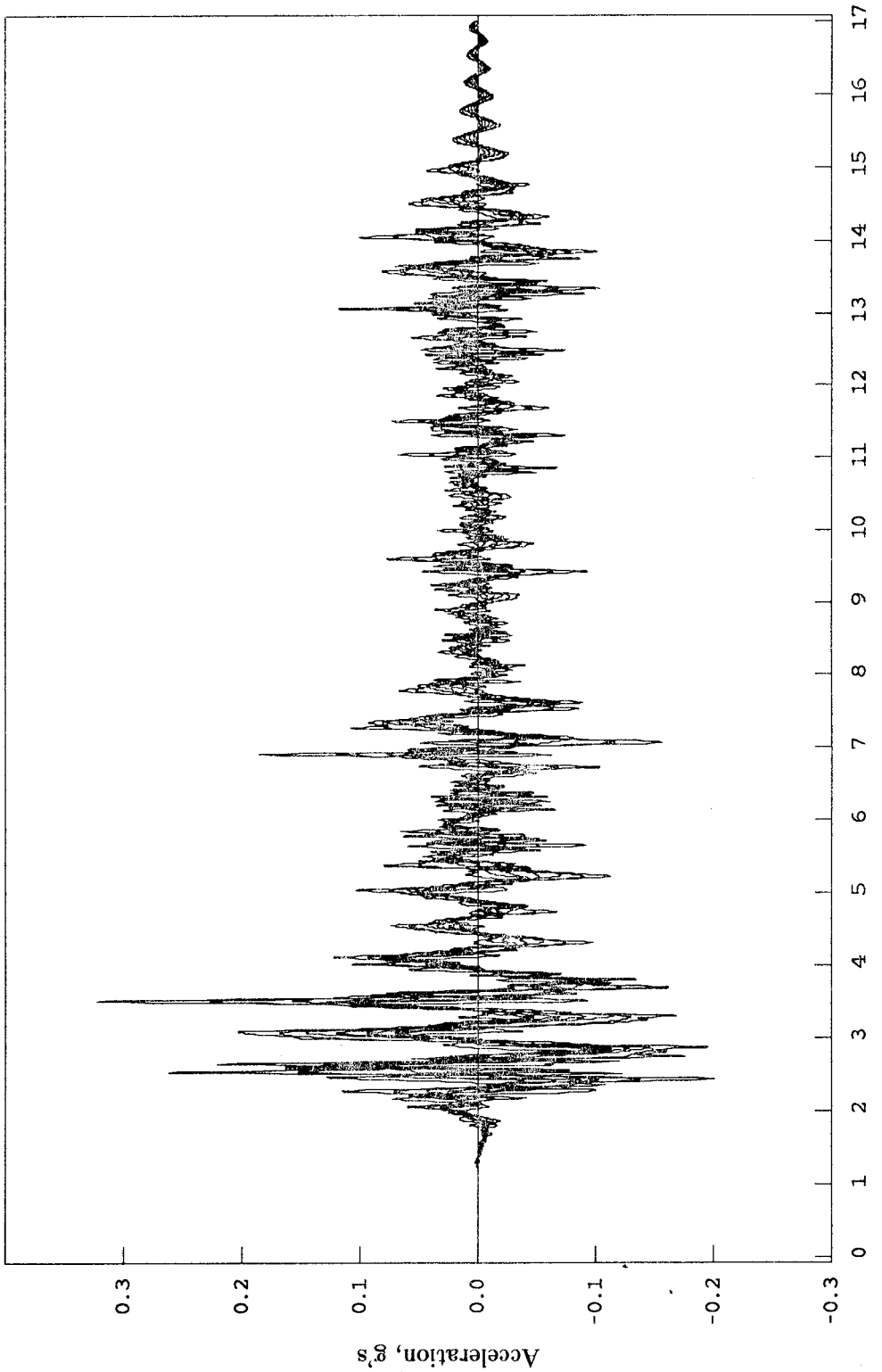

Figure 7.13 - Story Accelerations, Fixed-Base R.C. Model

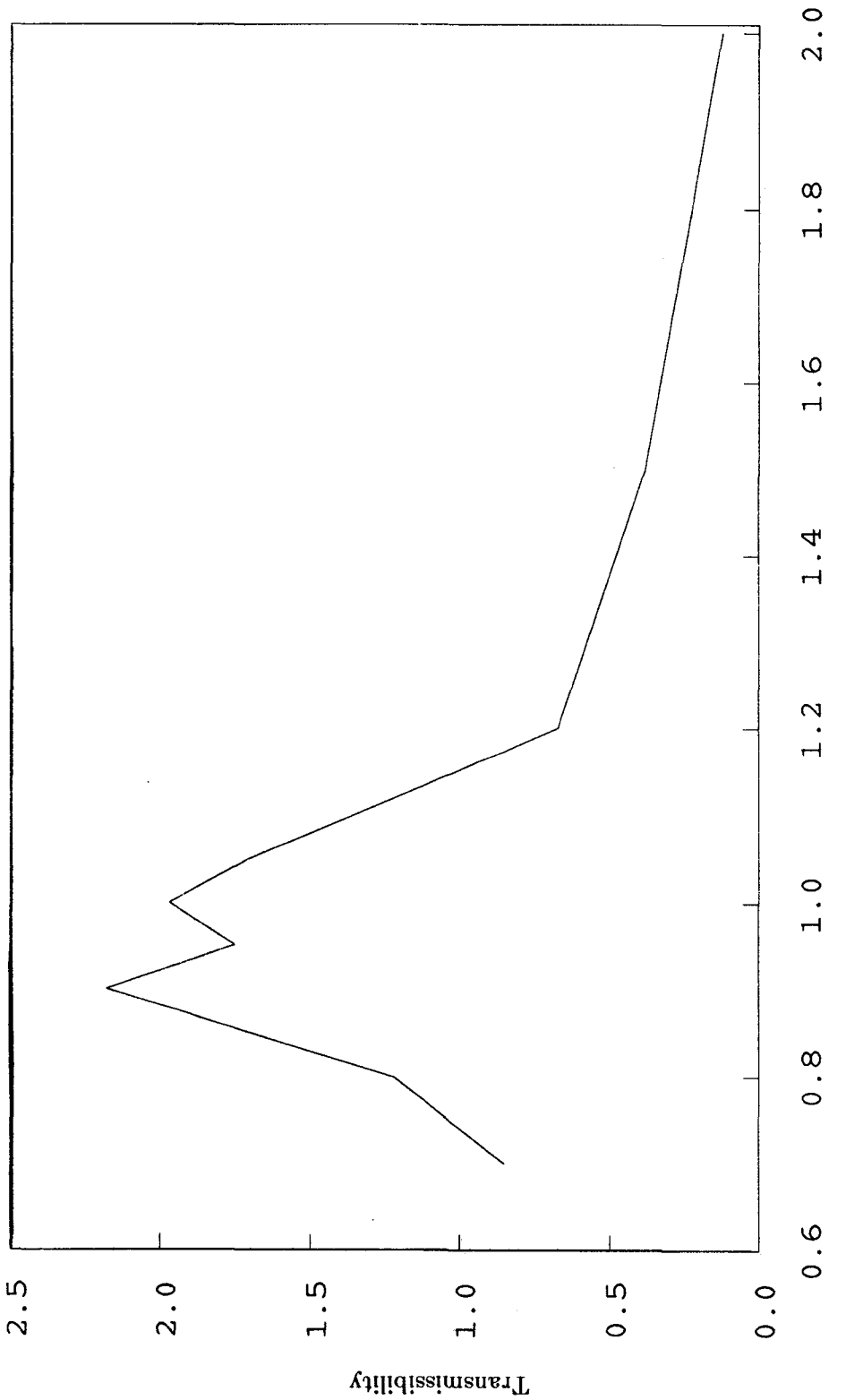

Figure 8.1 - Sine Test Transmissibility Plot, 3rd Set of Bearings

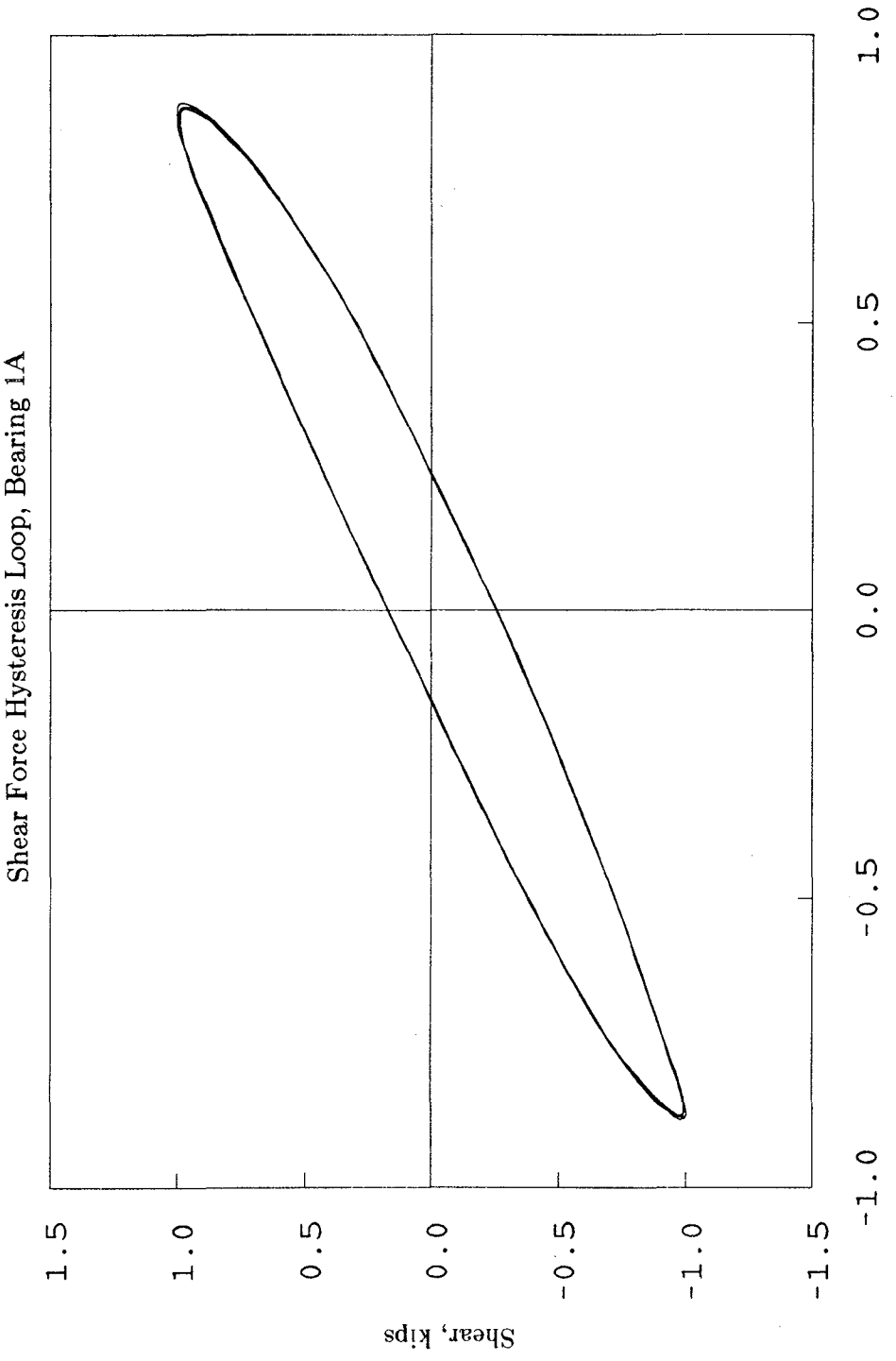

Figure 8.2 - Sine Test Hysteresis Loops, 3rd Set of Bearings

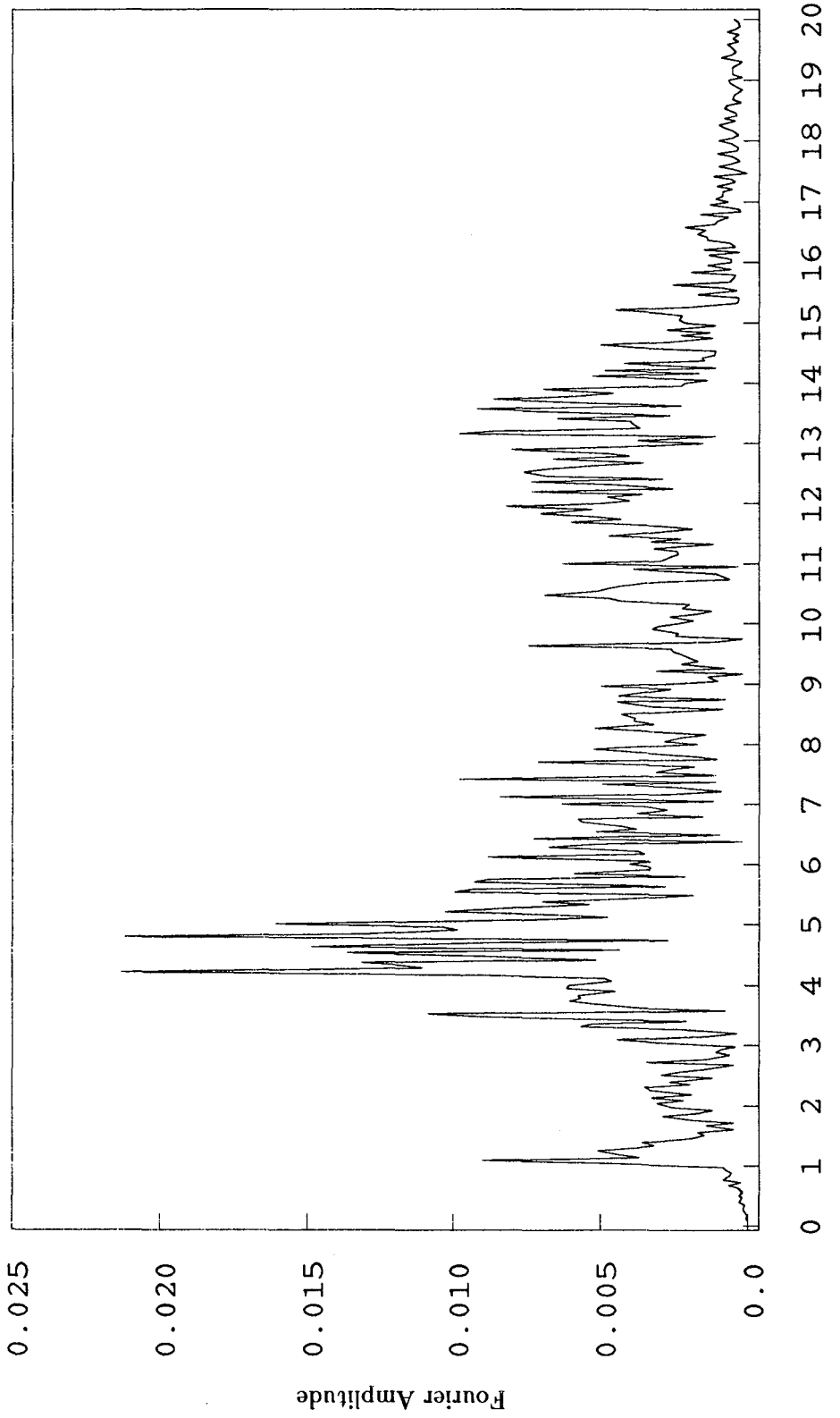

Figure 8.3 - White Noise Test, Roof Acceleration

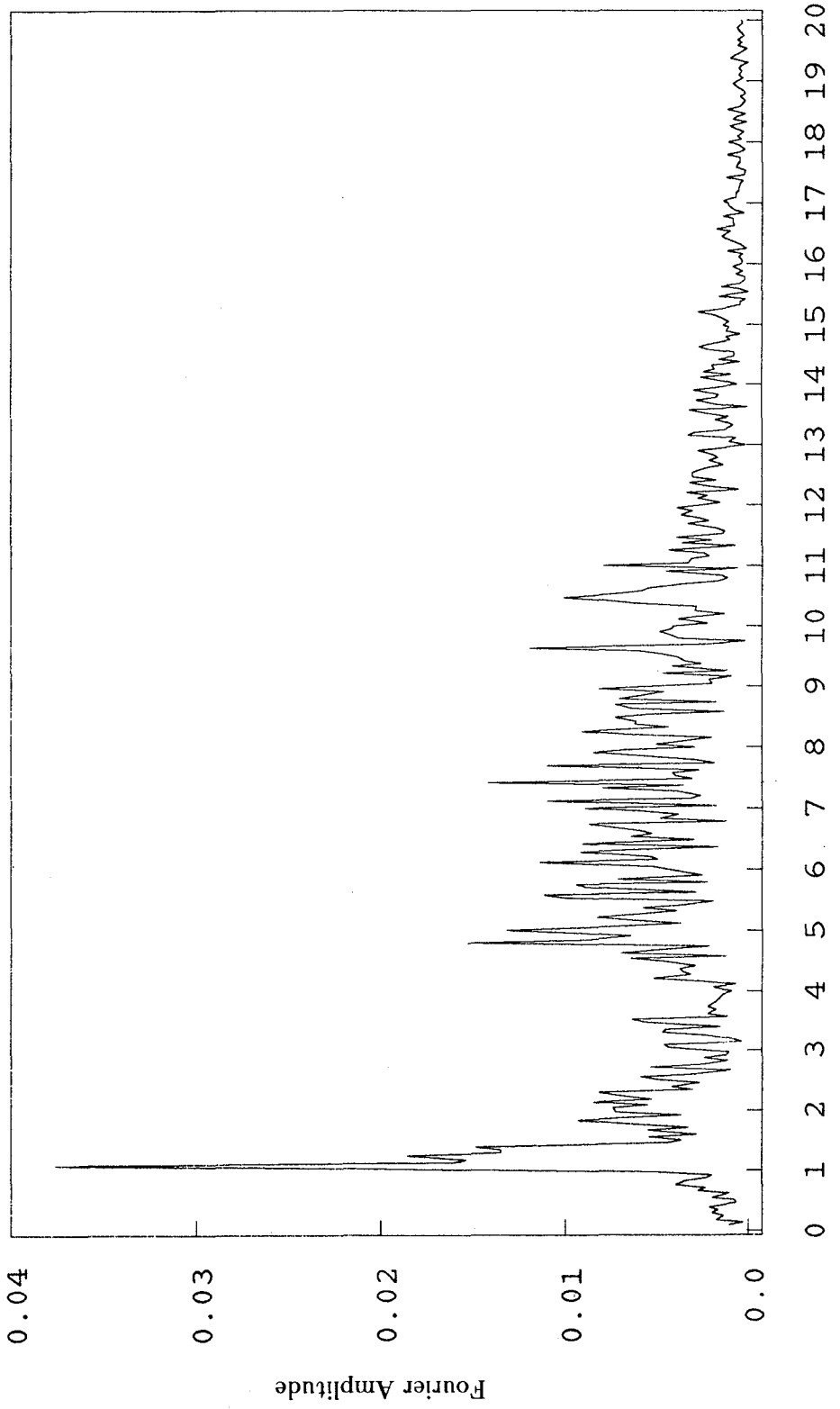

Figure 8.4 - White Noise Test, Bearing Displacement

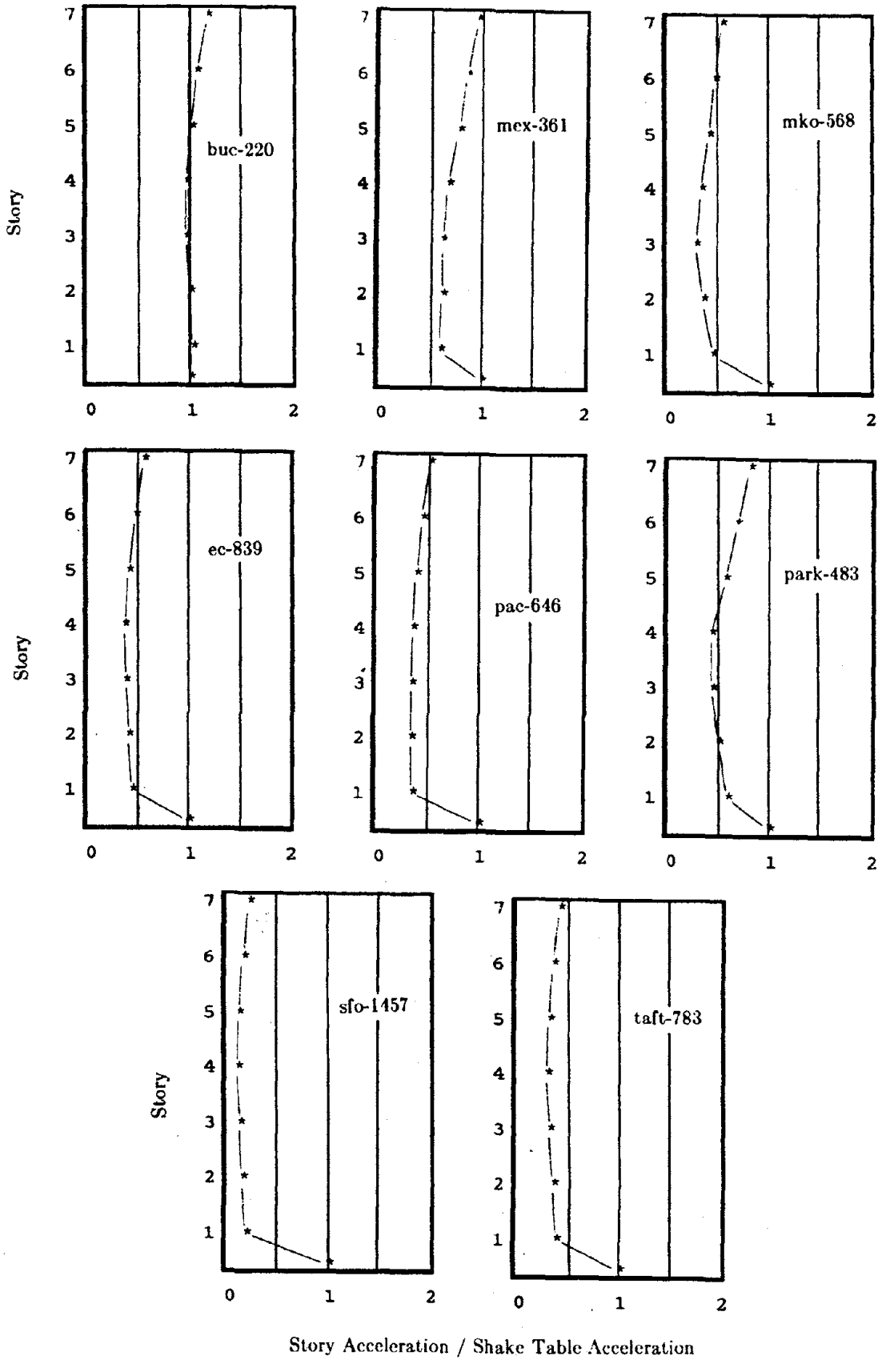

Figure 8.5 - Peak Acceleration Profiles, 3rd Set of Bearings

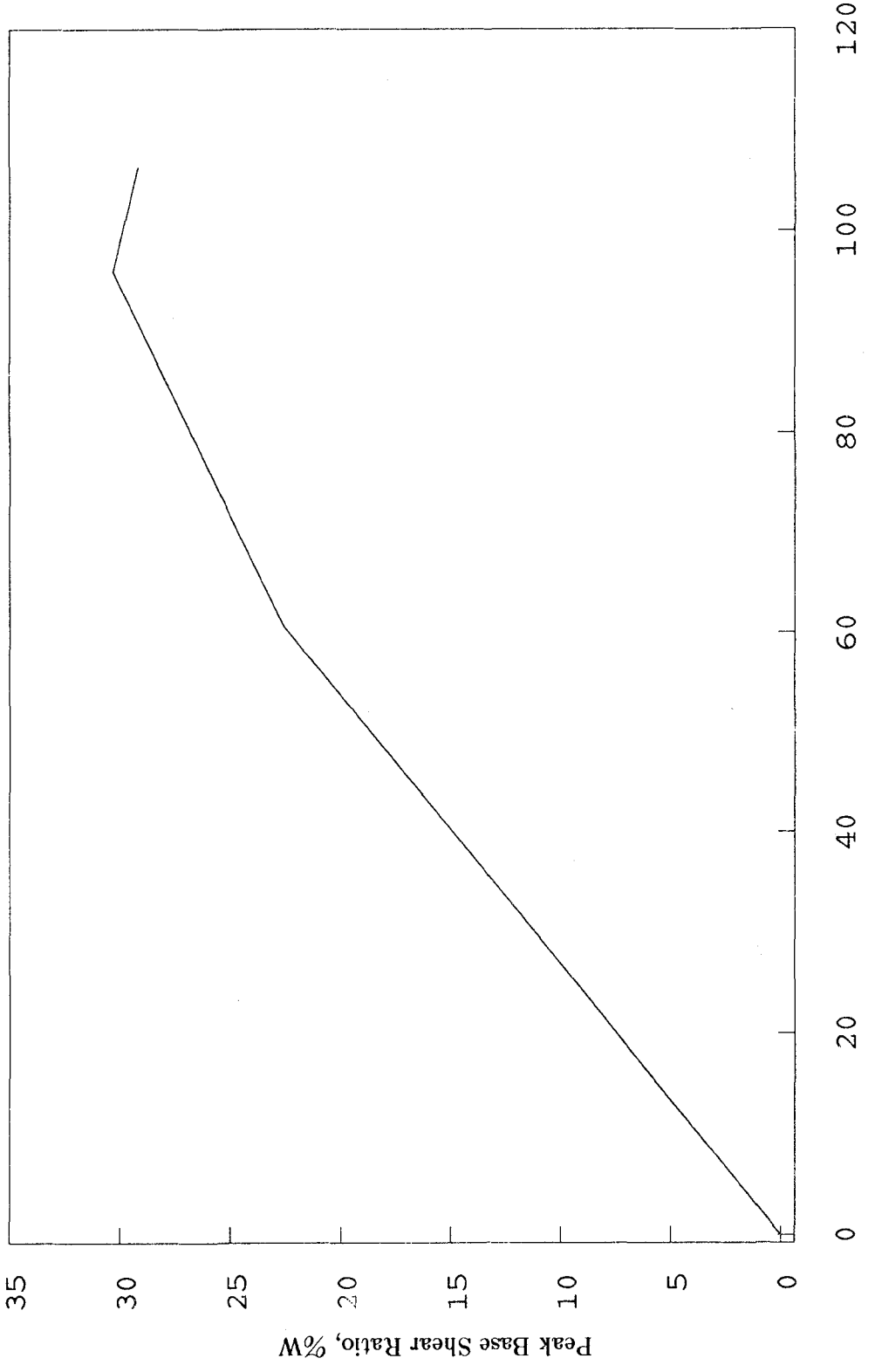

Figure 8.6 - Peak Base Shear Ratio for El Centro Earthquake 3rd Set of Bearings

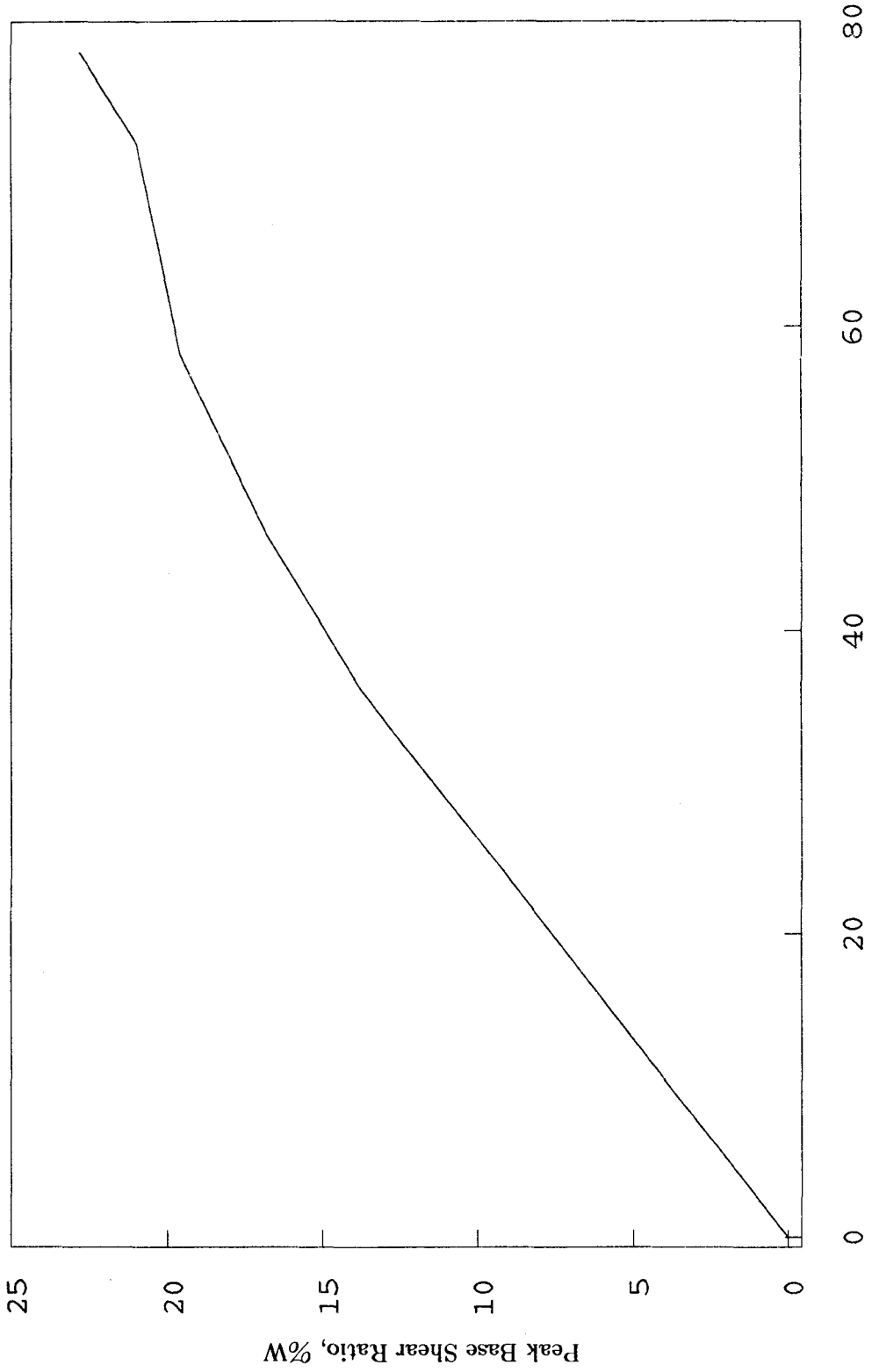

Figure 8.7 - Peak Base Shear Ratio for Mexico City Earthquake 3rd Set of Bearings

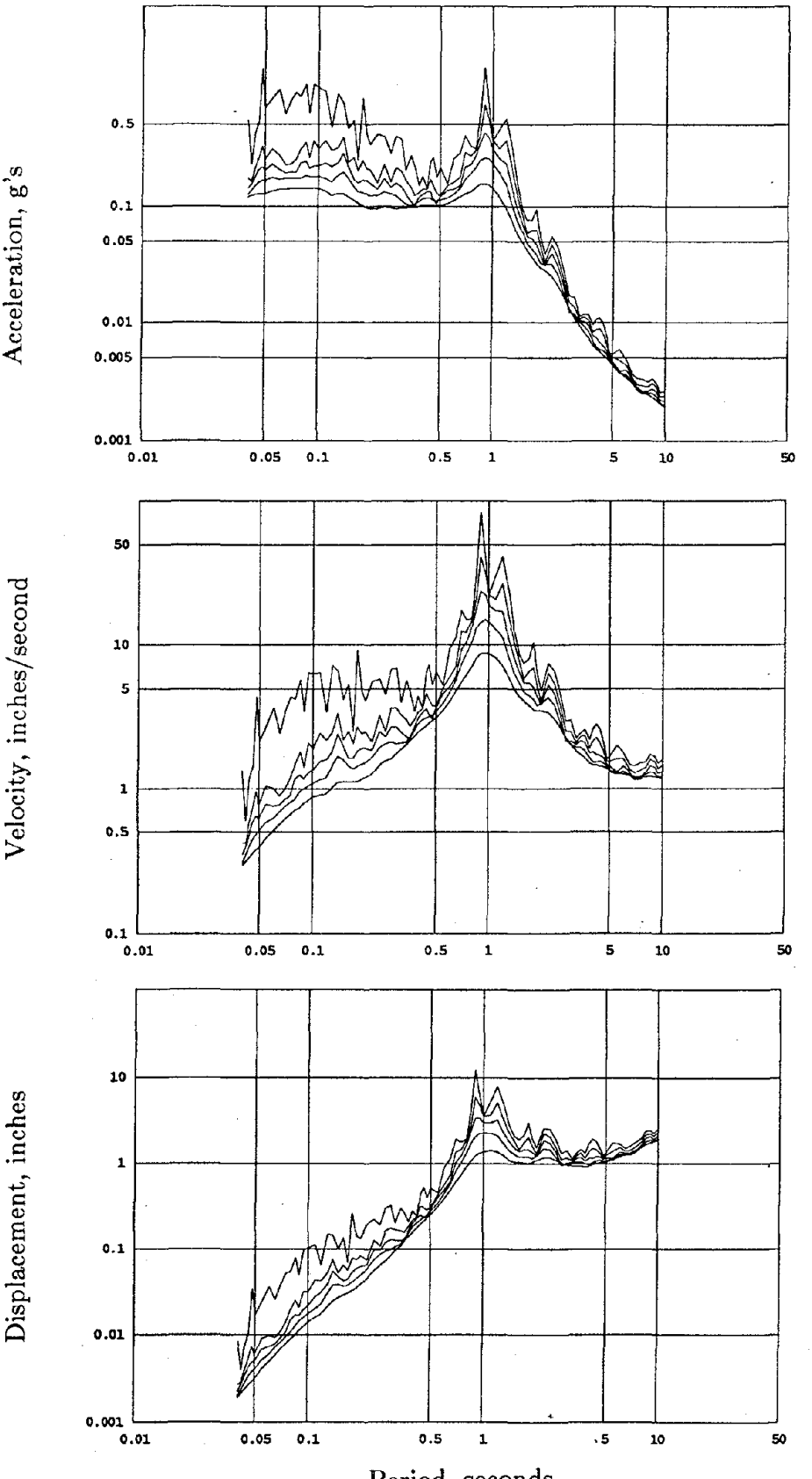

Damping Values: 0%, 2%, 5%, 10%, 20%

Figure 8.8 - Response Spectrum of Mexico City Shake Table Motion

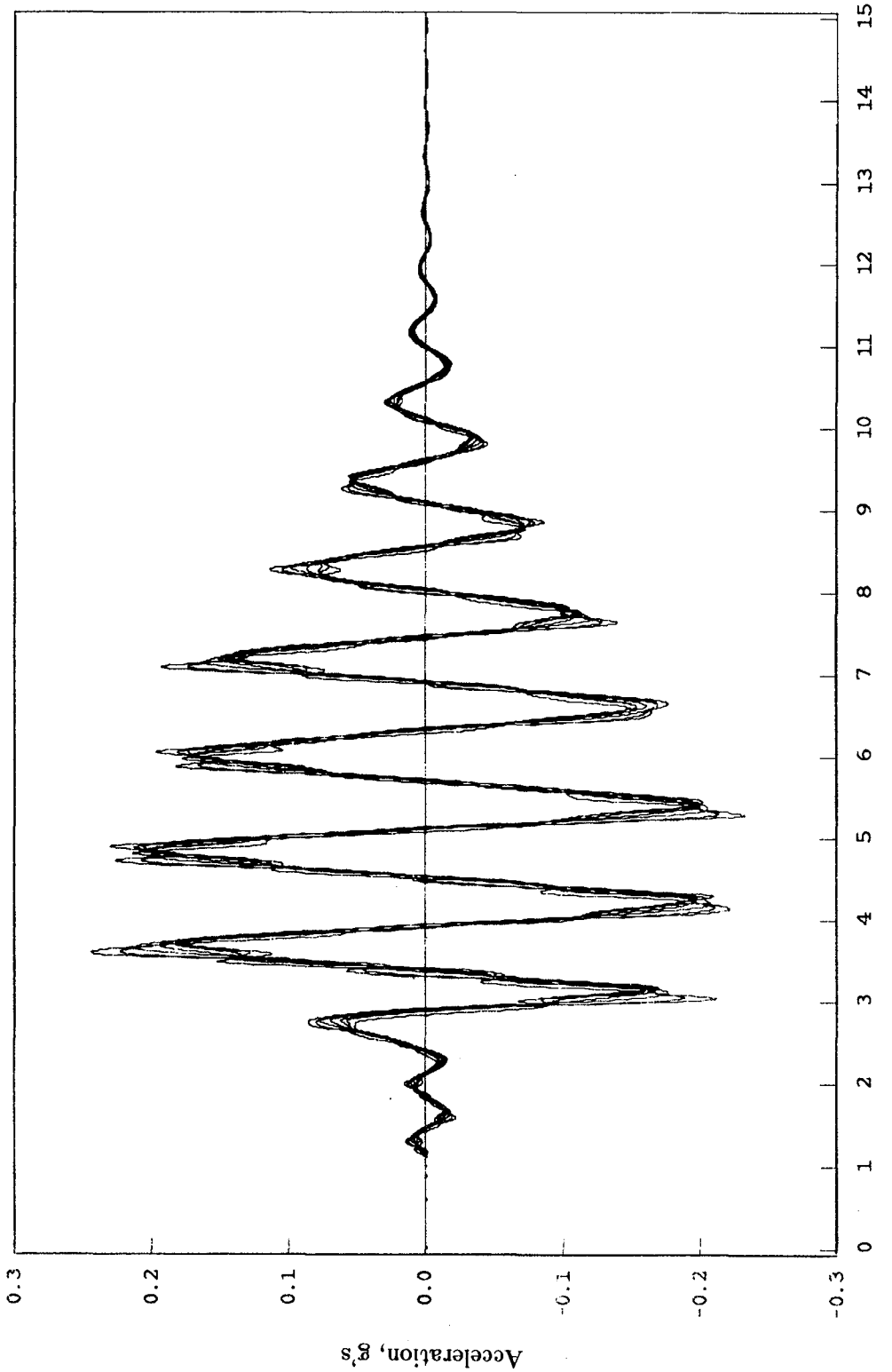

(a) Bucharest

Figure 8.9 - Story Accelerations, 3rd Set of Bearings

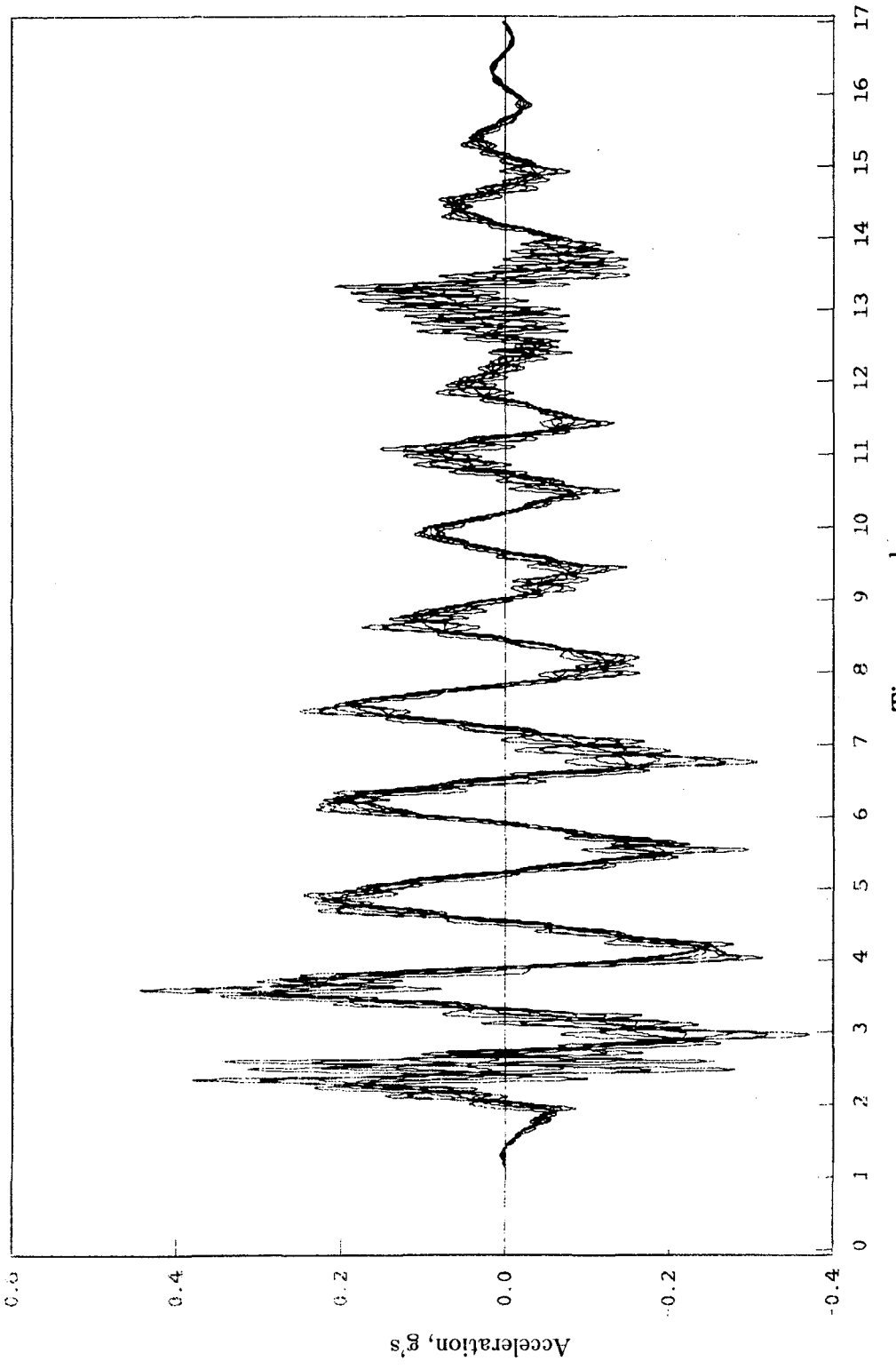

(b) El Centro

Figure 8.9 - Continued

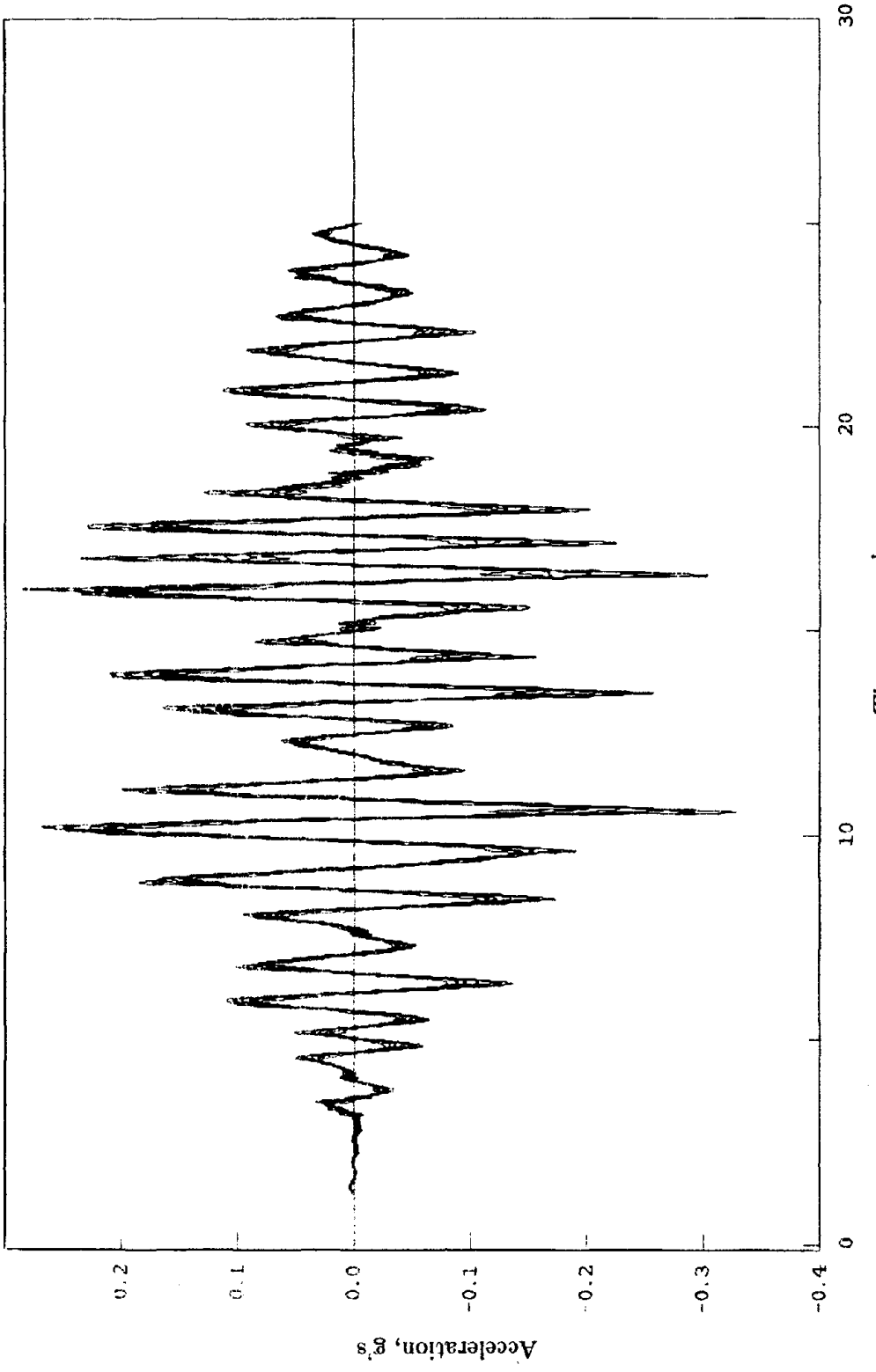

(c) Mexico City

Figure 8.9 - Continued

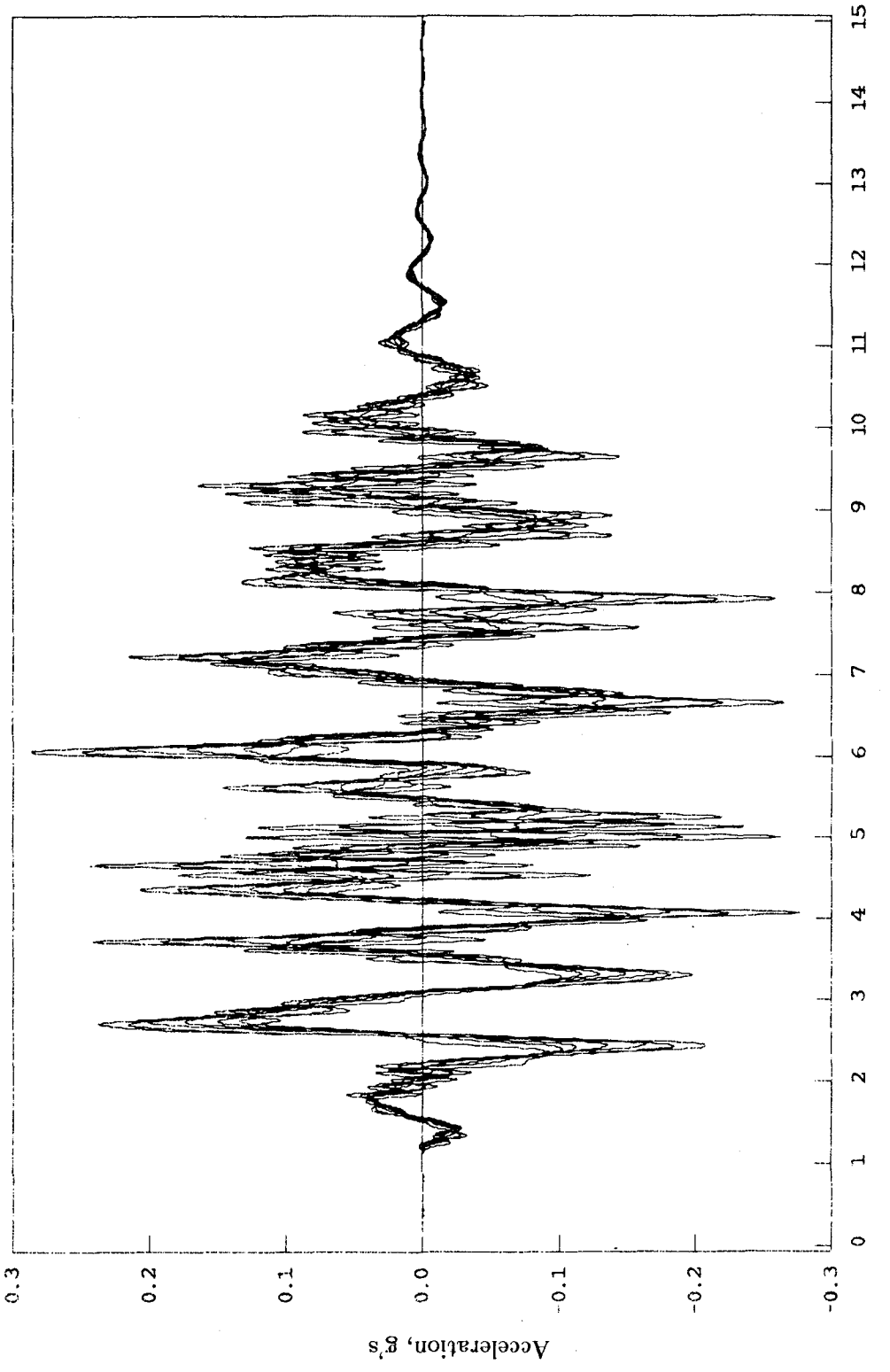

(d) Miyagi-Ken-Oki

Figure 8.9 - Continued

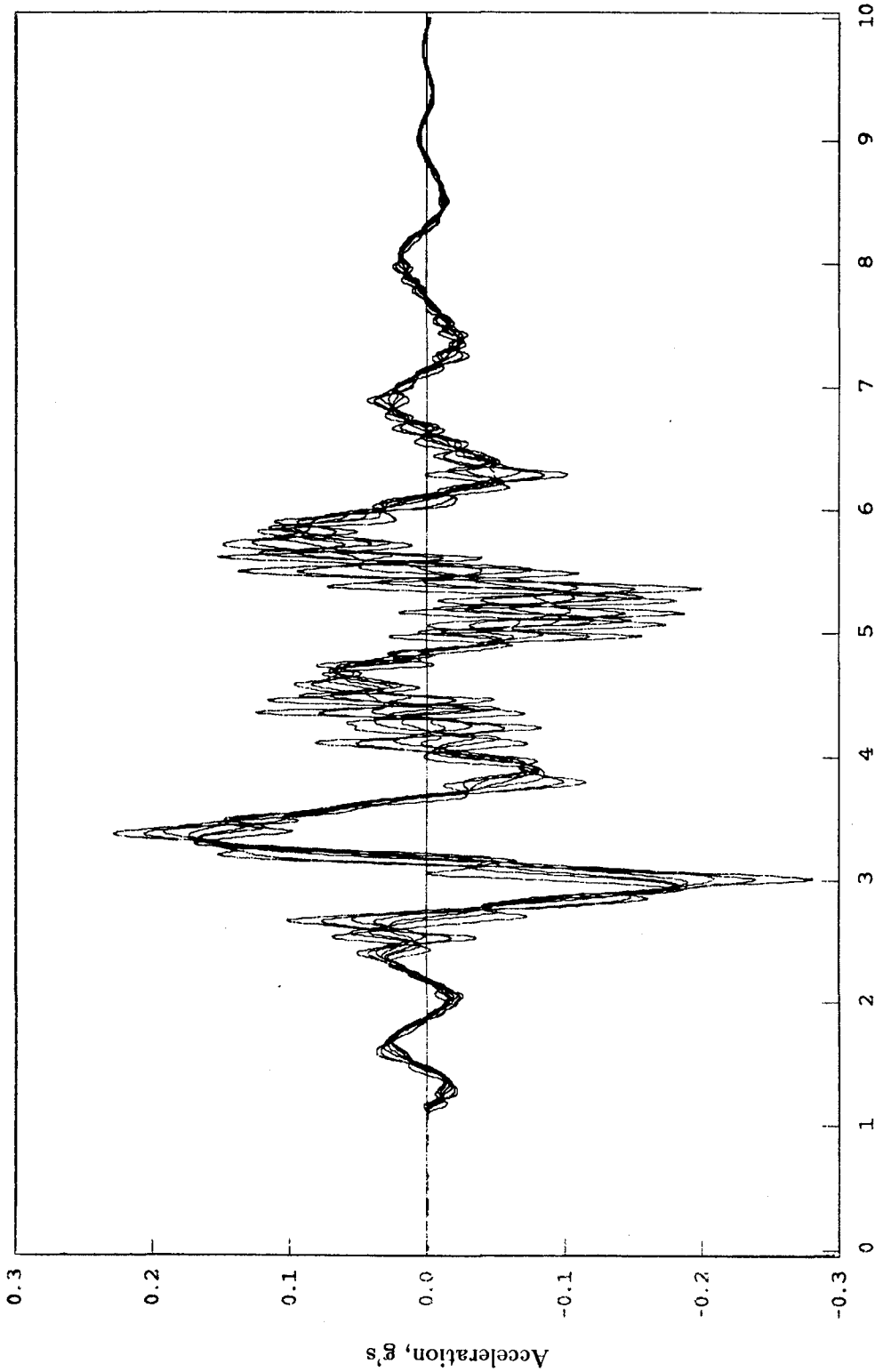

(e) Pacoima Dam

Figure 8.9 - Continued

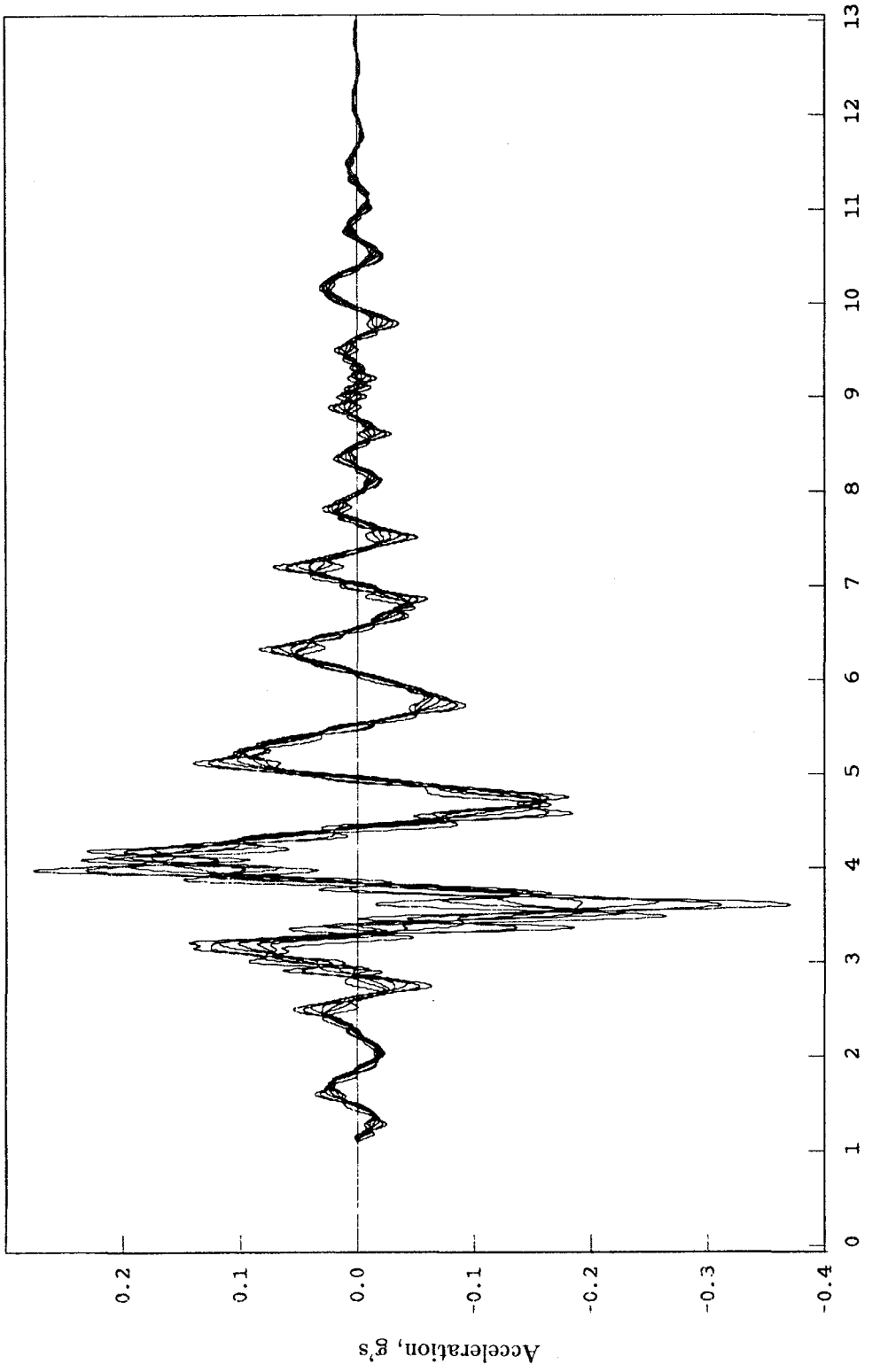

(f) Parkfield

Figure 8.9 - Continued

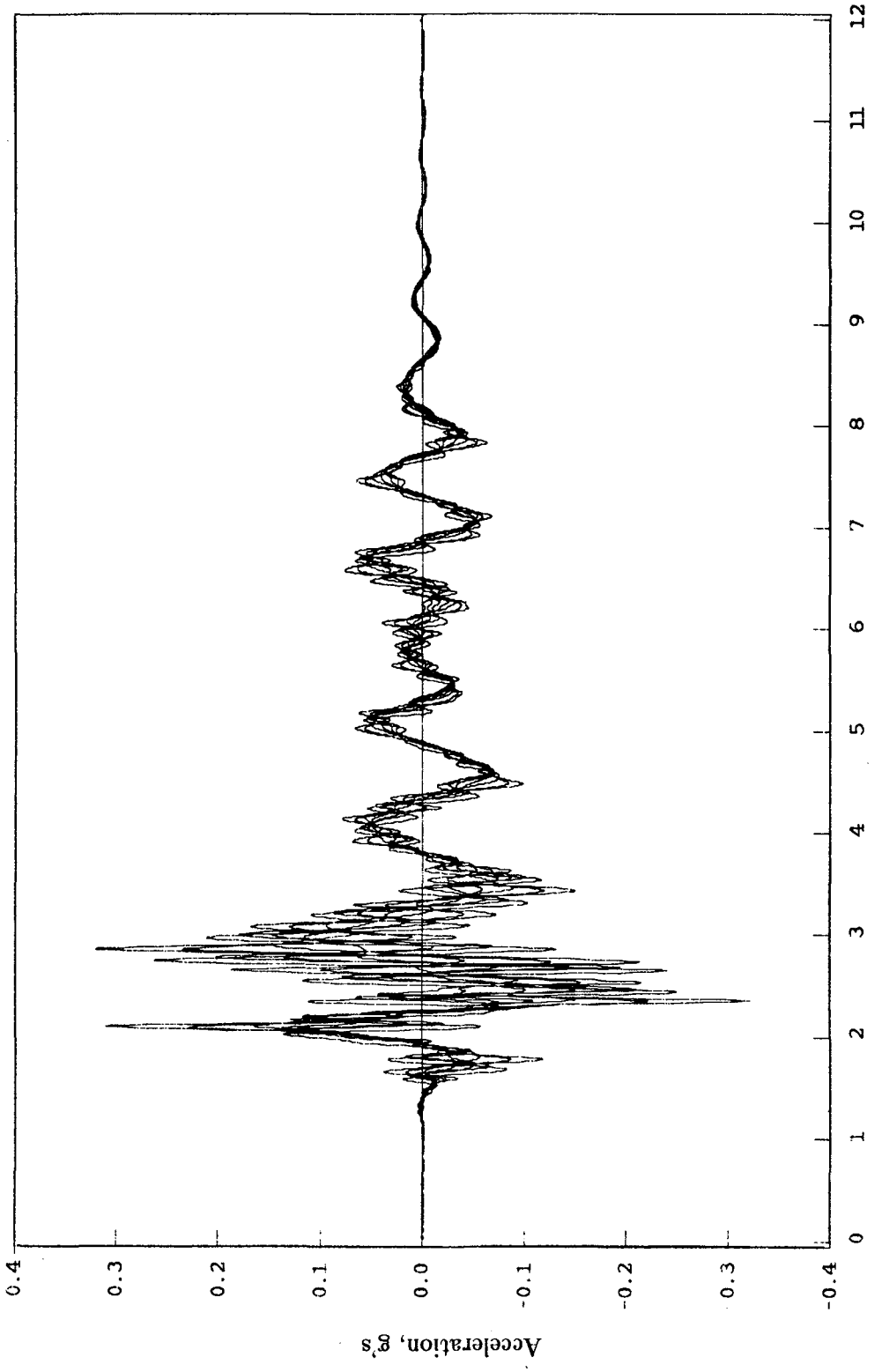

(g) San Francisco

Figure 8.9 - Continued

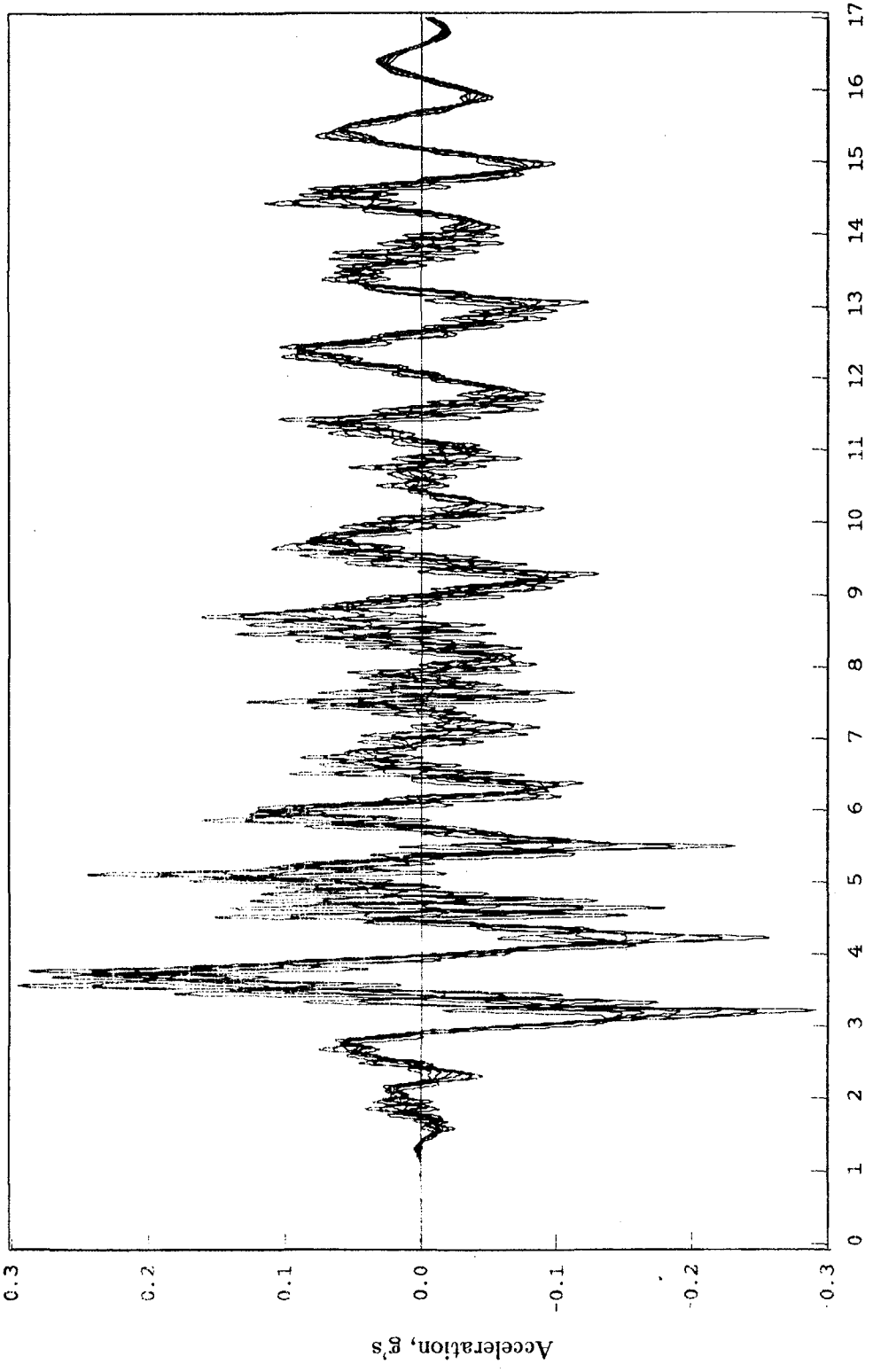

(h) Taft

Figure 8.9 - Continued

EARTHQUAKE ENGINEERING RESEARCH CENTER REPORT SERIES

EERC reports are available from the National Information Service for Earthquake Engineering(NISEE) and from the National Technical Information Service(NTIS). Numbers in parentheses are Accession Numbers assigned by the National Technical Information Service; these are followed by a price code. Contact NTIS, 5285 Port Royal Road, Springfield Virginia, 22161 for more information. Reports without Accession Numbers were not available from NTIS at the time of printing. For a current complete list of EERC reports (from EERC 67-1) and availablity information, please contact University of California, EERC, NISEE, 1301 South 46th Street, Richmond, California 94804.

UCB/EERC-80/01 "Earthquake Response of Concrete Gravity Dams Including Hydrodynamic and Foundation Interaction Effects," by Chopra, A.K., Chakrabarti, P. and Gupta, S., January 1980, (AD-A087297)A10.

UCB/EERC-80/02 "Rocking Response of Rigid Blocks to Earthquakes," by Yim, C.S., Chopra, A.K. and Penzien, J., January 1980, (PB80 166 002)A04.

UCB/EERC-80/03 "Optimum Inelastic Design of Seismic-Resistant Reinforced Concrete Frame Structures," by Zagajeski, S.W. and Bertero, V.V., January 1980, (PB80 164 635)A06.

UCB/EERC-80/04 "Effects of Amount and Arrangement of Wall-Panel Reinforcement on Hysteretic Behavior of Reinforced Concrete Walls," by Iliya, R. and Bertero, V.V., February 1980, (PB81 122 525)A09.

UCB/EERC-80/05 "Shaking Table Research on Concrete Dam Models," by Niwa, A. and Clough, R.W., September 1980, (PB81 122 368)A06.

UCB/EERC-80/06 "The Design of Steel Energy-Absorbing Restrainers and their Incorporation into Nuclear Power Plants for Enhanced Safety (Vol 1a): Piping with Energy Absorbing Restrainers: Parameter Study on Small Systems," by Powell, G.H., Oughourlian, C. and Simons, J., June 1980.

UCB/EERC-80/07 "Inelastic Torsional Response of Structures Subjected to Earthquake Ground Motions," by Yamazaki, Y., April 1980, (PB81 122 327)A08.

UCB/EERC-80/08 "Study of X-Braced Steel Frame Structures under Earthquake Simulation," by Ghanaat, Y., April 1980, (PB81 122 335)A11.

UCB/EERC-80/09 "Hybrid Modelling of Soil-Structure Interaction," by Gupta, S., Lin, T.W. and Penzien, J., May 1980, (PB81 122 319)A07.

UCB/EERC-80/10 "General Applicability of a Nonlinear Model of a One Story Steel Frame," by Sveinsson, B.I. and McNiven, H.D., May 1980, (PB81 124 877)A06.

UCB/EERC-80/11 "A Green-Function Method for Wave Interaction with a Submerged Body," by Kioka, W., April 1980, (PB81 122 269)A07.

UCB/EERC-80/12 "Hydrodynamic Pressure and Added Mass for Axisymmetric Bodies.," by Nilrat, F., May 1980, (PB81 122 343)A08.

UCB/EERC-80/13 "Treatment of Non-Linear Drag Forces Acting on Offshore Platforms," by Dao, B.V. and Penzien, J., May 1980, (PB81 153 413)A07.

UCB/EERC-80/14 "2D Plane/Axisymmetric Solid Element (Type 3-Elastic or Elastic-Perfectly Plastic)for the ANSR-II Program," by Mondkar, D.P. and Powell, G.H., July 1980, (PB81 122 350)A03.

UCB/EERC-80/15 "A Response Spectrum Method for Random Vibrations," by Der Kiureghian, A., June 1981, (PB81 122 301)A03.

UCB/EERC-80/16 "Cyclic Inelastic Buckling of Tubular Steel Braces," by Zayas, V.A., Popov, E.P. and Martin, S.A., June 1981, (PB81 124 885)A10.

UCB/EERC-80/17 "Dynamic Response of Simple Arch Dams Including Hydrodynamic Interaction," by Porter, C.S. and Chopra, A.K., July 1981, (PB81 124 000)A13.

UCB/EERC-80/18 "Experimental Testing of a Friction Damped Aseismic Base Isolation System with Fail-Safe Characteristics," by Kelly, J.M., Beucke, K.E. and Skinner, M.S., July 1980, (PB81 148 595)A04.

UCB/EERC-80/19 "The Design of Steel Energy-Absorbing Restrainers and their Incorporation into Nuclear Power Plants for Enhanced Safety (Vol.1B): Stochastic Seismic Analyses of Nuclear Power Plant Structures and Piping Systems Subjected to Multiple Supported Excitations," by Lee, M.C. and Penzien, J., June 1980, (PB82 201 872)A08.

UCB/EERC-80/20 "The Design of Steel Energy-Absorbing Restrainers and their Incorporation into Nuclear Power Plants for Enhanced Safety (Vol 1C): Numerical Method for Dynamic Substructure Analysis," by Dickens, J.M. and Wilson, E.L., June 1980.

UCB/EERC-80/21 "The Design of Steel Energy-Absorbing Restrainers and their Incorporation into Nuclear Power Plants for Enhanced Safety (Vol 2): Development and Testing of Restraints for Nuclear Piping Systems," by Kelly, J.M. and Skinner, M.S., June 1980.

UCB/EERC-80/22 "3D Solid Element (Type 4-Elastic or Elastic-Perfectly-Plastic) for the ANSR-II Program," by Mondkar, D.P. and Powell, G.H., July 1980, (PB81 123 242)A03.

UCB/EERC-80/23 "Gap-Friction Element (Type 5) for the Ansr-II Program," by Mondkar, D.P. and Powell, G.H., July 1980, (PB81 122 285)A03.

UCB/EERC-80/24 "U-Bar Restraint Element (Type 11) for the ANSR-II Program," by Oughourlian, C. and Powell, G.H., July 1980, (PB81 122 293)A03.

UCB/EERC-80/25 "Testing of a Natural Rubber Base Isolation System by an Explosively Simulated Earthquake," by Kelly, J.M., August 1980, (PB81 201 360)A04.

UCB/EERC-80/26 "Input Identification from Structural Vibrational Response," by Hu, Y., August 1980, (PB81 152 308)A05.

UCB/EERC-80/27 "Cyclic Inelastic Behavior of Steel Offshore Structures," by Zayas, V.A., Mahin, S.A. and Popov, E.P., August 1980, (PB81 196 180)A15.

UCB/EERC-80/28 "Shaking Table Testing of a Reinforced Concrete Frame with Biaxial Response," by Oliva, M.G., October 1980, (PB81 154 304)A10.

UCB/EERC-80/29 "Dynamic Properties of a Twelve-Story Prefabricated Panel Building," by Bouwkamp, J.G., Kollegger, J.P. and Stephen, R.M., October 1980, (PB82 138 777)A07.

UCB/EERC-80/30 "Dynamic Properties of an Eight-Story Prefabricated Panel Building," by Bouwkamp, J.G., Kollegger, J.P. and Stephen, R.M., October 1980, (PB81 200 313)A05.

UCB/EERC-80/31 "Predictive Dynamic Response of Panel Type Structures under Earthquakes," by Kollegger, J.P. and Bouwkamp, J.G., October 1980, (PB81 152 316)A04.

UCB/EERC-80/32 "The Design of Steel Energy-Absorbing Restrainers and their Incorporation into Nuclear Power Plants for Enhanced Safety (Vol 3): Testing of Commercial Steels in Low-Cycle Torsional Fatique," by Spanner, P., Parker, E.R., Jongewaard, E. and Dory, M., 1980.

UCB/EERC-80/33 "The Design of Steel Energy-Absorbing Restrainers and their Incorporation into Nuclear Power Plants for Enhanced Safety (Vol 4): Shaking Table Tests of Piping Systems with Energy-Absorbing Restrainers," by Stiemer, S.F. and Godden, W.G., September 1980, (PB82 201 880)A05.

UCB/EERC-80/34 "The Design of Steel Energy-Absorbing Restrainers and their Incorporation into Nuclear Power Plants for Enhanced Safety (Vol 5): Summary Report," by Spencer, P., 1980.

UCB/EERC-80/35 "Experimental Testing of an Energy-Absorbing Base Isolation System," by Kelly, J.M., Skinner, M.S. and Beucke, K.E., October 1980, (PB81 154 072)A04.

UCB/EERC-80/36 "Simulating and Analyzing Artificial Non-Stationary Earth Ground Motions," by Nau, R.F., Oliver, R.M. and Pister, K.S., October 1980, (PB81 153 397)A04.

UCB/EERC-80/37 "Earthquake Engineering at Berkeley - 1980," by , September 1980, (PB81 205 674)A09.

UCB/EERC-80/38 "Inelastic Seismic Analysis of Large Panel Buildings," by Schricker, V. and Powell, G.H., September 1980, (PB81 154 338)A13.

UCB/EERC-80/39 "Dynamic Response of Embankment, Concrete-Gavity and Arch Dams Including Hydrodynamic Interation," by Hall, J.F. and Chopra, A.K., October 1980, (PB81 152 324)A11.

UCB/EERC-80/40 "Inelastic Buckling of Steel Struts under Cyclic Load Reversal.," by Black, R.G., Wenger, W.A. and Popov, E.P., October 1980, (PB81 154 312)A08.

UCB/EERC-80/41 "Influence of Site Characteristics on Buildings Damage during the October 3,1974 Lima Earthquake," by Repetto, P., Arango, I. and Seed, H.B., September 1980, (PB81 161 739)A05.

UCB/EERC-80/42 "Evaluation of a Shaking Table Test Program on Response Behavior of a Two Story Reinforced Concrete Frame," by Blondet, J.M., Clough, R.W. and Mahin, S.A., December 1980, (PB82 196 544)A11.

UCB/EERC-80/43 "Modelling of Soil-Structure Interaction by Finite and Infinite Elements," by Medina, F., December 1980, (PB81 229 270)A04.

UCB/EERC-81/01 "Control of Seismic Response of Piping Systems and Other Structures by Base Isolation," by Kelly, J.M., January 1981, (PB81 200 735)A05.

UCB/EERC-81/02 "OPTNSR- An Interactive Software System for Optimal Design of Statically and Dynamically Loaded Structures with Nonlinear Response," by Bhatti, M.A., Ciampi, V. and Pister, K.S., January 1981, (PB81 218 851)A09.

UCB/EERC-81/03 "Analysis of Local Variations in Free Field Seismic Ground Motions," by Chen, J.-C., Lysmer, J. and Seed, H.B., January 1981, (AD-A099508)A13.

UCB/EERC-81/04 "Inelastic Structural Modeling of Braced Offshore Platforms for Seismic Loading," by Zayas, V.A., Shing, P.-S.B., Mahin, S.A. and Popov, E.P., January 1981, (PB82 138 777)A07.

UCB/EERC-81/05 "Dynamic Response of Light Equipment in Structures," by Der Kiureghian, A., Sackman, J.L. and Nour-Omid, B., April 1981, (PB81 218 497)A04.

UCB/EERC-81/06 "Preliminary Experimental Investigation of a Broad Base Liquid Storage Tank," by Bouwkamp, J.G., Kollegger, J.P. and Stephen, R.M., May 1981, (PB82 140 385)A03.

UCB/EERC-81/07 "The Seismic Resistant Design of Reinforced Concrete Coupled Structural Walls," by Aktan, A.E. and Bertero, V.V., June 1981, (PB82 113 358)A11.

UCB/EERC-81/08 "Unassigned," by Unassigned, 1981.

UCB/EERC-81/09 "Experimental Behavior of a Spatial Piping System with Steel Energy Absorbers Subjected to a Simulated Differential Seismic Input," by Stiemer, S.F., Godden, W.G. and Kelly, J.M., July 1981, (PB82 201 898)A04.

UCB/EERC-81/10 "Evaluation of Seismic Design Provisions for Masonry in the United States," by Sveinsson, B.I., Mayes, R.L. and McNiven, H.D., August 1981, (PB82 166 075)A08.

UCB/EERC-81/11 "Two-Dimensional Hybrid Modelling of Soil-Structure Interaction," by Tzong, T.-J., Gupta, S. and Penzien, J., August 1981, (PB82 142 118)A04.

UCB/EERC-81/12 "Studies on Effects of Infills in Seismic Resistant R/C Construction," by Brokken, S. and Bertero, V.V., October 1981, (PB82 166 190)A09.

UCB/EERC-81/13 "Linear Models to Predict the Nonlinear Seismic Behavior of a One-Story Steel Frame," by Valdimarsson, H., Shah, A.H. and McNiven, H.D., September 1981, (PB82 138 793)A07.

UCB/EERC-81/14 "TLUSH: A Computer Program for the Three-Dimensional Dynamic Analysis of Earth Dams," by Kagawa, T., Mejia, L.H., Seed, H.B. and Lysmer, J., September 1981, (PB82 139 940)A06.

UCB/EERC-81/15 "Three Dimensional Dynamic Response Analysis of Earth Dams," by Mejia, L.H. and Seed, H.B., September 1981, (PB82 137 274)A12.

UCB/EERC-81/16 "Experimental Study of Lead and Elastomeric Dampers for Base Isolation Systems," by Kelly, J.M. and Hodder, S.B., October 1981, (PB82 166 182)A05.

UCB/EERC-81/17 "The Influence of Base Isolation on the Seismic Response of Light Secondary Equipment," by Kelly, J.M., April 1981, (PB82 255 266)A04.

UCB/EERC-81/18 "Studies on Evaluation of Shaking Table Response Analysis Procedures," by Blondet, J. M., November 1981, (PB82 197 278)A10.

UCB/EERC-81/19 "DELIGHT.STRUCT: A Computer-Aided Design Environment for Structural Engineering," by Balling, R.J., Pister, K.S. and Polak, E., December 1981, (PB82 218 496)A07.

UCB/EERC-81/20 "Optimal Design of Seismic-Resistant Planar Steel Frames," by Balling, R.J., Ciampi, V. and Pister, K.S., December 1981, (PB82 220 179)A07.

UCB/EERC-82/01 "Dynamic Behavior of Ground for Seismic Analysis of Lifeline Systems," by Sato, T. and Der Kiureghian, A., January 1982, (PB82 218 926)A05.

UCB/EERC-82/02 "Shaking Table Tests of a Tubular Steel Frame Model," by Ghanaat, Y. and Clough, R.W., January 1982, (PB82 220 161)A07.

UCB/EERC-82/03 "Behavior of a Piping System under Seismic Excitation: Experimental Investigations of a Spatial Piping System supported by Mechanical Shock Arrestors," by Schneider, S., Lee, H.-M. and Godden, W. G., May 1982, (PB83 172 544)A09.

UCB/EERC-82/04 "New Approaches for the Dynamic Analysis of Large Structural Systems," by Wilson, E.L., June 1982, (PB83 148 080)A05.

UCB/EERC-82/05 "Model Study of Effects of Damage on the Vibration Properties of Steel Offshore Platforms," by Shahrivar, F. and Bouwkamp, J.G., June 1982, (PB83 148 742)A10.

UCB/EERC-82/06 "States of the Art and Pratice in the Optimum Seismic Design and Analytical Response Prediction of R/C Frame Wall Structures," by Aktan, A.E. and Bertero, V.V., July 1982, (PB83 147 736)A05.

UCB/EERC-82/07 "Further Study of the Earthquake Response of a Broad Cylindrical Liquid-Storage Tank Model," by Manos, G.C. and Clough, R.W., July 1982, (PB83 147 744)A11.

UCB/EERC-82/08 "An Evaluation of the Design and Analytical Seismic Response of a Seven Story Reinforced Concrete Frame," by Charney, F.A. and Bertero, V.V., July 1982, (PB83 157 628)A09.

UCB/EERC-82/09 "Fluid-Structure Interactions: Added Mass Computations for Incompressible Fluid," by Kuo, J.S.-H., August 1982, (PB83 156 281)A07.

UCB/EERC-82/10 "Joint-Opening Nonlinear Mechanism: Interface Smeared Crack Model," by Kuo, J.S.-H., August 1982, (PB83 149 195)A05.

UCB/EERC-82/11 "Dynamic Response Analysis of Techi Dam," by Clough, R.W., Stephen, R.M. and Kuo, J.S.-H., August 1982, (PB83 147 496)A06.

UCB/EERC-82/12 "Prediction of the Seismic Response of R/C Frame-Coupled Wall Structures," by Aktan, A.E., Bertero, V.V. and Piazzo, M., August 1982, (PB83 149 203)A09.

UCB/EERC-82/13 "Preliminary Report on the Smart 1 Strong Motion Array in Taiwan," by Bolt, B.A., Loh, C.H., Penzien, J. and Tsai, Y.B., August 1982, (PB83 159 400)A10.

UCB/EERC-82/14 "Shaking-Table Studies of an Eccentrically X-Braced Steel Structure," by Yang, M.S., September 1982, (PB83 260 778)A12.

UCB/EERC-82/15 "The Performance of Stairways in Earthquakes," by Roha, C., Axley, J.W. and Bertero, V.V., September 1982, (PB83 157 693)A07.

UCB/EERC-82/16 "The Behavior of Submerged Multiple Bodies in Earthquakes," by Liao, W.-G., September 1982, (PB83 158 709)A07.

UCB/EERC-82/17 "Effects of Concrete Types and Loading Conditions on Local Bond-Slip Relationships," by Cowell, A.D., Popov, E.P. and Bertero, V.V., September 1982, (PB83 153 577)A04.

UCB/EERC-82/18 "Mechanical Behavior of Shear Wall Vertical Boundary Members: An Experimental Investigation," by Wagner, M.T. and Bertero, V.V., October 1982, (PB83 159 764)A05.

UCB/EERC-82/19 "Experimental Studies of Multi-support Seismic Loading on Piping Systems," by Kelly, J.M. and Cowell, A.D., November 1982.

UCB/EERC-82/20 "Generalized Plastic Hinge Concepts for 3D Beam-Column Elements," by Chen, P. F.-S. and Powell, G.H., November 1982, (PB83 247 981)A13.

UCB/EERC-82/21 "ANSR-II: General Computer Program for Nonlinear Structural Analysis," by Oughourlian, C.V. and Powell, G.H., November 1982, (PB83 251 330)A12.

UCB/EERC-82/22 "Solution Strategies for Statically Loaded Nonlinear Structures," by Simons, J.W. and Powell, G.H., November 1982, (PB83 197 970)A06.

UCB/EERC-82/23 "Analytical Model of Deformed Bar Anchorages under Generalized Excitations," by Ciampi, V., Eligehausen, R., Bertero, V.V. and Popov, E.P., November 1982, (PB83 169 532)A06.

UCB/EERC-82/24 "A Mathematical Model for the Response of Masonry Walls to Dynamic Excitations," by Sucuoglu, H., Mengi, Y. and McNiven, H.D., November 1982, (PB83 169 011)A07.

UCB/EERC-82/25 "Earthquake Response Considerations of Broad Liquid Storage Tanks," by Cambra, F.J., November 1982, (PB83 251 215)A09.

UCB/EERC-82/26 "Computational Models for Cyclic Plasticity, Rate Dependence and Creep," by Mosaddad, B. and Powell, G.H., November 1982, (PB83 245 829)A08.

UCB/EERC-82/27 "Inelastic Analysis of Piping and Tubular Structures," by Mahasuverachai, M. and Powell, G.H., November 1982, (PB83 249 987)A07.

UCB/EERC-83/01 "The Economic Feasibility of Seismic Rehabilitation of Buildings by Base Isolation," by Kelly, J.M., January 1983, (PB83 197 988)A05.

UCB/EERC-83/02 "Seismic Moment Connections for Moment-Resisting Steel Frames.," by Popov, E.P., January 1983, (PB83 195 412)A04.

UCB/EERC-83/03 "Design of Links and Beam-to-Column Connections for Eccentrically Braced Steel Frames," by Popov, E.P. and Malley, J.O., January 1983, (PB83 194 811)A04.

UCB/EERC-83/04 "Numerical Techniques for the Evaluation of Soil-Structure Interaction Effects in the Time Domain," by Bayo, E. and Wilson, E.L., February 1983, (PB83 245 605)A09.

UCB/EERC-83/05 "A Transducer for Measuring the Internal Forces in the Columns of a Frame-Wall Reinforced Concrete Structure," by Sause, R. and Bertero, V.V., May 1983, (PB84 119 494)A06.

UCB/EERC-83/06 "Dynamic Interactions Between Floating Ice and Offshore Structures," by Croteau, P., May 1983, (PB84 119 486)A16.

UCB/EERC-83/07 "Dynamic Analysis of Multiply Tuned and Arbitrarily Supported Secondary Systems," by Igusa, T. and Der Kiureghian, A., July 1983, (PB84 118 272)A11.

UCB/EERC-83/08 "A Laboratory Study of Submerged Multi-body Systems in Earthquakes," by Ansari, G.R., June 1983, (PB83 261 842)A17.

UCB/EERC-83/09 "Effects of Transient Foundation Uplift on Earthquake Response of Structures," by Yim, C.-S. and Chopra, A.K., June 1983, (PB83 261 396)A07.

UCB/EERC-83/10 "Optimal Design of Friction-Braced Frames under Seismic Loading," by Austin, M.A. and Pister, K.S., June 1983, (PB84 119 288)A06.

UCB/EERC-83/11 "Shaking Table Study of Single-Story Masonry Houses: Dynamic Performance under Three Component Seismic Input and Recommendations," by Manos, G.C., Clough, R.W. and Mayes, R.L., July 1983, (UCB/EERC-83/11)A08.

UCB/EERC-83/12 "Experimental Error Propagation in Pseudodynamic Testing," by Shiing, P.B. and Mahin, S.A., June 1983, (PB84 119 270)A09.

UCB/EERC-83/13 "Experimental and Analytical Predictions of the Mechanical Characteristics of a 1/5-scale Model of a 7-story R/C Frame-Wall Building Structure," by Aktan, A.E., Bertero, V.V., Chowdhury, A.A. and Nagashima, T., June 1983, (PB84 119 213)A07.

UCB/EERC-83/14 "Shaking Table Tests of Large-Panel Precast Concrete Building System Assemblages," by Oliva, M.G. and Clough, R.W., June 1983, (PB86 110 210/AS)A11.

UCB/EERC-83/15 "Seismic Behavior of Active Beam Links in Eccentrically Braced Frames," by Hjelmstad, K.D. and Popov, E.P., July 1983, (PB84 119 676)A09.

UCB/EERC-83/16 "System Identification of Structures with Joint Rotation," by Dimsdale, J.S., July 1983, (PB84 192 210)A06.

UCB/EERC-83/17 "Construction of Inelastic Response Spectra for Single-Degree-of-Freedom Systems," by Mahin, S. and Lin, J., June 1983, (PB84 208 834)A05.

UCB/EERC-83/18 "Interactive Computer Analysis Methods for Predicting the Inelastic Cyclic Behaviour of Structural Sections," by Kaba, S. and Mahin, S., July 1983, (PB84 192 012)A06.

UCB/EERC-83/19 "Effects of Bond Deterioration on Hysteretic Behavior of Reinforced Concrete Joints," by Filippou, F.C., Popov, E.P. and Bertero, V.V., August 1983, (PB84 192 020)A10.

UCB/EERC-83/20 "Analytical and Experimental Correlation of Large-Panel Precast Building System Performance," by Oliva, M.G., Clough, R.W., Velkov, M. and Gavrilovic, P., November 1983.

UCB/EERC-83/21 "Mechanical Characteristics of Materials Used in a 1/5 Scale Model of a 7-Story Reinforced Concrete Test Structure," by Bertero, V.V., Aktan, A.E., Harris, H.G. and Chowdhury, A.A., October 1983, (PB84 193 697)A05.

UCB/EERC-83/22 "Hybrid Modelling of Soil-Structure Interaction in Layered Media," by Tzong, T.-J. and Penzien, J., October 1983, (PB84 192 178)A08.

UCB/EERC-83/23 "Local Bond Stress-Slip Relationships of Deformed Bars under Generalized Excitations," by Eligehausen, R., Popov, E.P. and Bertero, V.V., October 1983, (PB84 192 848)A09.

UCB/EERC-83/24 "Design Considerations for Shear Links in Eccentrically Braced Frames," by Malley, J.O. and Popov, E.P., November 1983, (PB84 192 186)A07.

UCB/EERC-84/01 "Pseudodynamic Test Method for Seismic Performance Evaluation: Theory and Implementation," by Shing, P.-S.B. and Mahin, S.A., January 1984, (PB84 190 644)A08.

UCB/EERC-84/02 "Dynamic Response Behavior of Kiang Hong Dian Dam," by Clough, R.W., Chang, K.-T., Chen, H.-Q. and Stephen, R.M., April 1984, (PB84 209 402)A08.

UCB/EERC-84/03 "Refined Modelling of Reinforced Concrete Columns for Seismic Analysis," by Kaba, S.A. and Mahin, S.A., April 1984, (PB84 234 384)A06.

UCB/EERC-84/04 "A New Floor Response Spectrum Method for Seismic Analysis of Multiply Supported Secondary Systems," by Asfura, A. and Der Kiureghian, A., June 1984, (PB84 239 417)A06.

UCB/EERC-84/05 "Earthquake Simulation Tests and Associated Studies of a 1/5th-scale Model of a 7-Story R/C Frame-Wall Test Structure," by Bertero, V.V., Aktan, A.E., Charney, F.A. and Sause, R., June 1984, (PB84 239 409)A09.

UCB/EERC-84/06 "R/C Structural Walls: Seismic Design for Shear," by Aktan, A.E. and Bertero, V.V., 1984.

UCB/EERC-84/07 "Behavior of Interior and Exterior Flat-Plate Connections subjected to Inelastic Load Reversals," by Zee, H.L. and Moehle, J.P., August 1984, (PB86 117 629/AS)A07.

UCB/EERC-84/08 "Experimental Study of the Seismic Behavior of a Two-Story Flat-Plate Structure," by Moehle, J.P. and Diebold, J.W., August 1984, (PB86 122 553/AS)A12.

UCB/EERC-84/09 "Phenomenological Modeling of Steel Braces under Cyclic Loading," by Ikeda, K., Mahin, S.A. and Dermitzakis, S.N., May 1984, (PB86 132 198/AS)A08.

UCB/EERC-84/10 "Earthquake Analysis and Response of Concrete Gravity Dams," by Fenves, G. and Chopra, A.K., August 1984, (PB85 193 902/AS)A11.

UCB/EERC-84/11 "EAGD-84: A Computer Program for Earthquake Analysis of Concrete Gravity Dams," by Fenves, G. and Chopra, A.K., August 1984, (PB85 193 613/AS)A05.

UCB/EERC-84/12 "A Refined Physical Theory Model for Predicting the Seismic Behavior of Braced Steel Frames," by Ikeda, K. and Mahin, S.A., July 1984, (PB85 191 450/AS)A09.

UCB/EERC-84/13 "Earthquake Engineering Research at Berkeley - 1984," by , August 1984, (PB85 197 341/AS)A10.

UCB/EERC-84/14 "Moduli and Damping Factors for Dynamic Analyses of Cohesionless Soils," by Seed, H.B., Wong, R.T., Idriss, I.M. and Tokimatsu, K., September 1984, (PB85 191 468/AS)A04.

UCB/EERC-84/15 "The Influence of SPT Procedures in Soil Liquefaction Resistance Evaluations," by Seed, H.B., Tokimatsu, K., Harder, L.F. and Chung, R.M., October 1984, (PB85 191 732/AS)A04.

UCB/EERC-84/16 "Simplified Procedures for the Evaluation of Settlements in Sands Due to Earthquake Shaking," by Tokimatsu, K. and Seed, H.B., October 1984, (PB85 197 887/AS)A03.

UCB/EERC-84/17 "Evaluation of Energy Absorption Characteristics of Bridges under Seismic Conditions," by Imbsen, R.A. and Penzien, J., November 1984.

UCB/EERC-84/18 "Structure-Foundation Interactions under Dynamic Loads," by Liu, W.D. and Penzien, J., November 1984, (PB87 124 889/AS)A11.

UCB/EERC-84/19 "Seismic Modelling of Deep Foundations," by Chen, C.-H. and Penzien, J., November 1984, (PB87 124 798/AS)A07.

UCB/EERC-84/20 "Dynamic Response Behavior of Quan Shui Dam," by Clough, R.W., Chang, K.-T., Chen, H.-Q., Stephen, R.M., Ghanaat, Y. and Qi, J.-H., November 1984, (PB86 115177/AS)A07.

UCB/EERC-85/01 "Simplified Methods of Analysis for Earthquake Resistant Design of Buildings," by Cruz, E.F. and Chopra, A.K., February 1985, (PB86 112299/AS)A12.

UCB/EERC-85/02 "Estimation of Seismic Wave Coherency and Rupture Velocity using the SMART 1 Strong-Motion Array Recordings," by Abrahamson, N.A., March 1985, (PB86 214 343)A07.

UCB/EERC-85/03 "Dynamic Properties of a Thirty Story Condominium Tower Building," by Stephen, R.M., Wilson, E.L. and Stander, N., April 1985, (PB86 118965/AS)A06.

UCB/EERC-85/04 "Development of Substructuring Techniques for On-Line Computer Controlled Seismic Performance Testing," by Dermitzakis, S. and Mahin, S., February 1985, (PB86 132941/AS)A08.

UCB/EERC-85/05 "A Simple Model for Reinforcing Bar Anchorages under Cyclic Excitations," by Filippou, F.C., March 1985, (PB86 112 919/AS)A05.

UCB/EERC-85/06 "Racking Behavior of Wood-framed Gypsum Panels under Dynamic Load," by Oliva, M.G., June 1985.

UCB/EERC-85/07 "Earthquake Analysis and Response of Concrete Arch Dams," by Fok, K.-L. and Chopra, A.K., June 1985, (PB86 139672/AS)A10.

UCB/EERC-85/08 "Effect of Inelastic Behavior on the Analysis and Design of Earthquake Resistant Structures," by Lin, J.P. and Mahin, S.A., June 1985, (PB86 135340/AS)A08.

UCB/EERC-85/09 "Earthquake Simulator Testing of a Base-Isolated Bridge Deck," by Kelly, J.M., Buckle, I.G. and Tsai, H.-C., January 1986, (PB87 124 152/AS)A06.

UCB/EERC-85/10 "Simplified Analysis for Earthquake Resistant Design of Concrete Gravity Dams," by Fenves, G. and Chopra, A.K., June 1986, (PB87 124 160/AS)A08.

UCB/EERC-85/11 "Dynamic Interaction Effects in Arch Dams," by Clough, R.W., Chang, K.-T., Chen, H.-Q. and Ghanaat, Y., October 1985, (PB86 135027/AS)A05.

UCB/EERC-85/12 "Dynamic Response of Long Valley Dam in the Mammoth Lake Earthquake Series of May 25-27, 1980," by Lai, S. and Seed, H.B., November 1985, (PB86 142304/AS)A05.

UCB/EERC-85/13 "A Methodology for Computer-Aided Design of Earthquake-Resistant Steel Structures," by Austin, M.A., Pister, K.S. and Mahin, S.A., December 1985, (PB86 159480/AS)A10 .

UCB/EERC-85/14 "Response of Tension-Leg Platforms to Vertical Seismic Excitations," by Liou, G.-S., Penzien, J. and Yeung, R.W., December 1985, (PB87 124 871/AS)A08.

UCB/EERC-85/15 "Cyclic Loading Tests of Masonry Single Piers: Volume 4 - Additional Tests with Height to Width Ratio of 1," by Sveinsson, B., McNiven, H.D. and Sucuoglu, H., December 1985.

UCB/EERC-85/16 "An Experimental Program for Studying the Dynamic Response of a Steel Frame with a Variety of Infill Partitions," by Yanev, B. and McNiven, H.D., December 1985.

UCB/EERC-86/01 "A Study of Seismically Resistant Eccentrically Braced Steel Frame Systems," by Kasai, K. and Popov, E.P., January 1986, (PB87 124 178/AS)A14.

UCB/EERC-86/02 "Design Problems in Soil Liquefaction," by Seed, H.B., February 1986, (PB87 124 186/AS)A03.

UCB/EERC-86/03 "Implications of Recent Earthquakes and Research on Earthquake-Resistant Design and Construction of Buildings," by Bertero, V.V., March 1986, (PB87 124 194/AS)A05.

UCB/EERC-86/04 "The Use of Load Dependent Vectors for Dynamic and Earthquake Analyses," by Leger, P., Wilson, E.L. and Clough, R.W., March 1986, (PB87 124 202/AS)A12.

UCB/EERC-86/05 "Two Beam-To-Column Web Connections," by Tsai, K.-C. and Popov, E.P., April 1986, (PB87 124 301/AS)A04.

UCB/EERC-86/06 "Determination of Penetration Resistance for Coarse-Grained Soils using the Becker Hammer Drill," by Harder, L.F. and Seed, H.B., May 1986, (PB87 124 210/AS)A07.

UCB/EERC-86/07 "A Mathematical Model for Predicting the Nonlinear Response of Unreinforced Masonry Walls to In-Plane Earthquake Excitations," by Mengi, Y. and McNiven, H.D., May 1986, (PB87 124 780/AS)A06.

UCB/EERC-86/08 "The 19 September 1985 Mexico Earthquake: Building Behavior," by Bertero, V.V., July 1986.

UCB/EERC-86/09 "EACD-3D: A Computer Program for Three-Dimensional Earthquake Analysis of Concrete Dams," by Fok, K.-L., Hall, J.F. and Chopra, A.K., July 1986, (PB87 124 228/AS)A08.

UCB/EERC-86/10 "Earthquake Simulation Tests and Associated Studies of a 0.3-Scale Model of a Six-Story Concentrically Braced Steel Structure," by Uang, C.-M. and Bertero, V.V., December 1986, (PB87 163 564/AS)A17.

UCB/EERC-86/11 "Mechanical Characteristics of Base Isolation Bearings for a Bridge Deck Model Test," by Kelly, J.M., Buckle, I.G. and Koh, C.-G., 1987.

UCB/EERC-86/12 "Effects of Axial Load on Elastomeric Isolation Bearings," by Koh, C.-G. and Kelly, J.M., 1987.

UCB/EERC-87/01 "The FPS Earthquake Resisting System: Experimental Report," by Zayas, V.A., Low, S.S. and Mahin, S.A., June 1987.

UCB/EERC-87/02 "Earthquake Simulator Tests and Associated Studies of a 0.3-Scale Model of a Six-Story Eccentrically Braced Steel Structure," by Whittaker, A., Uang, C.-M. and Bertero, V.V., July 1987.

UCB/EERC-87/03 "A Displacement Control and Uplift Restraint Device for Base-Isolated Structures," by Kelly, J.M., Griffith, M.C. and Aiken, I.G., April 1987.

UCB/EERC-87/04 "Earthquake Simulator Testing of a Combined Sliding Bearing and Rubber Bearing Isolation System," by Kelly, J.M. and Chalhoub, M.S., 1987.

UCB/EERC-87/05 "Three-Dimensional Inelastic Analysis of Reinforced Concrete Frame-Wall Structures," by Moazzami, S. and Bertero, V.V., May 1987.

UCB/EERC-87/06 "Experiments on Eccentrically Braced Frames with Composite Floors," by Ricles, J. and Popov, E., June 1987.

UCB/EERC-87/07 "Dynamic Analysis of Seismically Resistant Eccentrically Braced Frames," by Ricles, J. and Popov, E., June 1987.

UCB/EERC-87/08 "Undrained Cyclic Triaxial Testing of Gravels-The Effect of Membrane Compliance," by Evans, M.D. and Seed, H.B., July 1987.

UCB/EERC-87/09 "Hybrid Solution Techniques for Generalized Pseudo-Dynamic Testing," by Thewalt, C. and Mahin, S.A., July 1987.

UCB/EERC-87/10 "Investigation of Ultimate Behavior of AISC Group 4 and 5 Heavy Steel Rolled-Section Splices with Full and Partial Penetration Butt Welds," by Bruneau, M. and Mahin, S.A., July 1987.

UCB/EERC-87/11 "Residual Strength of Sand from Dam Failures in the Chilean Earthquake of March 3, 1985," by De Alba, P., Seed, H.B., Retamal, E. and Seed, R.B., September 1987.

UCB/EERC-87/12 "Inelastic Seismic Response of Structures with Mass or Stiffness Eccentricities in Plan," by Bruneau, M. and Mahin, S.A., September 1987.

UCB/EERC-87/13 "CSTRUCT: An Interactive Computer Environment for the Design and Analysis of Earthquake Resistant Steel Structures," by Austin, M.A., Mahin, S.A. and Pister, K.S., September 1987.

UCB/EERC-87/14 "Experimental Study of Reinforced Concrete Columns Subjected to Multi-Axial Loading," by Low, S.S. and Moehle, J.P., September 1987.

UCB/EERC-87/15 "Relationships between Soil Conditions and Earthquake Ground Motions in Mexico City in the Earthquake of Sept. 19, 1985," by Seed, H.B., Romo, M.P., Sun, J., Jaime, A. and Lysmer, J., October 1987.

UCB/EERC-87/16 "Experimental Study of Seismic Response of R. C. Setback Buildings," by Shahrooz, B.M. and Moehle, J.P., October 1987.

UCB/EERC-87/17 "Three Dimensional Aspects of the Behavior of R. C. Structures Subjected to Earthquakes," by Pantazopoulou, S.J. and Moehle, J.P., October 1987.

UCB/EERC-87/18 "Design Procedures for R-FBI Bearings," by Mostaghel, N. and Kelly, J.M., November 1987.

UCB/EERC-87/19 "Analytical Models for Predicting the Lateral Response of R C Shear Walls: Evaluation of their Reliability," by Vulcano, A. and Bertero, V.V., November 1987.

UCB/EERC-87/20 "Earthquake Response of Torsionally-Coupled Buildings," by Hejal, R. and Chopra, A.K., December 1987.

UCB/EERC-87/21 "Dynamic Reservoir Interaction with Monticello Dam," by Clough, R.W., Ghanaat, Y. and Qiu, X-F., December 1987.

UCB/EERC-87/22 "Strength Evaluation of Coarse-Grained Soils," by Siddiqi, F.H., Seed, R.B., Chan, C.K., Seed, H.B. and Pyke, R.M., December 1987.

UCB/EERC-88/01 "Seismic Behavior of Concentrically Braced Steel Frames," by Khatib, I., Mahin, S.A. and Pister, K.S., January 1988.

UCB/EERC-88/02 "Experimental Evaluation of Seismic Isolation of Medium-Rise Structures Subject to Uplift," by Griffith, M.C., Kelly, J.M., Coveney, V.A. and Koh, C.G., January 1988.